The haematological consequences of experimental visceral leishmaniasis

Dr. Gulab Fatima Rani
MBBS, MPhil (Haematology)

Doctor of Philosophy (PhD)

University of York

York Biomedical and Research Institute (YBRI)/Biology

May 2020

Abstract

Visceral leishmaniasis (VL) is a neglected tropical disease with high morbidity and mortality, presents with hepatosplenomegaly, immune dysregulation, haematological complications and high risk of co-/secondary infections. Thrombocytopenia is one of the predominant haematological features in infected humans and experimental models but the underlying mechanisms remain poorly understood. In this thesis, key aspects of platelet production and removal were examined in an experimental murine model of VL

First, ultrastructural morphology of bone marrow megakaryocytes (MKs) in *L. donovani*-infected mice was examined using transmission electron microscopy and quantitative image analysis. The cytoplasmic demarcation membranous system and associated platelet territories, features of normal thrombopoiesis, were reduced in MKs. Despite this, MKs retained the functional capacity to produce platelets when placed under stress following anti-CD41 mediated platelet removal. Thrombopoietin, a key regulator of thrombopoiesis, was differentially expressed in hepatocytes around the hepatic granulomas in chronically infected mice. To address platelet removal, depletion of tissue macrophages was performed. In uninfected mice, no change in platelet counts was suggestive of other clearance mechanisms under homeostatic conditions. Full depletion of macrophages could not be achieved in infected mice, leaving open the question of their role in platelet clearance during infection. However, infected mice had significant numbers of IgG bound platelets, suggestive of macrophage dependent clearance. Excessive platelet desialylation in infected mice was also observed, providing an alternate mechanism involving enhanced platelet clearance by hepatocytes.

To address the reversibility of these changes, a model of drug-induced parasite clearance was used. Blood parameters and tissue microarchitecture were restored after AmBisome® treatment. Finally, this model was extended to determine how previous VL affected the course of experimental malaria, as these two infections are commonly found in endemic countries. Malaria induced pronounced thrombocytopenia in mice with previous VL, but parasitaemia was delayed compared to control mice, suggestive of a residual cross protective immune response. Together, these data suggest a reversible multifactorial pathogenesis of thrombocytopenia with defective production and enhanced clearance. Delayed malaria kinetics post-treatment could be useful to study in human patients to avoid delayed and wrong diagnosis due to overlap of clinical presentations.

Table of contents

Abstract 2

Table of contents 3

List of Figures 8

List of Tables 13

Acknowledgements 14

Author's declaration 16

Chapter 1. General introduction 17

1.1 Megakaryopoiesis to thrombopoiesis 17

1.1.1 Overview of platelet production from haematopoietic stem cells 17

1.1.1.1 Regulation of platelet production 21

1.1.2 Platelet clearance and TPO production 21

1.1.3 Platelet disorders 25

1.1.4 Thrombocytopenia in infections 26

1.2 Leishmaniasis 29

1.2.1 Prevalence and epidemiology of leishmaniasis 29

1.2.2 Visceral leishmaniasis (VL) 29

1.2.3 Immune response in VL 32

1.2.4 Haematological complications in VL 33

1.2.5 Thrombocytopenia in VL 34

1.2.6 Treatment of VL 37

1.2.7 Leishmaniasis/co-infections 37

1.3 Tissue macrophages 38

1.3.1 Splenic macrophages 38

1.3.2 Liver architecture and Kupffer cells 41

1.3.3 Tissue macrophages as reservoirs of *L. donovani* amastigotes 43

1.3.4 Splenic macrophages are responsible for excessive platelet clearance resulting in thrombocytopenia....46
1.4 Experimental models of secondary infection....46
1.4.1 Malaria as a model of secondary infection....46
1.4.2 Malaria as a model of secondary infection in treated EVL....47
1.5 Overall Aims....48
Chapter 2. Materials and Methods....49
2.1 Animals and parasites:....49
2.1.1 Ethical approval....49
2.1.2 Mice....49
2.1.3 Parasites and infection....49
2.1.3.1 *L. donovani* passage and infection....50
2.1.3.2 *P. chabaudi* passage and infection....50
2.1.4 Estimation of parasite burden....51
2.1.4.1 Leishmania parasite burden....51
2.1.4.2 Malaria parasitaemia....52
2.2 Blood collection and analysis....52
2.3 Induced thrombocytopenia model....53
2.4 Exogenous thrombopoietin administration....53
2.5 *In vivo* bioluminescence imaging....53
2.6 *Ex vivo* bioluminescence imaging....54
2.7 Tissue macrophage depletion....54
2.8 AmBisome® preparation and administration....55
2.9 Developing a model of secondary infection....55
2.10 Detection of anti-platelet antibodies....55
2.11 Estimation of platelet desialylation....56
2.12 Quantification of serum TPO using enzyme-linked immunosorbent assay....58

2.13 Measurement of *Thpo* mRNA accumulation 59
2.13.1 RNA extraction: 59
2.13.2 Reverse transcription reaction 60
2.13.3 Quantitative polymerase-chain reaction 60
2.14 Sample processing for electron microscopy 61
2.15 Cryopreservation and Cryo-sectioning of tissues 62
2.16 Haematoxylin and Eosin (H & E) staining on tissue sections 63
2.17 Immunofluorescence staining on tissues sections 63
2.18 Segmentation image analysis on IF images 64
2.19 Statistical analysis 66
Chapter 3. Thrombopoiesis in visceral leishmaniasis 67
3.1 Introduction 67
3.2 Aims 69
3.3 Results 70
3.3.1 *L. donovani* infection results in progressive thrombocytopenia in an experimental mouse model 70
3.3.2 Bone marrow megakaryopoiesis is altered in experimental VL 76
3.3.3 Bone marrow megakaryocytes are capable of platelet production on stimulation 80
3.3.4 Thrombopoietin production is compromised during chromic EVL 89
3.3.5 BM megakaryocytes remain responsive to thrombopoietin stimulation 96
3.4 Discussion 108
Chapter 4. Splenic clearance and thrombocytopenia in visceral leishmaniasis 111
4.1 Introduction 111
4.2 Aims 113
4.3 Results: Macrophage depletion 114
4.3.1 Histological confirmation of tissue macrophage depletion 114
4.3.2 Effects of macrophage depletion on platelet counts 121

4.3.3 Effects of macrophage depletion on other blood cells and parasite burden.....121
4.4 Antiplatelet antibodies 129
4.4.1 Anti-platelet antibodies coating the circulating platelets 129
4.5 Platelet Desialylation 131
4.6 Discussion 133
Chapter 5. Post-treatment recovery of haematological parameters in experimental VL 136
5.1 Introduction 136
5.2 Aims 138
5.3 Results 139
5.3.1 Haematological profile after treatment 139
5.3.1.1 Platelet count recovery after treatment 139
5.3.1.2 Reversal of anaemia and red cell parameters 142
5.3.1.3 Leucocyte count recovery after treatment 142
5.3.1.4 Thrombopoietin production after treatment 143
5.3.2 Restoration of liver and spleen microarchitecture 148
5.3.3 Production of iNOS by macrophages during infection and after treatment.....158
5.4 Discussion 166
Chapter 6. Sequential secondary infection in drug-treated *L. donovani*-infected mice 168
6.1 Introduction 168
6.2 Aims 170
6.3 Results: Rodent malaria- a pilot experiment 171
6.3.1 Haematological profile of malaria infected mice 175
6.3.2 Tissue microarchitectural changes in malaria 175
6.4 Malaria as a secondary infection in drug-treated *L. donovani*-infected mice 183
6.4.1 Response to malaria in VL treated mice 183
6.4.2 Haematological response to malaria in VL treated mice 189

6.4.3 Thrombopoietin production in single and sequentially infected mice 190
6.4.4 Tissue remodelling after sequential secondary infection 198
6.5 Discussion 206
Chapter 7. Concluding Discussion 209
7.1 Thrombocytopenia in experimental VL is multifactorial 209
7.2 Haematological profile and tissue architecture is reversible after treatment 212
7.3 Delayed disease kinetics of *P. chabaudi* malaria in treated EVL mice 213
Appendix 215
Abbreviations 216
References 221
Publications/other contributions 247

List of Figures

Figure 1.1 Schematic of platelet production in the bone marrow……..20

Figure 1.2 Platelet desialylation and hepatic TPO production via JAK2-STAT3 signalling pathway……23

Figure 1.3 Role of tissue macrophages in platelet clearance…….24

Figure 1.4 Factors responsible for thrombocytopenia in chronic liver diseases (CLD)...28

Figure 1.5 Life-cycle of *Leishmania donovani*…….....31

Figure 1.6 Summary of thrombocytopenia mechanisms in VL known so far……...36

Figure 1.7 Microarchitecture of the murine spleen highlighting the localization of different splenic macrophage populations……40

Figure 1.8 Microarchitecture of the liver……..42

Figure 1.9 Microarchitectural alterations in the infected liver…….……44

Figure 1.10 Microarchitectural alterations in the infected spleen…..……...45

Figure 3.1 Schematic diagram of chronic infection murine model of *L. donovani* infection ……..……...72

Figure 3.2 Thrombocytopenia in *L. donovani*-infected BALB/c mice…….73

Figure 3.3 *L. donovani* infection in C57BL/6 mice results in thrombocytopenia and high parasite burden with organomegaly…….....74

Figure 3.4 Platelet counts during the course of *L. donovani* infection in C57BL/6 mice ……..... 75

Figure 3.5 Segmentation analysis strategy on Transmission Electron Microscopy (TEM) images……..77

Figure 3.6 Representative images of transmission electron microscopy and perimeter of demarcation membranes of mature bone marrow megakaryocytes……..78

Figure 3.7 Schematic of the induced immune thrombocytopenia in infected mice……...82

Figure 3.8 Spleen parasite burden and splenic weight in induced immune thrombocytopenia……...83

Figure 3.9 Platelet counts after anti-CD41 mAb administration in uninfected and infected C57BL/6 mice……..84

Figure 3.10 Anti-CD41 induced ITP restores the DMS in BM MKs in *L. donovani*-infected mice ...…….……...…….85

Figure 3.11 Thrombopoietin in circulation and tissues……91

Figure 3.12 Representative immunofluorescent (IF) staining of liver sections stained with anti-TPO antibodies ……92

Figure 3.13 Gating strategy to obtain the median fluorescence intensity of TPO^+ hepatocytes at various distances from the margin of granuloma……...94

Figure 3.14 Median fluorescence intensity of TPO^+ hepatocytes in the whole liver and around the hepatic granulomas at various distances……95

Figure 3.15 Schematic of the experiment involving exogenous administration of rTPO to mice infected with bioluminescent *L. donovani* parasites along with *in vivo* imaging.....98

Figure 3.16 Treatment with the recombinant TPO delays the onset of thrombocytopenia in infected mice……99

Figure 3.17 Effects of the rTPO treatment on circulating levels, tissue mRNA and tissue weights……...…100

Figure 3.18 Parasite burden and correlation between platelets and enlarged spleen…...101

Figure 3.19 *In vivo* detection of *L. donovani* parasites in control and rTPO-treated mice……...102

Figure 3.20 Parasite burden determined by *in vivo* imaging in mice infected with bioluminescent *L. donovani*……...103

Figure 3.21 *Ex vivo* images of mice spleens and livers……..104

Figure 3.22 Parasite burden in infected livers and spleens……105

Figure 4.1 Schematic of experiment showing the strategy to deplete tissue macrophages …….……..116

Figure 4.2 Representative IF stained spleen images of clodronate treated mice ……..……..117

Figure 4.3 Representative IF stained liver images of clodronate treated mice ……..…….118

Figure 4.4 Changes in area and perimeter of spleens and livers after clodronate treatment ……...……119

Figure 4.5 Tissue macrophages in response to clodronate treatment……..…120

Figure 4.6 Platelet count and MPV changes after clodronate treatment……..…122

Figure 4.7 Changes in organ weight after clodronate treatment…….....123

Figure 4.8 Parasite burden in infected mice after treatment with clodronate……..124

Figure 4.9 Correlation between platelet count and organ weights…….….125

Figure 4.10 Presence of anti-platelet antibodies in infected mice……...130

Figure 4.11 Platelet desialylation in infected mice…….132

Figure 5.1 Schematic of the experiment to study the effects of treatment……...140

Figure 5.2 Platelet count recovery after treatment…….….141

Figure 5.3 Anaemia and red cell parameters after treatment……...144

Figure 5.4 Leucocyte counts after treatment……...146

Figure 5.5 Thrombopoietin production after treatment……..147

Figure 5.6 Segmentation analysis on IF stained liver images of treated mice…….149

Figure 5.7 Representative IF stained liver images of treated mice.……...……..150

Figure 5.8 Organ weight in response to treatment..…… 151

Figure 5.9 Correlation between platelet count and organ weights……..152

Figure 5.10 Representative Haematoxylin and Eosin stained liver images of treated mice ……...……153

Figure 5.11 Representative Haematoxylin and Eosin stained spleen images of treated mice…….……..154

Figure 5.12 Representative IF stained spleen images of treated mice……155

Figure 5.13 Area and perimeter of spleen after treatment……...156

Figure 5.14 Response of splenic macrophages to treatment……...157

Figure 5.15 Reduction in hepatic iNOS expression in response to treatment……....160

Figure 5.16 iNOS expression in Kupffer cells…….....161

Figure 5.17 Splenic iNOS expression in response to treatment……..163

Figure 5.18 Splenic area in response to treatment……...164

Figure 5.19 iNOS expression in splenic RP macrophages……..165

Figure 6.1 Schematic of malaria infection in C57BL/6 mice…….……172

Figure 6.2 Parasitaemia and weight loss in infected mice……...173

Figure 6.3 Changes in the organ weights in response to malaria……..…...174

Figure 6.4 Thrombocytopenia in rodent malaria……176

Figure 6.5 Changes in erythrocyte counts and indices in malaria infected mice……..…177

Figure 6.6 Changes in leucocyte counts in malaria infected mice.……178

Figure 6.7 Representative H & E and IF stained spleen images of malaria infected mice.....179

Figure 6.8 Representative H & E and IF stained liver images of malaria infected mice …….....180

Figure 6.9 Area and perimeter analysis on IF stained images of malaria infected mice ……..…….181

Figure 6.10 Spleen and liver macrophages in response to malaria…….……182

Figure 6.11 Schematic of malaria as a secondary infection in drug treated *L. donovani*-infected mice…….....185

Figure 6.12 *P. chabaudi* parasitaemia and LDUs in infected mice……186

Figure 6.13 Weight loss in malaria infected mice…….....…..187

Figure 6.14 Organomegaly in response to malaria……188

Figure 6.15 Platelet count changes in VL treated and malaria infected mice…..……191

Figure 6.16 Erythrocyte count and red cell indices in VL treated and malaria infected mice ……..192

Figure 6.17 Leucocyte count changes in VL treated and malaria infected mice…….194

Figure 6.18 Correlation between platelet count and organ weights……...196

Figure 6.19 Serum thrombopoietin levels……..197

Figure 6.20 Area and perimeter analysis on IF stained images……...199

Figure 6.21 F4/80^{+} Kupffer cells in response to malaria…….....200

Figure 6.22 Splenic macrophages in response to malaria……..201

Figure 6.23 Representative IF stained liver images……202

Figure 6.24 Representative IF stained spleen images…….203

Figure 6.25 Representative H & E stained liver images……..204

Figure 6.26 Representative H & E stained spleen images……...205

Figure 7.1 Summary of thrombocytopenia mechanisms in VL including our findings...211

Supplementary Figure 1 No detectable human-TPO in hu-rTPO treated mice serum …….....215

List of Tables

Table 2.1 List of antibodies used for platelets flow cytometric assays……..57

Table 2.2 List of antibodies used for IF staining……...65

Table 3.1 Erythrocyte parameters on peripheral blood counts in infected vs uninfected mice, treated with anti-CD41 mAb to induce ITP…….87

Table 3.2 Leucocyte counts on peripheral blood counts in infected vs uninfected mice, treated with anti-CD41 mAb to induce ITP……..88

Table 3.3 Erythrocyte parameters in peripheral blood in infected vs uninfected mice, treated with rTPO……..106

Table 3.4 Leucocyte counts in peripheral blood in infected vs uninfected mice, treated with rTPO……..107

Table 4.1 Erythrocyte count and red cell indices in infected and uninfected mice treated with clodronate or PBS liposomes……126

Table 4.2 Leucocyte count in infected and uninfected mice treated with clodronate or PBS liposomes……..128

Acknowledgements

I would primarily like to extend my gratitude to my supervisors Prof. Paul M. Kaye and Prof. Ian S. Hitchcock for their mentorship and support throughout my PhD. In particular, I would like to thank both of them for giving me the opportunity to work on an interesting research topic, for devising my experimental plans and for their help and guidance whenever I needed it. Additionally, I would take this opportunity to acknowledge my thesis advisory panel/formal review of progress panel members, Prof. Paul Genever and Dr Allison Green for their support and useful advice.

I have greatly enjoyed these three years of my PhD at the York Biomedical Research Institute (YBRI) formerly Centre for Immunology and Infection. This thesis was not possible without the invaluable support of many colleagues at YBRI especially Kaye lab and Hitchcock lab members. I am greatly indebted to Dr Najmeeyah Brown for being an amazing human being, a great friend and a very kind teacher. Throughout these years, she has taught me a lot from basic pipetting to imaging and flow cytometry. This work would not have been possible without her support and training. I would also like to thank Dr Helen Ashwin for her enormous help with my experimental work and image analysis, beautiful immunofluorescent images and segmentation analysis would not have been possible without her help. I would also like to thank Dr Marcela Montes De Oca and Dr Tess Stanly for their support during the stressful days of thesis write up and for their useful comments and proofreading my thesis. Both of you have been a huge support in keeping me motivated for the thesis write up.

A very special thank you to all the present members of both groups, Dr. Mohamed Osman, Dr Katrien Van Bocxlaer, Dr Nidhi Dey and Dr Shoumit Dey in Kaye lab and Dr Julie Tucker, Dani Pulgar Prieto, Oliver Herd, Andy Stone and Dr Daniel Yee in Hitchcock lab for being wonderful colleagues. I would also like to thank past members, Dr Johannes Doehl, Dr Audrey Romano and Dr Ana Pinto for their technical support in my first year of PhD. I am also very grateful to Prof. Jeremey Mottram for providing bioluminescent *L. donovani* parasites for *in vivo* imaging experiments, and Prof. Jean Langhorne for providing parasites for malaria experiments. I am highly indebted to Dr Jayanthi Anand and Dr Elmarie Myburgh for their help in *in vivo* imaging and analysis. A big thank you to Dr Jayanthi Anand for being an amazing friend from the beginning of my PhD and for her support especially when I was homesick or stressed with failed experiments. She

along with her family (Dr Anand Manoharran, Mimi and Mini) have been a big support and like my second family in the UK, thanks for keeping me smiling throughout my hard PhD days.

I would like to thank all the academic members of YBRI for their support and motivation, members of Walrad and Mottram lab groups for being very nice and supportive. Last but not the least, I am very thankful to Dr James Hewitson and Dr Dimitris Lagos for their invaluable advice on my work and moral support during my bad experimental days. I am grateful to BSF staff for their help in conducting my experiments and biological technical facility (TF) staff in particular Dr Graeme Park, Dr Karen Hogg and Dr Karen Hodgkinson for their technical support in microscopy and flow cytometry. I would also like to thank Meg Stark in the TF for her help in electron microscopy and collecting the beautiful images of bone marrow megakaryocytes.

Many thanks to all the academic, research and support staff in the department for their immense moral support, motivating words and delicious food. I am greatly indebted to Monica Bandeira in biology graduate office for always being there to answer any question and very supportive in making this journey smooth for all PhD students.

I would like to acknowledge my funding bodies Higher Education Commission of Pakistan and Khyber Medical University, Pakistan. This work would have not been possible without their financial support throughout my PhD. I am also thankful to Prof. Abid Sohail Taj and Dr Safia Jalal, my mentors in haematology training in Pakistan who have a big role in making me what I am today. Thank you for training me under your supervision, and your continuous support and appreciation till date.

Lastly, I would like to thank my parents, sister, cousins, aunts and uncles for their encouragement and always being on my side in all moments. I have no words to express my gratitude and love for my parents who have supported me in every decision I have ever made in my life. It is their trust and support that I have accomplished what I have dreamt of in my life. A special thanks to my friends for their kind and motivating words, adventures and food parties. Their support and encouragement have helped me enjoy the hard days of PhD and especially bringing tasty food to the lab when I was working late nights was a great help in finishing my dream project. Thank you for making it so much fun and a great experience.

Author’s declaration

I declare that this thesis is a presentation of original work and I am the sole author. This work has not previously been presented for an award at this, or any other, University. All sources are acknowledged as References.

Chapter 1. General introduction

1.1 Megakaryopoiesis to thrombopoiesis

1.1.1 Overview of platelet production from haematopoietic stem cells

Platelets are one of the most important cellular components of the blood. Their main function is to maintain primary hemostasis of the body (1). Approximately 100 billion platelets are produced every day in an adult human bone marrow (BM) to maintain a circulating level of 150-400 x 10^3 platelets per µl (2). Apart from hemostasis, recent studies have emphasized on their role in the innate immune system.

Platelets play a vital role in the primary hemostasis and thrombosis by forming a primary platelet plug (aggregate or clot) on the endothelial wall in case of any vascular injury (3). This process involves various stages, starting from platelet adhesion to injured subendothelial extracellular matrix, platelet activation and recruitment of additional platelets to form a platelet aggregate (3). Vasoconstriction and platelet plug formation are the critical initial responses to stop bleeding from the site of injury (3). Apart from their role in coagulation and hemostasis, recent studies have shown that they are an integral part of the innate immune system and especially important against viral infections. Platelets can harbor pathogens on their plasma membrane as well as internally such as viruses, bacteria and parasites (4–7). Platelets express toll-like receptors on their membranes which are critical for their innate immune functions (8). Other than hemostasis and immunity, platelets are also involved in a variety of other processes including development of the lymphatic system, liver regeneration, inflammation and cancer through angiogenesis promotion (9). On the other hand, platelets have also been thought to play an important role in cerebral malaria and neurological complications such as in HIV (10,11).

Platelets are anucleated cellular components with complex cytoplasm containing small pockets loaded with alpha granules, dense granules, and lysosomes. There are about 60-80 alpha granules rich in vWF, TGF-β, fibrinogen, PF4 and around 4-6 dense granules in each platelet which contain ADP, calcium, serotonin. (3,12,13). These granules are released upon platelet activation and perform their hemostatic and immune functions.

Hypogranular platelets could lead to haemorrhagic complications despite normal counts and are often evident in malignancy or as a consequence of inherited disorders (14) (see **section 1.1.3**). Platelets are tiny cellular fragments, ranging from ~2-4 µm in size, produced mainly in the BM of the long bones in adults (15). Platelets have a half-life of 7-10 days in humans and 3-5 days in mice and are continuously produced by their BM precursors, megakaryocytes (MKs) which make up less than 1% of myeloid cells (16,17). The whole process of platelet production is tightly regulated by cytokines and any discrepancy in this process could result in defective or abnormal MKs and reduced or defective platelets leading to fatal outcomes.

Figure 1.1 shows a simplified schematic of platelet production from BM MKs. Briefly, haematopoietic stem cells (HSCs) differentiate into megakaryoblasts through repeated mitotic divisions under the influence of cytokines. HSCs divide into myeloid lineage committed cells which further differentiate into MK-erythroid progenitors (MEP) and then megakaryoblasts, the precursors of MKs. While these megakaryoblasts proliferate to transform into MKs, further proliferation is taken over by a unique mitotic process called endomitosis (18). Endomitosis is a special type of mitotic cell division where repeated mitotic divisions of the nucleus result in a multilobulated polyploid nucleus and maturation of cytoplasm (19). Due to multiple endomitotic divisions, MKs transform into giant polyploid cells with a multilobulated nucleus (ranging from ~50-100 µm in size), generally referred as megakaryopoiesis.

Giant MKs develop a network of membranes inside their cytoplasm as a result of endomitosis, known as the demarcation membranous system (DMS) which serve as platelet territories (20). They are also known as the invagination membranous system (IVS) as the recent data suggest that these membranes are the invaginations of the plasma membranes into the cytoplasm of MKs (20).

In addition to a polyploid nucleus and extensive cytoplasmic membranes, different types of the granules and organelles also develop and accumulate in the cytoplasm of maturing MKs. Upon maturation, these membranes surround the granules and extend long cytoplasmic extensions into the blood vessels as proplatelets (21,22). Electron microscopy (EM) analysis has shown that mature MKs are located in close proximity to the walls of BM sinuses (< 1µm distance from a sinus), critical for releasing immature platelets (proplatelets) into the general circulation (23). These proplatelets are remodeled

further in the tissue parenchyma or general circulation to transform into mature platelets (22,24). Production of platelets from MKs to their release into the circulation is generally regarded as thrombopoiesis.

As mentioned earlier, the process from differentiation and proliferation of HSCs to MK development and platelet production is tightly regulated by cytokines. These cytokines include thrombopoietin (TPO), stem cell factor (SCF), granulocyte-macrophage colony stimulating factor (GM-CSF) and certain interleukins (ILs) e.g. IL-3, IL-6, IL-11 along with FLT ligand, fibroblast growth factor (FGF) and erythropoietin (EPO) (25–27). TPO is the key regulator of megakaryocyte differentiation, supporting HSCs expansion, megakaryocyte lineage selection and megakaryopoiesis, whereas SCF and interleukins are important in the initial stages of MK production (28).

Any disparity in this process results in aberrant platelet production, ranging from abnormal platelet counts to functionally defective platelets, each resulting in distinct clinical complications. Apart from central BM causes, systemic diseases could also impact the process of platelet production. Chronic liver disease (CLD) refers to a group of diseases with progressive liver damage. In these diseases, normal liver parenchyma is gradually replaced by the extracellular matrix (ECM) leading to fibrosis and cirrhosis (29). CLD can occur due to several causes including viral infections, drugs, alcohol, autoimmune and metabolic disorders and are associated with thrombocytopenia most likely due to reduced TPO production (30).

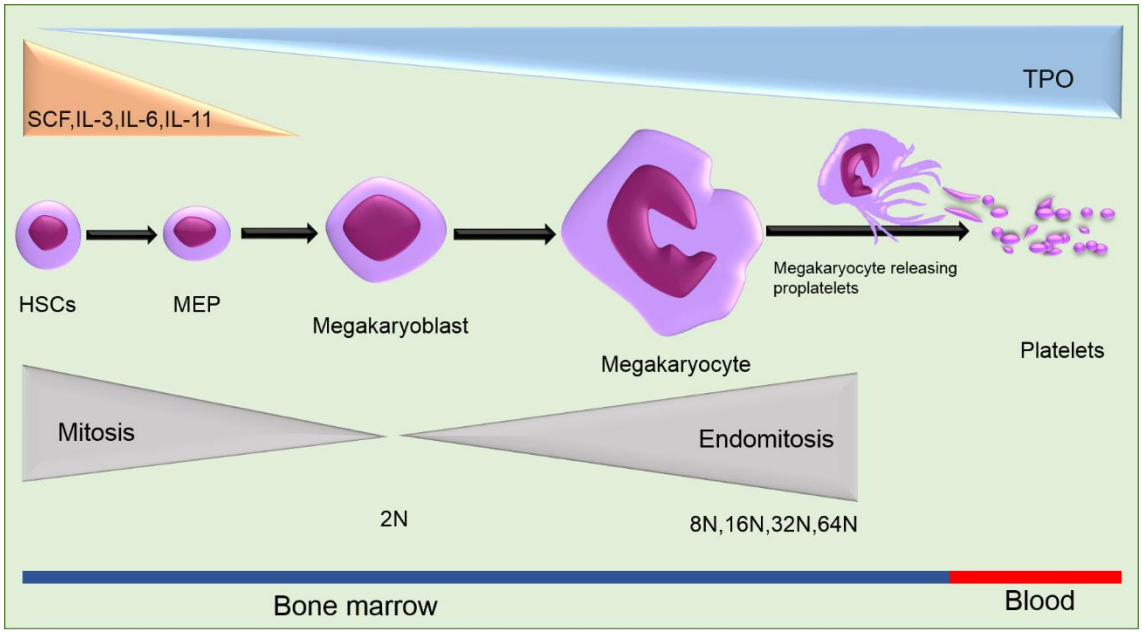

Figure 1.1 Schematic of platelet production in the bone marrow. Haematopoietic stem cells (HSCs) multiply by mitotic division into megakaryocyte-erythroid lineage committed cells under the influence of stem cell factor (SCF), IL-3, IL-6, IL-11 and thrombopoietin (TPO). Megakaryocyte-erythroid progenitors (MEP) differentiate into megakaryoblasts and then MKs thorough endomitotic divisions. Large polyploid MKs release immature proplatelets into the bone marrow blood sinuses. Proplatelets are remodeled into mature platelets in the circulation or tissue parenchyma. Image slightly modified from the original publication (31).

1.1.1.1 Regulation of platelet production

As shown in **Figure 1.1**, TPO is one of the major regulators of platelet production, secreted by hepatocytes (~90%) and kidneys (5-10%) with a small contribution from BM stromal cells and other tissues (23). The role of TPO is not only limited to megakaryopoiesis and thrombopoiesis but also in the differentiation and proliferation of HSCs along with SCF and interleukins (23). TPO is vital for endomitosis to produce large polyploid cells with a multilobulated nucleus and complex cytoplasm particularly the development of DMS (32).

Normal hepatocytes are crucial for the production of TPO and the liver diseases which damage the hepatic microarchitecture have been associated with thrombocytopenia (33). Therefore, thrombocytopenia is considered as an important parameter for grading and treatment response in liver diseases although the circulating TPO levels are not generally measured in liver disorders.

1.1.2 Platelet clearance and TPO production

Platelet counts are kept under strict control to maintain the level of circulating platelets within the normal range and avoid any complications due to high or low platelet counts. Thrombocytopenia, lower number of circulating platelets is associated with bleeding disorders while thrombocytosis, higher number of circulating platelets which can be reactive and self-limiting or clonal and life-threatening (34). Considering the complications and serious outcomes associated with the low or high number of circulating platelets, it shows how important it is to keep that process under tight control (see **section 1.1.3** on diseases associated with platelet dysfunction).

Various mechanisms have been proposed to explain the clearance of old and damaged platelets from the body under physiological and pathological conditions. Clinical and experimental studies have suggested the role of spleen and liver in removing old/damaged platelets from the circulation.

Glycoproteins (GPs) on the surface of platelet plasma membranes are coated with sialic acid terminals similar to other body cells. Platelets have a short life-span and get

desialylated in the circulation as they age. Platelet desialylation occurs due to loss of terminal sialic acid, exposing the galactose residues which have a capacity to bind to hepatocyte Ashwell-Morrell Receptor (AMR; hepatic asialoglycoprotein receptor). The AMR, a mammalian asialoglycoprotein receptor (ASGPR) is a heterodimer consisting of ASGPR1 and ASGPR2 subunits, binds to these desialylated platelets and removes them from the circulation (35). Binding of desialylated platelets to AMR not only removes the old platelets but also triggers TPO transcription via the JAK2-STAT3 pathway in hepatocytes **(Figure 1.2)**. Platelet desialylation has also been seen as a consequence of platelet storage at lower temperatures (4°C). *In vitro* studies have shown increased *Thpo* mRNA levels in HepG2 cells incubated with refrigerated platelets suggesting the critical role of desialylated platelet in TPO production (36). Interestingly, studies have also suggested that desialylated or the platelets with removed galactose residues on platelet GPs are more prone to clearance by Kupffer cells either directly or CLEC4F-mediated under physiological conditions (37,38) **(Figure 1.3)**.

The role of spleen in the clearance of blood cells under physiological and pathological conditions is well-studied. The professional macrophages in the spleen are known for their phagocytic capabilities and are described as one of the major mechanisms to clear effete or dead blood cells from the circulation especially erythrocytes and iron recycling (39). In immune-mediated disorders and infections, anti-platelet antibodies are produced making them susceptible to clear by phagocytic cells (40) **(Figure 1.3)**. The role of splenic macrophages in thrombocytopenia is well described in infections such as malaria, livers disorders with splenomegaly and hypersplenism. Although the role of splenic clearance of platelets have also been suggested in VL, the underlying mechanisms remain largely unknown.

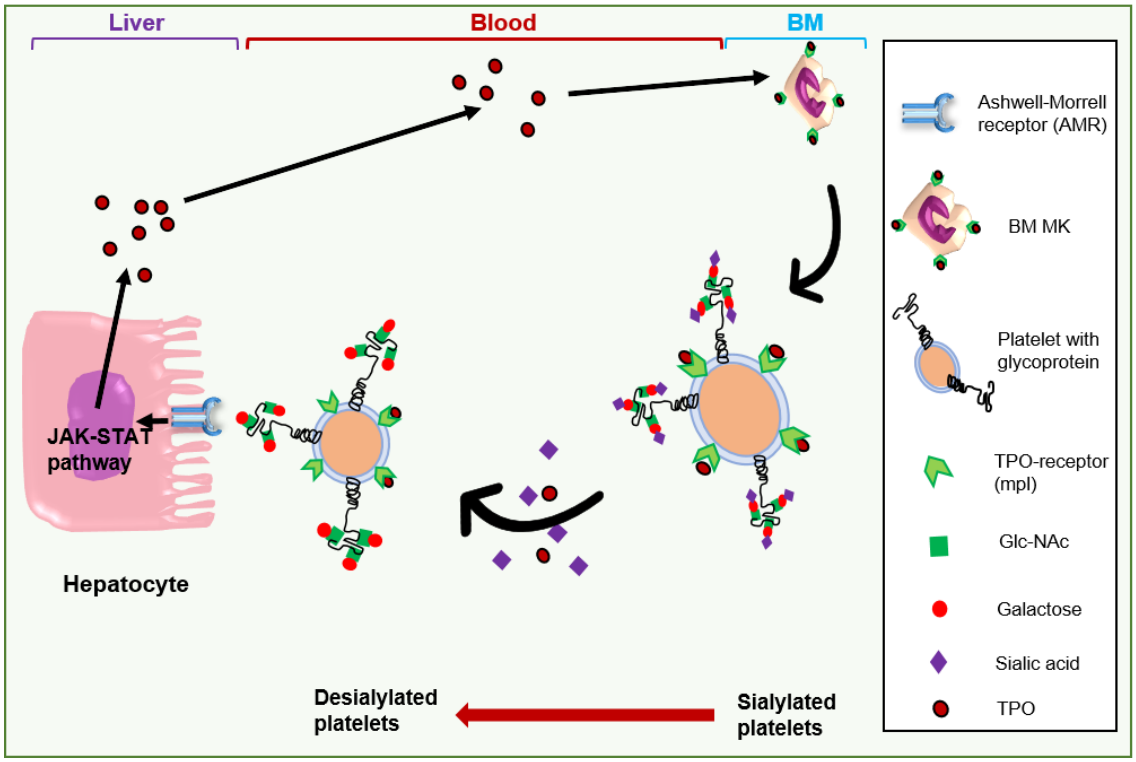

Figure 1.2 Platelet desialylation and hepatic TPO production via JAK2-STAT3 signalling pathway. Desialylated platelets are recognised by the hepatic Ashwell Morrell receptor (AMR) which then stimulates transcription of *Thpo* mRNA by activating the JAK2-STAT3 signalling pathway. Newly produced TPO is released into the circulation which then stimulates HSCs (not shown) and MKs in the bone marrow to produce new platelets. Young platelets have sialylated membrane glycoproteins which get desialylated by blood sialidases on ageing or by exogenous sialidases i.e. liberated during infection. Image modified from the original publication (35,41). Size and shapes are not true representative of the original.

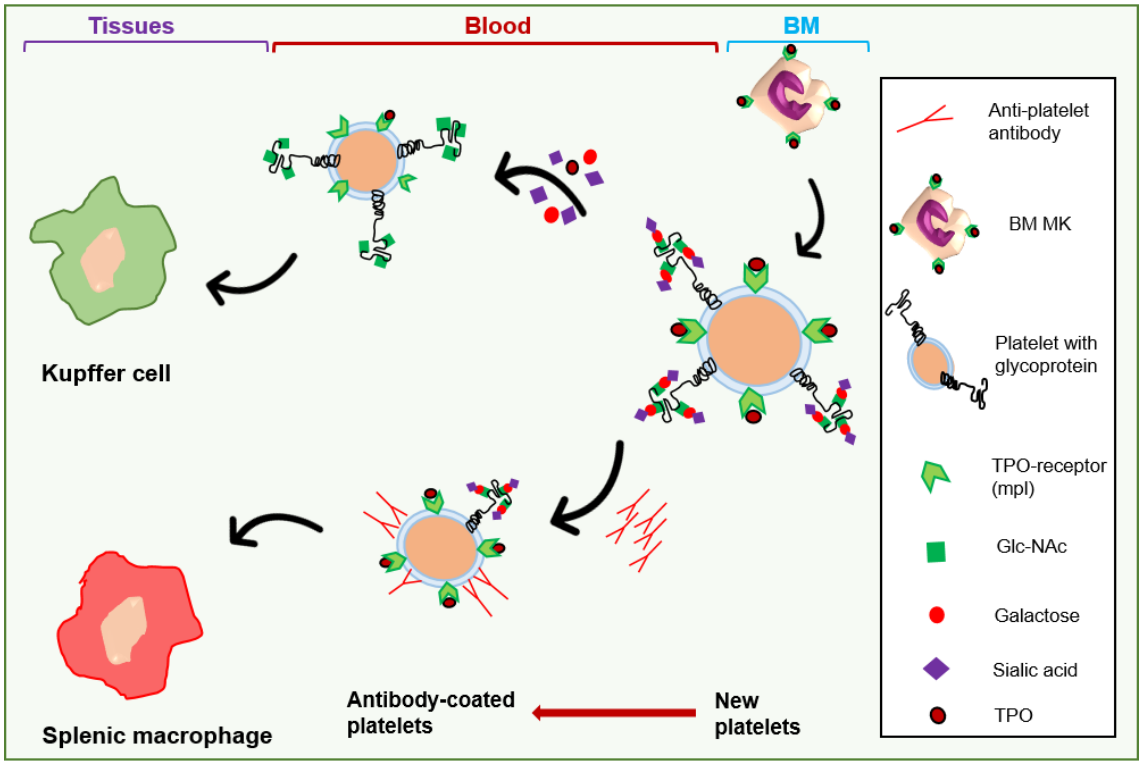

Figure 1.3 Role of tissue macrophages in platelet clearance. On aging or external insults, platelets lose their terminal sialic acid and galactose residues, platelets with exposed N-Acetylglucosamine (Glc-NAc) are taken up by Kupffer cell for clearance. Antibodies attached to platelet membranes are recognised by splenic macrophages particularly during infections and are removed by Fc-receptor mediated clearance. Image modified from the original publications (35,38,42). Size and shapes are not true representative of the original.

1.1.3 Platelet disorders

Platelet disorders are either quantitative (platelet count) or qualitative (poor functioning platelets). Thrombocytopenia is defined as the platelet count below the normal range for that particular population and gender. Normal range varies from one region to another due to various factors however, a platelet count of 150-450 x 10^3/µl is widely accepted as a normal range. Generally, a platelet count below 150 x 10^3/µl is considered as thrombocytopenia in humans however, clinically significant spontaneous bleeding usually occurs when platelet count drops below 10-20 x10^3/µl (43). Thrombocytopenia can occur in a variety of diseases either due to defective or fewer MKs, or systemic diseases.

Diseases like congenital amegakaryocytic thrombocytopenia (CAMT) occurs due to a mutation in TPO or the TPO-receptor (c-Mpl or TPO-R) resulting in a very low number of MKs in the BM (44,45). Inherited disorders could also manifest as defects in the platelet functions such as adhesion, activation, secretion, and aggregation defects and lead to haemorrhagic complications (46). Qualitative platelet disorders including Glanzmann thrombasthenia (GT), Bernard-Soulier Syndrome (BSS), Gray platelet syndrome (GPS) are inherited disorders with defective platelets, have low prevalence throughout the world, could lead to life-threatening bleeding after trauma (47,48). Platelet disorders are associated with multiple fatal complications such as prolonged bleeding time, delayed primary platelet clot formation. Apart from these disorders, local or systemic diseases could cause thrombocytopenia by various mechanisms such as excessive platelet sequestration due to the generation of autoantibodies against platelets (49). Thrombocytopenia in aplastic anaemia occurs due to hypocellular BM with the presence of very few MKs (50). Excessive desialylation, reduced TPO production in CLD and molecular mimicry also result in thrombocytopenia.

Thrombocytosis is defined as an increase in the number of circulating platelets, generally platelet count above the normal range for that region and population. Platelets are one of the acute phase reactants and an increased count is generally seen in acute insults to the body. Causes of thrombocytosis range from reactionary to malignancy i.e. Essential thrombocythaemia (ET) (14). Whether it is thrombocytopenia, thrombocytosis or the presence of defective platelets, all of them are associated with complications.

1.1.4 Thrombocytopenia in infections

Thrombocytopenia is one of the prominent haematological features during infections. Haematological complications are seen in both acute and chronic infections. Malaria, dengue, hepatitis (B & C), bacterial infections (*Salmonella*, *Mycobacterium*, *S. aureus*) and parasitic diseases (visceral leishmaniasis, Chagas disease and schistosomiasis) present with haematological complications including thrombocytopenia. These infections present with a varying degree of thrombocytopenia, ranging from mild asymptomatic to severe thrombocytopenia, with or without haemorrhagic complications.

Thrombocytopenia in infections is generally multifactorial (5). Studies suggest the role of hypersplenism, autoantibodies against platelets as well as defective production of TPO, all contribute to the development of thrombocytopenia (49,51–53). BM suppression has also been observed in HCV and other viral infections including EBV, HIV, parvovirus, varicella (54). Defective megakaryopoiesis, immature MK precursors and increased apoptosis is observed in HIV (55). Hypersplenism due to portal hypertension is a common feature of CLD and plays an important role in platelet sequestration (56). Loss of normal liver microarchitecture in CLD could be responsible for lower TPO production and hence, reduced platelet production (57). Similarly, successful liver transplantation in CLD has been shown to restore normal thrombopoiesis and reverse thrombocytopenia (58). **Figure 1.4** summarises the possible mechanisms of thrombocytopenia in liver diseases including chronic infections.

Previously, the circulating levels of TPO were thought to have an inverse relationship with the number of circulating platelets however, an increased or decreased, or even normal TPO levels are seen in thrombocytopenia due to different diseases, suggesting the complexity of TPO production and regulation. Interestingly, certain factors released by platelets have been noticed to play an important role in liver regeneration and restoration of normal parenchyma (59).

Desialylation with exposure to beta-galactose has also been suggested as a cause of cytopenias due to enhanced clearance from the circulation. Thrombocytopenia due to excessive platelet desialylation has been suggested in *Trypanosoma cruzi* infection, *Streptococcus pneumoniae* sepsis, dengue virus infection, ITP patients particularly non-responders, secondary ITP and non-ITP thrombocytopenia (60–63). Platelet desialylation

in *S. pneumoniae* is caused by pneumococcal neuraminidase A (NanA) leading to platelet hyper-reactivity with an increase in the level of exposed galactose residues, as shown by increase in lectin binding such as *Sambucus nigra* (SNA) and *Maackia amurensis* Lectin-II (MAL-II) (64). The effectiveness of Oseltamivir, a viral sialidase inhibitor in the reversal of thrombocytopenia in septic patients is suggestive of thrombocytopenia due to excessive platelet desialylation (65). Excessive desialylation is also observed in erythrocytes (66).

The role of cytokines (mainly TNF and IFNγ) and platelet phagocytosis have been well described in malaria (40). Exogenous IL-10 administration has been associated with thrombocytopenia while IFNα treatment in liver disorders has shown to increase platelet counts (67,68).

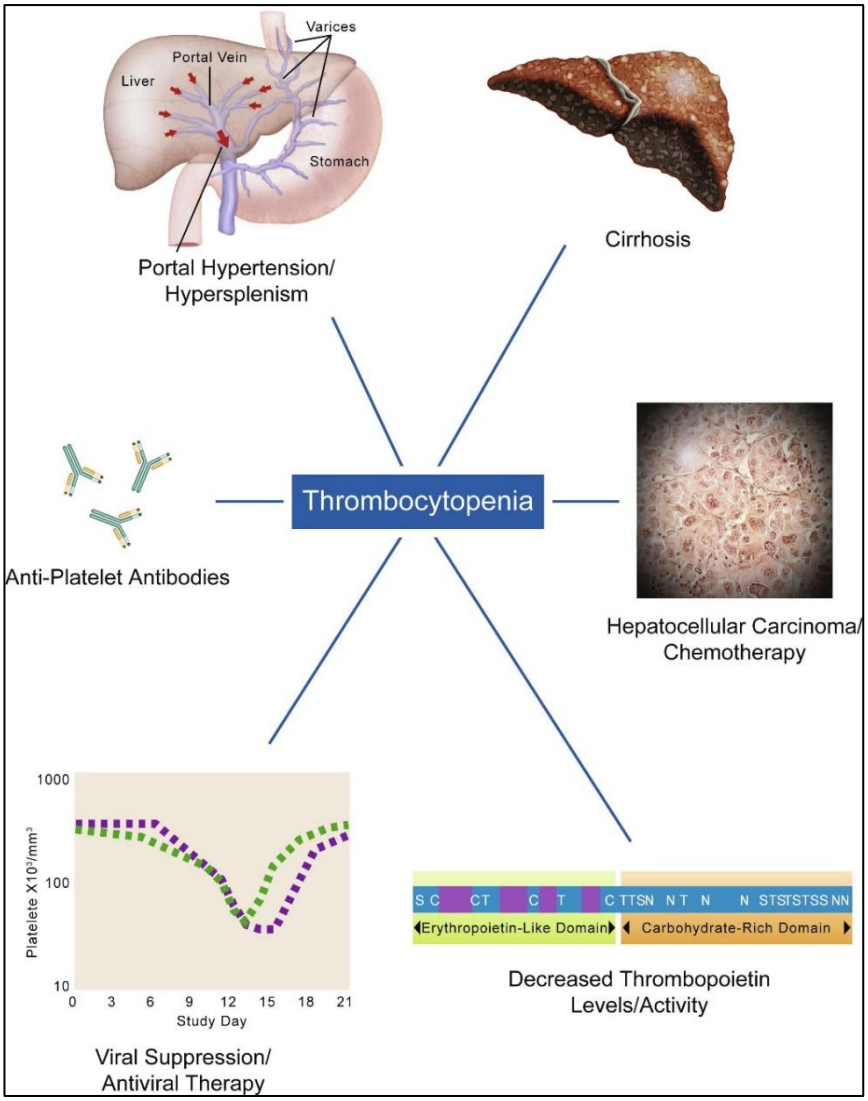

Figure 1.4 Factors responsible for thrombocytopenia in chronic liver diseases (CLD). CLD results in hypersplenism due to portal hypertension, liver fibrosis/cirrhosis, and direct effects of hepatocellular cancer or chemotherapy, production of antiplatelet antibodies, bone marrow suppression by viruses (e.g. HCV) or adverse effects of antiviral drugs and decreased or defective production and activity of thrombopoietin (TPO). Adapted from (28).

1.2 Leishmaniasis

Leishmaniasis belongs to a group of zoonotic diseases, caused by a unicellular protozoan of genus *Leishmania* (Kinetoplastida: Trypanosomatidae) (69). Leishmaniasis is a vector-borne disease, caused by the bite of blood sucking female sand flies, *Phlebotomus* in old world and *Lutzomyia* in the New World (70). Around 20 distinct species of *leishmania* have been known to infect humans and other mammals (71).

Clinically, leishmaniasis presents either as a cutaneous (CL), mucocutaneous (MCL) or visceral (VL) form of the disease. Visceral form of the disease is clinically more severe, hard to treat with a high risk of relapse or transformation into post-kala azar dermal leishmaniasis (PKDL) (72). CL and MCL present as ulcerative lesions on the skin and mucous membranes, respectively however, VL is a systemic disease with hepatosplenomegaly, cytopenias, fever, hypergammaglobinemia and immune dysregulations (70). VL is fatal if not treated properly, high risk of co-infections due to immune deficiency and post-treatment complication as PKDL which is difficult to treat.

1.2.1 Prevalence and epidemiology of leishmaniasis

Leishmaniasis is a disease of tropical and subtropical countries, prevalent in 89 countries of the world although the major burden of the disease comes from seven endemic countries including Brazil, Ethiopia, India, Kenya, Somalia, South Sudan and Sudan (72). VL is the second most deadly parasitic disease after malaria, with high morbidity and mortality (73). According to WHO report 2019, 700,000 to 1 million new cases of leishmaniasis are reported annually with a death rate of 26,000 to 65,000 a year worldwide (72). It is suspected that only 25-45% cases of VL are reported to WHO.

1.2.2 Visceral leishmaniasis (VL)

VL, also known as kala-azar (black fever) is a systemic disease, caused by different strains of the parasite in different regions of the world but mainly associated with *L.*

donovani in India and East Africa, *L. infantum* in Mediterranean region, and *L. chagasi*, *L. amazonensis* and *L. tropica* in South America (70).

Leishmania has a complicated life-cycle involving two morphologically distinct forms, promastigote (in the gut of its vector sandfly) and amastigote (tissue macrophages in host mammals), summarised in **Figure 1.5**. Briefly, the parasite exists as flagellated form called promastigote in the gut of sandfly, promastigote form is further classified into procyclic and metacyclic forms (74). Parasites are infective to the host in metacyclic form which are transmitted by the sandfly upon biting and are phagocytosed immediately by the mononuclear phagocyte system (74). Leishmania transforms itself into a-flagellated form, amastigote which multiplies and survives in the tissue macrophages mainly liver, spleen and the BM, and also in the draining lymph nodes (74).

Clinical manifestations of VL include fever, hepatomegaly, splenomegaly, cytopenias, hypocellular BM with haematological complications and immune dysregulations (70). VL is generally a diagnosis of exclusion and mostly confirmed on tissue biopsy (with the presence of parasites) (75). Although biopsy is the gold standard diagnostic test, it is invasive, expensive and needs expert advice. Non-invasive serological tests are also being used for the rapid diagnosis especially in remote areas i.e. rk39 and DAT are non-invasive, rapid and show comparable results (76).

VL is associated with high fatality rates due to limited access to treatment, unavailability of effective treatment and high treatment costs. Commonly used drugs include liposomal amphotericin B (AmBisome®), miltefosine and antimony compounds, with varying efficacy (77,78). No vaccines are currently available to combat and prevent the infection however, multiple clinical vaccine trials are currently ongoing (79).

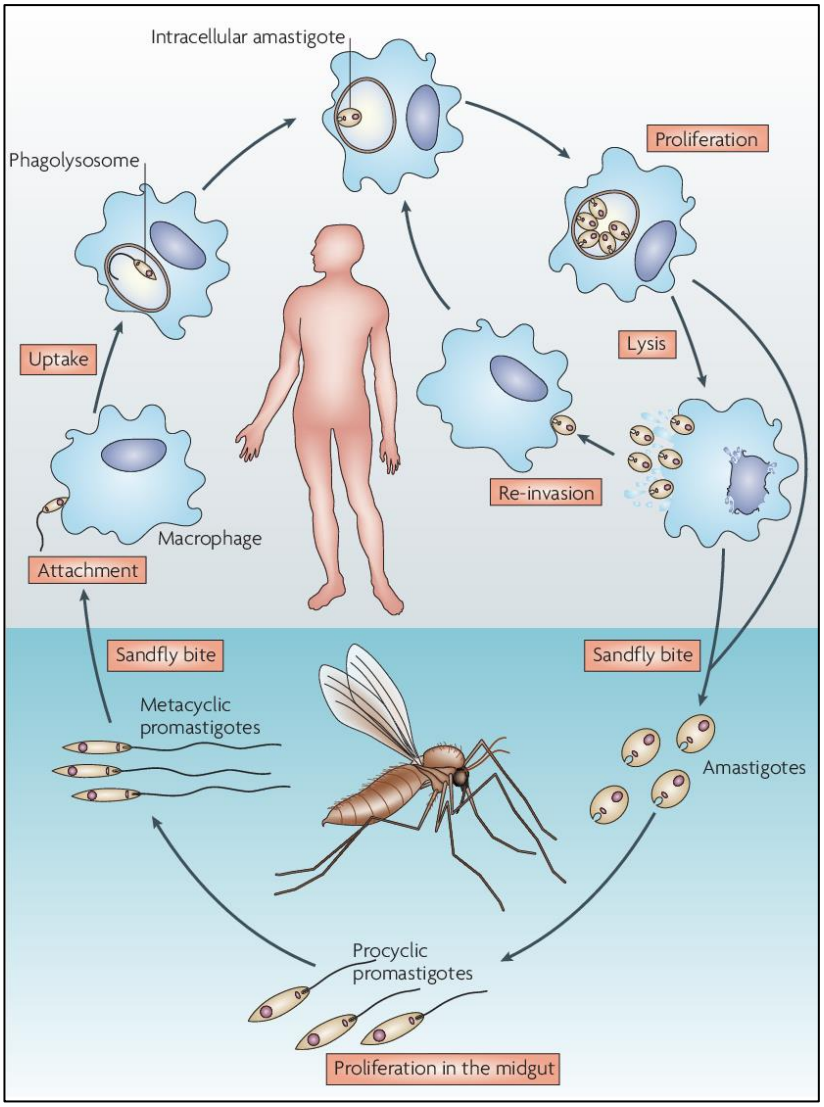

Figure 1.5 Life-cycle of *Leishmania donovani*. The metacyclic promastigote form of the parasite is transmitted via sand fly bite into the skin of a mammalian host. These parasites are phagocytosed by macrophages and dendritic cells in the skin forming a phagolysosome around the parasite. Parasites lose their flagella and transform into the amastigote form. Amastigotes proliferate inside host cells, macrophage re-invasion and then dissemination to liver, spleen and bone marrow. Adapted from (74).

1.2.3 Immune response in VL

Both parasite and host mechanisms are critical for the pathogenesis of VL. Parasites enter the tissue macrophages and establish an acute self-limiting infection in the liver and chronic infection in the spleen and BM by successfully avoiding host immune responses (80). The liver stage is generally asymptomatic and difficult to study in humans however, animal models have been used to understand the acute phase of disease. Experimental studies have suggested, a dominant Th1 immune response in the liver results in the clearance of parasites by forming granulomas around the infected Kupffer cells (71). Immediately after infection, the infected Kupffer cells release chemokines to attract phagocytes and T cells to produce cytokines such as IL-12, IFNγ, TNF (81). The production of IL-12 by antigen-presenting cells (APCs) and IFNγ by T cells are essential for leishmanicidal activity while TNF plays a key role in macrophage activation and killing of the parasites (81–83). Th1 mediated immune response is shown to produce reactive oxygen and nitrogen species (ROS, RNS) by phagocytic cells in various microbial infections (81,84,85). Microbicidal role of nitric oxide (NO) is well-studied in infections including leishmaniasis. NO is a labile factor therefore, the expression of inducible or type-2 NO synthase (iNOS or NOS2) is measured as a cell's capacity to produce NO in response to stimulation (84). Studies have shown that the synergistic effect of IFNγ with TNF results in the activation of iNOS in host macrophages to produce NO in both cutaneous and visceral forms of leishmaniasis (85–87). Increased expression of iNOS in macrophages with low number of parasites have been seen in the histological studies of VL infected dogs suggestive of the effectiveness of NO in controlling infection (88). $CD8^+$ T cells also play an important role in granulomatous response to parasites in the liver and impaired $CD8^+$ T cells response have been associated with delayed granuloma formation (89).

Chronic infection is established in the spleen and BM of infected mice due to ineffective Th1 cytokines response and T-cell exhaustion as seen in other chronic infections (90,91). Although the exact mechanisms remain poorly understood, various mechanisms are proposed based on the findings from experimental VL models. Marginal zone macrophages are the first contact with blood-borne parasites and are mainly dependent on Interferon Regulatory Factor-7 (IRF-7) for their leishmanicidal activity, independent of NO production (92). After disruption of marginal zone, the red pulp macrophages are

infected with the parasites and establish a chronic infection. Furthermore, activation of CD4, CD8 T cells and splenic dendritic cells (DCs) produce a wide range of cytokines such as IL-12, IL-17 and IFNγ in response to the parasite (71). Excessive production of IL-10 by $CD4^+$ T cells in the spleen are critical for establishing a chronic systemic disease in both humans and experimental models (93). The role of IL-10 is well established in VL and other infections like HCV, HIV, malaria, mycobacterium and extracellular parasites like pseudomonas and *S. pneumonia* (94). IL-10 is produced by multiple cell lineages in VL and IFN-γ is probably the major regulator, is also required for the production of antibodies by B cells which acts as a positive feedback to stimulate the production of IL-10 in an excessive manner (82). $IL\text{-}10^{-/-}$ or neutralizing anti-IL-10 antibody treated mice are highly resistant to *L. donovani* infection, IL-10 neutralization is associated with parasite clearance in *in vitro* assays and probably the major mediator of immunological defects during chronic infection (71). Together, the findings of the above mentioned studies suggest that immune responses in the spleen are not sufficient to resolve the infection leading to a chronic infection in human and experimental models.

Stromal macrophages in the BM are another site of chronic infection in both humans and mice models. However, the mechanisms of the parasite persistence in BM, its effects on the BM cells, BM microenvironment and cytokines production are poorly understood.

1.2.4 Haematological complications in VL

Haematological complications are a predominant finding in infections including VL (5,95). Anaemia and thrombocytopenia are commonly seen in naturally infected humans and dogs, and also in experimental models (96). Several mechanisms have been postulated by clinical and experimental studies however, the exact underlying mechanisms are still poorly understood.

VL results in haematological complications along with systemic effects and immune dysregulation. Haematopathology in VL includes anaemia, thrombocytopenia and abnormal leukocyte counts leading to immune dysfunctions (96,97). There is an excessive production of cytokines during active infection including IFNγ, IL-10, IL-6 and TNF, which could be responsible for defective production of blood cells either directly or due to exhaustion of HSCs (98,99). A direct correlation between parasite burden and

emergency haematopoiesis has also been found in experimental murine models of VL (100).

Anaemia in infections is a consequence of defective erythropoiesis or peripheral destruction of erythrocytes (95). In experimental VL models, defective medullary erythropoiesis and haemophagocytosis due to the presence of IgG antibodies against erythrocytes have been observed to play a vital role in VL induced anaemia (101–103). Electron microscopy analysis on the BM of infected patients has also shown hypocellular marrow with dyserythropoiesis (104).

Like anaemia, thrombocytopenia is another predominant finding in both natural infection and experimental models of the disease. The severity of thrombocytopenia varies from mild asymptomatic thrombocytopenia to life-threatening haemorrhagic consequences however, the underlying mechanisms remain poorly understood (see **section 1.2.5**).

1.2.5 Thrombocytopenia in VL

Thrombocytopenia is a common clinical finding in multiple infections including hepatitis, dengue, malaria and parasitic infections (as discussed in **section 1.1.4**). Little is known about the mechanisms responsible for thrombocytopenia in infections including VL (discussed in detail in **Chapter 3** and **Chapter 4**). Similar to anaemia, several underlying mechanisms have been proposed for thrombocytopenia including reduced/defective production or enhanced peripheral clearance. **Figure 1.6** summarizes the proposed mechanisms of thrombocytopenia in VL based on experimental studies so far. As seen in experimental VL, HSCs lose their self-reconstitution potential during chronic infection which might be responsible for hypocellular BM as a consequence of HSCs exhaustion and reduced potential to produce normal number of precursors and progenitors (99). Hence, reduced number of MKs would produce lesser platelets however, no reduction in the number of BM MKs is seen in EVL (O. Preham thesis; http://etheses.whiterose.ac.uk/13654/).

Parasites survive inside the tissue macrophages but the inflammatory responses to parasite result in the architectural changes to the parenchyma of these tissues (105). So far, very little is known about the effects of parasite presence on the neighbouring cells and their functions. There is a generous production of numerous cytokines in response to

parasites which might have stimulatory or inhibitory effects on the functions of surrounding cells including HSCs and progenitors/precursors in the BM (106). Although infection in the liver is self-resolving but a strong granulomatous response to the parasites result in damage to liver microarchitecture (105). As already discussed, normal liver architecture is critical for normal production of TPO (**section 1.1.4**). Damage to liver architecture in VL along with continuous production of cytokines might alter the JAK-STAT signalling pathways leading to decreased or increased TPO production however, the role of TPO in VL is not well-studied.

On the other hand, peripheral mechanisms responsible for excessive platelet clearance have also been studied in infections (40). Splenic macrophages are shown to play an important role in the clearance of platelets by Fc-mediated or complement-mediated phagocytosis (56). Increase in the number of plasma cells in the splenic red pulp (RP) with hyperglobulinemia, correlates with the severity of disease becoming normal after successful treatment is suggestive of increased antibody production against body cells including platelets (71). Increased production of IgG and IgM antibodies against platelets have been reported in dogs infected with *L. infantum*, might be responsible for enhanced platelet clearance and other coagulation defects seen in infected dogs (107,108).

Similarly, excessive production of cytokines like TNF, IFNγ and IL-10 in VL could be responsible for the suppression of platelet production. Although the effects of increased cytokine levels have been studied on haematopoiesis but not specifically on platelet production (99).

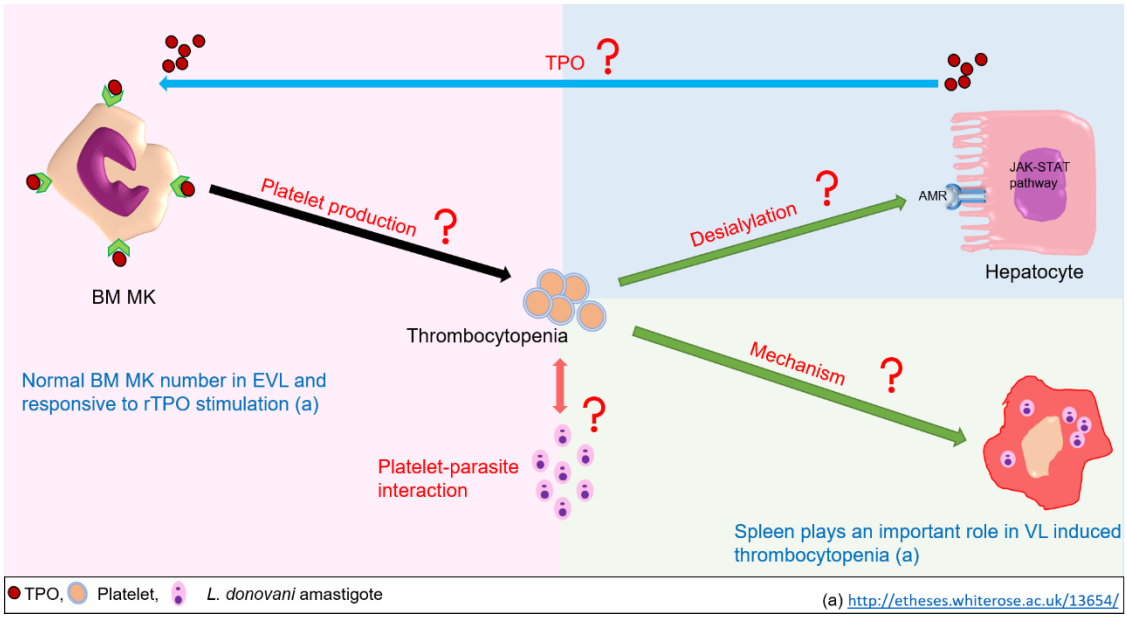

Figure 1.6 Summary of thrombocytopenia mechanisms in VL known so far. Multiple mechanisms have been proposed based on the findings of infection-induced thrombocytopenia in other infections however, not confirmed in VL induced thrombocytopenia. Experimental murine models of VL have suggested no obvious production defect but enhanced splenic clearance as a cause of thrombocytopenia (http://etheses.whiterose.ac.uk/13654/). There is no clinical or experimental data available on BM MKs ultrastructure, TPO production, mechanisms of splenic clearance, platelet desialylation and platelet-parasite interactions (discussed individually in result chapters).

1.2.6 Treatment of VL

Multiple drugs are used as monotherapy or in combination with other drugs for treating VL in human patients. Commonly used drugs have been associated with severe adverse effects, low efficacy, high risk of relapse, resistance to previously administered drugs, high treatment cost and need for hospitalization or expert health care (77,78,109).

One of the commonly used drugs is amphotericin B which is a repurposed antifungal antibiotic with promising results in Indian VL but less effective in African VL patients (110,111). Amphotericin B is known for its binding capacity to ergosterol in fungal and cholesterol in human cell membrane resulting in pore formation in the cell membranes leading to leakage and cell death (112). Liposomal formulation of amphotericin B (e.g. AmBisome®) is a potent source of targeted drug delivery with lesser adverse effects, widely used to treat human VL patients as well as in experimental models. Symptomatic relief and early parasitological cure are one of the prominent features of AmBisome® treatment however, patients with poor splenic responses have been associated with a high risk of relapse (113). Post-AmBisome® treatment transcriptome analysis in *L. donovani*-infected BALB/c mice have suggested a better resolution in the liver but not spleen despite complete parasitological cure (114).

Apart from organ response, patients with poor immunological response are also more prone to relapse, high risk of co- and secondary infections and drug resistance. The reversal of haematological parameters within the normal range has been seen in clinics after successful treatment as reviewed by Verma and Naseem (96). However, there is very limited data available on the rate of recovery of haematological parameters after treatment in humans and experimental models (**Chapter 5**).

1.2.7 Leishmaniasis/co-infections

Leishmaniasis shares the endemicity with other common infections due to environmental factors, poverty and poor health facilities (115,116). Polyparasitism is very common in most of the Asian and African countries where 80% of their population is a carrier of the infectious agents (117). Immunosuppression is well described in leishmaniasis especially later stages of VL (118). Immunosuppression carries a substantial risk of acquiring

multiple co-infections and secondary infections, worsening primary disease and treatment failure. Pathogens like helminths, plasmodia and HIV are seen as co-infections in CL and VL (117). Malnutrition is a common problem in these countries and studies have shown that malnutrition speeds up the progression of VL, high risk of co-infections, poor response to treatment and also exacerbates the primary infection (118). HIV/VL co-infection is commonly seen these days and is endemic in Mediterranean countries with varying severity. According to WHO, Leishmania-HIV co-infection (including both VL and CL) is endemic in about 35 countries (73). About ~30% cases of HIV/VL co-infection have been reported from Africa and Ethiopia, with an incidence of approximately 12.8% males and 4.2% females in asymptomatic VL cases (119,120). HIV/VL co-infection cases are also reported from the Indian region (121,122). Co-infections and secondary infections in VL are discussed in detail in **Chapter 6**.

1.3 Tissue macrophages

Tissue macrophages are an important member of the mononuclear phagocyte system (MPS) along with circulating monocytes, neutrophils and DCs (123). They are present in almost every organ of the body performing various specialized functions along with phagocytosis (124). Tissue macrophages are necessary for the maintenance of tissue homeostasis, inflammation regulation and cytokine production which are required for both innate and adaptive immune responses (125).

1.3.1 Splenic macrophages

Spleen is the largest secondary lymphoid organ in the body. Spleen is micro-anatomically divided into two discrete compartments i.e. Red pulp (RP) and White pulp (WP) separated by a distinct marginal zone **(Figure 1.7)**.

White pulp (WP) consisting of B cell follicles and T lymphocytes, arranged around branching arteries and perform their immune functions (126). Splenic macrophages are strategically arranged around the WP region as marginal zone macrophages and RP macrophages which allows them to perform their functions in an efficient way. Splenic

macrophages are critical for phagocytosis of blood-borne pathogens, dead or effete blood cells and iron recycling for erythropoiesis (126). WP is surrounded by two layers of marginal zone macrophages i.e. marginal metallophilic macrophages (MMM) and marginal zone macrophages (MZM). MZM macrophages express type-C Lectin, SIGNR1 and MARCO, their functions especially in phagocytosing microbial organisms including *Mycobacterium*, *E.coli*, *S. pneumonia* and HIV are well described (127). Splenic MMM macrophages express CD169, also known as Siglec-1 which recognizes sialic acid residues on the immune cells and pathogens (126). $CD169^{+}$ MMM macrophages are shown to phagocytose sialylated bacteria (128–131). MMM macrophages play a significant role in adaptive immunity by modulating T cell responses and clearance of various viruses. Both MMM and MZM macrophages are important for the early control of infections such as *L. monocytogenes* infection and *N. meningitides* (127). Apart from macrophages and lymphocytes, spleen contains a variety of immune cells such as splenic DCs.

Normal splenic architecture is essential for the optimal functioning of spleen. Diseases which damage the normal architecture are associated with compromised spleen function and also haematological complications (132). Splenectomy though uncommon these days could lead to immune complications e.g. risk of encapsulated bacterial infections and also changes in blood cells (133).

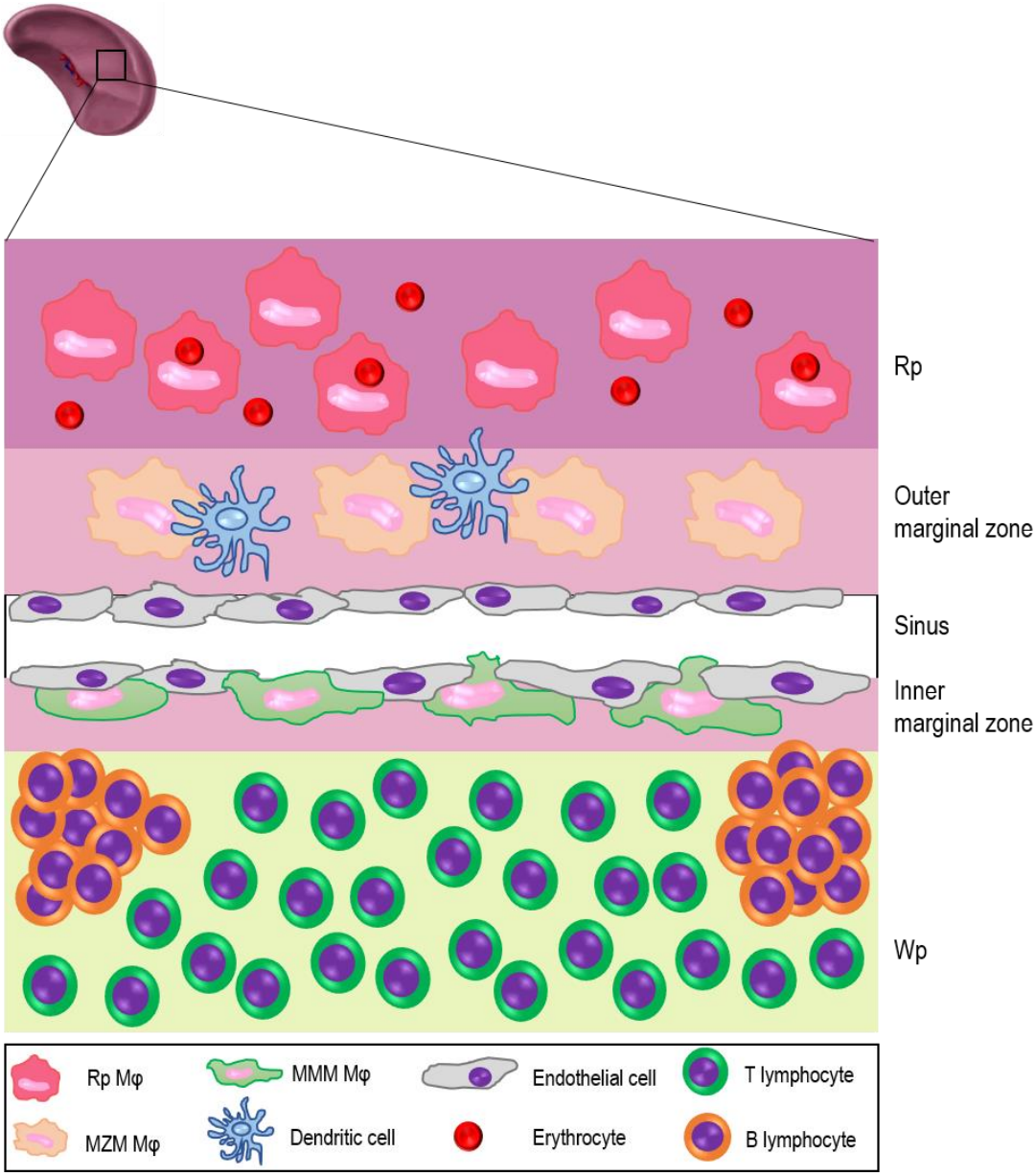

Figure 1.7 Microarchitecture of the murine spleen highlighting the localization of different splenic macrophage populations. Murine spleen has well-defined red pulp (RP or Rp) and white pulp (WP or Wp) regions, separated by a marginal zone (MZ). MZ is divided into two distinct zones i.e., Outer zone which contains marginal zone macrophages (MZM) and marginal zone metallophilic macrophages (MMM) arranged around the blood sinuses. WP shows the B cell follicles surrounded by CD4 and CD8 T cells. Image modified from the original publications (130,138). Size and shapes are not true representative of the original.

1.3.2 Liver architecture and Kupffer cells

Liver is the largest organ with the largest reticuloendothelial system in the body and plays an important role in defense against microbial organisms (136). Liver has a complex microarchitecture comprising of the vasculature, parenchyma (mainly hepatocytes), sinusoids, biliary network and stromal tissue (136). Hepatocytes alone make up around 78% of liver parenchyma while the rest of it is non-parenchymal cells e.g. endothelial cells, Kupffer cells, stellate cells and also extracellular space (136).

Figure 1.8 shows a simplified diagram of the liver with the major cell types and their organisation. Hepatocytes are polygonal cells with round to oval shaped nucleus and arranged in the form of cords, partly facing towards sinusoids forming a canalicular system with neighbouring hepatocytes (137). Hepatocytes have multiple functions such as innate immune response to microorganism e.g. bacteria, produce proteins involved in iron metabolisms, production of coagulation factors and also the production of TPO for the maintenance of HSCs and platelet production (138). Sinusoids are the channels for blood flow and are lined by endothelial cells and Kupffer cells. Kupffer cells are the resident liver macrophages, found inside the lumen of sinusoids and are critical for phagocytosis of microbes entering the liver through blood circulation. Bilzer and colleagues have summarized the functions of Kupffer cells as highly phagocytic cells, destruction of effete erythrocytes similar to splenic macrophages, adaptive immune responses and liver regeneration (139). Kupffer cells express toll-like receptors (TLRs) on their surfaces which have the capacity to sense any injury to the liver (136). Hepatic stellate cells (Ito cells) are present in the space of Disse, in between the layer of hepatocytes and endothelial cells and are important for the production of extracellular matrix proteins such as collagen I, II and IV, and play a principal role in liver fibrosis (140).

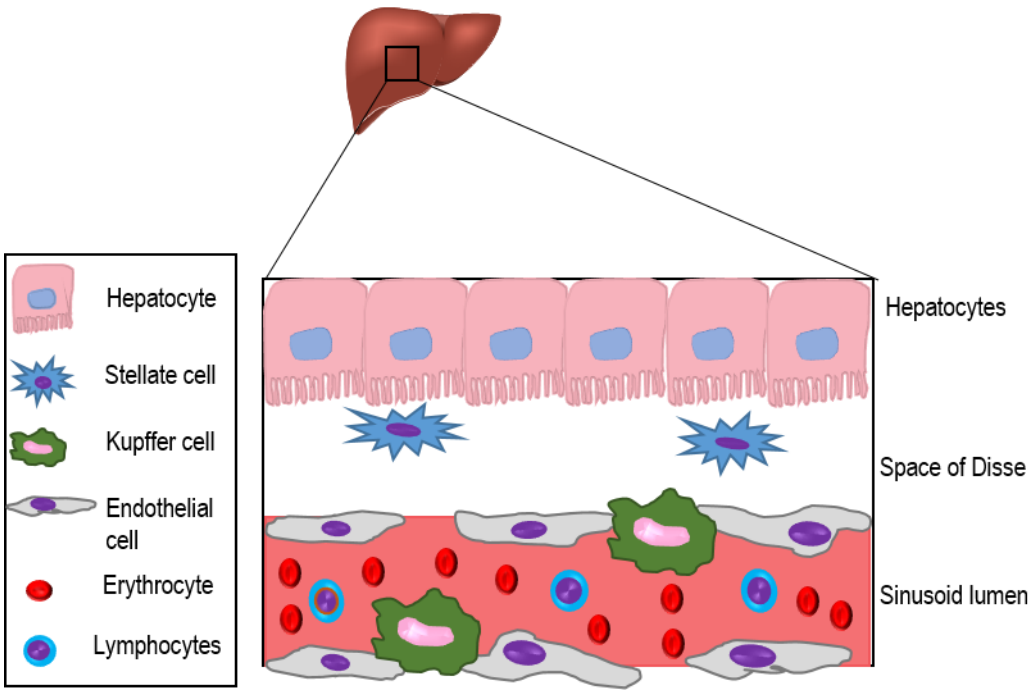

Figure 1.8 Microarchitecture of the liver. Schematic showing the organisation and composition of different cell types in a healthy liver. Polygonal hepatocytes lie adjacent to each other facing towards the sinusoid. Kupffer cells are located on the inner side of the sinusoid in order to capture the microbial agents entering the liver through blood flow. Space of Disse mainly comprises of stellate cells and secrete extracellular matrix proteins. Image modified from the original publications (136,141). Size and shapes are not true representative of the original.

1.3.3 Tissue macrophages as reservoirs of *L. donovani* amastigotes

In experimental murine models, an acute self-limiting infection starts in the liver immediately after the parasites are phagocytosed by the Kupffer cells. Efficient response to control hepatic phase of infection is dependent on the formation of granulomas (71). Kupffer cells play a central role by secreting cytokines to attract other immune cells i.e. neutrophils, monocytes and T cells which form the granulomas around the parasite loaded macrophages and restrict their growth (142,143). Dendritic cells (DCs) stimulate $CD4^+$ T cells to produce cytokines like IFNγ, TNF and IL-12 which are critical for killing the parasites along with $CD8^+$ T cells which are critical for the initiation of granulomatous response in liver (81,89). Additionally, the production of reactive oxygen intermediates (ROI) and reactive nitrogen intermediates (RNI) help in the resolution of infection in the liver by promoting granuloma formation and parasite clearance (144). Granulomatous response to parasites results in major architectural changes in the liver parenchyma, summarized in **Figure 1.9**. Architectural disruption could be responsible for haematological complications due to abnormal TPO production or excessive clearance by activated Kupffer cells. However, this has not been studied in detail.

Chronic infection involves the persistence of parasites in the spleen and BM macrophages. Parasites invade marginal zone splenic macrophages initially followed by RP macrophages resulting in the complete destruction of marginal zone and hyperplasia of RP macrophages (145,146). Loss of marginal zone also affects the WP organisation, and the splenic architecture is mainly replaced by RP macrophages. Presence of excessive amounts of TNF leads to a delayed response to granuloma formation and also destruction of splenic microarchitecture (145). Disrupted splenic microarchitecture in VL includes shrinkage of WP, expansion of RP and loss of marginal zone, summarized in **Figure 1.10**.

Stromal macrophages in the BM are another reservoir of the parasites and result in chronic infection. Chronically infected mice BM shows hypocellularity with peripheral pancytopenia, emergency haematopoiesis and increased myelopoiesis however, at the expense of long-term (LT) HSCs exhaustion as a consequence of chronic infection (99,100,147,148).

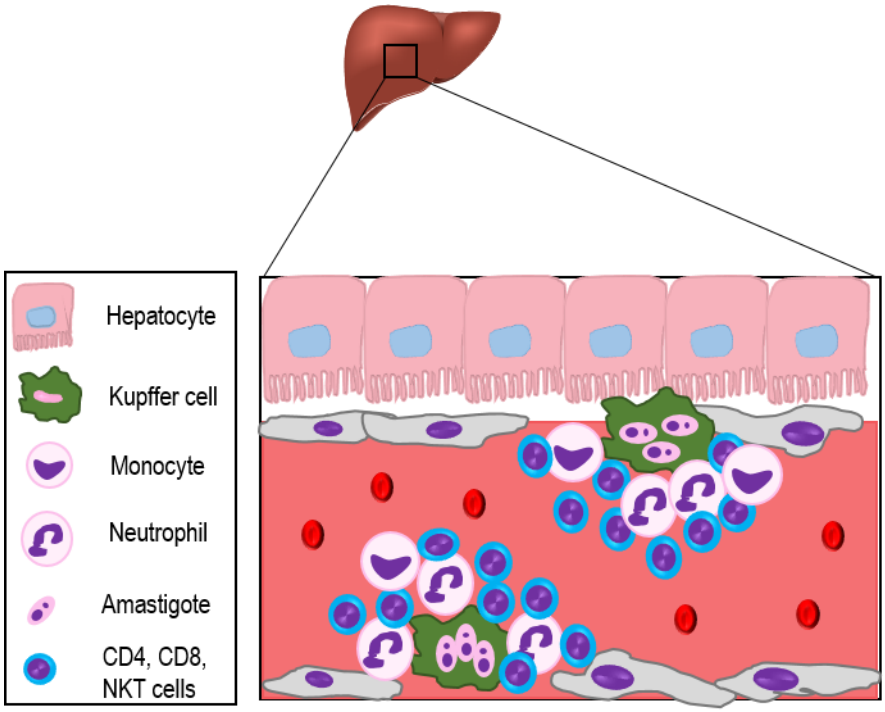

Figure 1.9 Microarchitectural alterations in the infected liver. Schematic showing the alterations which occur in response to parasite phagocytosis by Kupffer cells. Infected Kupffer cells attract inflammatory cells to form granulomas around the parasite harbouring macrophages. Size and shapes are not true representative of the original.

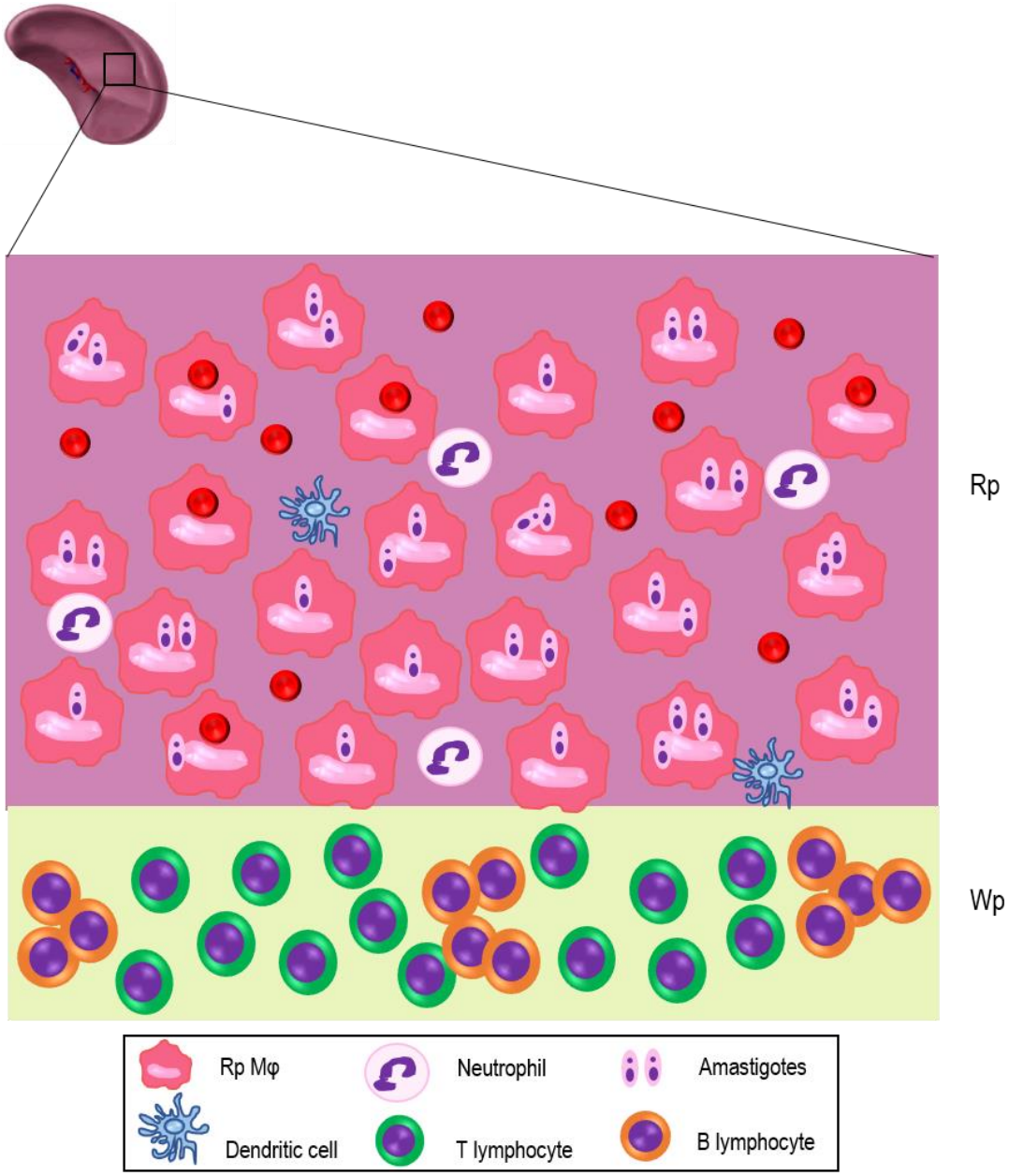

Figure 1.10 Microarchitectural alterations in the infected spleen. Schematic showing the microarchitectural alterations in response to parasite phagocytosis by splenic macrophages mainly Red pulp (RP or Rp) macrophages. Infection results in loss of marginal zone and shrinkage of white pulp (WP or Wp) and recruitment of myeloid/inflammatory cells. Size and shapes are not true representative of the original.

1.3.4 Splenic macrophages are responsible for excessive platelet clearance resulting in thrombocytopenia

Hypersplenism is defined as an enlargement of the spleen with cytopenias (149). Hypersplenism has been described as an important clinical finding in multiple diseases i.e. portal hypertension in liver disorders, cirrhosis, malaria, infectious mononucleosis, malignancies like polycythemia Vera and other myeloproliferative disorders (149). Cytopenias due splenic sequestration of blood cells have been known for a long time (49,150,151). Role of splenic sequestration has been proposed in infection-induced thrombocytopenia (152,153).

In both naturally infected humans and experimental mice models of VL, splenomegaly is a prominent feature of the infection along with thrombocytopenia. It is previously shown that thrombocytopenia is less severe in splenectomised infected mice with a better response to the exogenous cytokine stimulation (O. Preham thesis; http://etheses.whiterose.ac.uk/13654/). Although these findings are suggestive of spleen dependent platelet clearance however, it is not a direct evidence of the role of splenic macrophages in thrombocytopenia. Also, anti-platelet antibodies have been detected in canine VL but their role in platelet destruction in human and experimental VL is not well-studied (107).

1.4 Experimental models of secondary infection

1.4.1 Malaria as a model of secondary infection

Malaria is a parasitic disease with high morbidity and mortality and shares the geographical overlap and clinical presentation with a wide range of infections (154–161). Experimental models of malaria are well-characterised to study the role of immune system, disease severity, response to treatment and haematological complications. Due to the above mentioned features, rodent malaria models are widely studied as co-infection and secondary or primary infection model to understand the disease kinetics, immune response and treatment outcomes.

Rodent malaria is caused by various strains of rodent plasmodia similar to human malaria. *Plasmodium (P) berghei* presents with acute life-threatening disease with severe anaemia and cerebral malaria, similar to *P. falciparum* in humans while *P. chabaudi* and *P. yoelii* are studied as models of non-fatal chronic infection. All of these rodent strains have been studied as a model of co- and secondary infection. *P. berghei* as a co-infection in *Trypanosoma (T) brucei* infected mice have shown delayed disease kinetics and decreased severity of malaria along with protection against cerebral malaria (162). Moreover, no difference in parasitaemia was noticed between malaria only infected and co-infected $Rag^{-/-}$ mice in the same study (162). These findings suggest the possible role of lymphocytes in inhibiting malaria progression mainly due to increased IFNγ production in *T. brucei* infection (162). Similarly, a less severe *P. yoelii* infection was seen in mice infected with *Schistosoma (S) mansoni* (163). Similar findings were noticed in *P. chabaudi* and *S. mansoni* co-infection probably due to excessive IFNγ production (164). Protective role of *T. cruzi* has also been observed in *P. berghei* co-infection with reduced neurological and respiratory complications (165).

On the contrary, a severe *P. berghei* infection with high parasitaemia, severe anaemia, early death and overall decreased survival was noticed in mice co-infected with *S. mansoni* or *T. brucei* (155,166).

1.4.2 Malaria as a model of secondary infection in treated EVL

Malaria and VL are endemic in tropical and subtropical countries, and are classified as first and second most fatal parasitic diseases, respectively (154,167,168). Polyparasitism is commonly seen in bacterial, viral, parasitic and helminthic infections which impact each other either synergistically or antagonistically depending on various factors (169). Various causes of co-infections have been suggested including poor health and immune status which results in a prolonged infection with detrimental effects compared to single infection (170).

Both malaria and VL present with similar clinical features including fever, hepatosplenomegaly, anaemia and thrombocytopenia, therefore, making the correct diagnosis and treatment difficult (171,172). A high prevalence of VL/malaria co-infection is suggested by clinical studies (158,173). Studies involving malaria as a model of co-

infection in CL infected mice have suggested a protective role of malaria (156). Despite the geographical and clinical overlap, VL and malaria are not well-studied as co-infection or post-treatment infection using experiment models. Our study is the first of its kind to our knowledge using rodent malaria as a model of sequential secondary infection in treated *L. donovani*-infected mice (**Chapter 6**).

1.5 Overall Aims

1) To determine the role of BM MKs and hepatic TPO in the production of platelets in *L. donovani*-infected thrombocytopenic mice (**Chapter 3**).

2) To determine the role of platelet clearance in *L. donovani* induced thrombocytopenia (**Chapter 4**).

3) To investigate the recovery of haematological parameters and tissue microarchitecture after the clearance of parasites (**Chapter 5**).

4) To study the impact of a secondary sequential infection on haematological features and tissue microarchitecture in VL cured mice (**Chapter 6**).

Chapter 2. Materials and Methods

2.1 Animals and parasites:

2.1.1 Ethical approval

Ethical approval was obtained prior to any regulated procedure from the Animal Procedures and Ethics Committee of the Department of Biology, University of York, York. All procedures were performed under the Home Office Project License (Ref # PK49487014) and ARRIVE guidelines.

2.1.2 Mice

Female C57BL/6 and BALB/c wild type mice of six-eight weeks age were used for experiments due to ease of handling. These mice were bred and maintained at Biological services Facility (BSF), University of York under specific-pathogen free (SPF) conditions according to the Home Office guidelines. All experimental mice were kept in the containment level-3 (CL3) after infection with *L. donovani* parasites and the infected tissues were processed in the CL3 laboratories as per the Home Office recommendations. Mice were kept under strict 12 hour light-dark cycle especially malaria infected mice as the circadian rhythm of the parasite is critical for the progression of infection. All mice were sacrificed at the end of every experiment using schedule-1 killing (S1k) methods.

2.1.3 Parasites and infection

All visceral leishmaniasis experiments were performed using an Ethiopian strain of *L. donovani* (*LV9*) and rodent malaria experiments with a non-fatal strain of *Plasmodium chabaudi chabaudi AS* (*P.c.c AS*). *P. chabaudi* parasites used for malaria experiments (see **Chapter 6**) were kindly provided by Dr Jean Langhorne (The Francis Crick Institute London, UK). Bioluminescent *LV9*-RE9H parasites used for *in vivo* imaging experiment (see **Chapter 3**) were kindly provided by Prof. Jeremy Mottram (York Biomedical and Research Institute; YBRI, University of York, York, UK).

2.1.3.1 L. donovani passage and infection

L. donovani (LV9) amastigotes were maintained in serial passage in B6. *Rag*$^{-/-}$ mice for a minimum of three months (to fourteen months at maximum) prior to infection. Spleens of B6. *Rag*$^{-/-}$ passage mice were harvested in Roswell Park Memorial Institute (RPMI) 1640 medium (Gibco, ThermoFisher, Paisley, UK) after euthanasia with CO_2 in rising concentration followed by cervical dislocation. *LV9* amastigotes were isolated from freshly harvested spleens using a standardized protocol. Briefly, spleens of passage mice were crushed in a glass homogenizer (Fisher Scientific, UK) with RPMI medium and transferred into a 50 ml Falcon tube (Sarstedt AG & Co, Germany). Cell suspension was centrifuged in a Heraeus Multifuge 3S-R (DJB labcare, UK) at 137G for 5 minutes at room temperature (RT). The resultant supernatant was transferred into a new 50 ml Falcon tube containing 25 milligrams (mg) of Saponin (BDH, Leicestershire, UK) per 20 ml of the supernatant. The suspension was allowed to stand at RT for 5 minutes to ensure maximal erythrocyte lysis. The suspension was washed thrice in RPMI 1640 medium by centrifuging at 2063G for 10 minutes. Finally, the washed pellet was re-suspended in 20ml of RPMI 1640 medium and passed several times through a 26-gauge needle (BD Biosciences, San Jose, CA, USA) attached to a 10 ml syringe (BD Biosciences, San Jose, CA, USA) to break the parasite clumps.

Parasites were counted using a Thoma bacteriological counting chamber (Weber Scientific International, Middlesex, UK) as per manufacturer guidelines. The parasite suspension was then diluted or concentrated with RPMI 1640 medium to obtain a final concentration of 3 x 10^8 amastigotes/ml for a 100µl injection. Later, experimental mice were infected via a lateral tail vein injection of a bolus dose of 3x10^7 amastigotes in 100µl. Bioluminescent parasites were also isolated using the above mentioned protocol.

2.1.3.2 P. chabaudi passage and infection

P. chabaudi infected erythrocytes were obtained in cryovials from Francis Crick Institute (London, UK) and kept in liquid Nitrogen (LN2) tanks until needed. Parasites were recovered by passaging through C57BL/6 mice as per guidelines obtained with the parasites. Briefly, one stabilate was taken out of the LN2 at a time and kept on dry ice.

Stabilate was allowed to thaw slowly in gloved hands and 100µl of ice-cold sterile saline was added to defrosted stabilate and mixed well by gently flicking the tube several times. Mice were injected with 100µl of suspension via a lateral tail vein and monitored strictly for parasitaemia, weight loss and signs of disease severity from day 5 post-infection.

Infected erythrocytes were harvested at peak parasitaemia to infect experimental mice. Whole blood was collected from passage mice after anaesthetising the mice with Isoflurane inhalation in a secure chamber (Apollo TEC3 Isoflurane Vaporise, Sound Veterinary Equipment, Victoria, Australia). Blood was harvested via cardiac puncture with 26-gauge needle (BD Biosciences, USA) attached to a 1 ml syringe (BD Biosciences, San Jose, CA, USA) and transferred immediately into 1.5ml Eppendorf tubes containing 30-36µl Saline + 25IU/ml heparin, mixed well by gently flicking the tubes and placed on ice. Thin blood smears were stained with Hemacolor® staining kit (Merck, Darmstadt, Germany) and parasitaemia as calculated. Blood was re-suspended with sterile saline at a concentration of 1 x 10^5 infected erythrocytes and mice were infected via lateral tail vein injections.

2.1.4 Estimation of parasite burden

2.1.4.1 Leishmania parasite burden

A small fragment of freshly isolated livers and spleens of *L. donovani*-infected mice were cut and excess of blood was removed by gently pressing on tissue roll. Impression smears were made by briefly pressing the tissue on Superfrost slides (Thermo Fisher Scientific, UK). These slides were allowed to air dry and fixed in 100% methanol. Following fixation, slides were stained with Giemsa staining solution for 20-30 minutes at RT, thoroughly washed in running tap water and air-dried. For the estimation of parasite burden, a total of 1000 cell nuclei were counted for each sample along with the number of amastigotes per 1000 nuclei. Leishmania parasite burden is expressed as Leishman-Donovan units (LDUs) and calculated using the following formula,

LDUs = number of amastigotes/1000 cell nuclei x organ weight (in grams)

2.1.4.2 Malaria parasitaemia

Parasite load in malaria infected mice was manually calculated on thin blood smears from day 5 onwards. Mice were bled from a lateral vein and 30-50µl of blood was collected in EDTA coated tubes (Microvette CB300 EDTA, Sarstedt, Germany). Thin blood smears were made by putting a drop of blood on one of a slide and gently spreading towards the other end by another slide at an angle of 45°. Blood smears were air-dried and stained with Hemacolor® staining kit (Merck, Darmstadt, Germany). For the estimation of parasitaemia, a total of 1000 erythrocytes (both parasitised and unparasitised) were counted. A record of parasitised (infected) erythrocytes was kept while counting and parasitaemia was calculated as follow,

Parasitaemia (%) = number of parasitised erythrocytes/total erythrocytes counted x 100

2.2 Blood collection and analysis

Blood was collected in EDTA coated tubes (Microvette CB300 EDTA, Sarstedt, Germany) from a lateral tail vein of infected and uninfected mice at specified time-points for complete blood count (CBC) analysis. CBC analysis was done by running a sample of whole blood on scil Vet abc Plus+ (scil animal care company, Dumfries, Scotland, UK).

Blood smears were made by putting 5µl of whole blood on Superfrost glass slides (Thermo Fisher Scientific, UK). Slides were air-dried followed by staining with Hemacolor® staining kit (Merck, Darmstadt, Germany) as per manufacturer guidelines. Slides were allowed to stand at RT until completely dried and microscopy was done using brightfield microscope (Zeiss) at 20x and 63x oil immersion lens.

2.3 Induced thrombocytopenia model

Immune thrombocytopenia (ITP) was induced in infected and uninfected mice using the standard approach as described in the literature (174). Pilot experiments were conducted to determine the severity of disease and specify the time-points for the assessment of blood counts. Mice were injected intraperitoneally with a single dose of 0.2µg/g of anti-CD41 monoclonal antibody (Clone: MWReg30) in 100µl of sterile PBS. Control mice were injected with 100µl of sterile PBS. Mice were bled before and after antibody administration at indicated time-points for the platelet counts. Details of ITP experiments and results are discussed in **Chapter 3**.

2.4 Exogenous thrombopoietin administration

In order to study the effects of thrombopoietin (TPO) administration in infected mice, both infected and uninfected mice were treated with exogenous human recombinant TPO (hu-rTPO) at a dose of 750ng/mouse intraperitoneally, at the end of week 1, 2 and 3 post-infection. Control infected and uninfected mice were injected with sterile PBS at the same dose and time-points. Mice were bled before infection and weekly after infection for blood counts prior to rTPO/PBS administration. Details of this experiment are discussed in **Chapter 3**.

2.5 *In vivo* bioluminescence imaging

C57BL/6 mice were infected with 3x 10^7 bioluminescent *LV9*-RE9H parasites via lateral tail vein injections similar to infection with wild type *LV9* parasites. Both infected and uninfected mice were imaged using the IVIS Spectrum *in vivo* imaging system (PerkinElmer, UK) before infection and weekly after infection. Imaging was done as described by Duncan *et al.* with few modifications (175).

Briefly, mice were anaesthetized by the inhalation of 3.5% Isoflurane/1.5L O_2 per minute in a closed anaesthesia chamber and inoculated by intraperitoneal injection with 200µl of D-Luciferin (15mg/ml in Mg/Ca-free Dulbecco's modified PBS). Mice were imaged

within 10 minutes of D-Luciferin administration, in a group of 3 mice, and for 5 minutes on ventral and 5 minutes on lateral side, with an open emission filter for 30-60 seconds exposure, large binning and 1f/stop. Images were captured using a charge-coupled device (CCD) camera. After imaging, mice were monitored and kept on a heating pad until fully recovered from the anaesthesia. Images were analysed using Living Image Software (PerkinElmer, UK) by drawing regions of (ROI) of equal size around the whole body to quantify the amount of photon emission as total photon flux and expressed in photon per second. Data were exported to Microsoft Excel sheets for further analysis. The absolute unit of photon emission was expressed as radiance (photons/second/cm2/steradian).

2.6 *Ex vivo* bioluminescence imaging

Livers and spleens of infected and uninfected mice were harvested at the end of experiment and imaged using the same protocol as described above. Livers and spleens were placed in clean petri dishes and soaked in 1-2ml of D-Luciferin (15mg/ml in Mg/Ca-free Dulbecco's modified PBS) for few minutes followed by imaging for 1 minute, one mouse tissues at a time. Images were collected and analysed by drawing ROIs around the whole liver and spleen tissues, using Living Image software as described above. Data were exported to Microsoft Excel sheets for further analysis.

2.7 Tissue macrophage depletion

Clodronate (Cl_2MDP) liposomes (Clodrosome 5mg/ml; Brentwood, Tennessee, USA) were administered intravenously to uninfected and d28 infected mice. Control mice (uninfected and infected) were injected with empty liposomes (PBS only liposomes) at the same time.

Clodronate liposomes were pre-formulated at 5mg/ml on the day of delivery by the company and were kept at 4°C as per manufacturer recommendations. Mice were treated with a dose of 40µg/g (8µl/g) body weight on alternate days and were bled before and after clodronate administration at the indicated time-points. Experimental details and results are shown in **Chapter 4**.

2.8 AmBisome® preparation and administration

AmBisome® (Gilead Sciences International, Ltd, Cambridge, United Kingdom) was used at a dose of 8mg/kg for the experiments described in **Chapter 5** and **6**.

Infected mice were weighed to calculate the dose of AmBisome® per mouse for each experiment on the day of treatment. The required amount of drug was converted into µg/µl for administration and re-suspended in sterile 5% dextrose in distilled water. Each mouse was administered with a single dose of 100µl of AmBisome® intravenously at d28 of *LV9* infection.

2.9 Developing a model of secondary infection

To study the effects of a sequential second infection in VL treated experimental model, we developed a model of secondary infection using murine malaria (*P. chabaudi*). Parasites were stored, passaged and used for infection as described above. *L. donovani*-infected mice were treated with a single dose of AmBisome® followed by infection with *P. chabaudi* parasites. Details of the experiment and experiment outcomes are discussed in detail in **Chapter 6**.

2.10 Detection of anti-platelet antibodies

In order to detect the presence of anti-platelet antibodies in *L. donovani*-infected mice, we collected the whole blood in ACD (Acid Citrate Dextrose solution, Sigma-Aldrich Company Ltd., Dorset, UK) coated 5ml Falcon™ round-bottom polystyrene tubes (Thermo Fisher Scientific, UK) via cardiac puncture after anaesthetizing with Isoflurane as described above. Both needle and syringe were also coated with ACD solution before starting the procedure. Platelets were isolated from the whole blood immediately after collection, using the protocols already described in the literature (176). Briefly, whole blood was centrifuged at 60G for 7 minutes at RT without breaks to obtain platelet rich plasma (PRP). PRP was transferred into a fresh polystyrene tube and platelet wash buffer (150mM NaCl, 20mM HEPES, pH 6.5 at RT) was added. Platelet suspension was then

centrifuged at 240G for 10 minutes at RT without breaks. Excess of wash buffer was discarded and washed platelets were stained with conjugated anti-CD41 antibody (Clone: MWReg30; in platelet wash buffer) for 30 minutes followed by conjugated anti-mouse IgG and IgM antibodies for 30 minutes. Platelets were washed with wash buffer and acquired on BD LSR II Fortessa^{TM} flow cytometer (BD Biosciences, San Jose, CA, USA). Unstained and single colour (antibody fluorophore) controls were used for setting up the voltages and compensations before the acquisition. Extra care was taken at each step to avoid platelet activation or desialylation. Detail of antibodies is given in **Table 2.1**. Data analysed using FlowJo^{TM} v10.6.2 software (FlowJo, LLC, Oregan, United States).

2.11 Estimation of platelet desialylation

Platelets were isolated from the whole blood as described above and flow cytometric analysis was done for the estimation of desialylated platelets in infected and uninfected mice blood. Freshly isolated platelets were stained with conjugated anti-CD41 antibody (Clone: MWReg30; in platelet wash buffer) for 30 minutes at RT followed by biotinylated lectins (details in **Table 2.1**) for 30 minutes at RT. Platelets were stained with three biotinylated lectins in separate tubes. Platelets were washed in wash buffer and incubated with streptavidin labelled secondary antibody (details in **Table 2.1**) for 15 minutes. Platelets were washed to remove excess antibody and acquired on BD LSR II Fortessa^{TM} flow cytometer (BD Biosciences, San Jose, CA, USA). Unstained, single antibody stained and neuraminidase (Invitrogen) treated platelets were used as controls. For neuraminidase treatment, washed platelets were incubated with 0.3U/ml of neuraminidase (Invitrogen) at 37°C for 30 minutes followed by antibody staining. Neuraminidase treated platelets show maximal desialylation and were used as a positive control for the estimation of platelet desialylation in experimental samples.

Whole process was done at RT and all antibodies were brought to RT before adding to platelet solution as cold temperature is likely to accelerate platelet desialylation. Detail of antibodies is given in **Table 2.1**. Data analysed using FlowJo^{TM} v10.6.2 software (FlowJo, LLC, Oregan, United States) and FCS Express 7 (De Novo Software, Pasadena, CA91107, USA).

Table 2.1 List of antibodies used for platelets flow cytometric assays

Target	Fluorophore / conjugation	Primary/ Secondary	Manufacturer	Cat:/ product #	Clone	Host	Isotype	Dilution	Lectin specificity
Anti-platelet antibodies detection panel									
CD41	FITC	Primary	BioLegend	133904	MWReg -30	Rat	IgG1, κ	1:200	N/A
Anti-mouse IgG	AF647	Secondary	Invitrogen	A-32728	Poly-clonal	Goat	IgG	1:500	N/A
Anti-mouse IgM	PE-Cy7	Secondary	BD Biosciences	552867	R6-60.2	Rat	IgG2a, κ	1:500	N/A
Platelet desialylation panel									
CD41	FITC	Primary	BioLegend	133904	MWReg -30	Rat	IgG1, κ	1:200	N/A
RCA-I	Biotinylated	Primary	Vector laboratories	B-1085	-	-	-	0.5µg/ml	Galactose or N-acetylgalacto -samine residues of membrane glycoconjuga -tes
MAL-II	Biotinylated	Primary	Vector laboratories	B-1265	-	-	-	0.5µg/ml	α-2,3-sialoglycans
SNA	Biotinylated	Primary	Vector laboratories	B-1305	-	-	-	0.5µg/ml	α-2,6-sialoglycans
Streptavidin	PE	Secondary	BD Biosciences	554061	-	-	-	1:200	N/A

RCA = Ricinus Communis Agglutinin, MAL = Maackia Amurensis Lectin, SNA = Sambucus Nigra, N/A = Not applicable

2.12 Quantification of serum TPO using enzyme-linked immunosorbent assay

The serum levels of circulating TPO were measured using Mouse Thrombopoietin Quantikine ELISA Kit; MTP100 (R & D systems, Minneapolis, MN, USA) as per manufacturer's guidelines. Mice were euthanised by asphyxiation with Isoflurane inhalation prior to blood collection via cardiac puncture. Whole blood was collected in the 1.5ml Eppendorf tubes and allowed to stand for 2-3 hours at RT. Blood was centrifuged at 300G for 10 minutes for serum separation. Serum was carefully pipetted into another set of labelled Eppendorf tubes. Serum samples were stored at -80°C for long-term storage and samples were only taken out when needed.

Prior to the assay, serum samples were thawed on ice and then brought to RT. All the experimental serum samples, standards and mouse TPO control (provided with the assay kit) were prepared and assayed in duplicates as per manufacturer instructions. Serum samples were diluted up to 5-fold with the Calibrator Diluent (RD5-3) and allowed to stand for 20 minutes at RT prior to assay. Mouse standards were prepared in a serial dilution of 4000, 2000, 1000, 500, 250, 125, 62.5 and 0 (pg/ml) with the Calibrator Diluent (RD5-3) to generate a standard curve.

50µl of Assay Diluent (RD1-23) was added to each well of 96- well plates (provided with the assay kit) followed by 50µl of standard, control and diluted serum in duplicates. Assay plates were gently tapped for 1 minute to ensure proper mixing of samples with assay diluent, covered with the adhesive strip and incubated for 2 hours at RT. Each well was then washed five times with 300-400µl wash buffer (provided with the assay) and 100µl of Mouse TPO Conjugate was added to each well and plate was covered with a new adhesive strip. Samples were incubated for 2 hours at RT followed by five washes as described above. Substrate solution (colour reagents A + B in equal volumes) was prepared and added to each well (100µl/well) within 15 minutes of preparation and incubated for 30 minutes at RT in dark. To stop the enzymatic reaction, 100µl of Stop Solution was added to each well. Plates were gently tapped to ensure thorough mixing and the optical density (O.D) of each well was determined within 30 minutes of adding the stop solution. O.D was measured using iMark™ Microplate Absorbance Reader (Bio-

Rad Laboratories Ltd, Hertfordshire, UK) set at 450 nm with subtraction from 595 nm for wavelength correction.

2.13 Measurement of *Thpo* mRNA accumulation

2.13.1 RNA extraction:

Tissues fragments (~ 5mg) stored in RNAlater™ (Qiagen, Hilden, Germany) at -80°C were taken out and thawed to RT. Stainless steel beads (5mm, Qiagen) and defrosted tissues were added to 2ml round bottom Eppendorf tubes followed by 700µl of QIAzol Lysis Reagent (Qiagen). Tissues were lysed in Tissuelyser LT (Qiagen) at 50 oscillations for 60 seconds. Samples were left at RT for 5 minutes and ball bearings were removed. 140µl of Chloroform (Thermo Fisher Scientific) was added to each tube and shaken vigorously for few seconds. Samples were left for 2-3 minutes at RT followed by centrifuging at 12000G in a microcentrifuge (Microcentrifuge 5424R, Eppendorf) for 15 minutes at 4°C. The top clear aqueous layer (while avoiding white interface and pink organic phase) was transferred to the tube containing 525µl of ethanol and mixed well. Solutions were transferred onto the spin columns (700µl at a time) and centrifuged at ≥ 10,000G for 15 seconds at RT and the flowthrough was discarded. RWT buffer (350µl) as added to spin columns and centrifuged at ≥ 10,000G for 15 seconds at RT and the flowthrough was discarded. After that, 80µl of DNase-I working solution (Qiagen, prepared as per manufacturer's instructions) was added to the centre of spin column membrane and the samples were incubated at 20-30°C for 15 minutes followed by the addition of 350µl of RWT buffer. Spin columns were then centrifuged at 10,000G for 15 seconds at RT and the flowthrough was discarded. 500µl of RPE buffer was added to each spin column followed by centrifugation at 10,000G for 15 seconds at RT. 500µl of 80% ethanol was added to each spin column after discarding the flowthrough and spun at 10,000G for 15 seconds at RT. Flowthrough and collections tubes were discarded at this stage and the spin columns were placed on fresh 2ml collection tubes. Spin columns were dried by spinning the tubes with open lids for 2 minutes at RT. Both flowthrough and collection tubes were discarded, and spin columns were placed on 1.5ml collection tubes. 50µl of RNAse-free water was added to the centre of the spin column membrane and

centrifuged at full speed for 60 seconds at RT to collect the RNA. RNA quality and quantity were assessed by measuring the absorbance at 230, 260 and 280 nm with a NanoDrop™ 2000 spectrophotometer (Thermo Fisher Scientific, Loughborough, UK). The ratio of 260/280 and 260/230 were considered as the indicators of purity and considered acceptable when close to 2.0 and 2.2, respectively.

2.13.2 Reverse transcription reaction

The synthesis of cDNA was performed using High Capacity cDNA Reverse Transcription kit (Applied Biosystems™, Thermo Fisher Scientific) using manufacturer's protocol. The extracted mRNA was diluted to 1µg in 10µl of Nuclease-free water and mixed with 10µl of 2X reverse transcription (RT) master mix. Briefly, the RT master mix was prepared on ice with 2µl 10X RT buffer, 0.8µl 25x deoxynucleotides tri-phosphate (dNTP, 100mM) mix, 2.0µl 10X Random Primers, 1.0µl of MultiScribe™ Reverse Transcriptase, 1µl RNase inhibitor and 3.2µl Nuclease-free water, making up a total of 10µl per sample.

10µl of 2X RT master mix was added to each PCR reaction tube followed by 10µl of mRNA sample and mixed well by pipetting up and down twice. Tubes were sealed carefully and centrifuged at 10,000G for 5 seconds to remove any air bubbles. The cDNA synthesis reaction mixtures were then retrotranscribed in a thermal cycler. The thermal cycling conditions were set as 25°C for 10 minutes (annealing), 37°C for 120 minutes (reverse transcription), 85°C for 5 minutes (enzyme inactivation). The products were cooled down to 4°C until they were removed from the thermal cycler. The newly synthesized cDNA samples were stored at 4°C for short-term storage or -20°C for long-term storage.

2.13.3 Quantitative polymerase-chain reaction

Duplex quantitative polymerase-chain reaction (qPCR) was performed using TaqMan® gene expression assays (Applied Biosystems™, Thermo Fisher Scientific) with a FAM™ and a VIC® dye-labelled probes. The cDNA samples were diluted to 10ng/µl with Nuclease-free water and 4µl was used per reaction. A reaction mix was prepared with 1µl

20X FAM dye-labelled (*Thpo*), 1µl 20X VIC dye-labelled (primer-limited) (*Hrpt*), 10µl 2X Gene Expression master mix and 4µl RNAse-free water per reaction. The diluted cDNA samples were added to 200µl PCR tubes followed by 16µl of the reaction mix per tube. The tubes were centrifuged briefly to remove liquid trapped in the lid. Then qRT-PCRs were performed on QuantStudio® 3 Real-Time PCR system (Applied Biosystems™, Thermo Fisher Scientific) under the following cycling conditions: 95°C for 20 seconds followed by 40 cycles of 95°C for 1 second and 60°C for 20 seconds. Data were analysed using the QuantStudio® Design and Analysis software (Thermo Fisher Scientific, UK). *Thpo* mRNA expression levels were normalized to *Hprt* housekeeping gene using ΔΔCt calculations. Relative expression levels between control and experimental groups were calculated using the $2^{\wedge\Delta\Delta Ct}$ calculations.

2.14 Sample processing for electron microscopy

Femurs were harvested and fixed in 4% PFA + 1% glutaraldehyde in 0.1M Sodium cacodylate buffer (pH 7.4) for 4 hours at RT and then overnight at 4°C. Post-fixation treatment was done with Osmium Ferricyanide (1% Osmium Tetroxide and 1.5% Potassium Ferricyanide in 0.1M Sodium cacodylate buffer-pH 7.4) for 1 hour. Femurs were then washed in 0.1M Sodium cacodylate buffer and left in a decalcification solution (1.9% glutaraldehyde and 0.15M EDTA in 0.06M sodium cacodylate buffer) for 2 weeks. Femurs were cut into smaller pieces (both transverse and longitudinal) and passed through a series of ethanol solutions at 25%, 50%, 70%, 90% concentrations for 30 minutes to 1 hour at RT and 100% concentration overnight at 4°C.

These dehydrated bone pieces were then immersed in propylene oxide with continuous shaking for 30 minutes at RT and passed through a series of propylene oxide and epoxy resin (Epon-A) at various ratios (3:1 for 2 hours, 1:1 for 2-3 hours, 1:3 overnight) at RT followed by 100% epoxy resin (freshly made) for few hours at 37°C. Resin was polymerised in molds and allowed to embed the bone pieces at 60°C. Embedded bone pieces were then trimmed with a glass knife to expose the BM cavity and semithin sections of 0.5-1µm thickness were cut using Leica ultramicrotome (EM UC7, Leica microsystems, Wetzlar, Germany) with a diamond knife at 6° cutting angle.

These semithin sections were stained with saturated Uranyl Acetate (in 50% Acetate) for 10 minutes followed by Reynold's Lead Citrate for 10 minutes. Stained sections were then placed on EM mesh grids (200-Grid coated with Carbon support film).

Images were collected on Transmission Electron Microscope (TEM), FEI Tecnai $12G^2$ (Thermo Fisher Scientific, Oregon, USA) fitted with digital imaging system with SIS MegaView III camera (Ceta™16M, Thermo Scientific™, Waltham, Massachusetts, United States). Images were collected for each femur and saved as tiff files, about 5-25 megakaryocytes/femur. Segmentation analysis on these TEM images was done using Fiji ImageJ software (version 2.0.0-rc-65/1.51s; Madison, Wisconsin, United States) as described in **Chapter 3**.

2.15 Cryopreservation and Cryo-sectioning of tissues

Mice were sacrificed at the end of each experiment and tissues were harvested in RPMI 1640 medium. Tissues were cut into small pieces for the ease of embedding into cryomolds. Soft tissues such as spleen and liver do not need any further processing before embedding and were embedded directly after the harvest, using Tissue-Tek® OCT™ compound (Labtech, East Sussex, UK) on dry ice. Embedded tissues were transferred into -80°C freezer for long-term storage and were only taken out when ready for sectioning.

For tissue sectioning, cryomolds were transferred to CM1900 cryostat (Leica Microsystems, Wetzlar, Germany) on dry ice and allowed to stay inside cryostat for 10-15 minutes prior to cutting to equalize the temperature. OCT embedded tissues were mounted on to the cryostat knobs and extra OCT was trimmed. Tissues were cut at the desired thickness and picked up with the frosted glass slides and allowed to dry in the air. Slides were stored at -20°C for later use. All the liver and spleen sections were cut at a thickness of 8-10µm.

2.16 Haematoxylin and Eosin (H & E) staining on tissue sections

Tissue sections were cut at a thickness of 8-10µm as described above and allowed to air dry prior to staining. Tissue sections were fixed with ice-cold acetone for 5 minutes followed by staining with Harris Haematoxylin stain for 10 minutes. Slides were rinsed thoroughly in running water for few minutes followed by staining with 0.5% Eosin (1.5gram Eosin dissolved in 300ml of 95% ethanol). Slides were dipped 10-12 times in 0.5% Eosin and washed with running tap water until it stopped streaking. Slides were then dipped in a series of ethanol solutions of 50% ethanol (10 times), 75% ethanol (10 times), 95% ethanol (30 seconds) and 100% ethanol for 60 seconds or until ready for mounting. The whole staining process was carried out at RT. Slides were cover slipped with DePeX mounting medium (SLS, Nottingham, UK) in the fume hood. Slides were left at RT for drying and images were captured using AxioScan.Z1 slide scanner (Zeiss, Oberkochen, Germany) at 20x lens resolution.

2.17 Immunofluorescence staining on tissues sections

Immunofluorescence (IF) staining was done on liver and spleen cryosections. Slides with tissue sections were taken out of -80°C freezer and left at RT to equilibrate the temperature prior to staining. Tissues were fixed in acetone for 5 minutes after marking the tissue outlines with ImmEDGE™ Hydrophobic Barrier pen (Vector Laboratories Ltd., Peterborough, UK). Slides were washed with wash buffer (0.05% w/v bovine serum albumin; BSA (Sigma-Aldrich, USA) in sterile 1x PBS) followed by blocking with a dilution buffer containing 5% serum in wash buffer (serum of specie in which secondary antibody was raised). Dilution buffer was freshly made every time in order to block non-specific antibody binding. Slides were left in the dilution buffer for 30 minutes at RT and then washed with wash buffer prior to start antibody staining. An antibody mix of primary antibodies was made (antibodies detail and concentration is given in **Table 2.2**) and 100µl of antibody mix was added to each tissue section and allowed to stand for 45 minutes at RT or as per manufacturer guidelines.

Slides were washed three times in wash buffer while shaking continuously, for 3-5 minutes each wash to remove any unbound antibody. Tissue sections were then incubated

with secondary antibodies in case of unconjugated primary antibody (antibodies detail and concentration in **Table 2.2**) and were left for 30 minutes at RT. Slides were washed three times with wash buffer and two times with 1x PBS as described above. Later, the tissue sections were counter-stained with a nuclear stain i.e. 4′,6-diamidino-2-phenylindole (DAPI; 1µg/ml in 1x sterile PBS). Slides were washed twice with 1x PBS and mounted with coverslips using ProLong® gold antifade mountant (Thermo Fisher Scientific, UK). Slides were left at RT for few hours and then moved to -4°C refrigerator for short-term storage prior to imaging. The slide edges were sealed with nail varnish later. Images were captured using AxioScan.Z1 Slide scanner (Zeiss, Oberkochen, Germany) at 20x resolution or Zeiss LSM 710 upright confocal microscope (Zeiss, Oberkochen, Germany) using Zen software (Zeiss, Oberkochen, Germany) at 20x or 63x resolution with oil immersion lens.

2.18 Segmentation image analysis on IF images

Segmentation analysis was done on the IF images using StrataQuest TissueGnostics image analysis software (TissueGnostics, Vienna, Austria). Images were analysed either with the standard image analysis applications provided in the software or advanced mode by setting up a specific profile with the desired parameters. Details of the analysis and results are described in the result chapters.

Table 2.2 List of antibodies used for IF staining

Target	Fluorophore/ conjugation	Primary/ Secondary	Manufacturer	Catalog/ product #	Clone	Host	Isotype	Dilution
Spleen macrophage panel								
F4/80	AF647	Primary	BioLegend	123122	BM8	Rat	IgG2a, κ	1:200
CD169 (Siglec-1)	AF488	Primary	BioLegend	142419	3D6.112	Rat	IgG2a, κ	1:200
SIGNR1 (CD209b)	Unconjugated	Primary	eBiosciences	14-2093-82	eBio22D1 (22D1)	Armenian hamster	IgG	1:50
Anti-hamster	AF546	Secondary	Invitrogen	A-21111	Polyclonal	Goat	IgG	1:200
DAPI	Nuclear dye	Counter-stain	Thermo Fisher Scientific	D1306	-	-	-	1µg/µl (1:5000)
Liver macrophage panel								
F4/80	AF647	Primary	BioLegend	123122	BM8	Rat	IgG2a, κ	1:200
DAPI	Nuclear dye	Counter-stain	Thermo Fisher Scientific	D1306	-	-	-	1µg/µl (1:5000)
Liver TPO panel								
F4/80	AF647	Primary	BioLegend	123122	BM8	Rat	IgG2a, κ	1:200
TPO	Unconjugated	Primary	Abcam	ab196026	EPR14948	Rabbit	IgG	1:100
Anti-rabbit	AF488	Secondary	Invitrogen	A-11034	Polyclonal	Goat	IgG	1:200
DAPI	Nuclear dye	Counter-stain	Thermo Fisher Scientific	D1306	-	-	-	1µg/µl (1:5000)
Liver and spleen iNOS panel								
F4/80	AF488	Primary	BioLegend	123120	BM8	Rat	IgG2a, κ	1:300
iNOS	AF647	Primary	Abcam	ab209027	EPR16635	Rabbit	IgG	1:100
DAPI	Nuclear dye	Counter-stain	Thermo Fisher Scientific	D1306	-	-	-	1µg/µl (1:5000)

2.19 Statistical analysis

All the results were analyzed using GraphPad Prism 8 software (GraphPad Software, San Diego, CA). Data were analysed using appropriate statistical tests depending on the distribution of data and desired comparison. Parametric and non-parametric tests were used, commonly used tests include unpaired t test, Mann Whitney test, ANOVA with post-hoc tests and Kruskal Wallis with post-hoc tests. P value of less than 0.05 was taken as significant and expressed as non-significant (ns, more than 0.05), * (< 0.05), ** (< 0.01), *** (< 0.001) and **** (< 0.0001). All statistical information is provided in each figure legend.

Chapter 3. Thrombopoiesis in visceral leishmaniasis

3.1 Introduction

Thrombopoiesis, platelet production is a tightly regulated process which occurs mainly in the bone marrow (BM) of long bones in adults. The process of platelet production is already discussed in detail in **Chapter 1**. Briefly, haematopoietic stem cells (HSCs) differentiate into the progenitor cells i.e. megakaryoblasts, under the influence of various cytokines, mainly stem cell factor (SCF), thrombopoietin (TPO) and interleukins (27). Megakaryoblasts undergo repeated endomitotic divisions resulting in the formation of platelet precursors, the multi-lobulated polyploid giant cells "megakaryocytes" (MKs) (19). MKs are one of the largest cells in the body mainly present in the BM in adults. The number and normal morphology of MKs is an important factor for platelet production. Reduced number of MKs or defective progenitors and precursors results in fewer platelets being produced, resulting in thrombocytopenia. Abnormal MKs also produce fewer and/or defective platelets. The polyploid nucleus and mature cytoplasmic organelles are critical for the production of platelets. Immature MKs i.e. with hypoploid nuclei and less mature cytoplasm have been associated with many platelet disorders (177,178). Dilation or reduction in the demarcation membranes has been associated with thrombocytopenia in inherited disorders i.e. MYH9-related disorders (179). However, the status of the demarcation membranous system and their role in platelet production have not been explored in detail following infection.

As discussed in **Chapter 1**, thrombocytopenia is one of the predominant features seen in many infections. Various mechanisms have been postulated suggesting multifactorial pathogenesis. Some infections, such as Hepatitis C, have been associated with BM suppression along with peripheral mechanisms leading to excessive platelet clearance. Defective TPO production has also been noticed in infections, particularly when the liver is involved during active disease (57). VL patients present with haematological complications mainly anaemia and thrombocytopenia, yet few studies have examined the mechanisms underlying the effects of VL on haematopoiesis in general and thrombocytopenia in particular. The liver, BM and spleen are the major sites of infection during VL and these organs are also involved in the production, regulation and clearance of platelets under physiological and pathological conditions. Similar to anaemia, several

mechanisms from defective production of platelets to enhanced splenic clearance have been suggested. Experimental studies in murine models have shown that infection results in emergency haematopoiesis, most probably to compensate for pancytopenia, but at the expense of LT-HSCs resulting in HSCs exhaustion and reduced self-reconstitution potential (99,100). Ultrastructural changes in the BM and defective medullary erythropoiesis could be responsible for anaemia in VL (101,104). However, peripheral destruction of platelets as a consequence of splenomegaly cannot be neglected.

Tissue macrophages are the main reservoir of *Leishmania* amastigotes in all tissues involved and major microarchitectural changes occur in these tissues that facilitate long-term persistence of parasites (180). These morphological changes not only destroy the normal cellular architecture but also results in excessive production of an array of cytokines and chemokines which have a capacity to interfere with the normal physiological pathways (181). Granulomatous responses in the liver, damage to the marginal zone and expansion of RP in spleen, and hypocellular BM may all, therefore, be contributory factors for thrombocytopenia. The BM is the major site of platelet production and any direct effects on BM cells or the BM microenvironment could lead to compromised platelet production. The number of BM MKs and their gross morphology under light microscope was found to be unaltered in a C57BL/6 mouse model of chronic VL (O. Preham thesis; http://etheses.whiterose.ac.uk/13654/).

Here, we aim to determine how the production of platelets is affected in chronic infection using a murine model of VL, examining aspects of platelet production not previously examined. As *Leishmania* infected mice present with thrombocytopenia despite normal MKs count in the BM, we examined the ultrastructure of BM MKs of infected mice in comparison to uninfected mice BM MKs to potentially observe subtle changes in morphology that may have functional consequences. Due to a central role of TPO in the production of platelets and the known loss of normal microarchitecture of the liver during infection, we focused on the effects of hepatic infection on the production of TPO.

3.2 Aims

Thrombocytopenia is an important clinical finding in many infections with varying clinical consequences but the exact mechanisms remain poorly understood. Murine models have been used extensively to understand haematopoiesis and thrombopoiesis. Several studies have been conducted to study haematopoiesis in infections using mouse models, which have provided a valuable insight into the mechanisms responsible for infection-induced changes. Here, we used the well-characterised C57BL/6 mouse model to explore the production and regulation of platelets following *L. donovani* infection.

The specific aims of this study were to explore the following aspects of platelet production and regulation;

1. To determine the time course of thrombocytopenia following *L. donovani* infection
2. To characterise the ultrastructure of the BM MKs in infected compared to uninfected mice
3. To compare the capacity of BM MKs in uninfected and infected mice for platelet production, under conditions of enhanced thrombocytopenia due to experimentally-induced ITP
4. To establish the role of infection associated changes in hepatic TPO production in the regulation of platelet production.

3.3 Results

3.3.1 *L. donovani* infection results in progressive thrombocytopenia in an experimental mouse model

In order to study the mechanisms underlying thrombocytopenia, we adopted a well-characterised murine model of *L. donovani* infection (99,101) **(Figure 3.1)**. We first examined *L. donovani*-infected BALB/c mice and observed transient thrombocytopenia during the second week of infection followed by a recovery and then mild thrombocytopenia towards the end of fourth week post-infection **(Figure 3.2A and C)**. Mean platelet volume (MPV) only started increasing towards the fourth week of infection **(Figure 3.2B and D)**. Therefore, this model was not deemed a suitable model to study progressive thrombocytopenia. In contrast, analysis of peripheral blood samples at d28 of infection in C57BL/6 mice indicated moderate to severe thrombocytopenia (< $200x10^3$ platelets/µl; **Figure 3.3A)**. Giant platelets were also observed as shown by high mean platelet volume (MPV; **Figure 3.3B)**. By the fourth week of infection, mice had hepatomegaly and splenomegaly, and high parasite burden **(Figure 3.3C-E)**. Based on a reference interval defined by platelet counts in a cohort of n=15 uninfected mice, 73.3% (11/15) of infected mice were thrombocytopenic and were considered to have abnormally large platelets.

To evaluate the kinetics of development of thrombocytopenia, C57BL/6 mice were examined by CBCs before infection and weekly for four weeks following infection. Blood cell counts including platelet counts in uninfected mice remained consistent over the time course of these experiments. However, the platelet count in infected mice began to decrease in the second week of infection and mice were severely thrombocytopenic by the end of fourth week of infection **(Figure 3.4A)**. Platelets in infected mice were also significantly larger than in uninfected mice (MPV of 7.58 ± 0.36µl vs. 5.6 ±0.2µl in infected vs. uninfected mice, respectively; **Figure 3.4B**). Giemsa stained blood smears confirmed the presence of large/giant platelets (**Figure 3.4C and D**). No platelet satellitism was noticed on the blood smears.

Therefore, it was concluded that murine EVL in C57BL/6 mice induces significant progressive thrombocytopenia characterised by an increase in platelet volume and

provides a suitable model for evaluating mechanisms of thrombocytopenia that may be relevant in human disease.

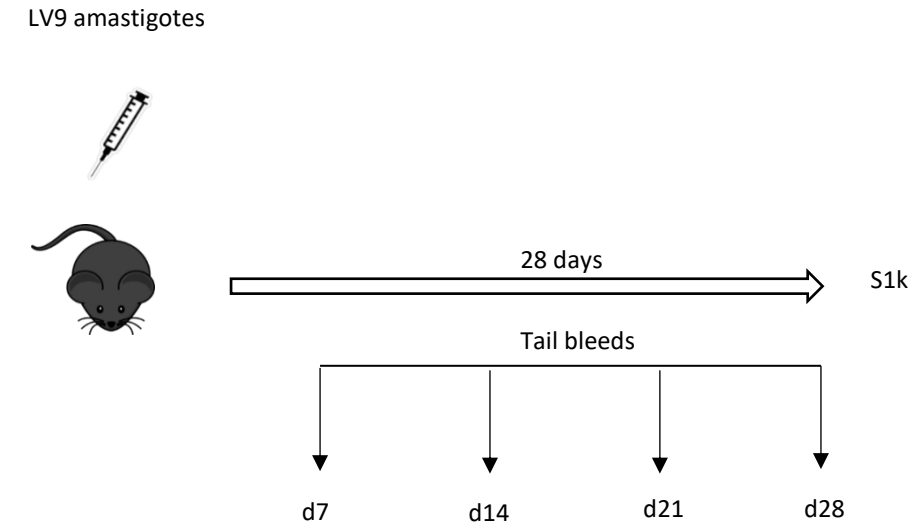

Experimental groups:

1. LV9 infected
2. Uninfected control

Figure 3.1 Schematic diagram of chronic infection murine model of *L. donovani* infection. Six-eight weeks old BALB/c or C57BL/6 mice were infected intravenously via tail vein with 3 x 10^7 amastigotes of *L. donovani* (*LV9* strain). Mice were bled from the lateral tail veins before and weekly after infection and complete blood counts (CBCs) obtained using an automated analyser. Experiments were terminated at d28 of infection for post-mortem analysis of tissues, assessment of parasite burden and further analyses.

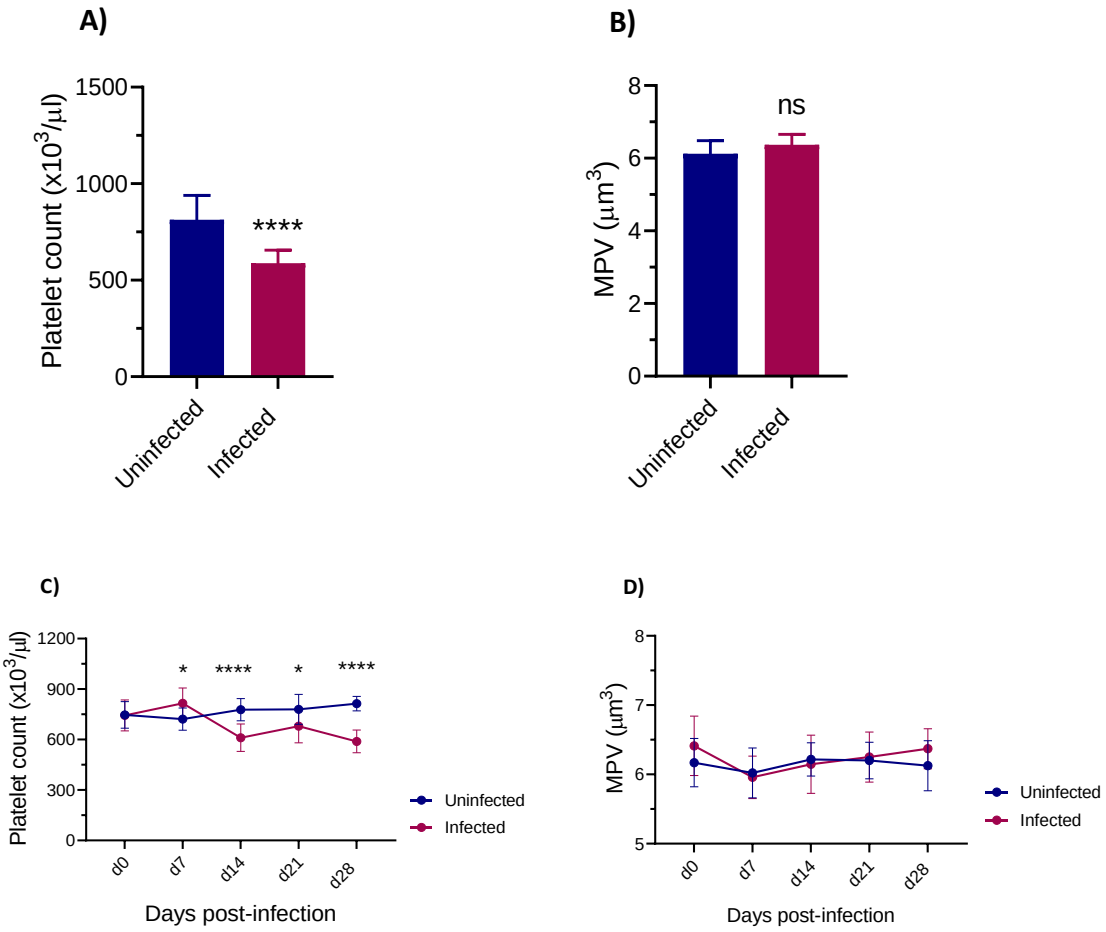

Figure 3.2 Thrombocytopenia in *L. donovani*-infected BALB/c mice. BALB/c mice infected with 3 x 10^7 *L. donovani* (*LV9*) amastigotes i.v were bled before and weekly after infection for platelet count measurement. Data show (A) the platelet count and (B) mean platelet volume (MPV) of d28 infected mice compared to uninfected mice, and (C) platelet count and (D) MPV of *L. donovani*-infected BALB/c mice monitored during the course of infection. Data are representative of a single experiment with n= 17 infected and n=8 uninfected BALB/c mice. Data expressed as mean ± SD and analysed using an unpaired t test between infected and uninfected groups, ns, non-significant; *, $p < 0.05$; ****, $p < 0.0001$.

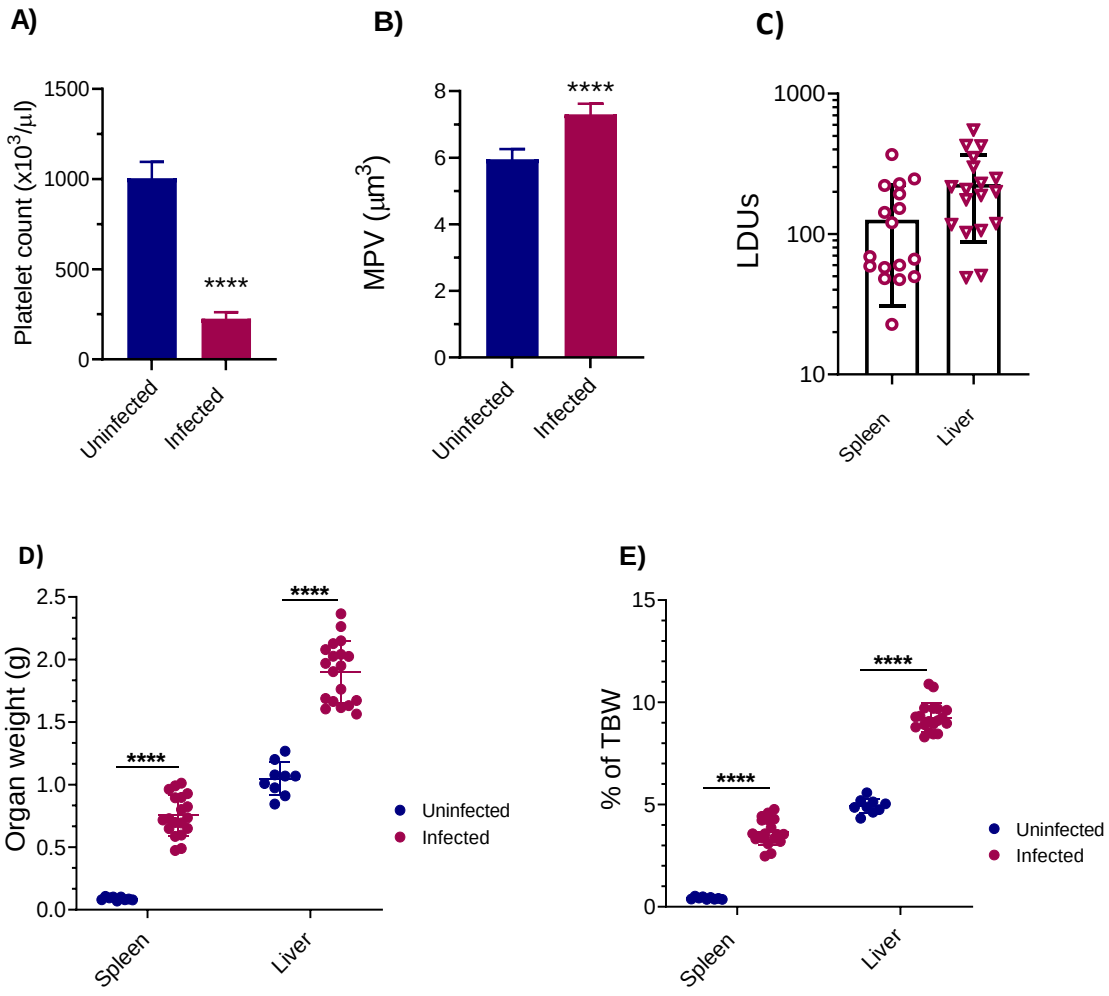

Figure 3.3 *L. donovani* infection in C57BL/6 mice results in thrombocytopenia and high parasite burden with organomegaly. Mice were sacrificed at d28 of infection for the assessment of thrombocytopenia and post-mortem hepatosplenomegaly and parasite burden. Mice were (A) severely thrombocytopenic at d28 post-infection with (B) higher than normal mean platelet volume (MPV) as compared to uninfected mice. Data show result of two independent experiments with n= 11 infected and n=15 uninfected. Data are analysed using an unpaired t test. Post-mortem (C) parasite burden was measured on liver (n=18) and spleen (n=17) impression smears as Leishman-Donovan units (LDUs), (D) spleen and liver weights in grams (g) and as a (E) percentage of spleen and liver size as a percentage of total body weight (TBW) as compared to uninfected mice. Data represent the result of three independent experiments with n= 9 uninfected and n= 19 infected mice. Data expressed as mean ± SD and analysed using unpaired t test between infected and uninfected groups. ****, $p < 0.0001$.

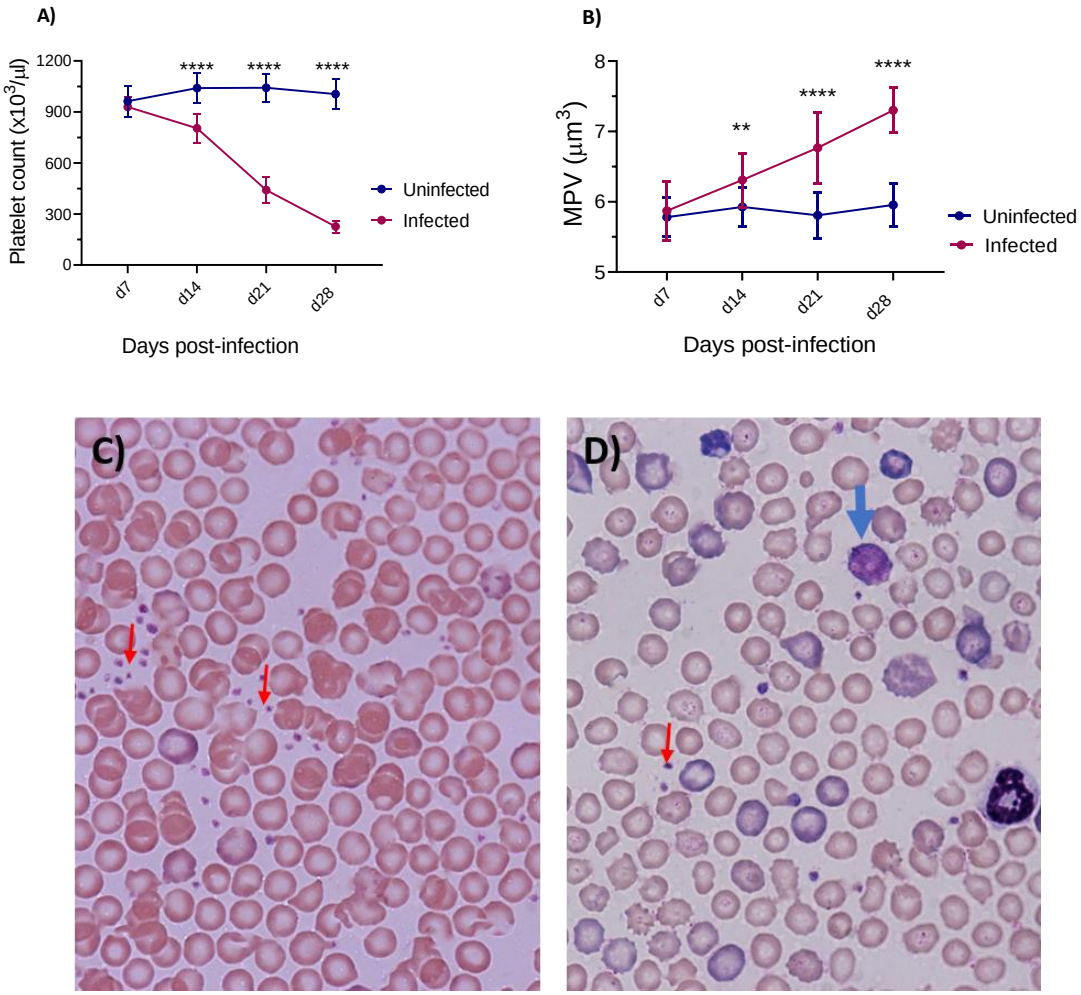

Figure 3.4 Platelet counts during the course of *L. donovani* infection in C57BL/6 mice. (A) Platelet counts and (B) MPV were monitored weekly in both infected and uninfected C57BL/6 mice. Graphs represent the mean (± SD) of n= 15 uninfected and n=12 infected mice from three independent experiments. Data were analysed using unpaired t test in uninfected vs infected mice at each time-point, **, $p < 0.01$; ****, $p < 0.0001$. Blood smears of (C) uninfected and (D) d28 infected C57BL/6 mice show the presence of giant platelets. Representative normal platelets (red arrows) and giant platelets (blue arrow) are indicated.

3.3.2 Bone marrow megakaryopoiesis is altered in experimental VL

We next investigated whether the production of platelets was defective in mice with *L. donovani* infection, by assessing the capacity of infected mice to produce platelets. A previous study had found no significant difference in the number of BM MKs at the time of maximal thrombocytopenia (O. Preham thesis; http://etheses.whiterose.ac.uk/13654/). Ultrastructural remodelling of MKs is important for the normal production of platelets and abnormalities in this process have been associated with abnormal platelet production (182). MKs contain demarcation membranes in the cytoplasm, developing granules and organelles and most importantly a polyploid nucleus. The demarcation membrane system (DMS) is an important structure in the cytoplasm of mature megakaryocytes, surrounding the developing platelets and elongating into blood vessels to release proplatelets. Defects in the DMS have been studied in congenital thrombocytopenic disorders (20). Hypogranular platelets i.e. with fewer or abnormal granules, hypoploid nucleus and reduced or less developed membranes are associated with multiple inherited and acquired disorders with a range of clinical pathologies (183,184).

To access the DMS of BM MKs, we applied quantitative image analysis to TEM images of the BM MKs (**Figure 3.5**). Analysis of the perimeter of the DMS indicated that these membranes were significantly reduced in the MKs of infected mice BM compared to uninfected mice (**Figure 3.6**). Reduction in the DMS of infected BM MKs suggests their capacity to produce a normal number of platelets may be impaired as a consequence of infection. Territories of the developing platelets were less pronounced in infected mice BM MKs suggestive of the lesser capacity of DMS to produce platelets **(Figure 3.6)**.

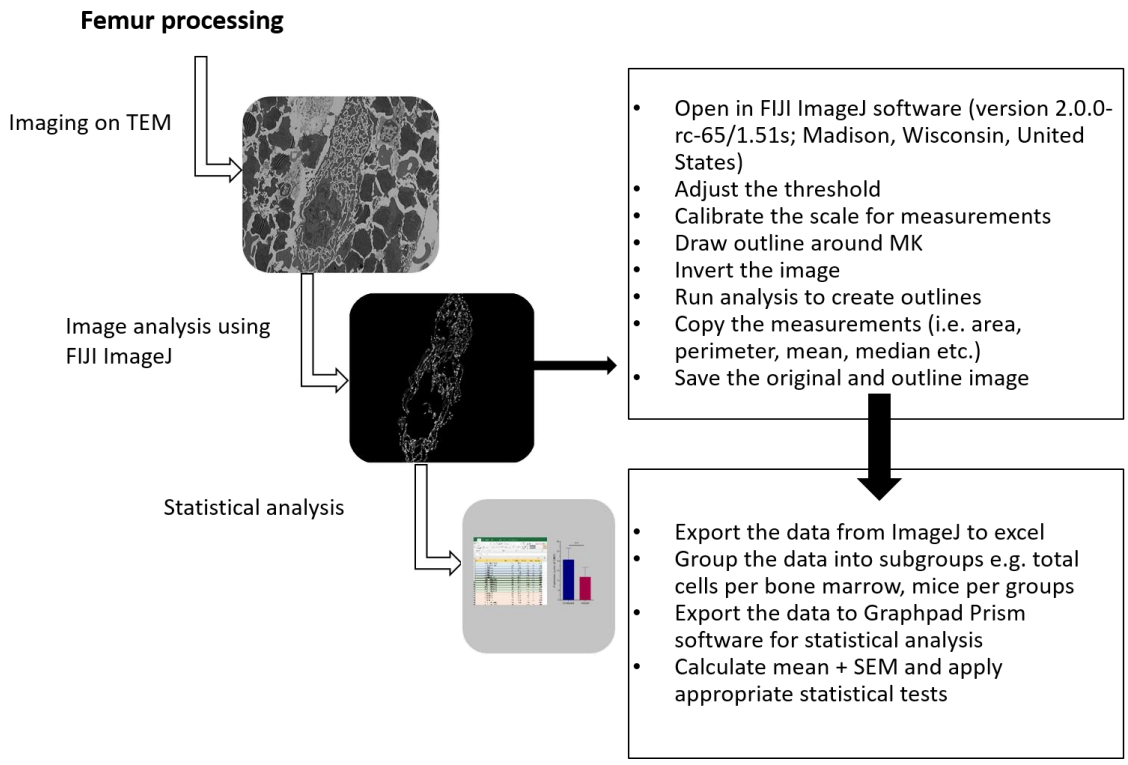

Figure 3.5 Segmentation analysis strategy on Transmission Electron Microscopy (TEM) images.

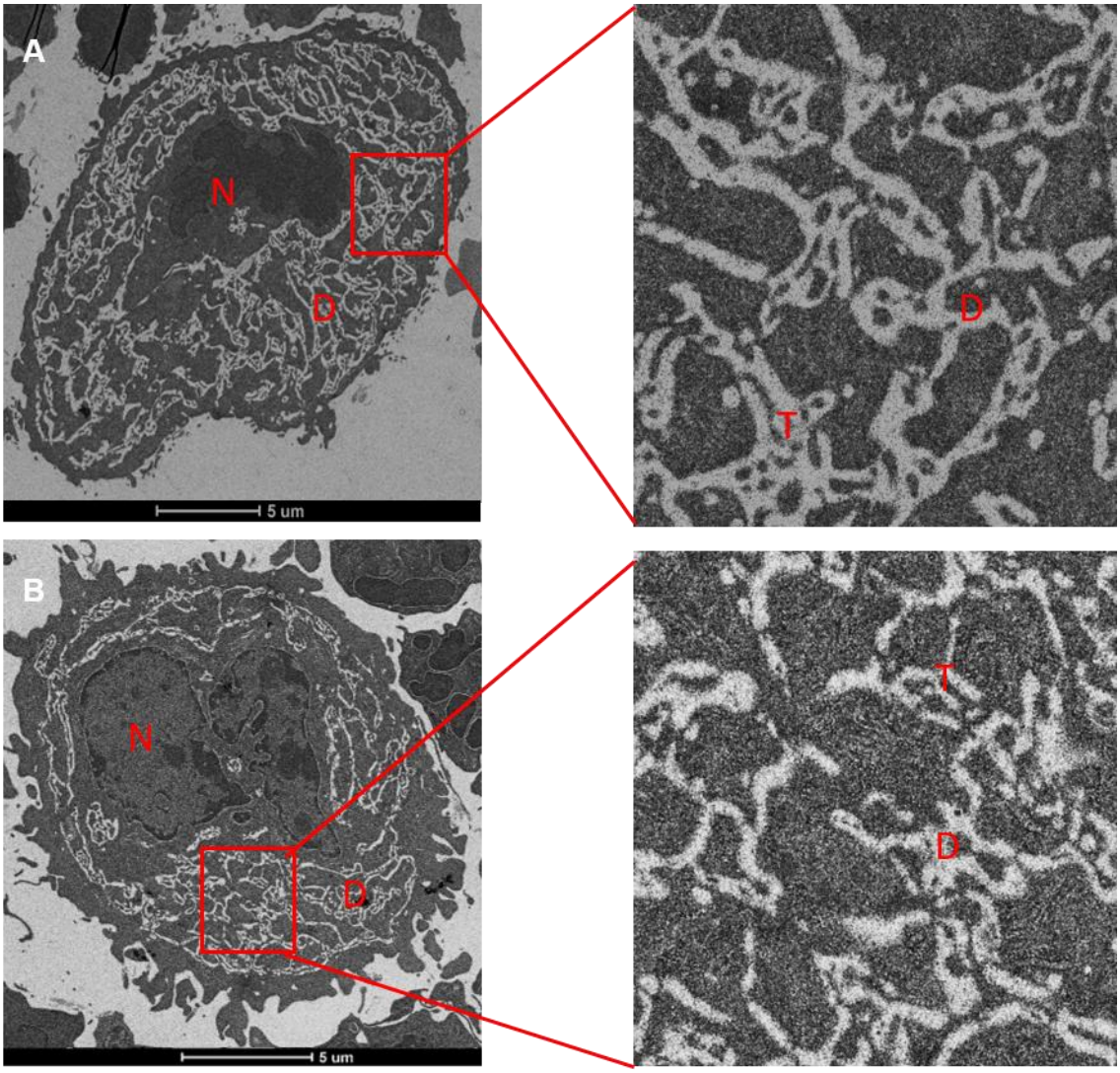
A
N
D
5 um
D
T
B
N
D
5 um
T
D

C)

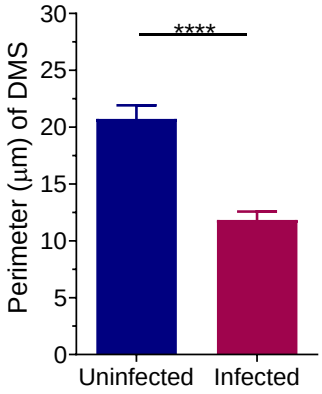
****
Perimeter (μm) of DMS
30
25
20
15
10
5
0
Uninfected
Infected

Figure 3.6 Representative images of transmission electron microscopy and perimeter of demarcation membranes of mature bone marrow megakaryocytes. Electron microscopy (TEM, FEI Tecnai $12G^2$) was performed on femur sections from (A) uninfected and (B) d28 infected mice. Note the presence of multi-lobulated nucleus and demarcation membranous system (DMS) within the cytoplasm. Scale bar; 5µm. N, nucleus; D, DMS; T, Platelet territories. Images were analysed by creating outlines of demarcation membranes using Fiji ImageJ software (refer **Figure 3.5**) and (C) perimeters were calculated with n= 25 uninfected, n=46 infected mice BM MKs. Data represent the mean (± SEM) across individual mice. Unpaired t test was applied to the means of the perimeter of membranes, ****, $p < 0.0001$, in uninfected vs infected mice.

3.3.3 Bone marrow megakaryocytes are capable of platelet production on stimulation

Although the segmentation analysis on the TEM images of BM MKs suggested alterations in the DMS which could be a major contributory factor in reduced platelet production, we wished to test whether these MKs retained their functional capacity.

To confirm the functional capacity of BM MKs for platelet production using an independent approach, we used a well-characterised model of anti-CD41 antibody driven induced ITP. Infected and uninfected mice were treated with anti-CD41 mAb and bled at specified times (**Figure 3.7)**. There was no difference in the splenic parasite burden and spleen weights in infected mice treated with anti-CD41 antibody and untreated infected mice **(Figure 3.8A and B)**. Erythrocyte count and indices as well as leucocyte counts were not altered after induced ITP (**Table 3.1** and **Table 3.2)**.

Administration of anti-CD41 mAb to uninfected mice led to a rapid fall in platelet count followed by a period of recovery, attributed to new platelet production by megakaryocytes (**Figure 3.9A**). When anti-CD41 mAb was administered to *L. donovani*-infected mice, a similar pattern of depletion followed by recovery was observed (**Figure 3.9A**). Interestingly, the rate of platelet drop followed by recovery was not different in either group when normalised to baseline platelet counts (**Figure 3.9B**). However, there was a 70% reduction in the platelet counts in infected mice as compared to > 92% in uninfected within 24 hours of antibody administration and slower recovery in infected mice. However, platelet count increased to >47% of baseline in both groups at day 7 post anti-CD41 antibody administration (**Figure 3.9C**). MPV was increased in anti-CD41 antibody treated uninfected mice within 24 hours followed by recovery in 4 days, and a slight decrease in MPV of antibody-treated infected mice at day 7 post antibody treatment was noticed (**Figure 3.9D**).

Intriguingly, anti-CD41 treatment of infected mice also normalised the MK DMS (17.66 ± 5.68μm vs 11.84 ± 4.94 μm vs 20.73 ± 5.96 μm anti-CD41 treated infected mice, untreated infected mice and uninfected mice, respectively; **Figure 3.10A-C)**. Although no significant difference in the DMS of uninfected anti-CD41 treated mice was noticed however, platelet territories were prominent in both uninfected and infected mice treated with anti-CD41 antibody **(Figure 3.10A and B)**. Not only do these data indicate that MK

production of platelets is functionally intact, but they also suggest that other factors besides megakaryocyte number and integrity of the DMS impose a limitation on the peripheral platelet count that is achievable in infected mice.

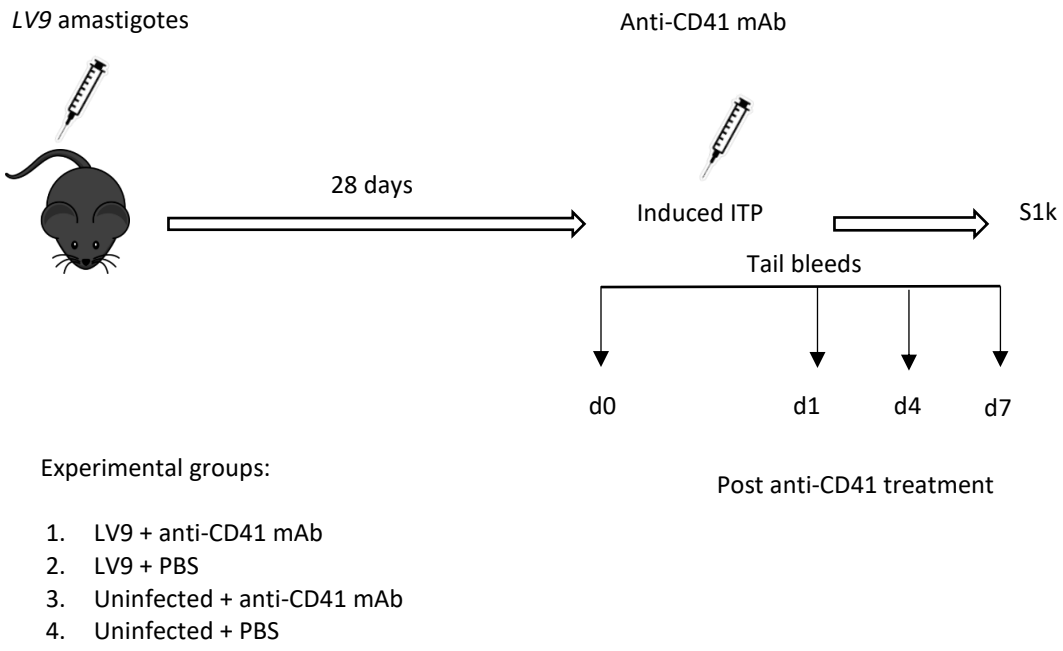

Figure 3.7 Schematic of the induced immune thrombocytopenia in infected mice. C57BL/6 mice were infected with *L.donovani* (*LV9*) amastigotes for 28 days to develop severe thrombocytopenia. Mice were treated with a single dose (0.2µg/g body weight) of anti-CD41 monoclonal antibody (Clone: MWReg30) to induce immune thrombocytopenia (ITP) and bled before and after antibody adminstration at specified times as shown in the diagram. Blood counts were done on peripheral blood and mice were sacrificed after 7 days of induced ITP. Post-mortem analyses of spleen size, spleen parasite burden (LDUs) and transmission electron microscopy on femurs for BM MKs were performed.

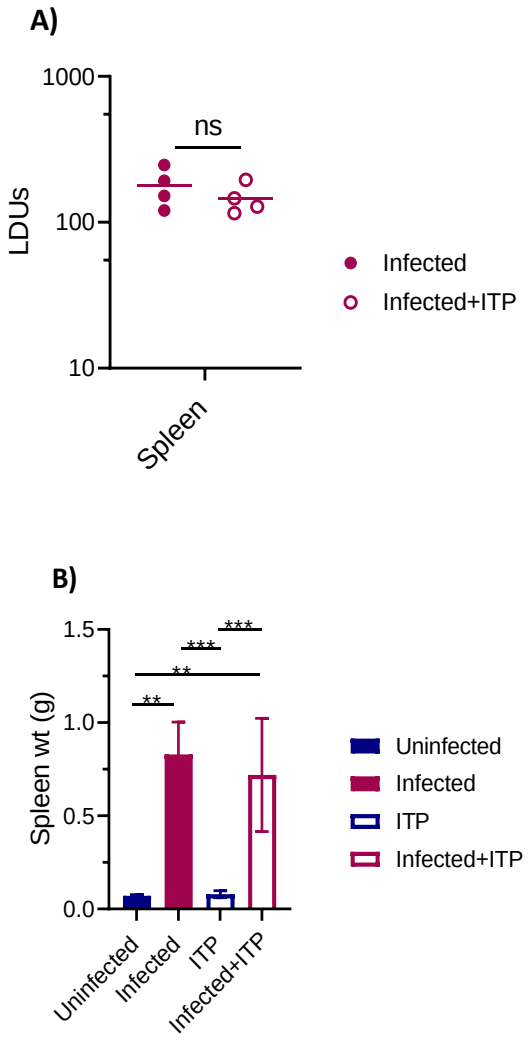

Figure 3.8 Spleen parasite burden and splenic weight in induced immune thrombocytopenia. (A) Parasite burden is represented as Leishman-Donovan units (LDUs). The number of parasites per 1000 cell nuclei were counted on the Giemsa stained spleen impression smears of anti-CD41 treated infected (n=4) and infected controls (n=4) mice at d7 post-antibody treatment. Data analysed unpaired t test, ns, non-significant. Post-mortem (B) spleen weight (g) was measured in each group in n= 2 uninfected, n=5 infected, n=6 anti-CD41 treated (ITP) and n=9 infected anti-CD41 treated (infected+ITP) mice. Data represent mean (± SD) of each group, statistically analysed using ANOVA with post-hoc Tukey's test on the mean of each group, **, $p < 0.01$; ***, $p < 0.001$.

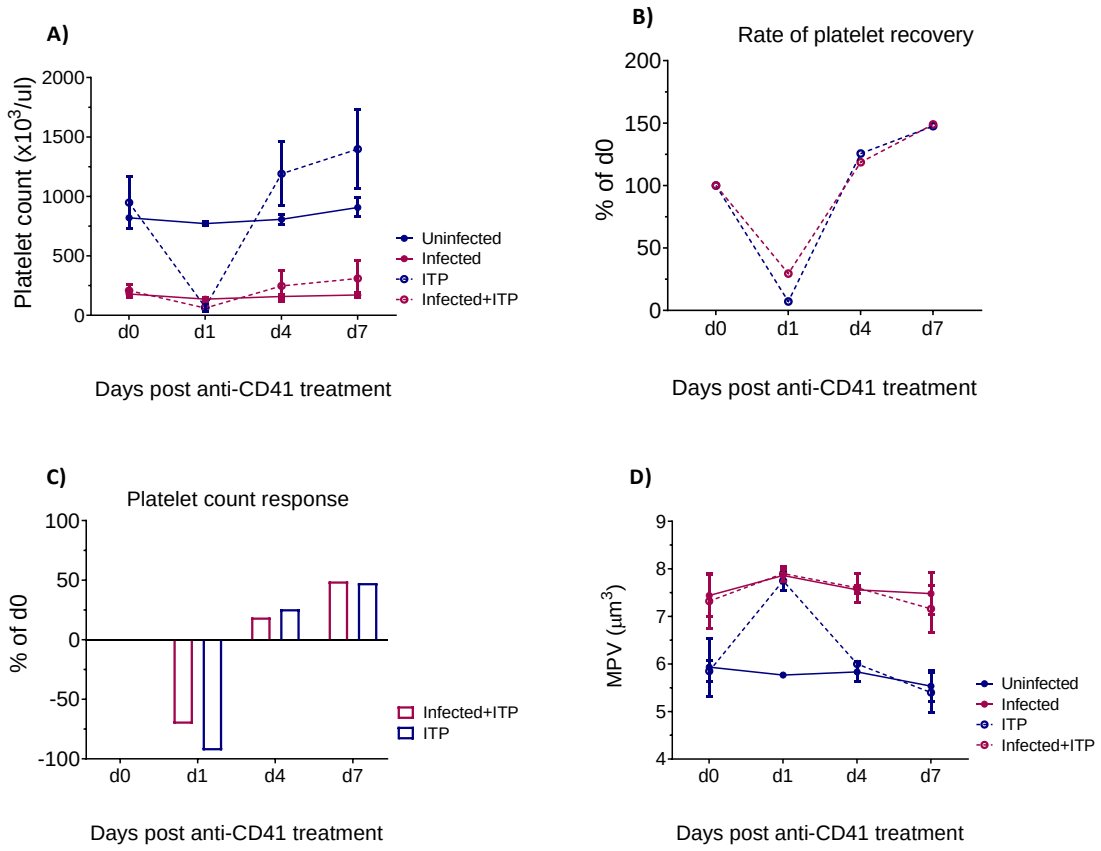

Figure 3.9 Platelet counts after anti-CD41 mAb administration in uninfected and infected C57BL/6 mice. Uninfected and infected mice were randomised into groups and injected intraperitoneally with 0.2µg/g body weight of anti-CD41 monoclonal antibody (Clone: MWReg30). Platelet counts were recorded in all groups at d0 (before antibody administration), d1, d4 and d7 post-injections. Data are representative of (A) Platelet count (x 10^3 per ul) from three different independent experiments, (B) Rate of recovery of platelet counts in anti-CD41 treated uninfected and infected mice, (C) platelet count as percentage change during the course of ITP in infected vs uninfected mice and (D) MPV measured at each time-point. Data show the results of three independent experiments (n=3 uninfected, n=9 anti-CD41, n=5 infected and n=10 infected + anti-CD41 treated), expressed as mean ± SD and % change.

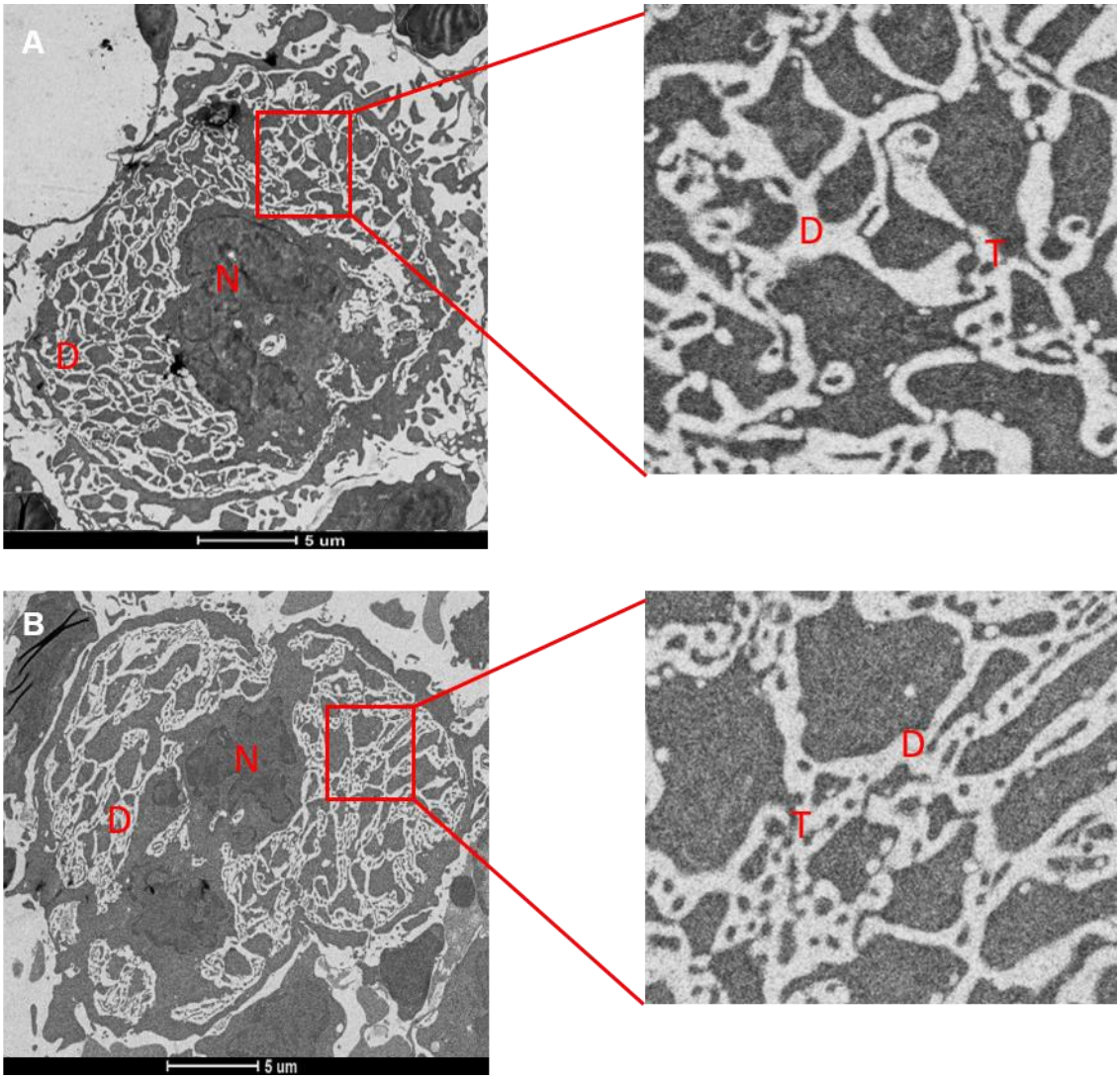
A
N
D
5 um
D
T
B
N
D
5 um
D
T

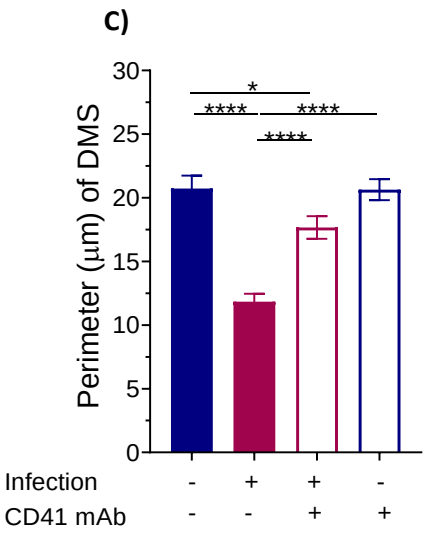
C)
Perimeter (μm) of DMS
30
25
20
15
10
5
0
*
****
****
****
Infection
CD41 mAb
- + + -
- - + +

Figure 3.10 Anti-CD41 induced ITP restores the DMS in BM MKs in *L. donovani*-infected mice. Electron microscopy was done on the femurs of (A) infected and (B) uninfected mice for BM MKs after treatment with anti-CD41 antibody. Data were analysed by creating the outlines of the perimeter of DMS in the cytoplasm of mature MKs using Fiji ImageJ software as described in **Figure 3.4**. Scale bar; 5µm, N, nucleus; D, DMS; T, Platelet territories. Statistical analysis was done using ANOVA with post-hoc Tukey's test on the mean (± SEM) of the perimeter of DMS, *, $p < 0.05$; ****, $p < 0.0001$. Data show the results of BM MKs of n=25 uninfected, n=20 anti-CD41, n=46 infected and n=30 infected + anti-CD41 treated (part of the data, n=25 uninfected and n=46 infected mice BM MKs is shown in **Figure 3.6**).

Table 3.1 Erythrocyte parameters on peripheral blood counts in infected vs uninfected mice, treated with anti-CD41 mAb to induce ITP

	Infected/ITP (Mean ± SD)	**Infected** (Mean ± SD)	**Uninfected** (Mean ± SD)	**ITP** (Mean ±SD)
Haemoglobin (Hb) g/dl				
d0	11.171 ± 1.378	11.533 ± 1.619	16.400 ± 0.700	16.000 ± 0.739
d1	11.514 ± 1.291	11.540 ± 0.753	15.185 ± 0.935	15.283 ± 0.466
d4	12.100 ± 1.274	11.733 ± 0.350	15.325 ± 1.178	14.900 ± 0.624
d7	11.480 ± 1.018	11.000 ± 0.832	16.050 ± 0.695	15.550 ± 1.244
RBC count (x 10^6/mm^3)				
d0	6.514 ± 1.409	5.685 ± 0.821	9.893 ± 0.745	9.623 ± 0.448
d1	6.887 ± 0.688	6.260 ± 0.559	10.300 ± 0.608	9.225 ± 0.958
d4	6.647 ± 1.652	6.450 ± 0.340	9.373 ± 0.484	9.238 ± 0.823
d7	6.715 ± 1.371	5.877 ± 0.596	9.970 ± 0.637	9.106 ± 1.449
Haematocrit (Hct) %				
d0	31.671 ± 4.456	31.575 ± 5.302	48.233 ± 3.203	47.000 ± 2.116
d1	33.155 ± 8.725	31.575 ± 5.302	45.766 ± 5.227	46.450 ± 2.254
d4	36.350 ± 2.980	34.880 ± 2.333	47.800 ± 2.426	44.550 ± 4.788
d7	33.225 ± 7.962	35.740 ± 0.887	45.700 ± 2.451	44.480 ± 4.161
Mean cell volume (MCV) µm^3				
d0	53.714 ± 2.288	53.285 ± 3.352	48.666 ± 2.081	48.571± 0.534
d1	53.250 ± 2.314	55.800 ± 2.774	48.666 ± 1.154	48.000 ± 0.000
d4	53.142 ± 1.214	55.600 ± 2.302	48.666 ± 1.154	48.000 ± 0.632
d7	52.833 ± 1.471	55.600 ± 2.880	48.666 ± 1.154	47.833 ± 0.408
Mean cell haemoglobin (MCH) pg				
d0	18.580 ± 1.088	19.340 ± 0.559	16.875 ± 0.518	16.840 ± 0.497
d1	18.033 ± 0.602	18.600 ± 0.894	15.900 ± 0.663	16.166 ± 0.136
d4	17.811 ± 0.679	18.360 ± 0.743	15.800 ± 0.264	16.022 ± 1.163
d7	18.511 ± 0.933	19.120 ± 1.103	16.566 ± 0.763	16.300 ± 0.178
Mean cell haemoglobin concentration (MCHC) g/dl				
d0	35.380 ± 0.771	35.400 ± 0.809	33.133 ± 0.901	34.000 ± 0.707
d1	33.933 ± 1.071	33.140 ± 0.364	32.366 ± 0.404	32.150 ± 0.212
d4	33.316 ± 0.549	33.020 ± 0.148	32.400 ± 0.264	32.850 ± 0.494
d7	34.777 ± 0.635	34.500 ± 0.595	32.966 ± 0.057	33.300 ± 0.141
Red blood cell distribution width (RDW) %				
d0	21.850 ± 1.421	24.000 ± 0.678	16.800 ± 0.700	16.466 ± 0.445
d1	21.600 ± 1.341	23.400 ± 0.894	17.000 ± 0.000	17.033 ± 0.694
d4	20.700 ± 1.513	21.740 ± 0.986	17.333 ± 0.152	17.116 ± 0.711
d7	21.460 ± 2.383	21.200 ± 0.644	17.500 ± 0.360	17.033 ± 0.320

Table 3.2 Leucocyte counts on peripheral blood counts in infected vs uninfected mice, treated with anti-CD41 mAb to induce ITP

	Infected/ITP (Mean ± SD)	**Infected** (Mean ± SD)	**Uninfected** (Mean ± SD)	**ITP** (Mean ±SD)
WBC count (x 10^3/mm^3)				
d0	5.640 ± 2.083	5.920 ± 2.106	9.000 ± 1.253	10.600 ± 2.835
d1	5.860 ± 1.368	7.140 ± 0.820	8.914 ± 2.012	10.383 ± 3.424
d4	5.844 ± 1.735	6.760 ± 1.750	11.166 ± 1.320	8.860 ± 2.389
d7	5.162 ± 1.263	4.740 ± 1.178	9.833 ± 1.527	9.966 ± 4.354
Neutrophil count (x 10^3/mm^3)				
d0	1.170 ± 0.459	1.360 ± 0.482	1.966 ± 0.450	1.666 ± 0.602
d1	1.500 ± 0.497	1.780 ± 0.216	1.800 ± 0.469	1.666 ± 0.404
d4	1.222 ± 0.349	1.720 ± 0.396	1.666 ± 0.288	1.625 ± 0.419
d7	1.177 ± 0.468	1.380 ± 0.238	2.100 ± 0.141	1.733 ± 0.378
Lymphocyte count (x 10^3/mm^3)				
d0	4.544 ± 1.359	4.420 ± 1.525	5.625 ± 2.247	6.040 ± 2.506
d1	4.300 ± 0.965	5.000 ± 0.707	8.125 ± 1.931	7.620 ± 2.709
d4	4.455 ± 1.364	4.820 ± 1.325	8.425 ± 1.537	7.425 ± 2.385
d7	3.762 ± 0.942	3.260 ± 0.884	7.333 ± 1.106	7.866 ± 1.450
Monocyte count (x 10^3/mm^3)				
d0	0.200 ± 0.133	0.140 ± 0.151	0.333 ± 0.057	0.260 ± 0.230
d1	0.212 ± 0.064	0.280 ± 0.083	0.300 ± 0.100	0.333 ± 0.121
d4	0.187 ± 0.099	0.220 ± 0.044	0.333 ± 0.057	0.250 ± 0.104
d7	0.137 ± 0.051	0.100 ± 0.070	0.366 ± 0.057	0.240 ± 0.181
Eosinophil counts (x 10^3/mm^3)				
d0	0.089 ± 0.076	0.084 ± 0.018	0.092 ± 0.079	0.126 ± 0.118
d1	0.080 ± 0.025	0.100 ± 0.000	0.075 ± 0.035	0.055 ± 0.031
d4	0.098 ± 0.117	0.076 ± 0.036	0.082 ± 0.034	0.136 ± 0.122
d7	0.047 ± 0.013	0.114 ± 0.094	0.056 ± 0.030	0.060 ± 0.017

3.3.4 Thrombopoietin production is compromised during chromic EVL

Thrombopoietin (TPO) is one of the major regulators of HSC differentiation, proliferation and platelet production as discussed in detail in **Chapter 1**. To assess the role of the liver in the production of TPO during *L. donovani* infection, we measured circulating unbound TPO in uninfected control mice and infected mice at d28 post-infection. The level of circulating TPO in infected mice was significantly reduced at d28 as compared to uninfected control mice (600.527 ± 25.82025 vs 75.8935 ± 26.7535, in uninfected and infected mice respectively; **Figure 3.11A**).

We next evaluated *Thpo* mRNA in the liver using qRT PCR to determine whether this reflected transcriptional regulation. The mRNA levels in the d28 infected hepatic tissues were reduced by around 50% compared to uninfected controls (**Figure 3.11B)**. Although renal pathology is not extensively reported in murine models of VL, we also measured *Thpo* mRNA accumulation in the kidneys of infected and uninfected mice, as the kidneys are the main site of TPO production after the liver. No difference was seen in renal *Thpo* mRNA accumulation in the kidneys of infected compared to uninfected mice **(Figure 3.11C**), indicating that the reduction in *Thpo* mRNA accumulation was tissue specific.

Finally, to assess TPO protein production by hepatocytes, we stained liver sections of uninfected control and d28 infected mice with anti-TPO antibody and analysed the resulting staining pattern using a quantitative segmentation analysis. By this approach, we observed a reduction in the number of hepatocytes per unit area that were positive for TPO, most probably due to the formation of granulomas and an increase in the number of non-parenchymal inflammatory cells **(Figure 3.12A-D).**

The JAK-STAT signalling pathway is important for the production of TPO. As liver granulomas secrete a range of cytokines which affect the JAK-STAT pathway, we sought to determine whether there was a reduction in the TPO expression on hepatocytes that reflected their spatial positioning relative to granulomas. Using liver tissues stained with anti-TPO antibody and an in-house developed StrataQuest TissueGnostics image analysis package, we determined the median fluorescence intensity (MFI) of TPO positive hepatocytes in uninfected vs d28 infected mice, and at different distances (0-30µm and 30-60µm from granuloma) from the margin of individual granulomas on infected mice livers **(Figure 3.13**). Based on this analysis, TPO expression was higher in infected as

compared to uninfected mice hepatocytes, and also in hepatocytes closer (0-30µm) to granuloma as compared to ones at intermediate distances away from granulomas **(Figure 3.14A and B)**. TPO expression beyond 60µm from granuloma was not taken into account as there was a risk of including hepatocytes closer to another granuloma.

Together these data suggest that although the production of TPO, as determined from the serum measurements, is reduced during *L. donovani* infection, hepatocytes in infected mice produce more TPO and also the hepatocytes which are in close proximity to the inflammatory cells seem to produce more TPO as compared to the ones at a greater distance. This could be due to increased activity of the JAK-STAT pathway or excessive phosphorylation of STATs due to the excess of cytokines around. Importantly, these data suggest spatial regulation of TPO protein production in the infected liver.

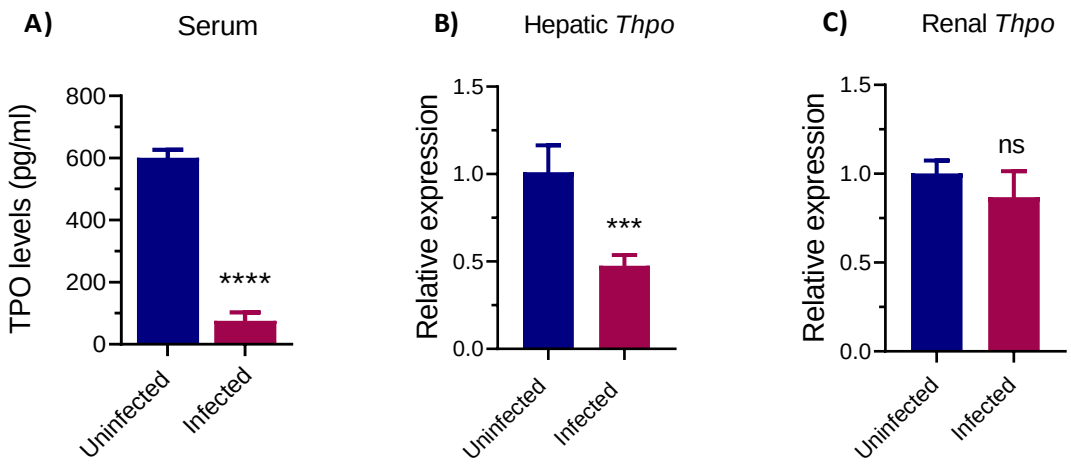

Figure 3.11 Thrombopoietin in circulation and tissues. (A) Circulating TPO levels were measured in uninfected and d28 infected C57BL/6 mice. (B) Hepatic and (C) renal *Thpo* mRNA accumulations were assessed in uninfected vs infected mice. Data were analysed using unpaired t test, p value, ns, non-significant; ***, $p < 0.001$; ****, $p < 0.0001$ on n=4 uninfected and n=5 infected mice, and expressed as mean ± SD.

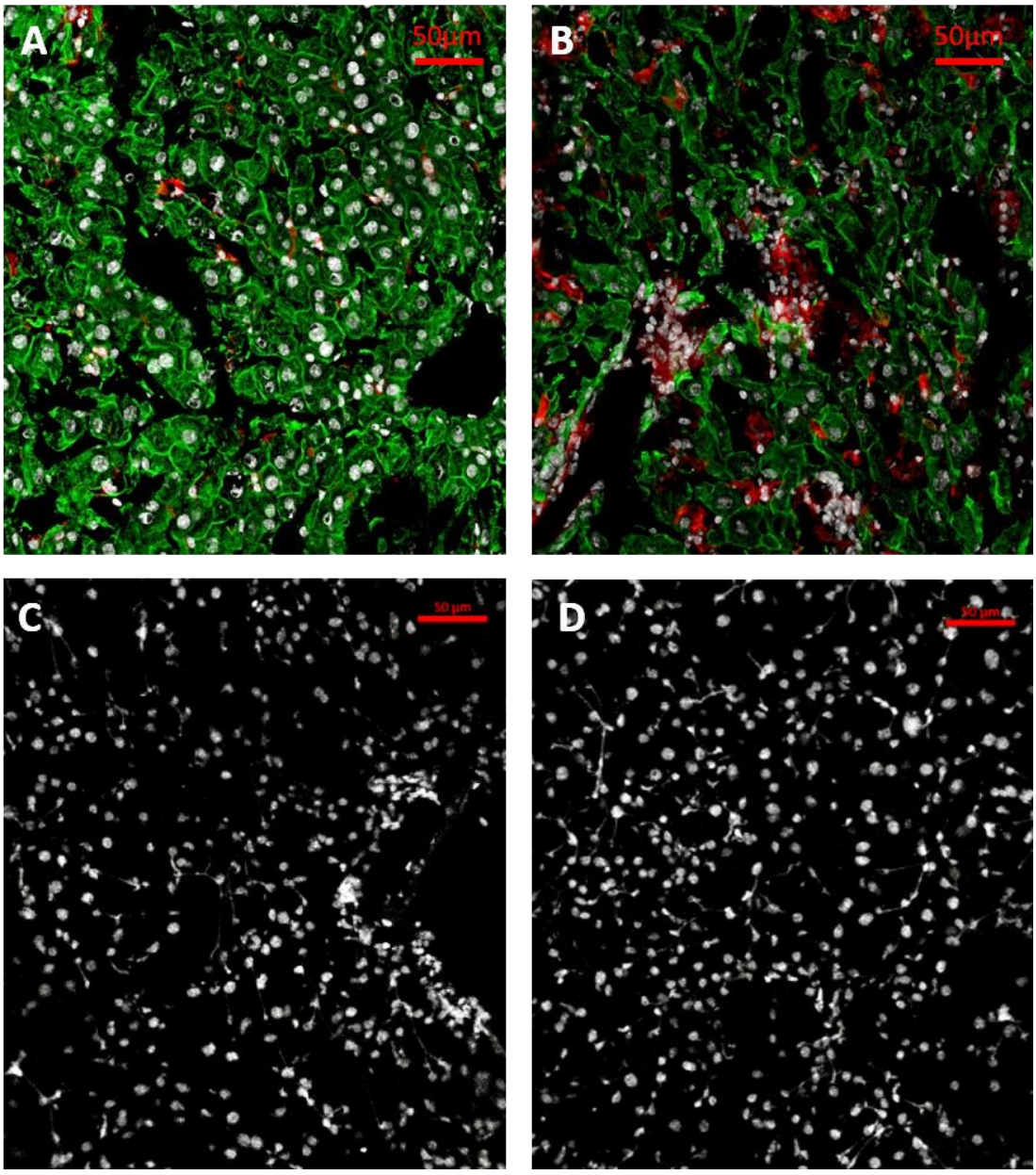
A
50µm
B
50µm
C
D

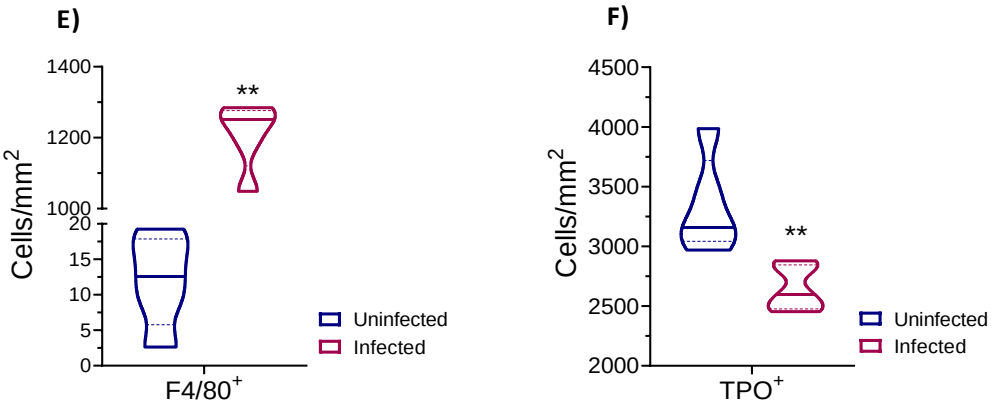
E)
1400
1200
1000
20
15
10
5
0
Cells/mm2
**
F4/80+
Uninfected
Infected
F)
4500
4000
3500
3000
2500
2000
Cells/mm2
**
TPO+
Uninfected
Infected

Figure 3.12 Representative immunofluorescent (IF) staining of liver sections stained with anti-TPO antibodies. Frozen liver sections (8µm thickness) of (A) uninfected and (B) d28 infected C57BL/6 mice were stained with immunofluorescent markers (F4/80 for Kupffer cells and anti-TPO antibody for TPO-producing hepatocytes) and images were collected using a confocal microscope (LSM 710) at 63x oil immersion lens. Single control images, (C) primary anti-TPO antibody only and (D) goat anti-rabbit AF488 antibody only were captured at 20x resolution. Segmentation analysis was performed using StrataQuest TissueGnostics software for both (E) F4/80 and (F) TPO positive cells on n=15 uninfected and n=15 infected tissues sections. Data represent median with quartiles, statistical analysis was done using Mann-Whitney non-parametric test, **, $p < 0.01$. Red= F4/80, Green= TPO, White= DAPI. Scale bar = 50µm.

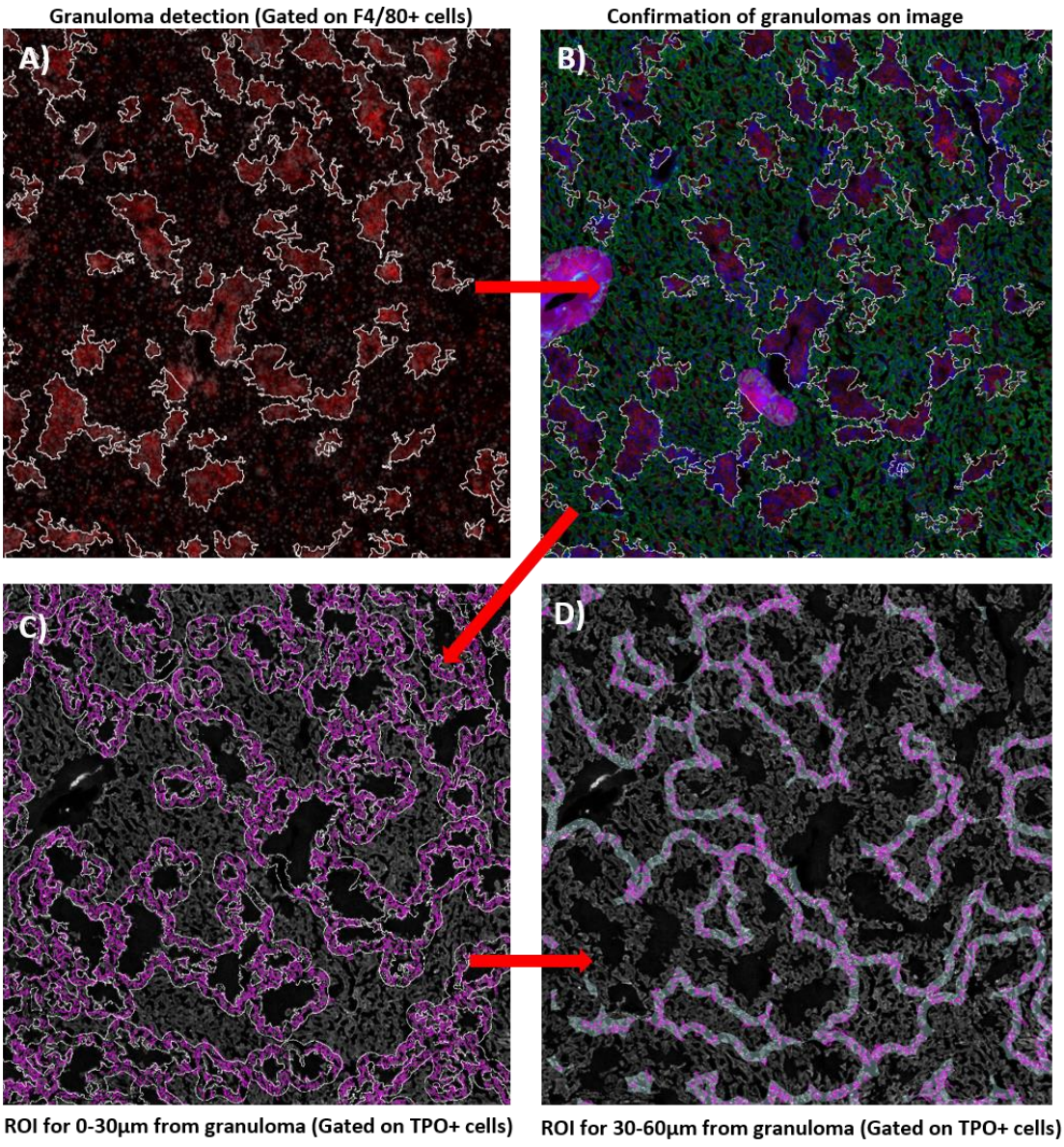

Figure 3.13 Gating strategy to obtain the median fluorescence intensity of TPO$^+$ hepatocytes at various distances from the margin of granuloma. Liver sections were gated for granulomas detection (A & B) using F4/80$^+$ and nuclear size as a marker followed by drawing masks around the granulomas (white lines around F4/80$^+$ cells) to create regions of interest (ROIs) at (C) 0-30µm and (D) 30-60µm from the margin of each granuloma (pink masks with grey background). Only hepatocytes with >50% of their nucleus and cytoplasm in the region of interests (masks) were included in the analysis. Data were analysed to generate intensity for each individual cell using an in-house app (StrataQuest image analysis software) and exported to Microsoft Excel for further analysis.

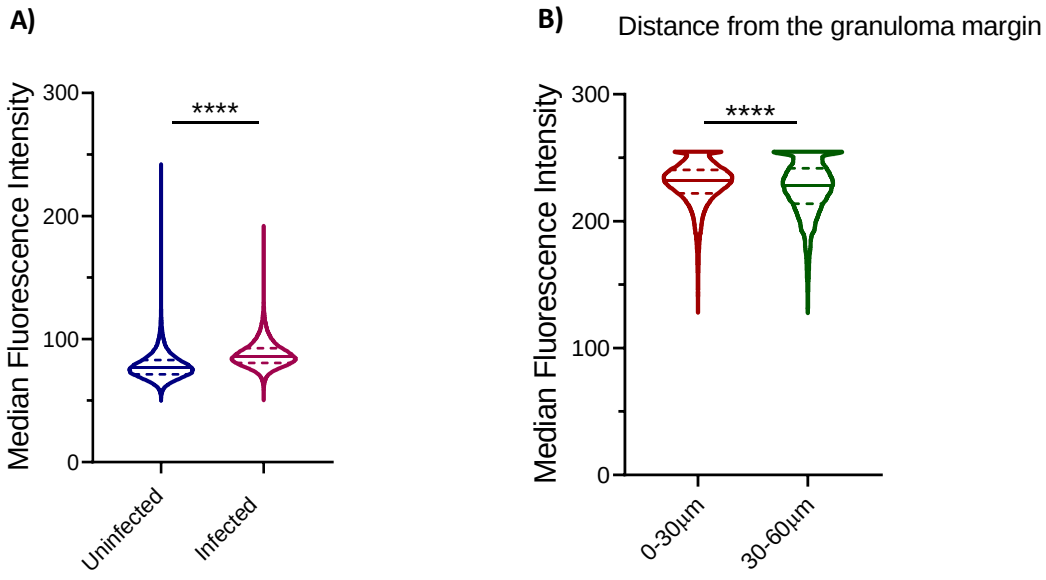

Figure 3.14 Median fluorescence intensity of TPO$^+$ hepatocytes in the whole liver and around the hepatic granulomas at various distances. Liver sections stained with anti-TPO antibody and F4/80 for Kupffer cells were analysed using StrataQuest TissueGnostics software, as explained in **Figure 3.13**. Median fluorescence intensity of TPO$^+$ hepatocytes in (A) the whole liver and (B) each region of interest around granuloma was calculated using non-parametric Mann-Whitney statistical test, ****, p <0.0001. Data show the results of the analysis of 11-38 x 10^3 hepatocytes in each ROI (region of interest) derived from n=12 uninfected liver sections of n=3 uninfected mice and n= 15 infected liver sections of n= 5 infected mice.

3.3.5 BM megakaryocytes remain responsive to thrombopoietin stimulation

As already discussed in **section 3.3.4**, the level of circulating TPO was reduced in infected mice as compared to uninfected mice at d28 of infection along with a reduction in *Thpo* mRNA accumulation in the liver and difference in the intensities of TPO producing hepatocytes. Therefore, we next evaluated the impact of increasing TPO levels on the platelet count through the administration of exogenous human recombinant-TPO (hu-rTPO). A schematic of the experiment is shown in **Figure 3.15**. For this experiment, C57BL/6 mice were infected with bioluminescent *L. donovani* amastigotes in order to allow non-invasive serial monitoring of parasite burden.

Platelet counts in uninfected mice showed a progressive increase following rTPO treatment, followed by a slight drop in the fourth week. A similar trend was observed in infected mice after treatment with rTPO and the platelet count started decreasing in the third week of infection, with mice becoming thrombocytopenic at the end of fourth week **(Figure 3.16A)**. The development of thrombocytopenia despite hu-rTPO administration could be due to the MK exhaustion or the development of antibodies against hu-rTPO. Platelet volume was lower in mice treated with rTPO in both the groups as compared to controls **(Figure 3.16B)**. However, the MPV in infected mice was slightly higher in the second week of infection but not significantly different in treated vs untreated groups after the third week of infection. Serum mu-TPO levels were measured (using a murine TPO-specific ELISA) at the end of fourth week of infection. Circulating TPO levels were decreased in uninfected rTPO treated mice as compared to uninfected controls while no significant difference in infected treated and untreated mice **(Figure 3.17A)**. No hu-TPO was detectable in murine-TPO ELISA confirming that the TPO levels are representative of mouse serum level **(Supplementary Figure 1)**.

Hepatic *Thpo* mRNA accumulation was unaltered in uninfected mice but increased in infected treated mice as compared to infected untreated mice **(Figure 3.17B).** No difference was noted in renal *Thpo* mRNA in any of the groups **(Figure 3.17C)**. Post-mortem organ weights showed an increase in the size of livers and spleens of rTPO administered mice as compared to infected and uninfected control mice (**Figure 3.17D, E & F**).

Interestingly, despite an increase in the sizes of liver and spleen of rTPO-treated infected mice, there was no significant difference in the d28 parasite burden in between these two groups (**Figure 3.18A**). There was a correlation between post-mortem spleen and liver sizes and pre-cull platelet counts at the end of fourth week suggesting that splenomegaly plays an important role in thrombocytopenia (**Figure 3.18B).** There was no noticeable difference in the counts of other blood cells in any of the groups. Other blood counts are shown in **Table 3.3** and **Table 3.4**.

In vivo imaging was performed before and weekly after infection to assess the progression of parasite load in rTPO-treated and PBS treated infected mice. This indicated no significant difference in the parasite burden in either group throughout the infection **(Figure 3.19A and B** and **Figure 3.20)**.

In order to increase the sensitivity of parasite detection, post-mortem *ex vivo* imaging of liver and spleen was also performed at d28 post-infection in all groups and these images were analysed as above (**Figure 3.21A and B**). Our data suggest that the parasite burden was slightly higher in both livers and spleens of infected mice treated with rTPO as compared to infected control mice **(Figure 3.22A and B)**.

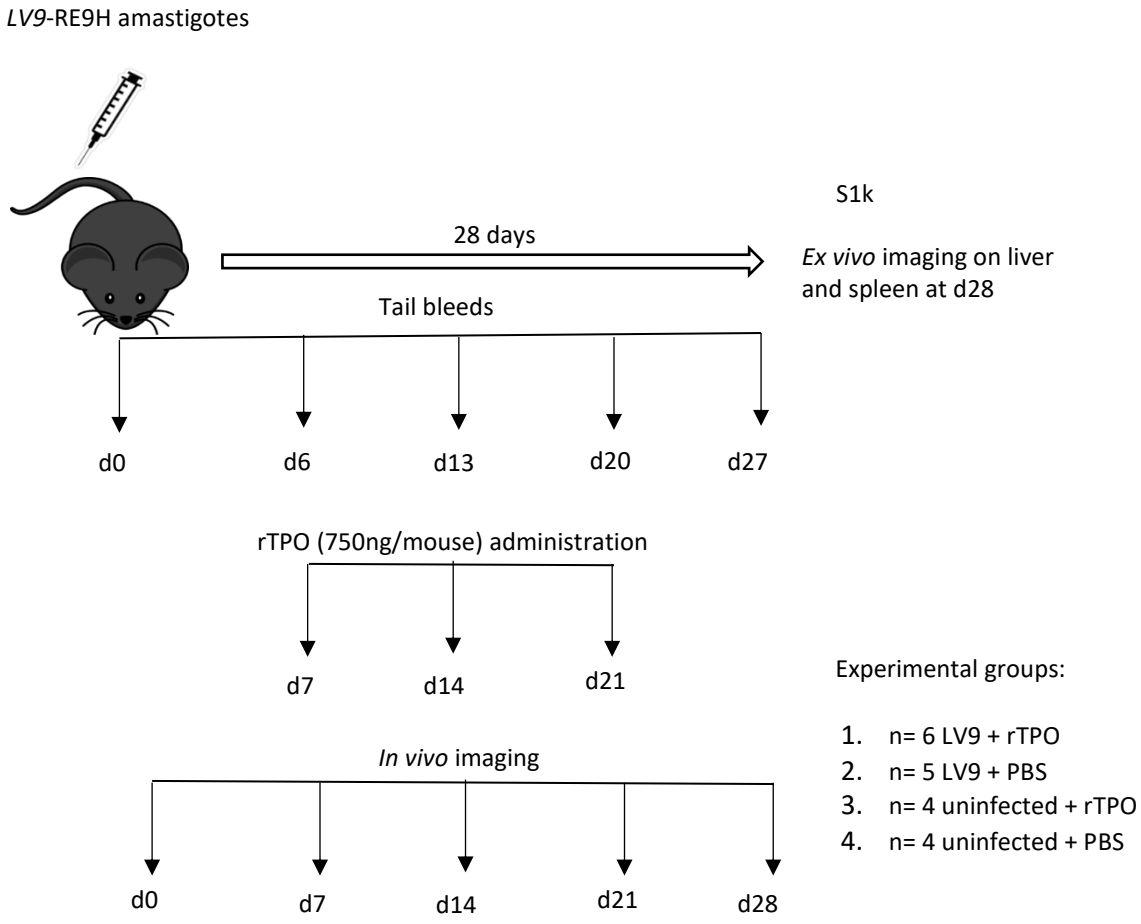

Figure 3.15 Schematic of the experiment involving exogenous administration of rTPO to mice infected with bioluminescent *L. donovani* parasites along with *in vivo* imaging. Six-eight weeks old C57BL/6 mice were infected with 3x 10^7 bioluminescent *L. donovani*-RE9H (*LV9*) amastigotes. Mice were bled before and weekly after infection for blood counts and human recombinant thrombopoietin (hu-rTPO) was administered intraperitoneally at 750ng/mouse at d7, d14 and d21 post-infection. *In vivo* imaging using the IVIS was done pre-infection and weekly post-infection (both ventral and lateral view) to estimate the parasite load throughout the course of infection. Mice were anaesthetised with Isoflurane and injected intraperitoneally with 200µl of D-Luciferin (15 mg/ml in Mg/Ca-free Dulbecco's modified PBS) and imaged after 10 minutes of injection, with 5 minutes on ventral and 5 minutes on the lateral side. *Ex vivo* imaging on livers and spleens was performed at the d28 of infection. Mice were allowed to recover from anaesthesia and monitored throughout for any signs of stress.

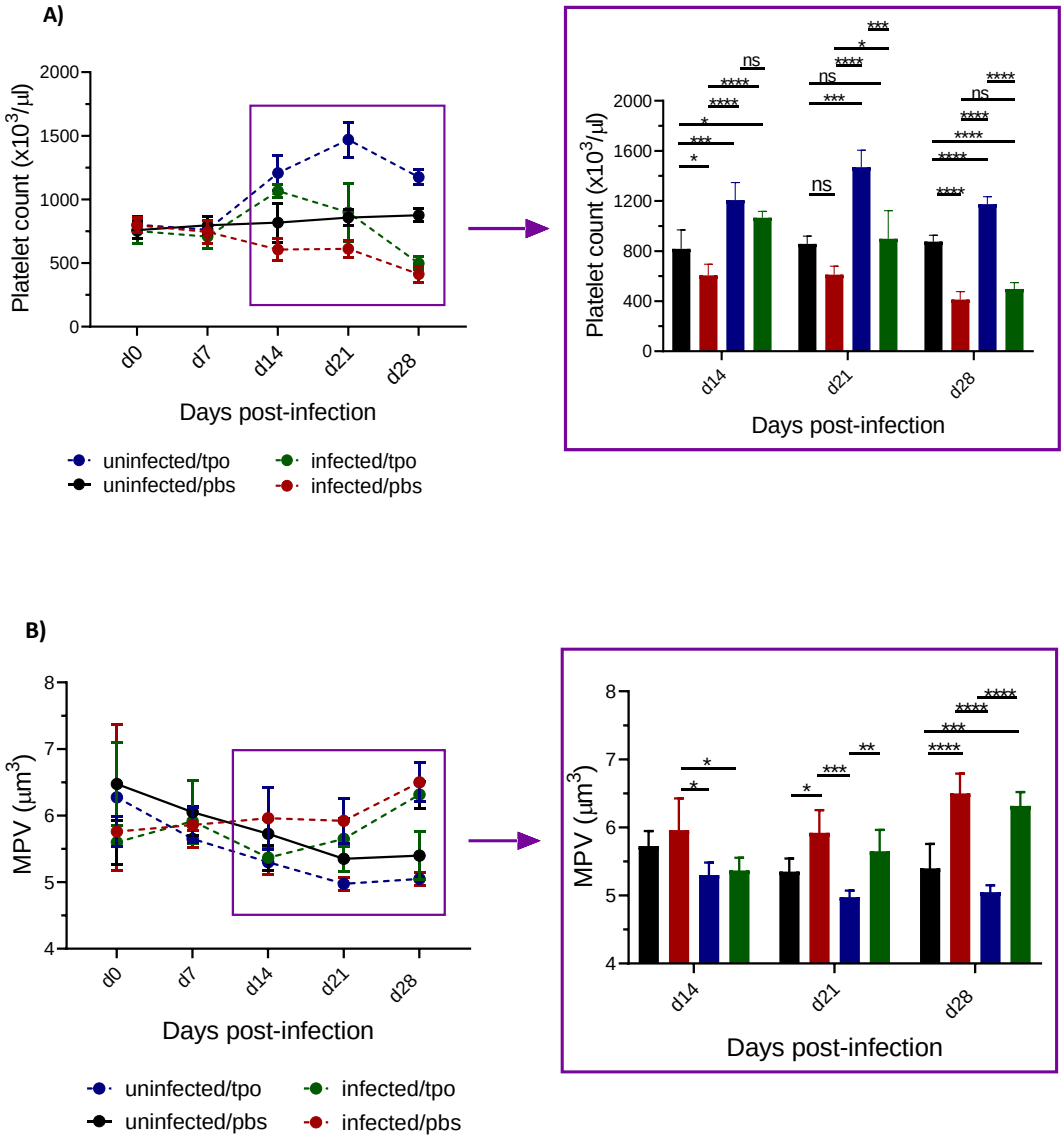

Figure 3.16 Treatment with the recombinant TPO delays the onset of thrombocytopenia in infected mice. (A) Platelet counts and (B) MPV were measured on the blood samples from uninfected and infected mice treated with 750ng rTPO or PBS. Data represent the results of a single experiment with n=5 PBS-treated infected mice and n=6 rTPO-treated infected mice, n=4 PBS-treated uninfected and n=4 TPO-treated uninfected mice. Statistical analysis done using ANOVA (with Tukey's post-hoc test) on the mean (±SD) of each group, ns, non-significant; *, $p < 0.05$; **, $p < 0.01$; ***, $p < 0.001$; ****, $p < 0.0001$.

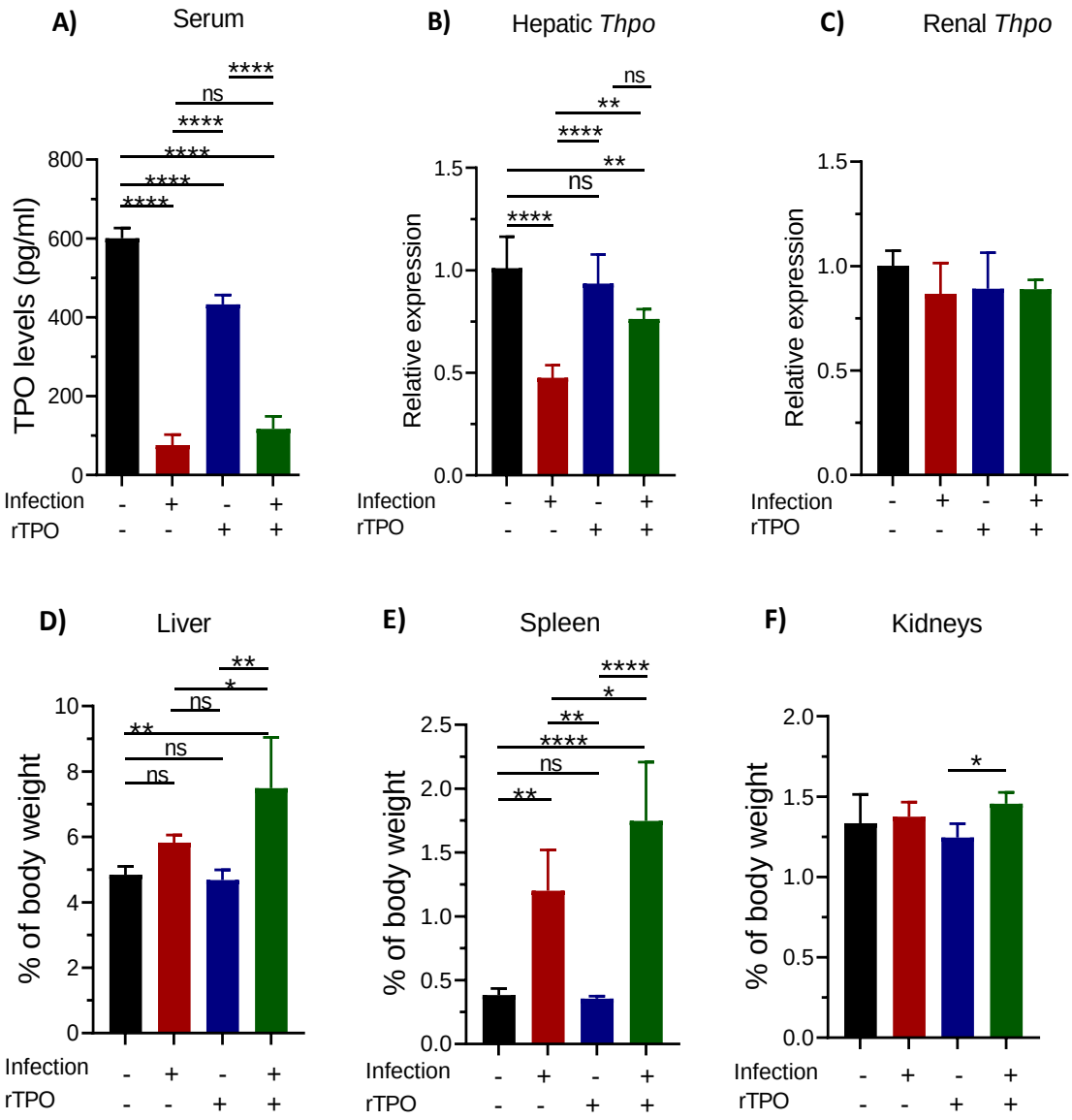

Figure 3.17 Effects of the rTPO treatment on circulating levels, tissue mRNA and tissue weights. (A) Circulating levels of TPO were measured in the serum samples of uninfected and infected mice treated with rTPO or PBS and *Thpo* mRNA accumulation in (B) hepatic and (C) renal samples (Part of the data is shown in **Figure 3.10**). Post-mortem body weight and weights of the (D) liver, (E) spleen and (F) kidneys were measured for each mouse and represented as the percentage of total body weight. Data represent the results of a single experiment with n=5 PBS-treated infected mice and n=6 rTPO-treated infected mice, n=4 PBS-treated uninfected and n=4 TPO-treated uninfected mice. Statistical analysis done using ANOVA (with Tukey's post-hoc test) on the mean (±SD) of each group, ns, non-significant; *, $p < 0.05$; **, $p < 0.01$; ****, $p < 0.0001$.

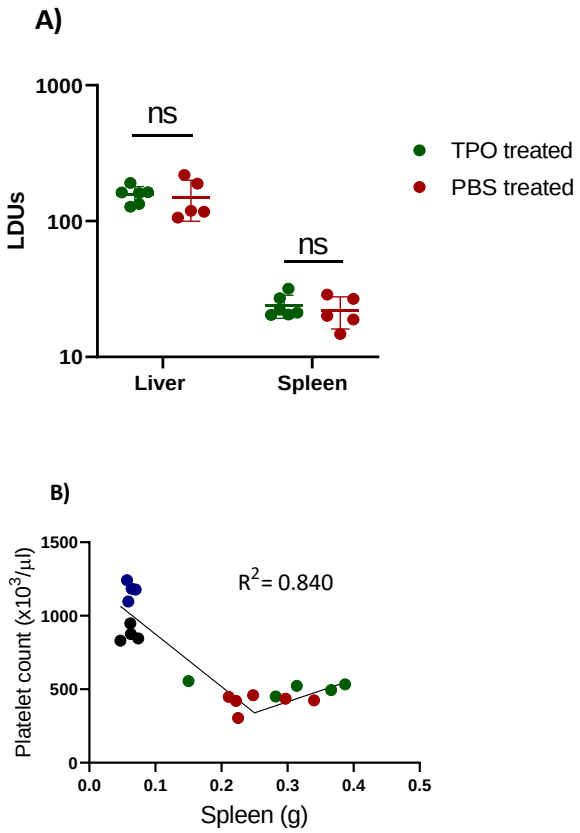

Figure 3.18 Parasite burden and the correlation between platelets and enlarged spleen. (A) Parasite burden was assessed as LDUs on impression smears of livers and spleens from d28 infected mice, treated with rTPO or PBS. Data represent the results of a single experiment with n=6 infected + TPO treated and n=5 infected + PBS treatment mice. Data analysed using unpaired t test, ns, non-significant and expressed as mean ± SD. (B) Correlation between d28 post-infection platelet count vs post-mortem spleen weight (g) of n= 6 infected + TPO treated (green dots), n= 5 infected + PBS treated (red dots), n= 4 uninfected + TPO treated (blue dots) and n=4 uninfected + PBS treated (black dots) mice. Data analysed using segmented linear regression.

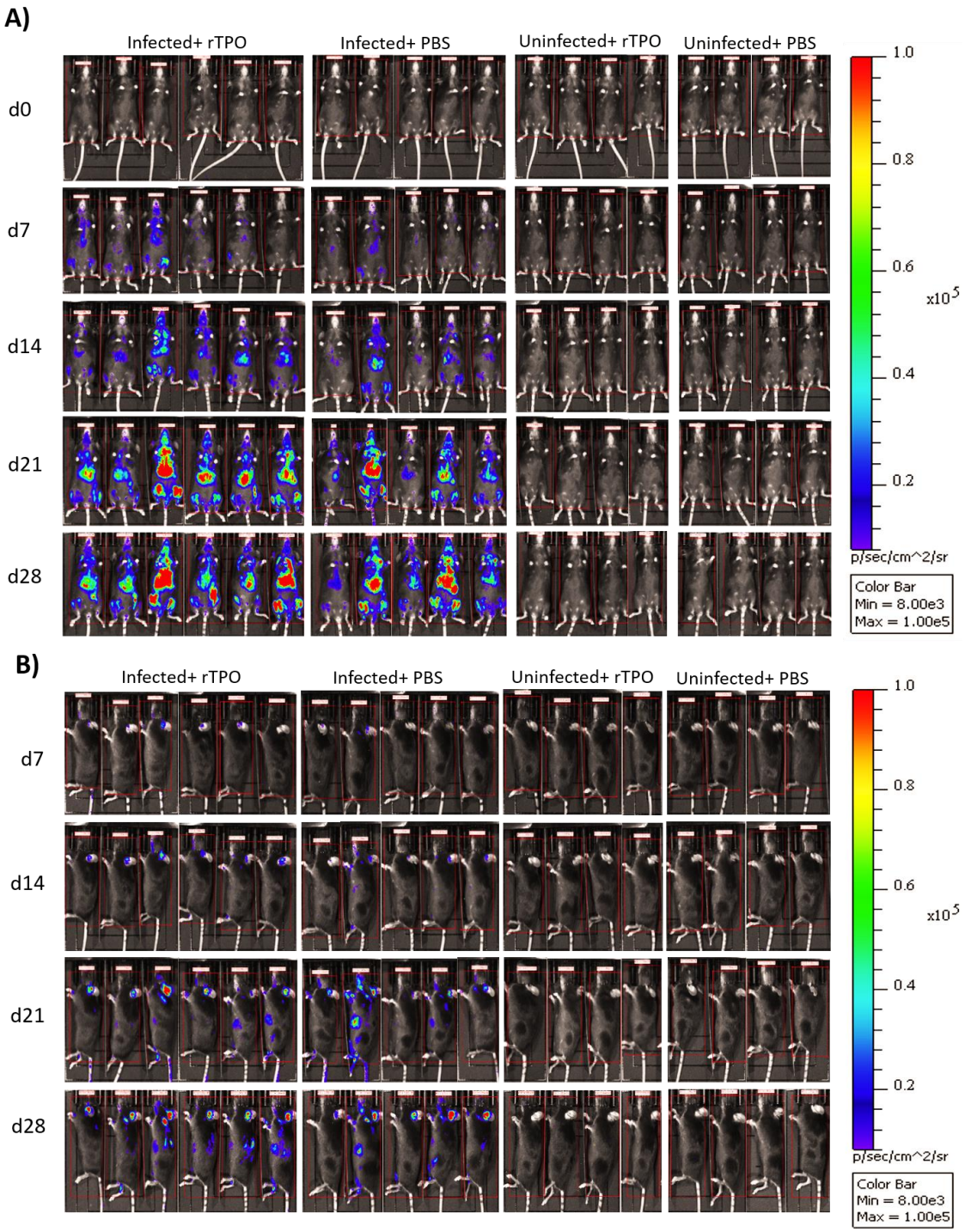

Figure 3.19 *In vivo* detection of *L. donovani* parasites in control and rTPO-treated mice. C57BL/6 mice were infected with bioluminescent *LV*9-RE9H parasites and imaged before and weekly after infection. Mice were imaged in (A) supine and (B) right lateral position to assess the parasite loads in tissues. Scale bar represents total flux = p/sec/cm^2/sr.

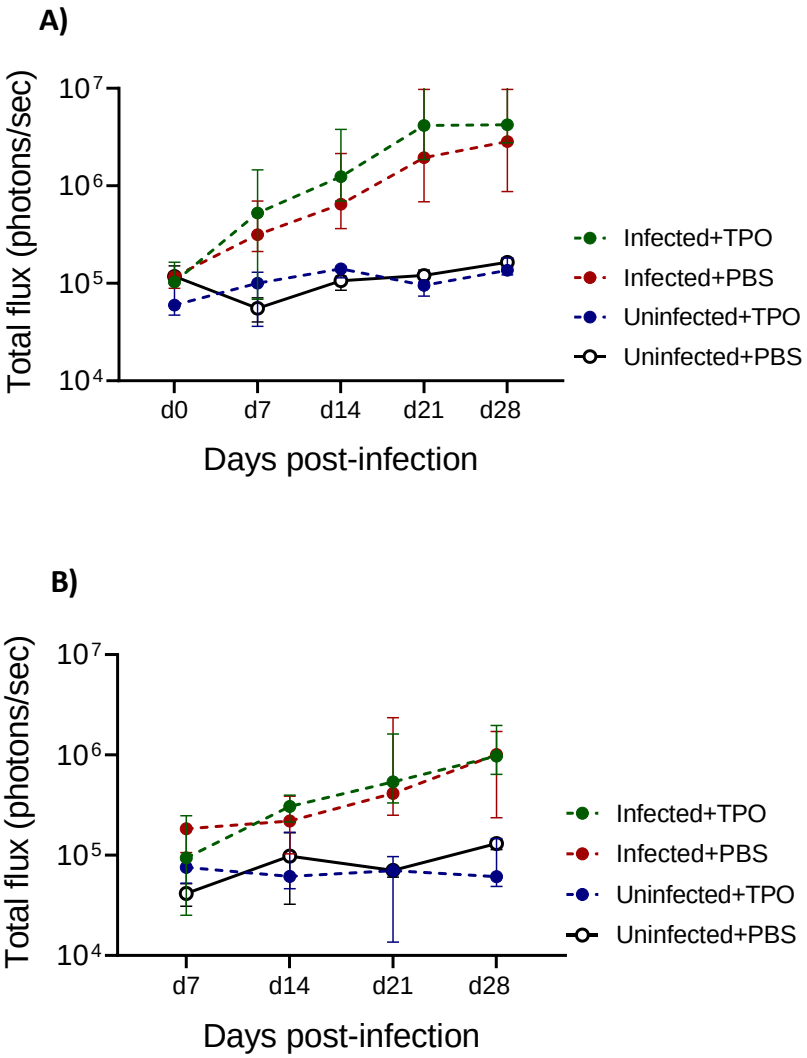

Figure 3.20 Parasite burden determined by *in vivo* imaging in mice infected with bioluminescent *L. donovani*. C57BL/6 mice were infected with bioluminescent *LV9* parasites and imaged weekly after infection along with the administration of rTPO. Data show the results of *in vivo* imaging in (A) supine and (B) right lateral positions at specified time-points of n= 6 infected + TPO treated, n=5 infected + PBS treated, n=4 uninfected + TPO treated and n=4 uninfected + PBS treated mice. Data analysed using Living Image software. No significant difference was observed in either group at any time-point throughout the experiment, represented as median with 95% confidence interval (C.I). Data are shown as total flux = number of photons per second (photons/sec) from the entire mouse.

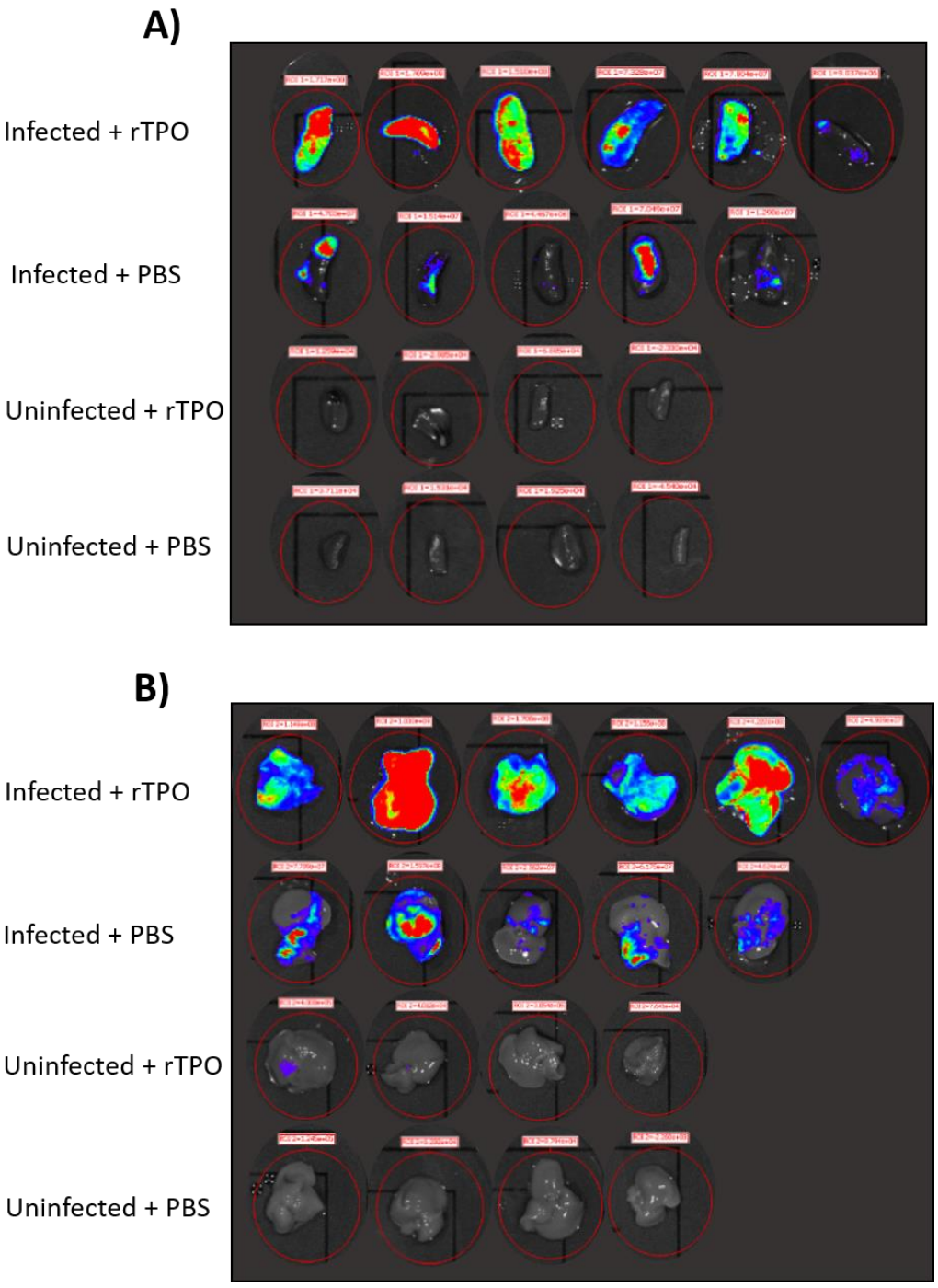

Figure 3.21 *Ex vivo* images of mice spleens and livers. Mice were sacrificed at d28 of infection and tissues were harvested. (A) Spleens and (B) livers were soaked in D-Luciferin and imaged immediately after the harvest to measure the parasite burden in all groups.

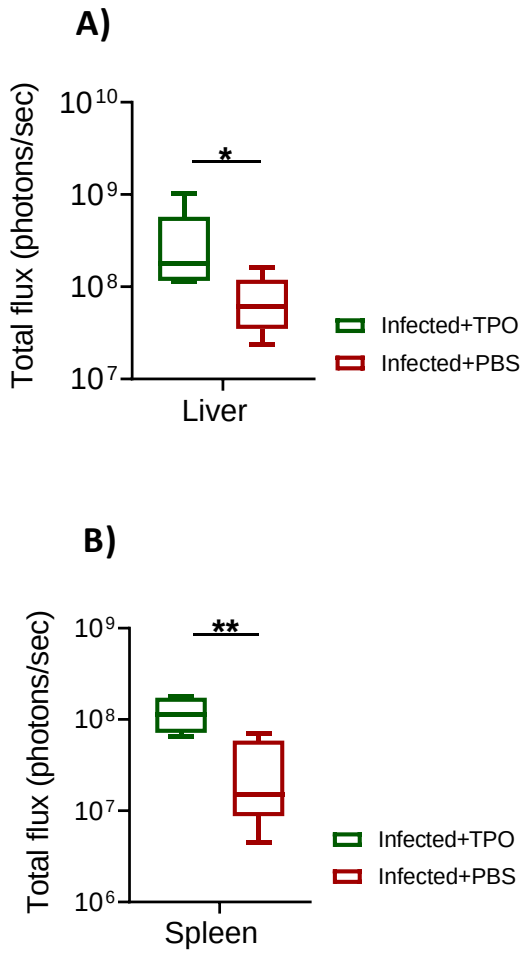

Figure 3.22 Parasite burden in infected livers and spleens. Livers and spleens were harvested and imaged *ex vivo* and the data were analysed using Living Image software. Parasite burden in (A) livers and (B) spleens were compared between infected mice treated with rTPO or PBS, shown as box and whisker plots (min to max). Data analysed using non-parametric tests Mann-Whitney in n=5 infected + PBS and n= 6 infected + TPO treated mice, *, $p < 0.05$; **, $p < 0.01$.

Table 3.3 Erythrocyte parameters in peripheral blood in infected vs uninfected mice, treated with rTPO

	Infected/TPO (mean ± SD)	**Infected** (mean ± SD)	**Uninfected/TPO** (mean ± SD)	**Uninfected** (mean ± SD)
Haemoglobin (Hb) g/dl				
d0	14.833 ± 1.958	15.300 ± 0.678	15.400 ± 0.698	14.350 ± 0.370
d7	15.483 ± 1.408	15.650 ± 0.356	15.775 ± 0.818	14.900 ± 1.054
d14	15.917 ± 0.773	15.620 ± 0.996	15.667 ± 0.611	15.750 ± 0.443
d21	15.517 ± 0.662	15.617 ± 0.637	15.825 ± 0.310	15.150 ± 0.858
d28	12.620 ± 0.545	12.920 ± 0.698	14.450 ± 0.370	13.550 ± 0.465
RBC count x 10^6/mm^3				
d0	8.628 ± 1.130	8.817 ± 0.531	8.995 ± 0.541	8.353 ± 0.357
d7	8.853 ± 0.886	8.898 ± 0.294	8.980 ± 0.535	8.573 ± 0.695
d14	9.002 ± 0.443	8.782 ± 0.686	8.877 ± 0.352	8.925 ± 0.202
d21	8.645 ± 0.378	8.738 ± 0.392	8.878 ± 0.282	8.478 ± 0.528
d28	7.698 ± 0.449	8.104 ± 0.532	9.098 ± 0.317	8.508 ± 0.358
Haematocrit (Hct) %				
d0	41.450 ± 5.766	42.583 ± 2.396	43.375 ± 2.504	41.100 ± 1.192
d7	42.200 ± 4.267	42.717 ± 1.207	43.450 ± 2.294	41.200 ± 3.105
d14	42.583 ± 2.342	41.700 ± 3.163	42.967 ± 1.617	43.125 ± 0.954
d21	40.267 ± 1.510	41.267 ± 1.573	42.525 ± 1.350	40.525 ± 2.506
d28	36.000 ± 2.682	38.100 ± 2.216	43.100 ± 1.407	40.175 ± 1.563
Mean cell volume (MCV) μm^3				
d0	47.833 ± 0.753	48.500 ± 0.548	48.250 ± 0.500	49.500 ± 1.000
d7	47.833 ± 0.408	48.000 ± 0.000	48.250 ± 0.500	48.000 ± 1.000
d14	47.167 ± 0.408	47.600 ± 0.548	48.000 ± 0.000	48.250 ± 0.500
d21	46.500 ± 0.548	47.333 ± 0.516	48.000 ± 0.000	47.750 ± 0.500
d28	46.800 ± 0.837	47.000 ± 0.707	47.500 ± 0.577	47.250 ± 0.500
Mean cell haemoglobin (MCH) pg				
d0	17.183 ± 0.279	17.367 ± 0.418	17.150 ± 0.332	17.175 ± 0.395
d7	17.467 ± 0.216	17.567 ± 0.320	17.550 ± 0.129	17.367 ± 0.208
d14	17.717 ± 0.232	17.820 ± 0.327	17.700 ± 0.173	17.600 ± 0.283
d21	17.967 ± 0.294	17.867 ± 0.234	17.825 ± 0.250	17.875 ± 0.330
d28	16.420 ± 0.497	15.980 ± 0.319	15.875 ± 0.287	15.925 ± 0.206
Mean cell haemoglobin concentration (MCHC) g/dl				
d0	35.833 ± 0.653	35.820 ± 0.698	35.525 ± 0.714	34.925 ± 0.250
d7	36.733 ± 0.505	36.580 ± 0.540	36.300 ± 0.141	36.100 ± 0.400
d14	37.417 ± 0.392	37.440 ± 0.564	36.500 ± 0.346	36.475 ± 0.299
d21	38.533 ± 0.659	37.780 ± 0.512	37.225 ± 0.591	37.375 ± 0.377
d28	35.160 ± 1.297	34.120 ± 0.705	33.575 ± 0.457	33.750 ± 0.379
Red blood cell distribution width (RDW) %				
d0	18.217 ± 0.717	18.700 ± 0.430	19.800 ± 2.712	21.950 ± 0.645
d7	18.050 ± 0.302	18.280 ± 0.383	18.325 ± 0.818	19.800 ± 0.700
d14	17.717 ± 0.349	17.580 ± 0.110	17.900 ± 0.608	17.875 ± 0.532
d21	17.700 ± 0.237	17.940 ± 0.541	17.250 ± 0.404	17.075 ± 0.320
d28	18.833 ± 1.167	18.580 ± 0.476	17.900 ± 0.424	17.500 ± 0.356

Table 3.4 Leucocyte counts in peripheral blood in infected vs uninfected mice, treated with rTPO

	Infected/TPO (mean ± SD)	**Infected** (mean ± SD)	**Uninfected/TPO** (mean ± SD)	**Uninfected** (mean ± SD)
WBC count (x 10^3/mm^3)				
d0	7.217 ± 1.225	7.120 ± 1.537	8.700 ± 1.058	8.475 ± 1.220
d7	8.150 ± 1.821	7.320 ± 1.078	8.525 ± 1.053	7.400 ± 1.652
d14	8.920 ± 0.766	6.380 ± 0.850	7.475 ± 0.763	7.025 ± 0.250
d21	8.300 ± 0.456	7.700 ± 1.279	8.450 ± 0.911	7.800 ± 0.920
d28	7.300 ± 1.375	7.225 ± 1.621	7.425 ± 0.763	8.275 ± 2.156
Lymphocyte count (x 10^3/mm^3)				
d0	5.917 ± 1.120	5.640 ± 1.361	7.700 ± 1.705	7.025 ± 0.793
d7	6.083 ± 1.520	5.120 ± 0.853	6.425 ± 0.741	6.775 ± 1.839
d14	6.300 ± 1.262	4.825 ± 0.776	5.900 ± 0.356	5.900 ± 0.183
d21	6.033 ± 0.427	5.660 ± 0.924	6.450 ± 0.806	6.150 ± 0.823
d28	5.940 ± 0.829	5.625 ± 1.569	5.775 ± 0.695	7.433 ± 1.617
Monocyte count (x 10^3/mm^3)				
d0	0.283 ± 0.041	0.300 ± 0.071	0.375 ± 0.050	0.300 ± 0.000
d7	0.367 ± 0.103	0.360 ± 0.055	0.300 ± 0.082	0.300 ± 0.100
d14	0.367 ± 0.052	0.240 ± 0.055	0.267 ± 0.058	0.200 ± 0.000
d21	0.333 ± 0.052	0.280 ± 0.084	0.325 ± 0.050	0.200 ± 0.000
d28	0.280 ± 0.084	0.300 ± 0.000	0.375 ± 0.050	0.233 ± 0.058
Neutrophil count (x 10^3/mm^3)				
d0	1.017 ± 0.232	1.217 ± 0.248	1.625 ± 0.450	1.150 ± 0.451
d7	1.700 ± 0.283	1.900 ± 0.268	1.800 ± 0.455	1.275 ± 0.310
d14	1.833 ± 0.356	1.517 ± 0.117	1.350 ± 0.379	0.925 ± 0.250
d21	1.933 ± 0.186	1.750 ± 0.315	1.675 ± 0.320	1.450 ± 0.129
d28	1.383 ± 0.349	1.233 ± 0.186	1.275 ± 0.126	1.200 ± 0.337
Eosinophil count (x 10^3/mm^3)				
d0	0.055 ± 0.016	0.060 ± 0.017	0.198 ± 0.289	0.160 ± 0.181
d7	0.107 ± 0.055	0.115 ± 0.062	0.108 ± 0.075	0.058 ± 0.005
d14	0.083 ± 0.022	0.085 ± 0.067	0.080 ± 0.039	0.040 ± 0.008
d21	0.093 ± 0.012	0.068 ± 0.023	0.075 ± 0.026	0.068 ± 0.022
d28	0.077 ± 0.024	0.067 ± 0.008	0.073 ± 0.017	0.060 ± 0.016

3.4 Discussion

Haematological complications are commonly seen in infections which mainly includes anaemia, thrombocytopenia or even pancytopenia. Infection with *L. donovani* presents as VL in both humans and rodents which includes haematological complications along with immune dysregulation and systemic effects (96). Anaemia and thrombocytopenia are widely reported in clinical and experimental studies but the mechanisms are poorly understood. Studies conduction in experimental models have proposed various mechanisms from HSC exhaustion to dysregulated erythropoiesis as the cause of anaemia in VL (99,101). In addition, splenic phagocytosis has been shown to play an important role in anaemia, due to excessive phagocytosis of erythrocytes by activated red pulp macrophages (126). Thrombocytopenia is a prominent haematological feature, seen in VL patients and rodents at a variable range in different regions of the world. Similar to anaemia, thrombocytopenia is either primary driven by impaired BM production or enhanced splenic sequestration and destruction (96). The usual laboratory definition of thrombocytopenia is of a platelet count below 150 x 10^3/µl, though it varies slightly depending on the region.

Although varying degrees of thrombocytopenia and coagulopathy are seen in infected patients, the correlation between these is not fully understood. Some postulate that this is due to thrombocytopenia or abnormal clotting secondary to liver involvement (185). Although spontaneous bleeding occurs only when the platelet count drops below 10-20 x 10^3 /µl, systemic diseases with multi-organ involvement have been associated with bleeding without very low platelet counts (43). Acute VL mainly involves the liver but is generally asymptomatic and patients are diagnosed with chronic disease and sometimes at a much progressed stage. Therefore, it is very hard to study the mechanisms of haematological complications, including coagulopathies, in humans from the onset. Not surprisingly, therefore, few clinical studies have been conducted to explore the mechanisms of anaemia and thrombocytopenia in VL infection. The difficulties are further compounded by ethical challenges and need for technical expertise and facilities often lacking in VL endemic countries. Therefore, we were interested to study the mechanisms responsible for thrombocytopenia in detail using a murine model of VL. Experimental murine models of VL have been widely used to study different aspects of the infection at both acute and chronic phase of infection and have been shown to

reproduce some though not all aspects of human disease. In EVL, mice are infected for 28 days which shows the features consistent with the beginning of chronic human VL. Mild to severe thrombocytopenia has been seen in the human VL cases and is also apparent in EVL. Thrombocytopenia could either be due to impaired BM production or excessive splenic clearance of platelets. However, the role of liver cannot be neglected given its role as the major producing organ for TPO. Here, we have taken a multi-organ holistic approach to addressing whether infection affects platelet production and the data provided in this chapter advance our understanding in a number of ways.

First, we show that infected C57BL/6 mice develop progressive thrombocytopenia with the presence of giant platelets in circulation. Although earlier work had suggested that the number of MKs was similar in control and infected mice (O. Preham thesis; http://etheses.whiterose.ac.uk/13654/), we now show using more sensitive ultrastructural techniques that MKs in infected mice have a defect in the DMS. Defective MKs with reduced DMS have been seen in congenital thrombocytopenic disorders. Furthermore, we have shown that these membranes are recoverable after stimulation of MKs to produce platelets as evident by the increased territories of newly developing platelets, by employing a novel approach of co-induction of ITP with anti-CD41 antibodies on the background of chronic infection with *L. donovani*. Infected mice showed a similar pattern of platelet count recovery as uninfected mice suggesting i) that the MKs retain their functional capability and ii) other factors contribute to keeping the number of circulating platelets low.

Second, we have shown that BM MKs in infected mice respond directly to stimulation with recombinant-huTPO. The onset of thrombocytopenia in infected mice was delayed on rTPO stimulation suggesting that the MKs were effectively producing platelets at higher than normal rate. Though there were changes in the sizes of liver and spleen along with circulating TPO levels and hepatic mRNA, no difference in the progression of infection was noted.

Third, different lines of evidence indicated that infection was associated with alteration in TPO production in the liver. Total hepatic mRNA accumulation was decreased, though this may reflect an influx of inflammatory cells leading to dilution of hepatocyte mRNA representation. This interpretation was supported by a reduction in the number of TPO-expressing hepatocytes as judged by immunohistology. The levels of circulating TPO correlate inversely with the number of platelets but we found a significant decrease in the levels of circulating TPO in infected mice at d28 post-infection. Platelets and MKs

express a high-affinity receptor for TPO, c-Mpl or TPO-R. Platelets bind to unbound TPO in the circulation which then regulates the production of TPO from the hepatocytes. Therefore, a decrease in the number of platelets would normally result in an increase in the level of TPO in the blood. However, in platelet disorders such as ITP, the level of TPO remains within the normal range despite thrombocytopenia (186). In contrast, increased TPO levels are found in aplastic anaemia which presents with thrombocytopenia and bone marrow failure (186). Interestingly, our results show a reduction in the number of TPO^+ hepatocytes most probably due to the architectural changes as a result of granuloma formation. The median fluorescence intensity of the TPO was higher in the hepatocytes closer to the margin of granuloma as compared to the hepatocytes away from granulomas, suggesting the role of cytokines produced by inflammatory cells in the activation of the JAK-STAT signalling pathway, needed for TPO transcription in the hepatocyte nucleus. This represents the first description of spatial regulation of TPO production occurring during liver infection.

Finally, we have shown for the first time, the impact of selectively modulating platelet production by exogenous TPO administration on the parasite burden during infection. Although thrombocytopenia is associated with VL, it was not known whether this affected host resistance to infection in any way. The experiments conducted here, though preliminary, suggest that total parasite load as determined by *in vivo* imaging is unaltered by rTPO administration even though the thrombocytopenia is retarded in its progression. Nevertheless, *ex vivo* imaging indicated a significant elevation of parasite load in the two main target tissues for infection, spleen and liver. This result suggests that platelets may also impact on host resistance mechanisms by as yet unidentified mechanisms, in keeping with an increasing awareness of their role as innate immune effectors.

Together our data suggest that the thrombocytopenia in VL is progressive with complicated pathophysiology. Defective BM MKs and impaired TPO production from the infected liver play a major role in thrombocytopenia however, these effects do not result in permanent damage to the BM MK compartment. Despite the obvious defects in the production of platelets in VL, excessive clearance of platelets cannot be neglected as seen in other infections therefore, we wished to determine the role of splenic and hepatic clearance mechanism in details. The role of splenic macrophages in clearing antibody bound platelets and platelet desialylation are discussed in **Chapter 4**.

Chapter 4. Splenic clearance and thrombocytopenia in visceral leishmaniasis

4.1 Introduction

Infection with *L. donovani* results in splenomegaly with characteristic increase in red pulp (RP) macrophages harbouring the parasites in them. Splenic macrophages are well known for their phagocytic capabilities, remove old or damaged blood cells especially erythrocytes allowing iron to be recycled for erythropoiesis (130,131). Splenomegaly and hypersplenism have been described to play an important role in disease-related cytopenias and have been well-studied in the context of infections with haematological complications (187,188).

Normal splenic architecture (discussed in **Chapter 1**) is important for defence against blood-borne infections and to maintain the blood cells within their normal range. Briefly, the RP comprises mainly of F4/80^{+} macrophages with highly phagocytic properties and involved in the removal of aberrant red blood cells (127). The white pulp (WP) comprises predominantly of lymphocytes i.e. B and T cells and some other immune cells (126). The marginal zone separates the WP from the RP and is composed of CD169^{+} marginal metallophilic macrophages (MMMs) and SIGNR1^{+} marginal zone macrophages (MZMs), as well as subsets of B cells and other lymphocytes. Both MMMs and MZMs have been associated with the filtration of microbes entering the spleen (127).

In experimental VL, spleen enlargement along with the destruction of the normal microarchitecture is a common finding (146). Disruption of the splenic microarchitecture and parasite harbouring RP macrophages could be responsible for altered immune functions as well as excessive clearance of blood cells by activated RP macrophages (189). Although the role of spleen is well-studied in infection-induced anaemia including VL, thrombocytopenia due to splenic clearance remains poorly understood. *L. donovani* infection in splenectomised mice results in less severe thrombocytopenia as compared to sham-operated mice suggesting the role of spleen in the destruction of platelets (O. Preham thesis; http://etheses.whiterose.ac.uk/13654/).

Immune thrombocytopenia (ITP) is an immune-mediated disorder which presents as isolated thrombocytopenia (190). The presence of antibodies against platelets, the role

cytotoxic $CD8^+$ T cells and platelet desialylation have been suggested to play a key role in the causation of thrombocytopenia in ITP (191,192). Antibodies against platelets have also been observed in various infections and ITP secondary to infection may be due to excessive clearance by macrophages and resultant thrombocytopenia (193).

Platelet clearance by hepatocytes is another way of removal of old platelets from the circulation. Platelets become desialylated due to loss of terminal sialic acid exposing galactose residues which can bind to the hepatic AMR (61). Binding of the desialylated platelets to AMR activates the JAK-STAT signalling pathway which is vital for the transcription and production of TPO by hepatocytes. Excessive desialylation of platelets leading to enhanced clearance has been studied in platelets stored at lower temperatures and sepsis but their effect on TPO production, especially in infection, is poorly understood (61,194). The role of TPO has been discussed in detail in **Chapter 3**.

In this study, we were interested to determine the role of splenic macrophages on platelet clearance by depleting the tissue macrophages post-infection, flow cytometric analysis for the presence of antibodies against platelets in infected mice and the effects of *L. donovani* infection on platelet desialylation.

4.2 Aims

The main aims of this study were to explore the role of the following factors in the clearance of platelets in VL-induced thrombocytopenia.

1. To characterise the role of splenic macrophages in platelet clearance
2. To determine the role of anti-platelet antibody-mediated clearance of platelets
3. To compare the levels of platelets desialylation in *L. donovani*-infected and uninfected control mice

4.3 Results: Macrophage depletion

Previously, it has been shown that splenectomy reduces the extent of thrombocytopenia when compared to sham-operated infected mice, suggesting a role of spleen in VL induced thrombocytopenia (O. Preham thesis; http://etheses.whiterose.ac.uk/13654/). In this study, splenectomy was performed prior to infection but no change in the baseline platelet counts of mice was noticed. Although the effect of infection on thrombocytopenia could be studied better by performing splenectomy after infection, surgical interventions at this time are likely to significantly affect ongoing immune responses. Therefore, we attempted macrophage depletion in C57BL/6 mice infected with *L. donovani* as a more targeted approach to evaluate the role of macrophages in platelet clearance. Based on published approaches (195,196), the experimental scheme is summarised in **Figure 4.1**. Infected and uninfected mice were randomised into groups and treated with either liposomal clodronate or empty (PBS) liposomes on alternate days and bled for blood counts and post-mortem tissue analysis **(Figure 4.1)**.

4.3.1 Histological confirmation of tissue macrophage depletion

In order to confirm the depletion of tissue macrophages, frozen sections of the livers and spleens were stained with immunofluorescent (IF) macrophage markers followed by segmentation image analysis.

Spleen and liver frozen sections were stained with F4/80 antibody for RP macrophages in the spleen and Kupffer cells in the liver. Additionally, spleen sections were stained with anti-CD169 and SIGNR1 antibodies for MMM and MZM macrophages respectively (detail of antibodies in **Chapter 2**). Images were collected on a slide scanner (AxioScan) using Zeiss ZenBlue software.

There was a clearly visible depletion of tissue macrophages, including MZM, MMM and RP macrophages in uninfected mice spleens treated with liposomal clodronate as compared to uninfected mice treated with PBS liposomes (**Figure 4.2A and B)**. Infection-induced architectural changes had already resulted in significant disruption to the MMM and MZM populations. However, no difference was noticed in the abundance of RP

macrophages in spleens from infected mice treated with liposomal clodronate compared to those from PBS treated infected mice (**Figure 4.2C and D)**.

Liver sections of the infected and uninfected mice treated with clodronate or PBS showed similar results. There was near complete depletion of Kupffer cells in clodronate treated uninfected mice (**Figure 4.3A and B)** with no observable difference in infected clodronate treated mice (**Figure 4.3C and D)**.

To confirm this subjective analysis, we used quantitative segmentation-based image analysis using StrataQuest TissueGnostics image analysis software. There was no significant difference in the area (mm^3) and perimeter (mm) of tissue sections **(Figure 4.4A-D**). No difference in the number of macrophages was seen between infected clodronate vs PBS treated groups, in contrast to the situation in uninfected mice **(Figure 4.5A-C**). Similar findings were seen in the liver images analysis **(Figure 4.5D)**.

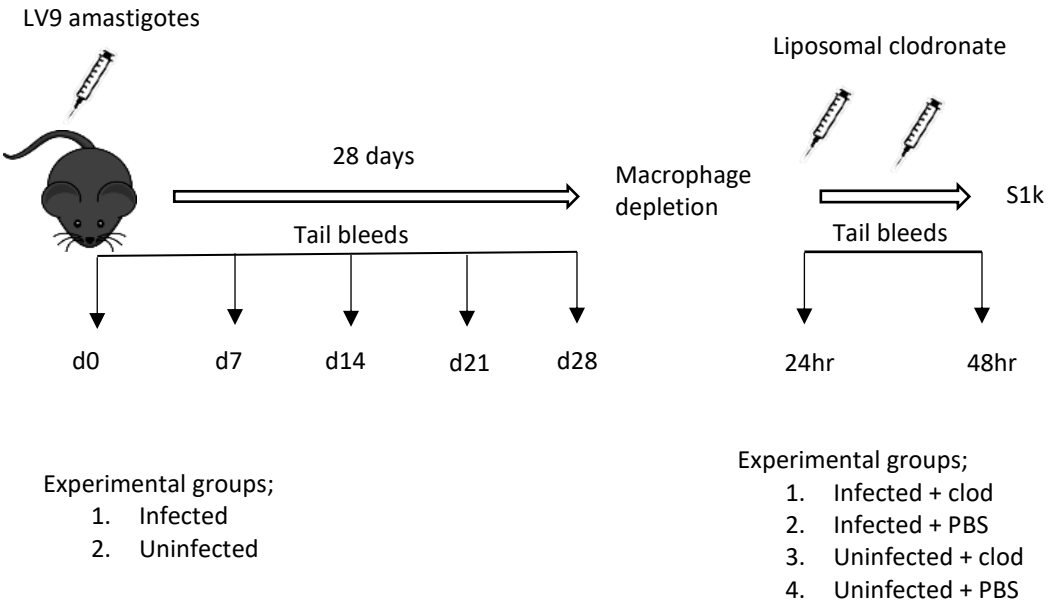

Figure 4.1 Schematic of experiment showing the strategy to deplete tissue macrophages. C57BL/6 mice were infected with *L. donovani* for 28 days and bled before and weekly after infection for blood counts. Uninfected and infected mice were treated with two doses (8µl/g; 40µg/g body weight) of clodronate or PBS (empty) liposomes on alternate days and bled 24 hours post-clodronate treatment. Mice were killed after 48 hours and tissues were harvested for further analysis.

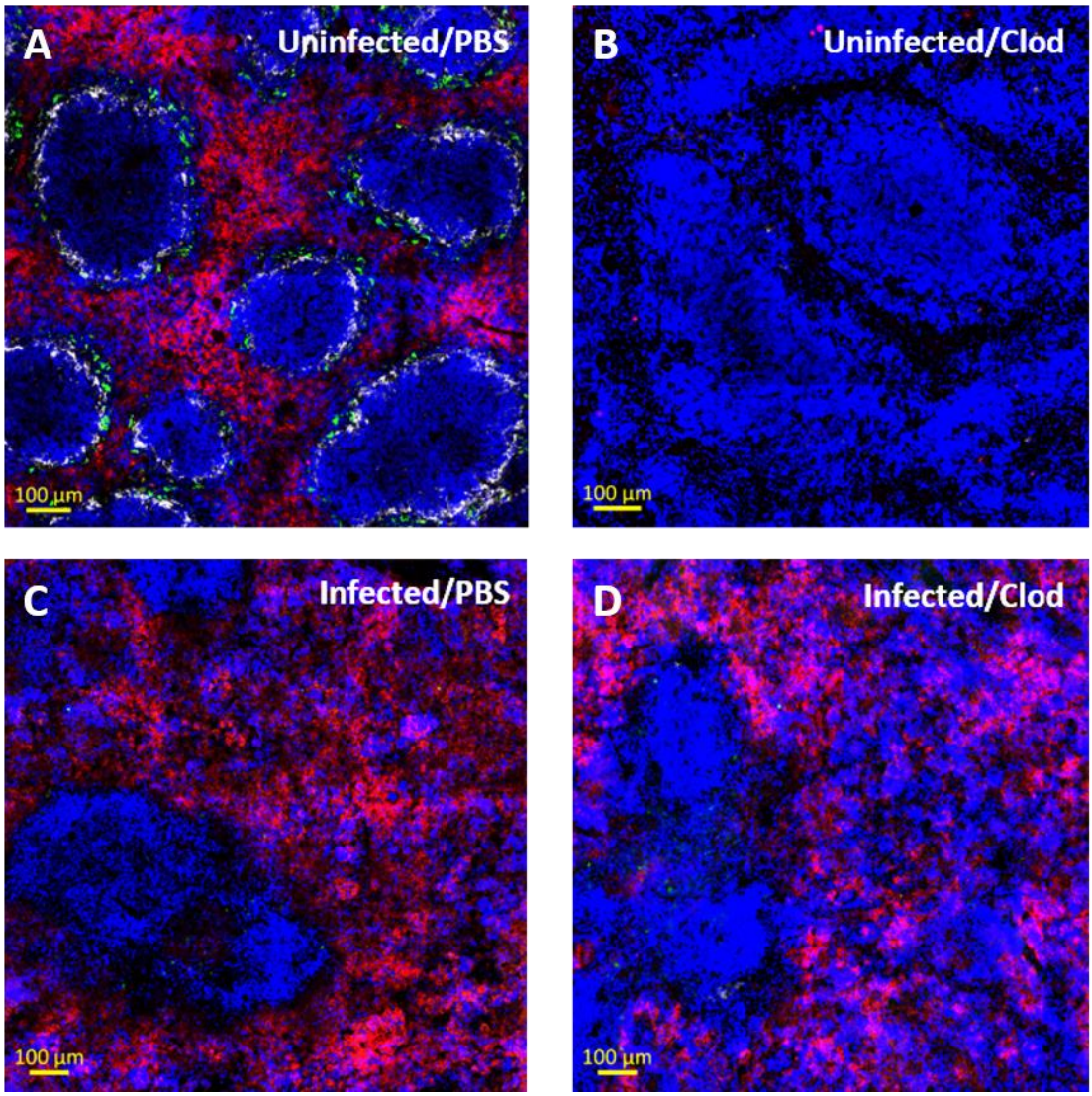

Figure 4.2 Representative IF stained spleen images of clodronate treated mice. Frozen spleen sections (8-10µm thickness) of uninfected (A & B) and infected (C & D) mice treated with PBS or clodronate liposomes were stained with macrophage markers. Tissue sections were stained with F4/80 for splenic RP macrophages (red), anti-CD169 (white) and SIGNR1 (green) for splenic MMM and MZM, respectively. Tissue sections were counterstained with DAPI for nuclei (blue). Images were collected on AxioScan Slide scanner using 20x lens. Scale bar, 100µm; Clod= clodronate liposomes treated, PBS= empty liposomes treated.

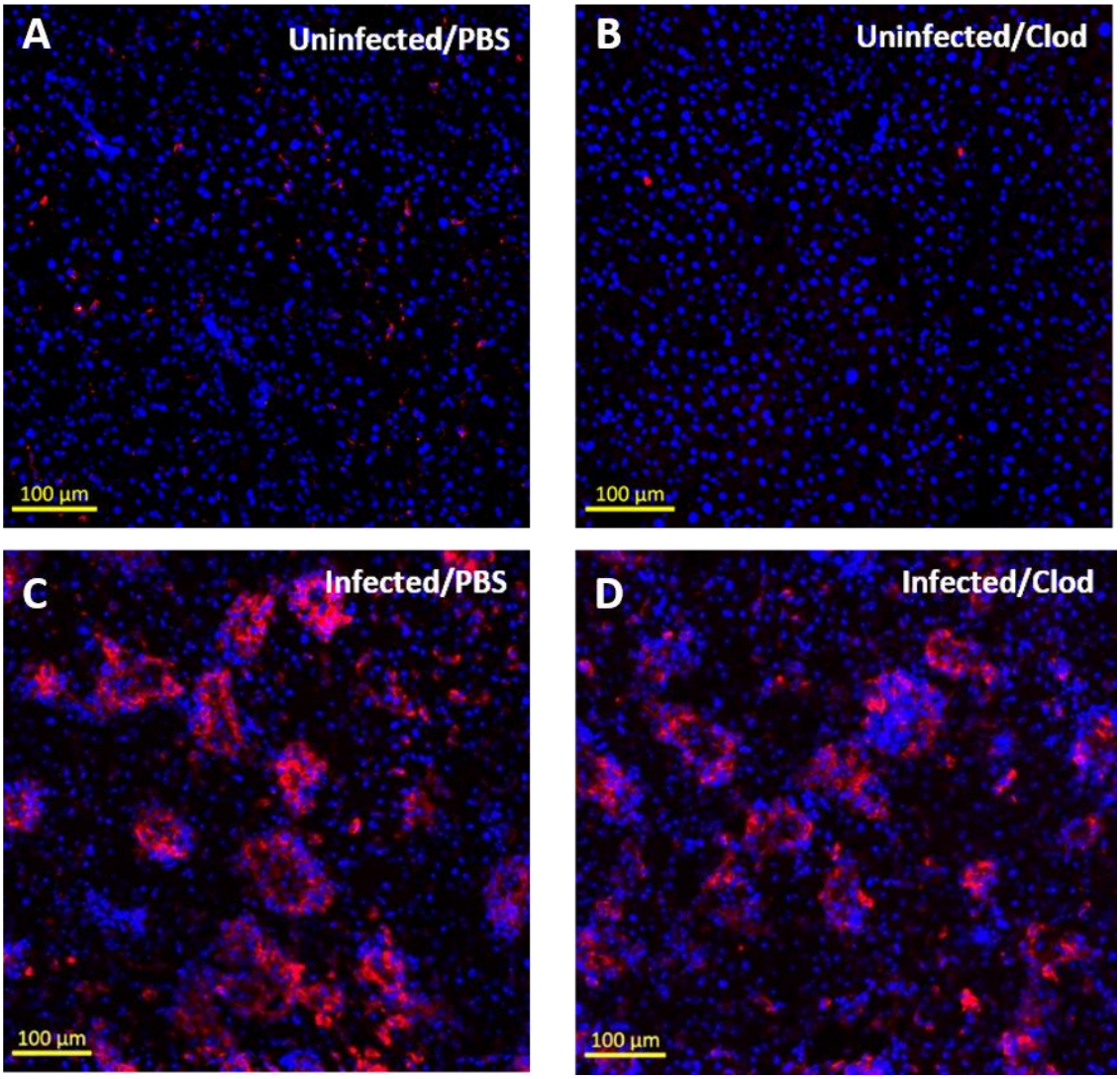

Figure 4.3 Representative IF stained liver images of clodronate treated mice. Frozen liver sections of uninfected (A & B) and infected (C & D) mice treated with PBS or clodronate liposomes were stained with F4/80 for Kupffer cells (red). Tissue sections were counterstained with DAPI for nuclei (blue). Images were collected on AxioScan Slide scanner using 20x lens. Scale bar, 100µm; Clod= clodronate liposomes treated, PBS= empty liposomes treated.

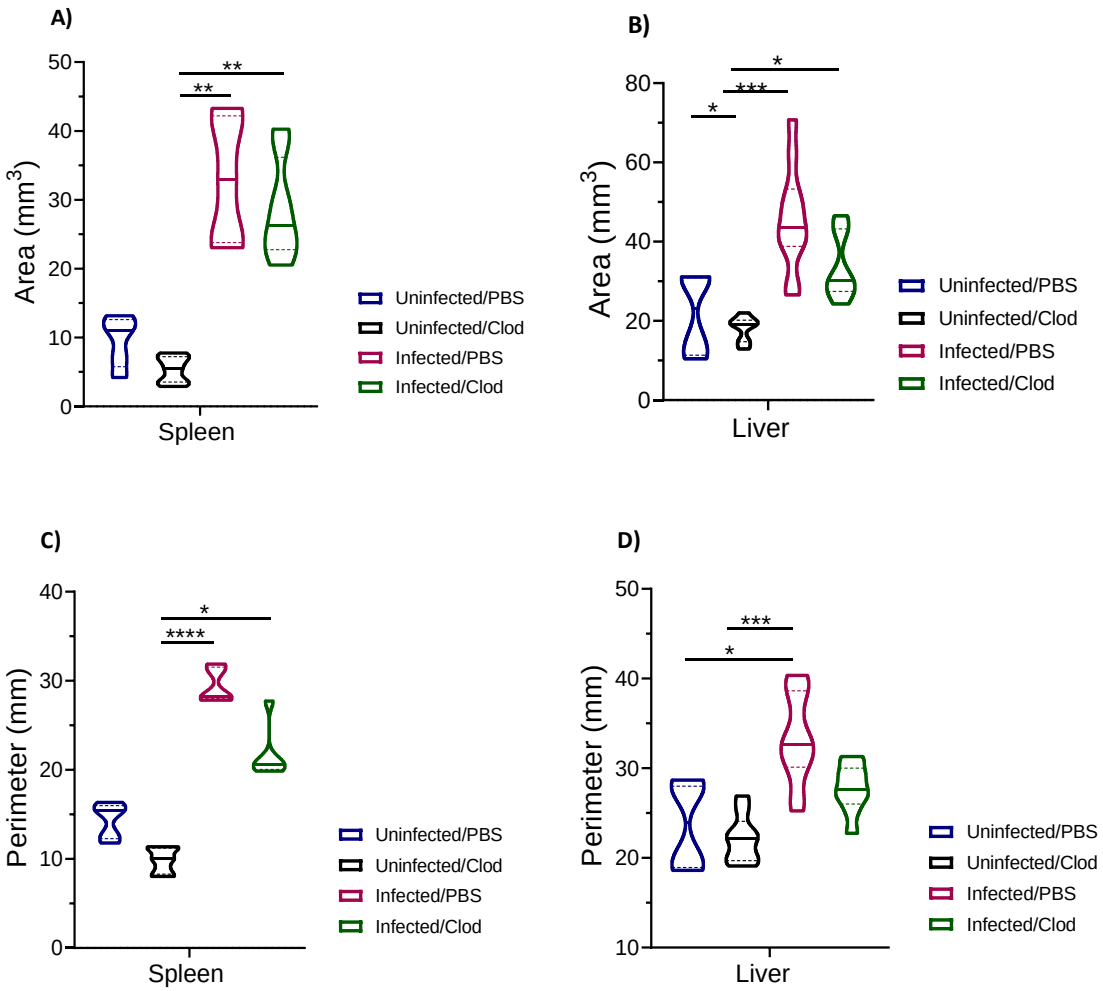

Figure 4.4 Changes in area and perimeter of spleens and livers after clodronate treatment. Image segmentation analysis was done on the spleen and liver sections of uninfected and infected mice treated with clodronate or PBS liposomes. Area of (A) spleens and (B) livers, and perimeter of (C) spleens and (D) livers was calculated by drawing outlines around the stained tissue sections, using StrataQuest TissueGnostics image analysis software. Data show the results of n= 3 uninfected/PBS, n= 3 uninfected/clod, n= 4 infected/PBS and n= 5 infected/Clod mice with 2-3 tissue sections/mouse. Data represent the median with quartiles and analysed using Kruskal-Wallis with post-hoc Dunn's test. *, $p < 0.05$; **, $p < 0.01$; ***, $p < 0.001$; ****, $p < 0.0001$.

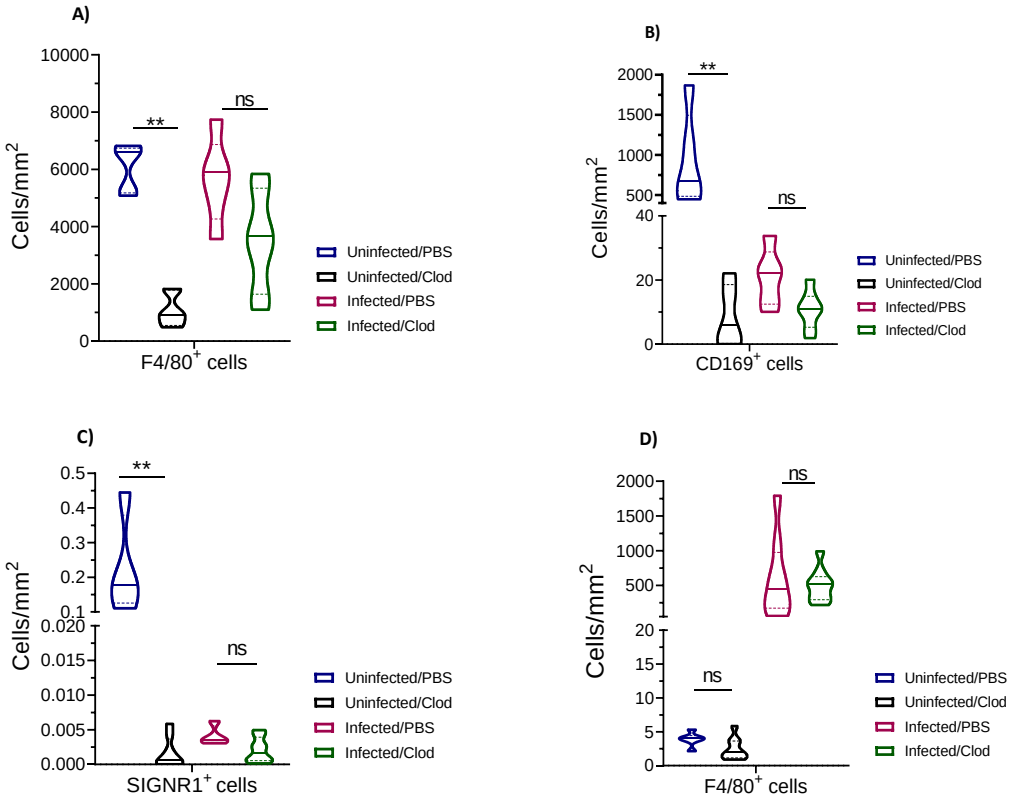

Figure 4.5 Tissue macrophages in response to clodronate treatment. IF stained spleen and liver frozen sections were analysed for macrophage depletion using tissue segmentation analysis. Image analysis was done on cell count/unit area of spleen sections for (A) F4/80$^+$ RP macrophages, (B) CD169$^+$ MMM and (C) SIGNR1$^+$ MZM and on liver sections for (D) F4/80$^+$ Kupffer cells. Data represent the median with quartiles and analysed using Kruskal-Wallis with post-hoc Dunn's test, ns, non-significant; **, $p < 0.01$, of n= 3 uninfected/PBS, n= 3 uninfected/clod, n= 4 infected/PBS and n= 5 infected/Clod mice with 2-3 tissue sections/mouse. Statistics only shown for PBS treated vs clodronate treated groups for clarity. Clod= clodronate liposomes treated, PBS= empty liposomes treated.

4.3.2 Effects of macrophage depletion on platelet counts

Mice were bled 24 hours after the administration of every dose of clodronate or PBS liposomes and CBCs were performed. No significant change in the number of circulating platelets was observed in any group after two doses of clodronate, given on alternate days **(Figure 4.6A)**. There was also no change in MPV after clodronate treatment (**Figure 4.6B**).

4.3.3 Effects of macrophage depletion on other blood cells and parasite burden

CBCs were monitored in uninfected and infected mice after the administration of clodronate. Mice infected for 28 days were anaemic before the administration of liposomal clodronate or PBS, no significant difference was noticed in erythrocyte count and other red cell indices in either group after clodronate treatment **(Table 4.1)**. Leucocyte counts were also analysed in all the groups. Our results suggest no significant difference in the leucocytes after clodronate treatment **(Table 4.2)**.

Mice were sacrificed after two doses of liposomal clodronate and tissues were harvested for further analysis. Post-mortem weights of liver and spleen were measured in infected and uninfected mice treated with clodronate or PBS. Interestingly, there was a significant reduction in the weight of spleens in infected mice treated with clodronate as compared to PBS treated infected mice **(Figure 4.7A and B)**. Liver weights also showed a small reduction in clodronate treated infected mice **(Figure 4.7A and B)**. Spleen and liver weights in uninfected mice remain unchanged in either group.

Parasite burden was measured on Giemsa stained tissue impression smears in both the livers and spleens of infected mice and calculated as Leishman-Donovan units (LDUs), as described earlier. There was no significant difference in the parasite burden in either organ in infected mice treated with clodronate compared to PBS liposomes **(Figure 4.8)**.

Although there was no change in the platelet counts in infected mice after clodronate treatment, we observed a strong correlation between the platelet count and spleen weight, and platelet count and liver weight **(Figure 4.9A and B)**.

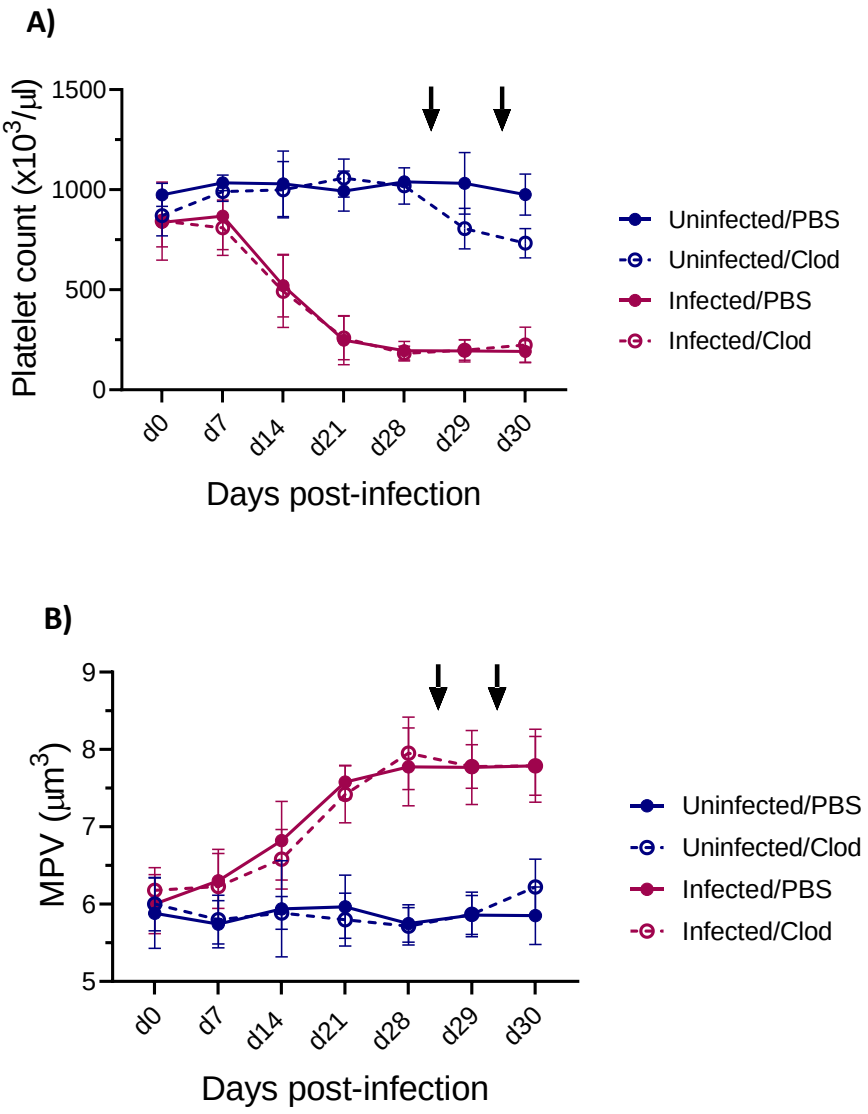

Figure 4.6 Platelet count and MPV changes after clodronate treatment. Uninfected or *L. donovani*-infected mice were bled before and weekly post-infection, and at 24h and 48h post-clodronate administration for (A) platelet counts and (B) mean platelet volume (MPV). Data show the results of two independent experiments with n= 6 uninfected/PBS, n=7 uninfected/clodronate, n=9 infected/PBS, n=10 infected/clodronate-treated mice. Thick black arrows show the administration of liposomal clodronate or PBS on alternate days, mice were bled 24 hours after each dose for blood counts. Clod= clodronate liposomes treated, PBS= empty liposomes treated.

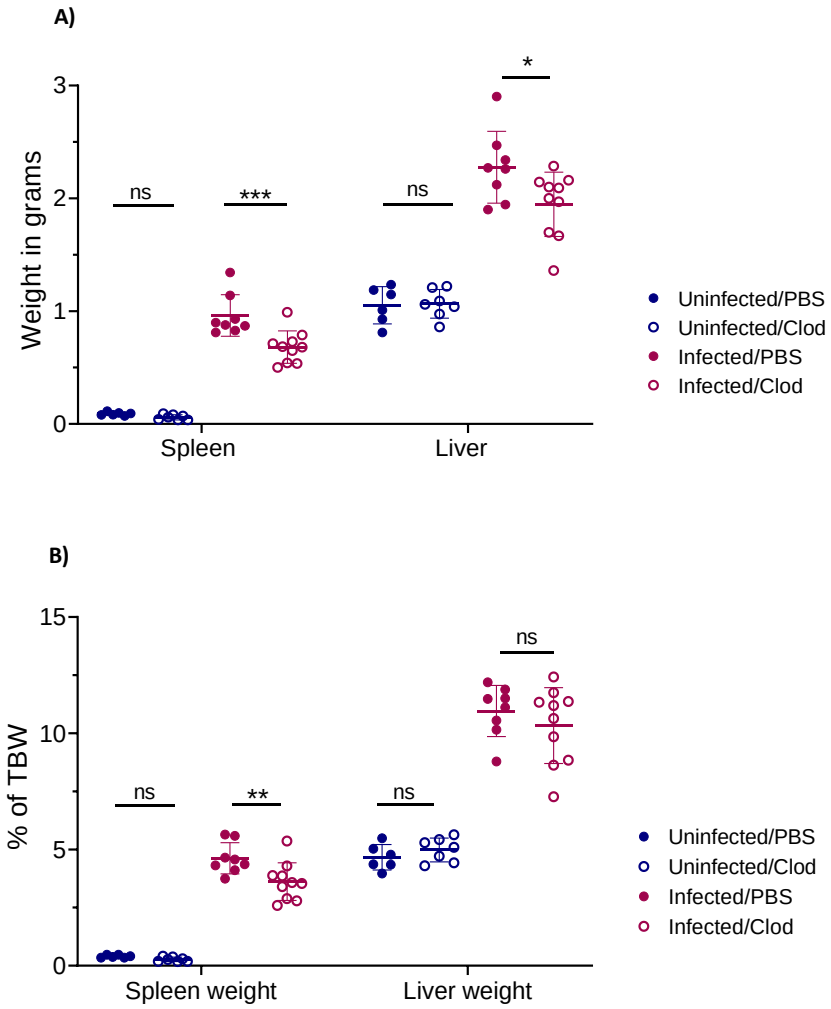

Figure 4.7 Changes in organ weight after clodronate treatment. Post-mortem liver and spleen weights were measured in infected and uninfected mice, treated with liposomal clodronate or PBS. Data are represented as (A) organ weight in grams and (B) percentage (%) of the total body weight (TBW). Data show the results of two independent experiments with n= 6 uninfected/PBS, n=7 uninfected/clodronate-treated, n=8 infected/PBS, n=10 infected/clodronate-treated. Data analysed using ANOVA with Tukey's post-hoc test, p value = ns, non-significant; *, $p < 0.05$; **, $p < 0.01$; ***, $p < 0.001$; only the comparisons between treated and non-treated groups are shown for clarity. Clod= clodronate liposomes treated, PBS= empty liposomes treated.

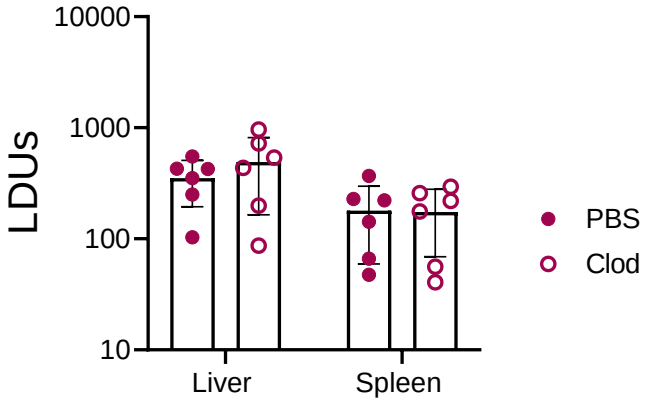

Figure 4.8 Parasite burden in infected mice after treatment with clodronate. Liver and spleen parasite burdens were calculated on Giemsa stained tissue impression smears in both groups. No significant difference in parasite burden was noticed. Data are shown as mean LDU ± SD from two independent experiments with n= 6 infected/PBS and n=6 infected/clodronate-treated mice. Clod= clodronate liposomes treated, PBS= empty liposomes treated.

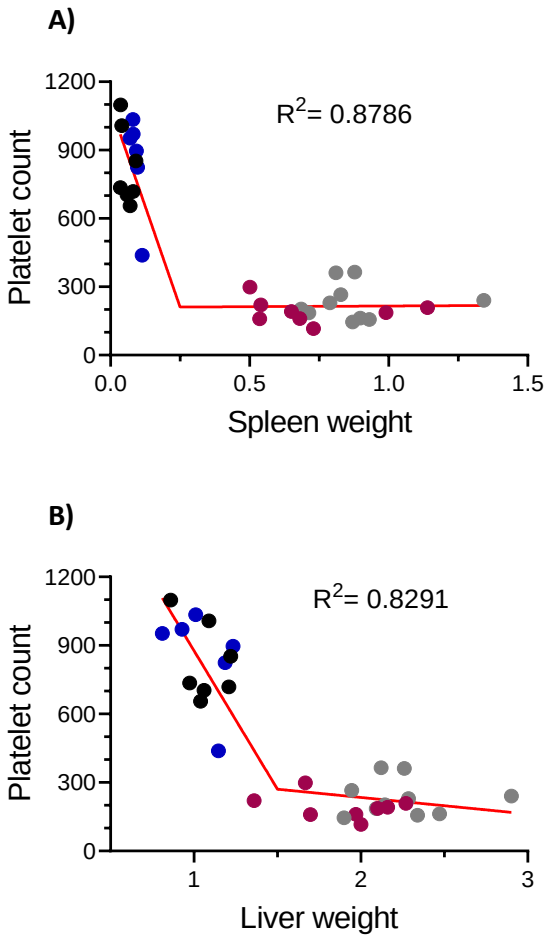

Figure 4.9 Correlation between platelet count and organ weights. A correlation between pre-mortem platelet counts and post-mortem (A) spleen and (B) liver weights (grams) was observed. Data are representative of two independent experiments with n= 6 uninfected/PBS (blue dots), n=7 uninfected/clodronate-treated (black dots), n=8 infected/PBS (magenta dots), n=10 infected/clodronate-treated (grey dots). A segmentation non-linear regression was applied to each data set.

Table 4.1 Erythrocyte count and red cell indices in infected and uninfected mice treated with clodronate or PBS liposomes.

	Uninfected/Control (mean ± SD)	**Uninfected/Clod** (mean ± SD)	**Infected/Control** (mean ± SD)	**Infected/Clod** (mean ± SD)
RBC count (10^6/mm^3)				
d0	7.478 ± 1.229	8.632 ± 1.297	7.946 ± 1.806	7.965 ± 1.682
d7	8.186 ± 2.025	8.204 ± 1.637	8.788 ± 1.605	8.381 ± 1.798
d14	8.772 ± 1.490	9.631 ± 0.733	8.310 ± 1.928	7.418 ± 2.738
d21	9.729 ± 0.750	8.975 ± 1.212	5.708 ± 2.332	5.585 ± 2.360
d28	9.145 ± 0.541	9.626 ± 0.600	5.700 ± 0.517	5.114 ± 1.407
24hrs	9.180 ± 1.017	9.042 ± 1.001	5.696 ± 1.240	5.848 ± 1.715
48hrs	8.616 ± 1.363	9.873 ± 1.026	5.326 ± 0.991	5.754 ± 2.190
Haemoglobin (Hb) g/dl				
d0	14.825 ± 1.709	14.500 ± 2.255	14.329 ± 1.161	13.450 ± 2.717
d7	14.800 ± 2.121	15.733 ± 1.759	15.450 ± 3.334	14.140 ± 2.813
d14	15.467 ± 2.895	16.117 ± 1.162	13.510 ± 3.173	14.089 ± 3.855
d21	16.600 ± 2.433	15.267 ± 2.519	13.029 ± 3.132	12.029 ± 3.192
d28	15.657 ± 1.235	15.971 ± 1.024	10.533 ± 1.046	9.950 ± 1.522
24hrs	15.483 ± 1.477	14.733 ± 1.707	11.388 ± 1.382	11.122 ± 1.790
48hrs	14.420 ± 1.363	16.200 ± 1.778	10.286 ± 1.346	10.878 ± 2.923
Haematocrit (Hct) %				
d0	43.763 ± 5.515	43.320 ± 6.814	44.483 ± 3.053	42.029 ± 7.044
d7	45.880 ± 8.809	41.157 ± 8.135	43.833 ± 9.287	40.044 ± 7.976
d14	43.480 ± 7.485	47.600 ± 2.952	37.567 ± 8.612	38.938 ± 10.559
d21	49.880 ± 5.034	45.433 ± 7.158	34.983 ± 7.151	31.129 ± 8.763
d28	46.075 ± 2.662	47.171 ± 2.618	29.500 ± 2.371	26.886 ± 6.340
24hrs	47.967 ± 2.860	43.260 ± 5.454	29.725 ± 5.948	29.986 ± 4.022
48hrs	45.033 ± 5.255	48.425 ± 5.914	30.229 ± 4.674	27.200 ± 3.550
Mean cell volume (MCV) μm^3				
d0	49.500 ± 0.577	49.800 ± 0.447	50.286 ± 0.756	50.375 ± 1.061
d7	50.000 ± 0.632	50.429 ± 0.787	50.222 ± 0.833	49.800 ± 1.135
d14	50.167 ± 0.983	50.571 ± 0.787	48.889 ± 1.269	48.500 ± 1.509
d21	51.000 ± 0.816	50.333 ± 1.506	49.778 ± 1.202	49.300 ± 0.823
d28	49.714 ± 0.756	49.286 ± 1.254	51.875 ± 1.458	50.900 ± 1.663
24hrs	50.667 ± 1.966	48.833 ± 0.983	54.375 ± 1.302	52.444 ± 2.186
48hrs	50.167 ± 1.602	48.400 ± 0.894	54.286 ± 0.951	51.500 ± 1.780
Mean cell haemoglobin (MCH) pg				
d0	17.150 ± 0.311	16.800 ± 0.235	17.257 ± 0.299	16.938 ± 0.518
d7	17.500 ± 0.755	17.183 ± 0.665	17.286 ± 0.706	17.190 ± 0.456
d14	17.183 ± 0.886	17.400 ± 0.894	16.825 ± 0.406	16.990 ± 0.689
d21	17.525 ± 0.685	17.050 ± 0.675	17.600 ± 0.332	17.460 ± 0.504
d28	16.900 ± 0.852	16.833 ± 0.720	18.143 ± 0.461	17.860 ± 0.822
24hrs	16.750 ± 0.389	16.267 ± 0.197	19.180 ± 0.709	18.514 ± 1.030
48hrs	17.283 ± 0.431	16.267 ± 0.208	18.957 ± 0.632	17.613 ± 0.740
Mean cell haemoglobin concentration (MCHC) g/dl				
d0	34.625 ± 0.263	33.480 ± 0.277	34.286 ± 0.672	33.675 ± 0.676
d7	34.400 ± 0.753	34.000 ± 0.911	34.511 ± 1.178	34.480 ± 0.466
d14	34.167 ± 1.271	34.033 ± 1.042	34.678 ± 1.060	34.970 ± 1.165

d21	34.425 ± 0.873	33.650 ± 1.001	35.256 ± 0.820	35.400 ± 1.068
d28	33.943 ± 1.163	33.871 ± 0.810	34.950 ± 0.727	35.070 ± 0.830
24hrs	33.486 ± 1.275	33.875 ± 0.206	35.322 ± 1.672	34.610 ± 1.422
48hrs	34.400 ± 0.908	33.440 ± 0.261	34.300 ± 1.069	34.930 ± 1.206
Red blood cell distribution width (RDW) %				
d0	17.400 ± 2.467	18.460 ± 0.856	21.120 ± 0.646	19.529 ± 1.262
d7	17.683 ± 1.386	18.214 ± 0.836	18.511 ± 0.521	18.060 ± 0.360
d14	17.267 ± 0.258	17.557 ± 0.506	18.089 ± 0.556	17.720 ± 0.316
d21	17.225 ± 0.150	17.283 ± 0.331	20.678 ± 1.821	20.160 ± 1.996
d28	17.157 ± 0.190	17.386 ± 0.302	23.300 ± 1.695	23.120 ± 1.422
24hrs	17.833 ± 1.368	17.200 ± 0.341	23.189 ± 1.563	23.650 ± 0.809
48hrs	17.633 ± 1.446	17.060 ± 0.385	22.150 ± 1.121	22.371 ± 0.966

Table 4.2 Leucocyte count in infected and uninfected mice treated with clodronate or PBS liposomes.

	Uninfected/Control (mean ± SD)	**Uninfected/Clod** (mean ± SD)	**Infected/Control** (mean ± SD)	**Infected/Clod** (mean ± SD)
WBC count (10^3/mm^3)				
d0	5.875 ± 1.526	7.220 ± 1.663	5.086 ± 1.356	4.538 ± 1.302
d7	5.880 ± 2.493	6.229 ± 1.788	7.011 ± 2.155	5.744 ± 1.441
d14	7.225 ± 1.884	7.367 ± 1.697	5.344 ± 1.719	4.920 ± 1.888
d21	8.000 ± 2.263	6.300 ± 1.463	4.513 ± 1.594	3.750 ± 1.318
d28	7.060 ± 1.350	6.900 ± 1.074	4.578 ± 0.628	3.756 ± 1.275
24hrs	7.200 ± 2.309	6.833 ± 1.271	5.660 ± 1.006	3.744 ± 1.056
48hrs	7.086 ± 1.716	7.425 ± 1.150	5.013 ± 0.806	3.900 ± 0.907
Lymphocyte count (10^3/mm^3)				
d0	4.825 ± 1.078	5.550 ± 0.947	3.214 ± 0.941	4.350 ± 1.176
d7	3.580 ± 1.418	4.800 ± 0.896	4.550 ± 1.021	4.171 ± 0.778
d14	5.675 ± 1.215	5.440 ± 1.232	4.130 ± 1.158	4.257 ± 0.732
d21	5.700 ± 0.424	4.383 ± 1.225	3.688 ± 1.037	3.313 ± 0.749
d28	5.700 ± 1.068	5.117 ± 0.615	3.589 ± 0.749	2.913 ± 0.452
24hrs	5.200 ± 1.826	5.650 ± 1.084	4.889 ± 1.028	3.100 ± 0.490
48hrs	5.300 ± 1.257	5.500 ± 0.819	3.550 ± 0.586	2.943 ± 0.611
Monocyte count (10^3/mm^3)				
d0	0.125 ± 0.050	0.160 ± 0.055	0.129 ± 0.049	0.129 ± 0.049
d7	0.120 ± 0.045	0.143 ± 0.053	0.200 ± 0.093	0.167 ± 0.071
d14	0.200 ± 0.082	0.243 ± 0.098	0.160 ± 0.084	0.157 ± 0.053
d21	0.225 ± 0.096	0.129 ± 0.049	0.100 ± 0.000	0.086 ± 0.069
d28	0.214 ± 0.069	0.200 ± 0.058	0.114 ± 0.038	0.080 ± 0.045
24hrs	0.200 ± 0.063	0.120 ± 0.045	0.120 ± 0.045	0.100 ± 0.000
48hrs	0.171 ± 0.049	0.160 ± 0.055	0.129 ± 0.049	0.100 ± 0.000
Neutrophil count (10^3/mm^3)				
d0	0.925 ± 0.435	1.220 ± 0.676	0.957 ± 0.230	0.763 ± 0.239
d7	1.243 ± 1.162	0.886 ± 0.445	1.470 ± 0.799	1.080 ± 0.461
d14	1.386 ± 0.649	1.600 ± 0.569	1.280 ± 0.648	1.070 ± 0.593
d21	1.950 ± 0.759	1.129 ± 0.610	0.640 ± 0.237	0.770 ± 0.481
d28	1.471 ± 0.585	1.314 ± 0.291	1.100 ± 0.304	0.700 ± 0.200
24hrs	1.443 ± 0.395	0.986 ± 0.344	1.656 ± 0.588	0.840 ± 0.337
48hrs	1.300 ± 0.277	1.520 ± 0.502	1.350 ± 0.239	0.740 ± 0.353
Eosinophil count (10^3/mm^3)				
d0	0.037 ± 0.015	0.038 ± 0.015	0.045 ± 0.006	0.063 ± 0.052
d7	0.050 ± 0.024	0.063 ± 0.029	0.056 ± 0.029	0.043 ± 0.036
d14	0.073 ± 0.048	0.078 ± 0.059	0.083 ± 0.041	0.060 ± 0.018
d21	0.080 ± 0.062	0.076 ± 0.040	0.048 ± 0.014	0.067 ± 0.040
d28	0.060 ± 0.024	0.051 ± 0.012	0.110 ± 0.060	0.082 ± 0.041
24hrs	0.062 ± 0.032	0.071 ± 0.080	0.092 ± 0.040	0.113 ± 0.057
48hrs	0.055 ± 0.020	0.058 ± 0.036	0.060 ± 0.032	0.083 ± 0.048

4.4 Antiplatelet antibodies

4.4.1 Anti-platelet antibodies coating the circulating platelets

In many thrombocytopenic disorders, anti-platelet antibodies have been detected coating platelets, facilitating their clearance by the tissue macrophages. Antiplatelet antibodies have been detected in immune-mediated thrombocytopenic disorders and infections, and play an important role in thrombocytopenia (197). As shown previously, splenectomy not only reduces the extent of thrombocytopenia but also a better response to cytokine stimulation in VL infected mice. Data from splenectomised infected mice suggest a role of the enlarged spleen in excessive platelet clearance in VL infected mice. Therefore, we assayed for the presence of anti-platelet antibodies in the blood of *L. donovani*-infected mice. Platelets were isolated from freshly collected blood of uninfected and infected mice and stained with anti-CD41 antibody followed by anti-mouse IgG and anti-mouse IgM antibodies.

CD41 positive platelets were gated for binding of anti-IgG and anti-IgM antibodies **(Figure 4.10A and B)**. Our findings suggest that approximately 30% of the platelets from infected mice were positive for bound IgG antibodies as compared to platelets from uninfected mice **(Figure 4.10C)**. Approximately 5% of the platelets from infected mice were also positive for bound IgM antibodies **(Figure 4.10D)**.

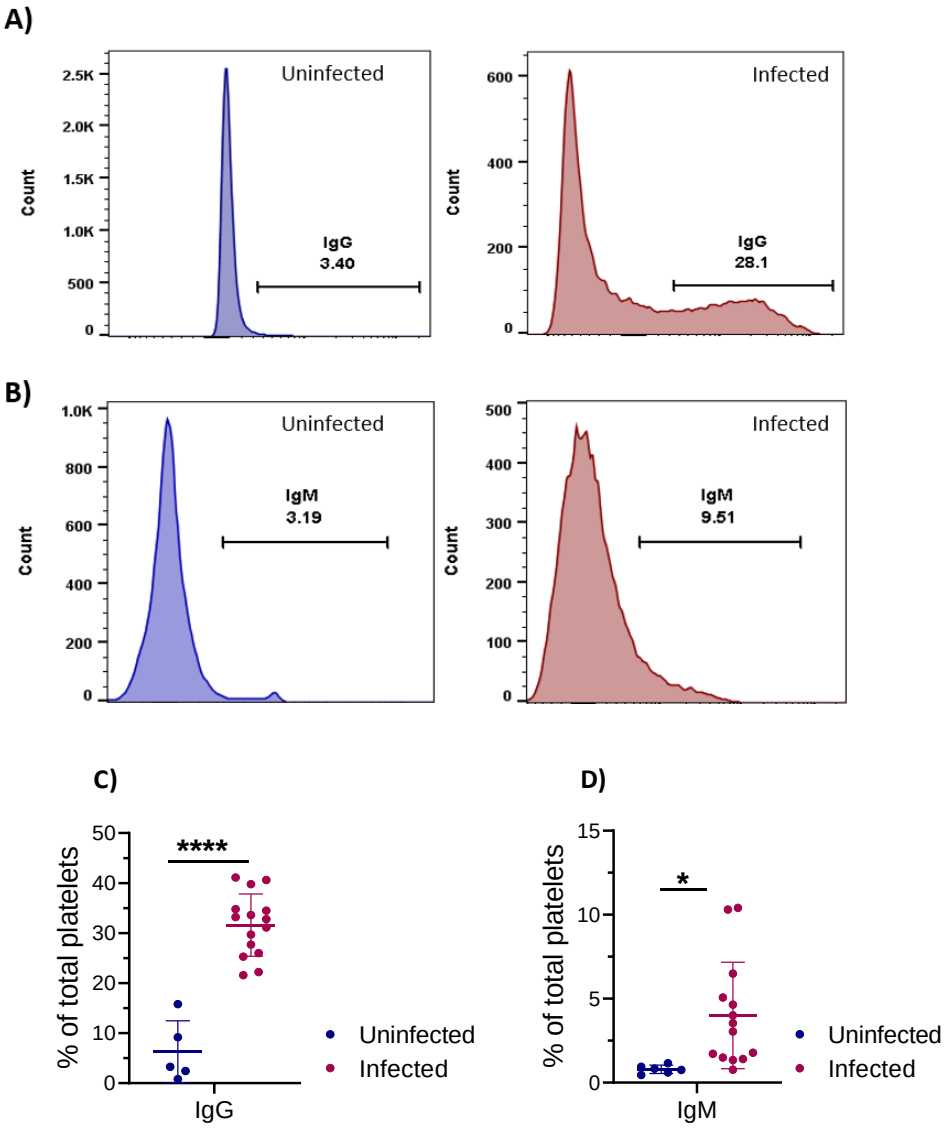

Figure 4.10 Presence of anti-platelet antibodies in infected mice. Blood was collected from d28 infected and uninfected mice by cardiac puncture and platelets were isolated. Freshly isolated platelets were stained with anti-CD41 antibody followed by anti-mouse IgG AF647 and anti-mouse IgM PECY7 antibodies and flow cytometric analysis was performed. Anti-CD41 positive platelets were gated for (A) IgG and (B) IgM antibodies. Data show the percentage of platelets positive for (C) IgG and (D) IgM antibodies, n= 5 uninfected and n=15 infected mice for IgG and n=6 uninfected and n=14 for infected for IgM, from two independent experiments. Data analysed using unpaired t test, *, $p < 0.05$ and ****, $p < 0.0001$ comparing mean ± SD between uninfected and infected mice.

4.5 Platelet Desialylation

The membrane of mature platelets is coated with terminal sialic acids in the circulation and this is lost as platelets age. Studies have shown that the loss of terminal sialic acids result in the exposure of galactose residues for the AMR expressed by hepatocytes. Binding of desialylated platelets to AMR is not only important for the production of TPO through the activation of the JAK-STAT pathway but also a way of clearance of old platelets from the circulation. Increased platelet desialylation could lead to an excessive clearance of platelets by hepatocytes and could cause thrombocytopenia, as observed in various infections (64,65).

To examine whether platelets from infected mice were desialylated, platelets were isolated from uninfected and infected mice blood and stained with anti-CD41 antibody followed by biotinylated lectins and streptavidin labelled PE antibody. We used three lectins i.e. *Ricinus Communis* Agglutinin-I (RCA-I), *Maackia amurensis* Lectin II (MAL-II) and *Sambucus nigra* (SNA), which have already been described in the literature (37). The binding specificities of these lectins are given in **Table 2.1** (**Chapter 2**).

Our data suggest that platelets from infected mice were more commonly desialylated as compared to in uninfected mice. Approximately 60% platelets were positive for RCA-I and MAL=II compared to < 5% in uninfected mice. In contrast, there was no change in binding of SNA **(Figure 4.11A, B and C)**.

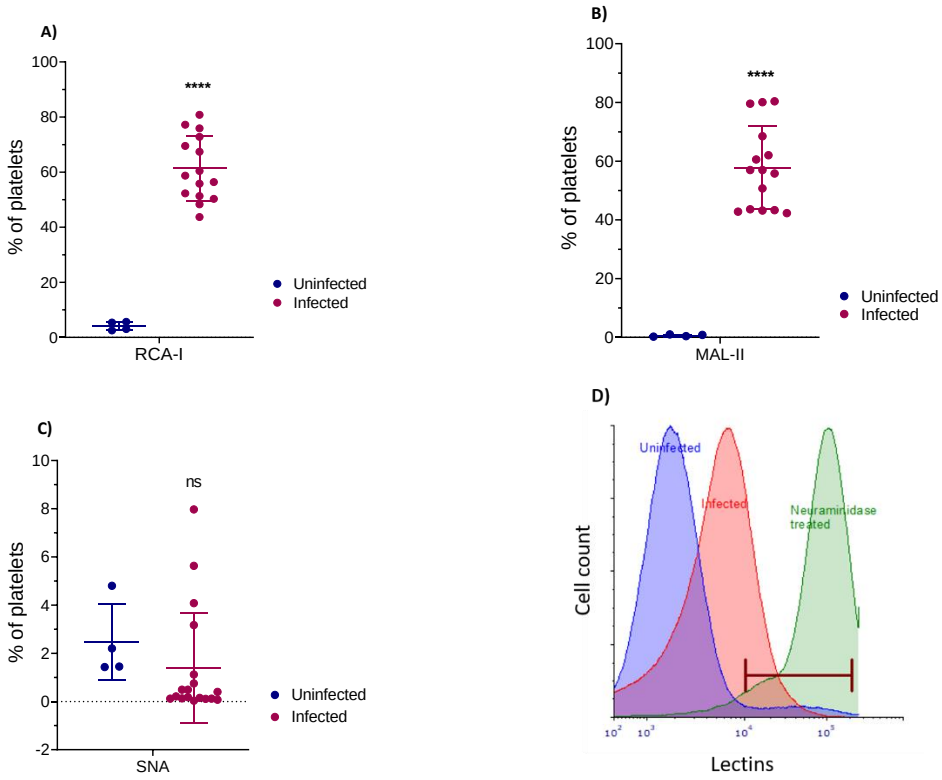

Figure 4.11 Platelet desialylation in infected mice. Platelets were isolated from cardiac blood of uninfected and d28 infected mice. Freshly isolated platelets were stained with anti-CD41 antibody and biotinylated lectins (A) RCA-I, (B) MAL-II and (C) SNA. (D) Histogram representative of gating for lectin positive platelets in infected and uninfected mice blood, with neuraminidase treated platelets as positive control (maximum desialylation). Data represent the results of two independent experiments with n=4 uninfected and n= 17 infected mice. Data analysed using unpaired t test with p value, ns, non-significant; ****, $p < 0.0001$, comparing mean ± SD between uninfected and infected mice.

4.6 Discussion

The role of the spleen has been frequently discussed in the literature due to its multiple functions under normal physiological conditions and in response to pathology. The spleen is one of the largest secondary lymphoid organ in the body, filters blood-borne pathogens from entering the general circulation and is critical for the removal of old or aberrant erythrocytes and recycle the iron for further erythropoiesis (126). On the other hand, splenomegaly, commonly known as hypersplenism, results in excessive phagocytosis of blood cells resulting in cytopenias. Haematological complications due to hypersplenism are commonly seen in infections and malignancies e.g. in malaria, viral hepatitis and hepatic disorders (149). Hence, the spleen may play a dual role in infection, promoting immunity yet leading to immune dysregulation and haematological complications.

Splenomegaly is one of the most common clinical findings in humans with VL and in experimental models. Splenic infiltration of *L. donovani* parasites leads to chronic infection due to ineffective immune responses unable to clear parasites (146). RP macrophages which act as a major reservoir for the parasite, though highly phagocytic however, parasites avoid its microbicidal effects leading to a chronic infection. Studies have shown that splenomegaly in VL leads to anaemia along with defective medullary erythropoiesis (101).

Very little is known about the role of splenomegaly in VL-induced thrombocytopenia however. Experiments on splenectomised infected mice have shown less severe thrombocytopenia with a better response to exogenous rTPO stimulation as compared to sham-operated control mice (O. Preham thesis; http://etheses.whiterose.ac.uk/13654/).

To explore the impact of splenic macrophages in thrombocytopenia, we attempted to use clodronate liposomes for macrophage depletion after the onset of chronic infection. Although our protocol was successful in reducing the number of RP macrophages, MZMs and MMMs in the spleen of uninfected mice, it was minimally effective in infected mice with pre-existing splenomegaly.

Although it is very difficult to explain the reason behind the inefficiency of clodronate liposomes to deplete tissue macrophages in infected mice, there are few possible explanations. First, our clodronate doses were insufficient to deplete the tissue

macrophages in infected mice, although our calculations were based on published literature with promising results but these studies were conducted on mice with normal size spleens. Clodronate treatment early in the course of infection would probably be effective in depleting macrophages but less informative as thrombocytopenia peaks towards the end of fourth week of infection. Second, the effectiveness of clodronate liposomes was compromised by the inflammatory microenvironment inside the tissues including macrophages. There is a possibility that the liposomes were denatured/damaged due to inflammatory microenvironment resulting in pre-mature release of clodronate in the circulation or tissue parenchyma before entering the macrophages or unable to penetrate the plasma membrane of macrophages. A previous study on EVL mice has shown similar results with partial macrophage depletion on clodronate treatment (198). Third, clodronate acts by the activation of apoptotic pathways in the macrophages while the presence of *L. donovani* parasites deactivates the apoptotic pathways in the resident macrophage. It is likely that the clodronate despite its release into the macrophage cytoplasm fails to activate these apoptotic pathways.

Of note, even complete depletion of tissue macrophages in uninfected mice did not lead to an elevated platelet count. Although further studies will be required using other approaches to deplete macrophages e.g inducible Cre-mediated deletion, *lys*M-Cre/DTR mice or other genetic models (199–201), our data nevertheless suggest that platelet clearance is not dependent on tissue macrophages under normal physiological condition.

Although we were unable to see the direct effects of macrophage depletion on the platelet counts in infected mice, we were able to demonstrate the presence of antibodies against platelets in circulation. Anti-platelet antibodies have been detected in ITP and infection-induced thrombocytopenia (202). Flow cytometric analysis on freshly isolated platelets demonstrated bound IgG and to a lesser extent IgM antibodies. We also observed that platelets in infected mice were more heavily desialylated compared to uninfected mice. Excessive platelet desialylation has been shown in sepsis and infections which could lead to enhanced platelet clearance by hepatocytes (202). Excessive desialylation either as a direct consequence of infection or due to other unknown mechanisms could result in thrombocytopenia with an effect on the production of TPO. However, disruption of normal hepatic microarchitecture might alter the signalling pathways for the production of TPO despite efficient JAK-STAT pathway stimulation by binding of desialylated platelets to the AMR.

In conclusion, these data are suggestive of enhanced platelet clearance by phagocytic cells in the spleen and / or following desialylation. However, the role of other factors could not be neglected. As discussed in detail in **Chapter 3**, defective megakaryopoiesis might contribute to lower platelet production. Together, our findings suggest that the mechanisms responsible for thrombocytopenia in *L. donovani* infection are multifactorial involving both defective BM production and excessive clearance by peripheral tissues.

Chapter 5. Post-treatment recovery of haematological parameters in experimental VL

5.1 Introduction

VL has a fatality rate of more than 95% around the world if left untreated (203). Multiple drugs have been used to treat VL in endemic regions, but with a variable response (204). Currently, pentavalent antimonials, miltefosine and amphotericin B are widely used as monotherapy or in combination (77,78).

Pentavalent antimonials have been in use for over 50 years to treat VL, widely used in developing countries but associated with rapidly evolving drug resistance (205–207) Miltefosine is the only orally administered drug approved for the treatment of VL. Though effective in South Asia, its efficacy in African region remains poor (208). Clinical trials on miltefosine efficacy have shown good response to treatment in India and Bangladesh. Increasing resistance, low haemoglobin levels and gastrointestinal adverse effects remained an issue (208,209). These conventional therapeutics have been associated with severe adverse reactions, parenteral administration which requires technical expertise and hospitalisation. The high cost of newer drugs remains a stress on the health system of countries with poor economic conditions (207). Amphotericin B, a polyene fungal antibiotic with high efficacy against fungal infections has shown promising results against VL. However, it is associated with severe adverse effects and high cost of therapy mainly due to hospitalisation (210). AmBisome® is a liposomal formulation of amphotericin B, widely used to treat VL have lesser adverse effects however, high cost is still a limiting factor for low income countries. Although AmBisome® is highly effective in treating Indian VL, efficacy remains poor in treating VL patients in East Africa and in VL/HIV co-infection (111,211) Due to rapidly evolving drug resistance similar to malaria and tuberculosis, a combination of drugs have been tried to achieve better outcomes. AmBisome® in combination with miltefosine or antimonials has been showing encouraging results in VL and VL/HIV co-infection (212).

Successful treatment is mainly attributed to relief from clinical symptoms in humans and clearance of parasites along with a reduction in the size of the liver and spleen. As already discussed in previous chapters, haematological complications in VL are studied less in

clinical settings, and there is very little data available on the post-treatment recovery of haematological profiles (96). Post-treatment clinical studies are mainly focused on the immune response to treatment while none have formally addressed haematological parameters. Therefore, we used our well-defined model of VL to study the restoration of haematological profiles alongside conventional parameters such as parasite clearance and the recovery of tissue microarchitecture.

The murine VL model is widely used to study the efficacy of drugs and immune response to the treatment and is an essential pre-clinical tool underpinning the progression of drugs for human VL. However, most studies have focused only on early time-points post-treatment (114). These studies indicate that a single dose of AmBisome® results in a significant reduction in parasite burden within in 24-72 hours, and complete clearance of parasite from liver and spleen within one week post-treatment (114).

Our data on understanding the mechanisms of thrombocytopenia in VL are suggestive of multifactorial pathogenesis with defects in both production and clearance of platelets during infection. Hypersplenism has been studied in multiple infections which are suggestive of excessive phagocytosis of blood cells by activated macrophages (188). As already discussed in **Chapter 1**, NO production is critical for the Th1 mediated immune response by phagocytic cells in infections including VL and associated with decreased parasite burden as seen in infected dogs (88). Increased expression of iNOS in VL suggests the increased activity of tissue macrophages in an attempt to kill the intracellular parasites however, this is not very effective in chronic infection. Tissue macrophages particularly splenic red pulp (RP) macrophages are phagocytic and a reservoir of parasites, might be responsible for excessive phagocytosis/destruction of blood cells. Although cytopenias due to splenic clearance have been suggested in infections however, the association between cytopenias and excessive iNOS production by tissue macrophages have not been studied. Therefore, we wanted to study the role of iNOS production by parasite harbouring tissue macrophages during infection and after treatment to indirectly assess the role of tissue macrophages in VL induced cytopenias.

5.2 Aims

The main aims of this study were;

1. To determine the time course of restoration of the haematological profile after treatment of experimental *L. donovani* infection.
2. To determine to the rate of recovery of tissue architecture post-treatment.
3. To determine the effects of inducible nitric oxide synthase (iNOS) expression on blood counts and parasite clearance.

5.3 Results

5.3.1 Haematological profile after treatment

Haematological complications are one of the predominant features of VL, though the severity varies from region to region. VL has been associated with pancytopenia however, isolated cytopenias or bicytopenia have also been reported (96). Post-treatment recovery of blood counts has been shown in few clinical studies however, no data are available in experimental models. Therefore, we were interested in determining the effects of treatment on the recovery of abnormal haematological profile using this model of infection. We assessed post-mortem reduction in organ sizes and parasite clearance as surrogates of clinical cure.

Infected mice were treated with a single dose of AmBisome® and monitored weekly for blood counts as shown in **Figure 5.1**. Post-mortem tissue analysis was done to assess parasite burden, the extent of organomegaly and tissue microarchitecture.

5.3.1.1 Platelet count recovery after treatment

Infected mice were treated with AmBisome® and bled weekly for blood counts. Platelet counts started to recover within one week post-treatment and reached normal range at four weeks post-treatment **(Figure 5.2A).**

MPV in infected mice also started decreasing within one week achieving a complete recovery within four weeks post-treatment **(Figure 5.2B)**. Together, these results indicate recovery of platelet homeostasis, irrespective of the underlying mechanisms; defective production or excessive clearance.

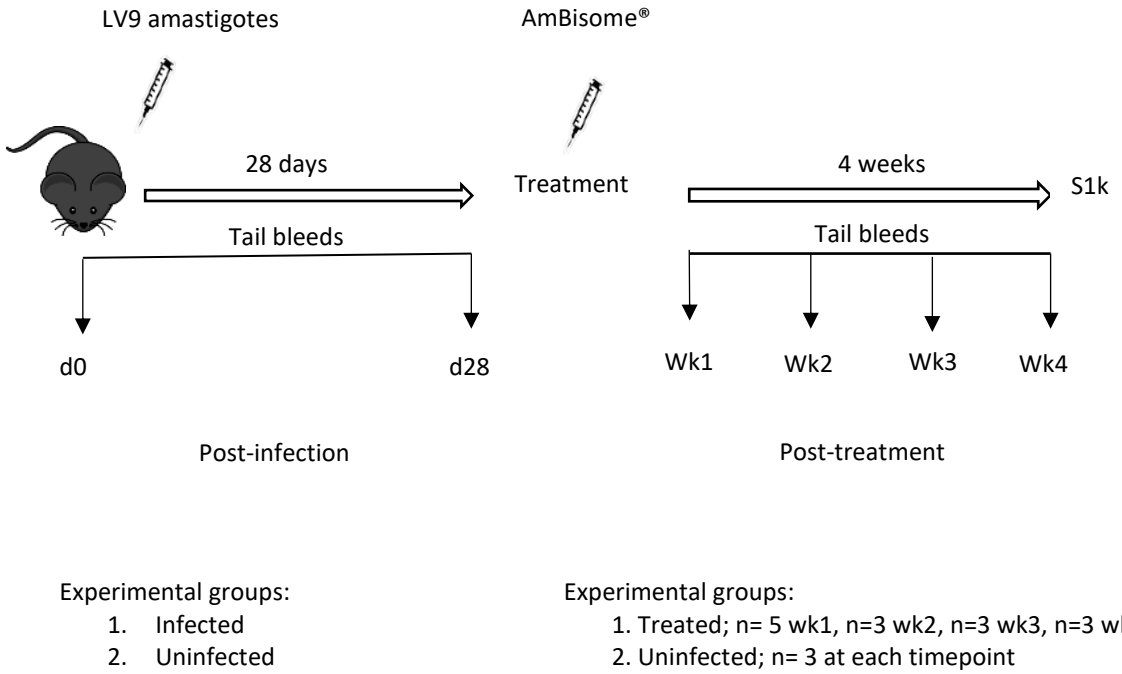

Figure 5.1 Schematic of the experiment to study the effects of treatment. C57BL/6 mice infected for 28 days with $3x10^7$ *L. donovani* amastigotes were treated with a single dose of 8mg/kg AmBisome® via tail vein injection. Mice were bled before and at d28 of infection, and then weekly post-treatment for four weeks. Groups of mice (n= 3-5 treated, n=3 uninfected) were killed every week for four weeks post-treatment and tissues were harvested for further analysis. Wk = Week, S1k = Schedule-1 killing.

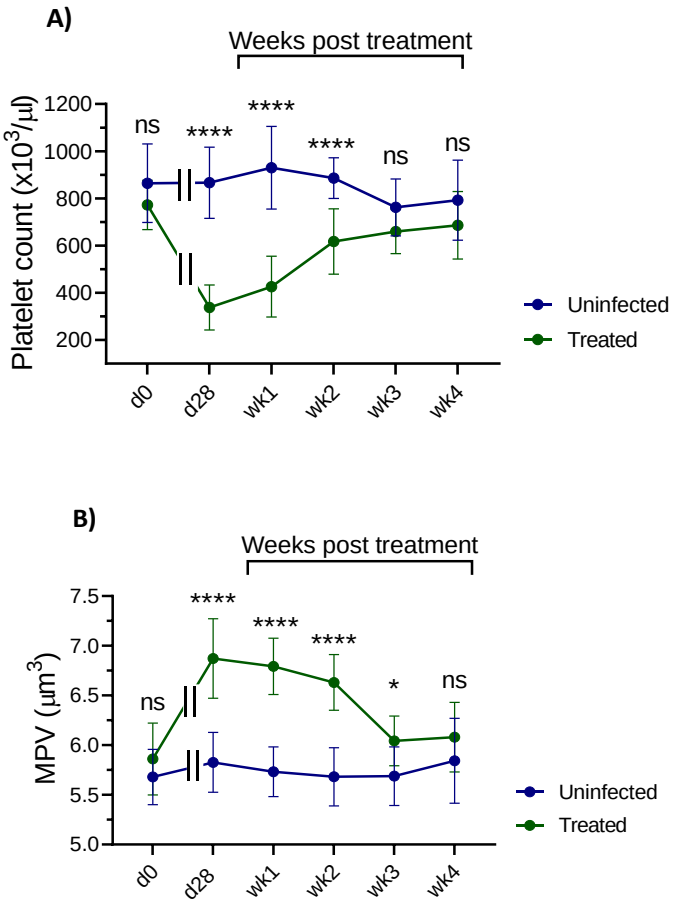

Figure 5.2 Platelet count recovery after treatment. *L. donovani*-infected C57BL/6 mice were treated with a single dose of AmBisome® at d28 of infection, and both treated and uninfected mice were bled weekly for platelet counts. (A) Platelet counts and (B) MPV recovered completely within 4 weeks post-treatment with AmBisome®. Data represent the results of n=16 uninfected and n=19 treated mice at d0, d28 and wk1, n=13 uninfected and n=14 treated at wk2, n=10 uninfected and n=10 treated at wk3, n= 5 uninfected and n= 7 treated at wk4. Data were analysed using unpaired t test comparing mean ± SD of uninfected vs treated groups at each time-point, with p value, ns=non-significant; *, $p < 0.05$; **, $p < 0.01$; ***, $p < 0.001$; ****, $p < 0.0001$.

5.3.1.2 Reversal of anaemia and red cell parameters

Anaemia is another predominant haematological complication in infected humans and experimental models. Clinical studies have shown that the anaemia is reversible after the clinical cure is achieved in infected patients. However, the rate of recovery of anaemia has not been studied in detail using experimental models.

Our data indicate that, like thrombocytopenia, anaemia is reversible after treatment. RBC count, haemoglobin (Hb) levels and haematocrit (Hct) all increased within one week post-treatment, achieving a complete recovery to homeostatic levels within four weeks post-treatment **(Figure 5.3A-C)**. Other red cell indices were also monitored throughout the experiment to assess any change in the size and shape of cells along with the concentration of Hb. Data are shown as mean cell volume (MCV), mean cell haemoglobin and mean cell haemoglobin concentration (MCH & MCHC) and red cell distribution width (RDW) **(Figure 5.3D-G)**. No change in the size of erythrocytes (MCV) was noticed throughout the experiment on CBCs but a significant increase in the concentration of Hb in total and in red blood cells. RDW increases during infection followed by a progressive decline, suggesting that erythrocytes of variable sizes are a feature of chronic disease however, reversible after treatment. Aniso-poikilocytosis with the presence of large polychromatic cells during infection and recovery after treatment was confirmed on the blood smears at each time-point (data not shown).

5.3.1.3 Leucocyte count recovery after treatment

Pancytopenia has also been reported as a feature of human *L. donovani* infection. Although our data on platelet counts and erythrocyte counts are suggestive of complete recovery of blood counts after treatment, we were interested to study the peripheral leucocyte counts in chronic infection and any changes in response to treatment in our experimental mice model.

Our results show that the total leucocytes count (White blood cell count; WBC) decreases during infection followed by recovery after treatment **(Figure 5.4A)**. Individual leucocyte counts i.e. lymphocyte count, monocyte count, neutrophil count and eosinophil count show a similar pattern as shown by total leucocyte counts **(Figure 5.4B-E)**. Together,

these results are indicative of leucopenia during infection most probably due to the recruitment of leucocytes in the inflamed tissues or reduced production due to hypocellular BM however, recovers to normal levels after the resolution of infection.

5.3.1.4 Thrombopoietin production after treatment

We previously showed that the level of circulating TPO is decreased during infection along with reduced *Thpo* RNA accumulation (**Chapter 3**). We, therefore, asked whether the levels of circulating TPO and *Thpo* RNA accumulation are altered during treatment. Our results indicate that the level of circulating TPO increases after treatment correlating with the recovery of platelet counts **(Figure 5.5A)**. Hepatic *Thpo* RNA also showed a progressive restoration after treatment reaching normal range within 3-4 weeks post-treatment **(Figure 5.5B)**.

Liver sections were stained for TPO to assess the production of TPO by hepatocytes. No significant difference in the number of hepatocytes producing TPO was observed after treatment as compared to uninfected mice livers **(Figure 5.6A)**. The number of $F4/80^{+}$ Kupffer cells increases during infection as discussed in previous chapters however, a progressive reduction was seen after treatment **(Figure 5.6B)**. IF stained liver images with F4/80 and TPO antibodies are shown in **Figure 5.7A-E**.

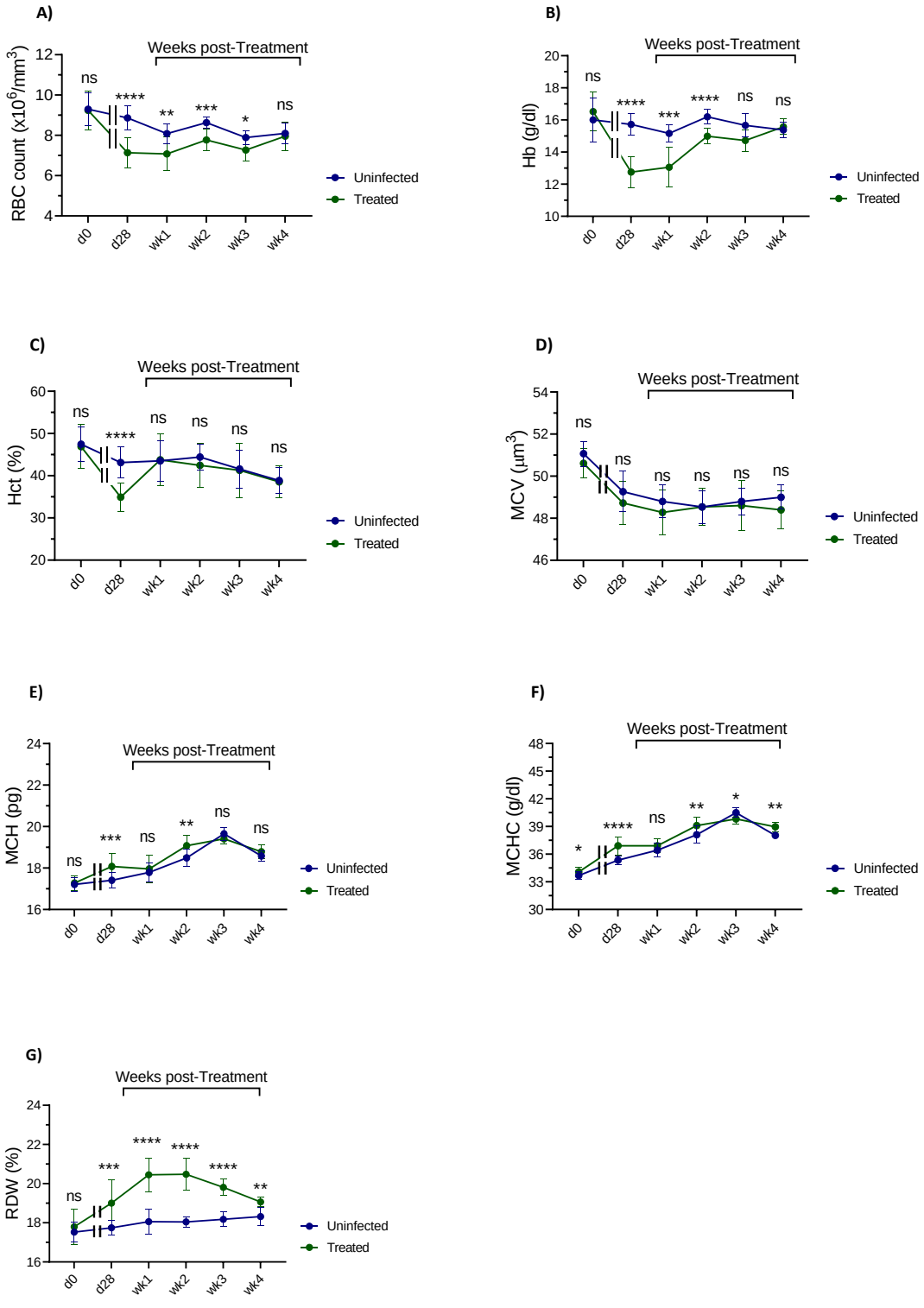

Figure 5.3 Anaemia and red cell parameters after treatment. *L. donovani*-infected C57BL/6 mice were treated with a single dose of AmBisome®, and both treated and uninfected mice were bled weekly to monitor the rate of recovery of erythrocytes and red

cell parameters. (A) RBC count, (B) Hemoglobin (Hb) and (C) Haematocrit (Hct) were monitored at each time-point to assess the extent of anaemia during infection and the rate of recovery after treatment. Other red cell parameters including (D) MCV, (E) MCH, (F) MCHC and (G) RDW were also checked to assess the volume of erythrocytes, concentration of Hb and variation in the size of cells. Data were analysed using unpaired t test, comparing mean ± SD of uninfected vs treated at each time-point, with n=16 uninfected and n=19 treated mice at d0, d28 and wk1, n=13 uninfected and n=14 treated at wk2, n=10 uninfected and n=10 treated at wk3, n= 5 uninfected and n= 7 treated at wk4, with p value, ns= non-significant; *, $p < 0.05$; **, $p < 0.01$; ***, $p < 0.001$; ****, $p < 0.0001$.

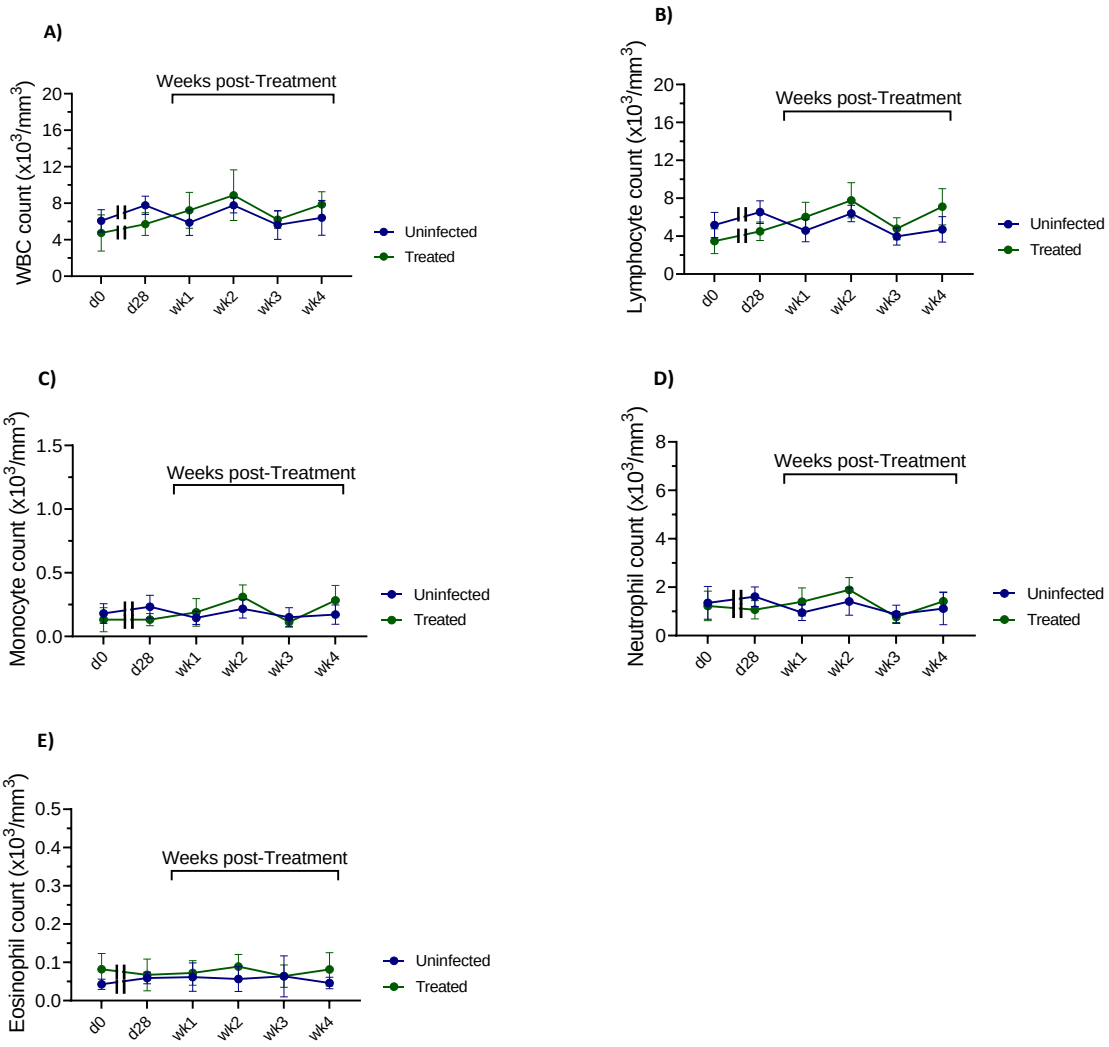

Figure 5.4 Leucocyte counts after treatment. C57BL/6 infected mice were treated with a single dose of AmBisome®, both treated and uninfected mice were bled weekly to monitor the rate of recovery of leucocytes. Mice were monitored for (A) WBC count, (B) Lymphocyte count, (C) Monocyte count, (D) Neutrophil count and (E) Eosinophil count during infection and weekly after treatment. Data are representative of n=16 uninfected and n=19 treated mice at d0, d28 and wk1, n=13 uninfected and n=14 treated at wk2, n=10 uninfected and n=10 treated at wk3, n= 5 uninfected and n= 7 treated at wk4. Data shown as mean ± SD for both groups.

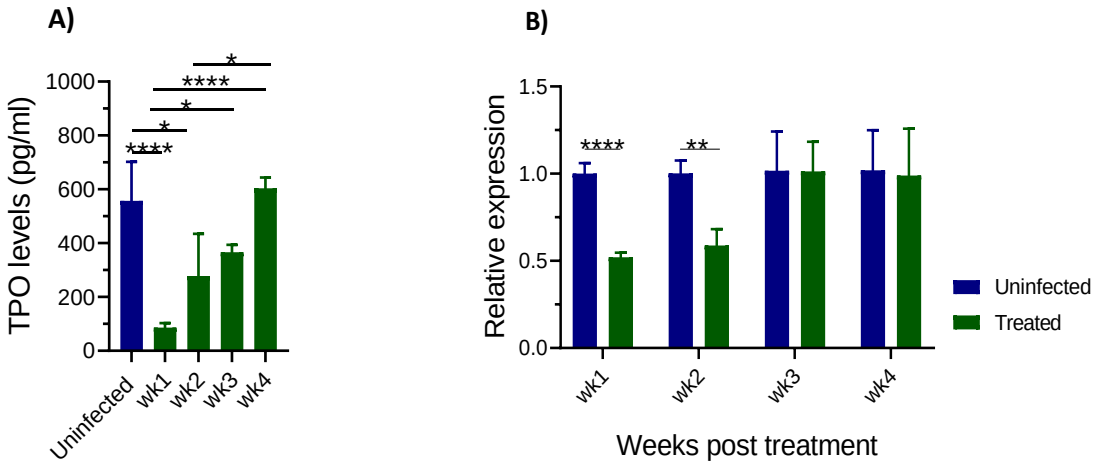

Figure 5.5 Thrombopoietin production after treatment. C57BL/6 VL treated mice were sacrificed every week post-treatment and tissues were harvested for further analysis. Serum TPO levels were measured using Mouse Thrombopoietin Quantikine ELISA Kit (R&D Systems, Minneapolis, USA) for each time-point. Data are representative of (A) serum TPO levels of n= 5 uninfected (1-2 from each time-point), n=3 treated at wk1, wk2 and wk3 post-treatment. Data analysed using ANOVA with Tukey's post-hoc test. Post-mortem liver RNA samples were measured for (B) the levels of *Thpo* RNA for each time-point by quantitative qPCR on n=3 uninfected and n=3 Treated mice at wk1, wk2, wk3 and wk4 post-treatment. Data analysed using unpaired t test comparing uninfected vs treatment, *, $p < 0.05$; **, $p < 0.01$; ****, $p < 0.0001$. Data are shown as mean ± SD for each time-point.

5.3.2 Restoration of liver and spleen microarchitecture

Enlargement of the liver and spleen is an important feature of systemic infection seen in humans and mice models. Following treatment, there was a gradual reduction in the sizes of liver and spleen **(Figure 5.8A and B)**, with hepatomegaly recovering earlier than splenomegaly most probably due to the earlier clearance of parasites and complete resolution of infection in the liver in chronic infection. Although there was a significant reduction in the size of the spleen, splenomegaly remained persistent even after four weeks post-treatment.

Parasite burden was measured on impression smears of infected livers and spleens to assess the parasite burden post-treatment. No parasites were found on the Giemsa stained impression smears at any stage of treatment suggesting a complete clearance. No signs of relapse or any parasite on the impression smears were noticed up to the fourth weeks post-treatment when the experiment was terminated. Our data on correlation between platelets and liver or spleen weights shows a stronger correlation at the end of first week of treatment however, that correlation is lost after two weeks post-treatment **(Figure 5.9)**. It could be due to increased production of platelets by recovering BM and reduction in the number of platelet clearing tissue macrophages.

Liver and spleen histology was used to study the effects of parasite clearance on the tissue architecture. H & E staining on liver sections showed a reduction in the sizes of hepatic granulomas with the restoration of normal liver architecture (**Figure 5.10A-E**). There was also a significant reduction in the number of Kupffer cells post-treatment (data shown in **Figure 5.6B**).

Post-mortem spleen sections were also stained with H & E and IF macrophage markers. As already discussed that RP splenic macrophages are abundant during infection with destruction of splenic architecture and loss of MMMs and MZMs. Tissue sections stained with H & E **(Figure 5.11)** and IF splenic macrophage markers **(Figure 5.12)** were analysed with a tissue segmentation analysis approach using StrataQuest Tissue Gnostics software. Our results are consistent with the recovery of splenic architecture after treatment with a reduction in the area and perimeter and also a reduction in $F4/80^{+}$ RP macrophages and slow restoration of marginal zone macrophages, MMM ($CD169^{+}$) and MZM ($SIGNR1^{+}$) **(Figure 5.13 and Figure 5.14)**.

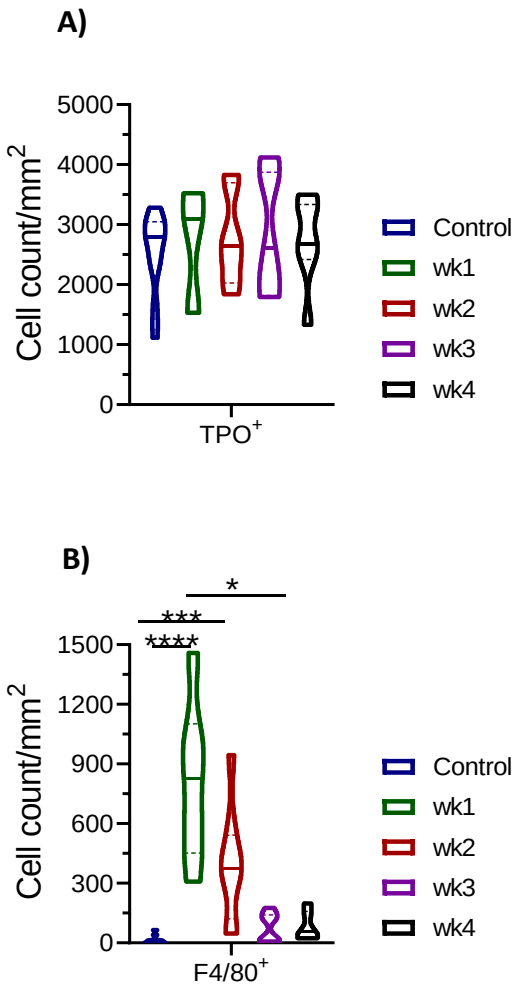

Figure 5.6 Segmentation analysis on IF stained liver images of treated mice. Segmentation analysis using StrataQuest analysis was done on the IF stained liver images of treated mice. Data show the results of (A) TPO^+ hepatocytes and (B) $F4/80^+$ cells for n=3 uninfected and n=3 Treated mice at wk1, wk2, wk3 and wk4 post-treatment. Data expressed as median with quartiles and analysed using Kruskal Wallis with Dunn's post-hoc test, *, $p < 0.05$; ***, $p < 0.001$; ****, $p < 0.0001$.

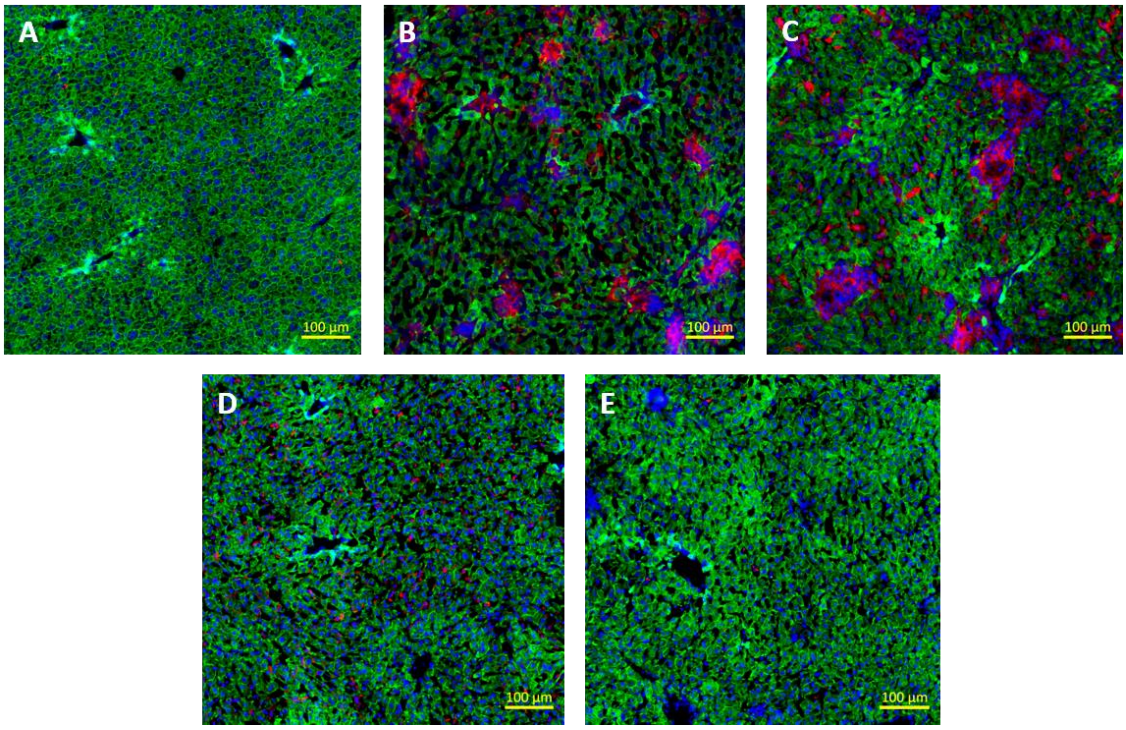

Figure 5.7 Representative IF stained liver images of treated mice. Post-mortem frozen liver sections of 8-10µm thickness were stained with F4/80 for Kupffer cells (red) and TPO for hepatocytes (green). Images were counterstained with DAPI for nuclei (blue). Images are representative of (A) uninfected, (B) wk1 post-treatment, (C) wk2 post-treatment, (D) wk3 post-treatment and (E) wk4 post-treatment groups. Subsequent segmentation analysis was done using StrataQuest TissueGnostics image analysis software for quantification of TPO^+ hepatocytes and $F4/80^+$ Kupffer cells. Scale bar = 100µm.

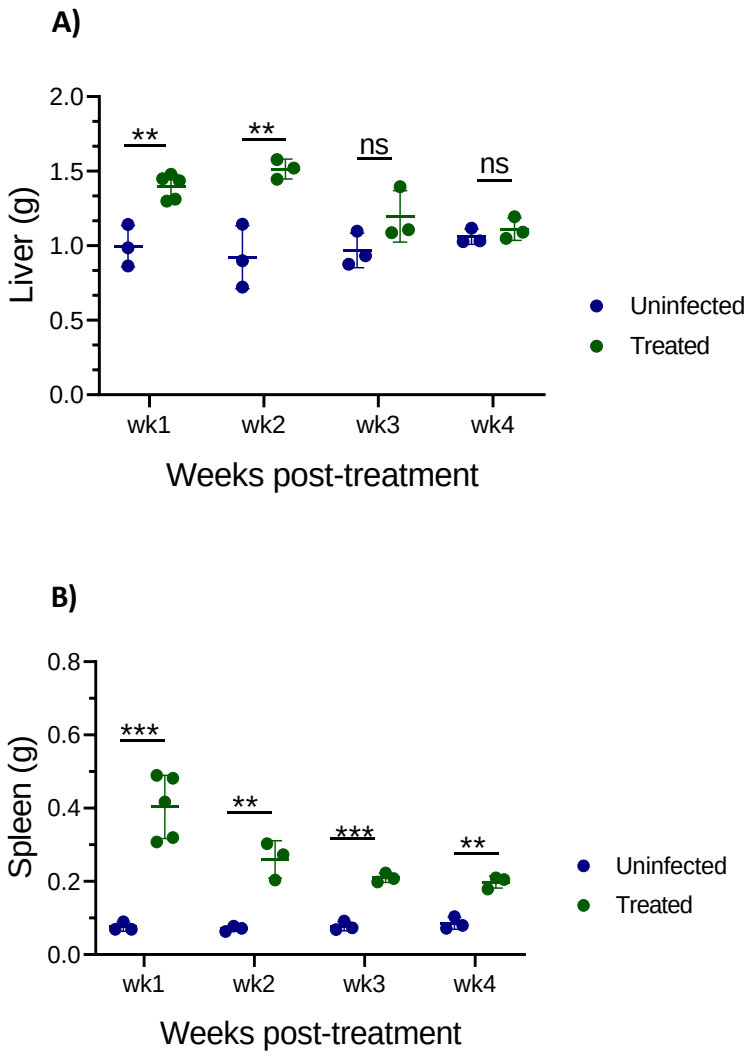

Figure 5.8 Organ weight in response to treatment. Mice were sacrificed weekly after treatment and tissues were harvested. Post-mortem (A) liver and (B) spleen weights were measured at wk1, wk2, wk3 and wk4 after treatment. Data show the result of n=3 uninfected/untreated mice at each time-point and n= 5 treated at wk1, n=3 at wk2, wk3 and wk4. Statistical analysis was done using unpaired t test comparing mean ± SD of uninfected vs treated at each time-point, p value, ns=non-significant; *, $p < 0.05$; **, $p < 0.01$; ***, $p < 0.001$.

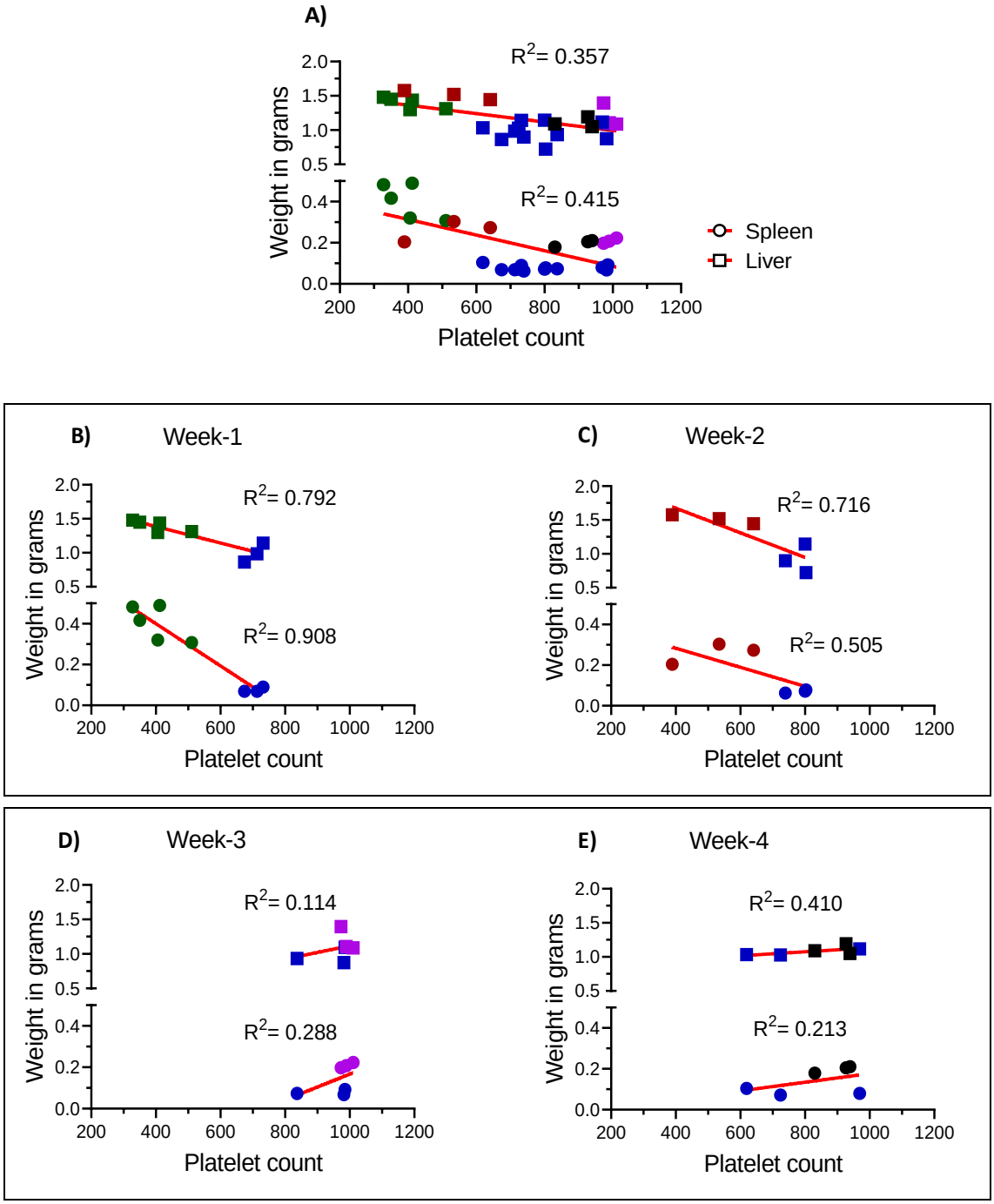

Figure 5.9 Correlation between platelet count and organ weights. Pre-mortem platelet counts and post-mortem organ weights (Liver & spleen) at each cull point were correlated using non-linear regression. Graph (A) shows the combined data of n= 11 uninfected (blue) and n= 3-5 treated from each timepoint {wk1; green, wk2; red, wk3; purple and wk4; black, of treatment}. Graphs (B-E) show the data from each week post-treatment including an uninfected group at that timepoint.

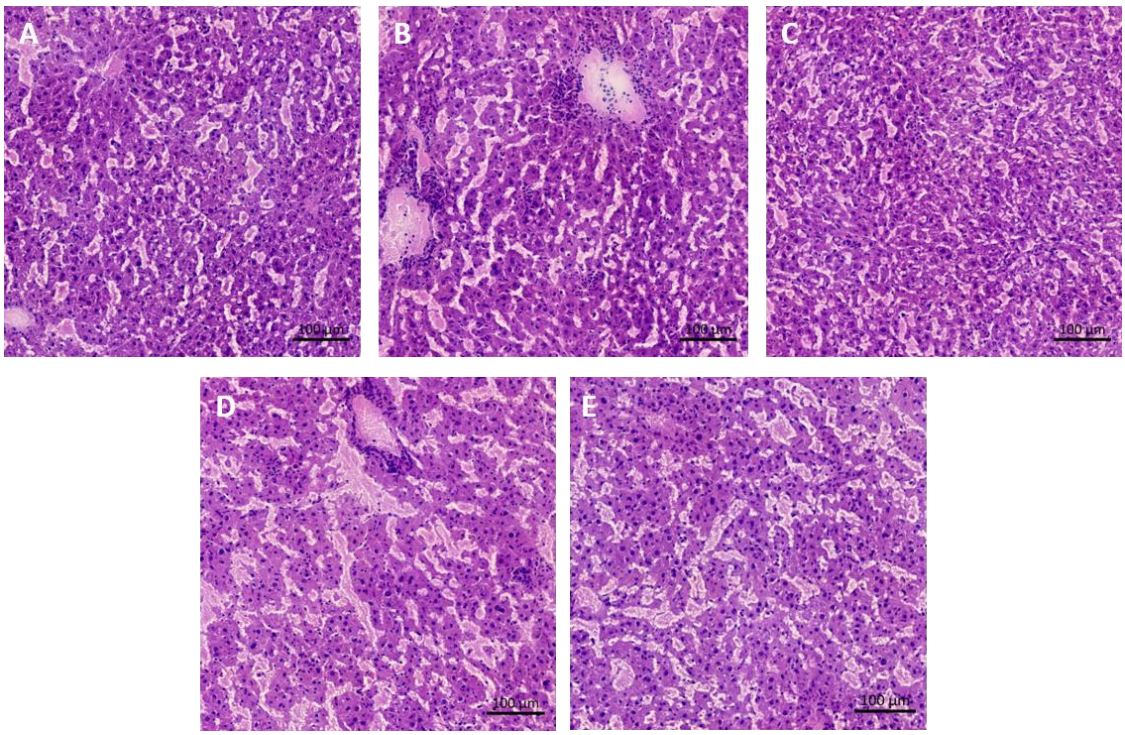

Figure 5.10 Representative Haematoxylin and Eosin stained liver images of treated mice. Post-mortem livers were harvested and cryopreserved. Frozen sections of 8-10µm thickness were stained with Haematoxylin and Eosin (H & E) as described in **Chapter 2** (Methods and Materials). Images are representative of (A) uninfected, (B) wk1 post-treatment, (C) wk2 post-treatment, (D) wk3 post-treatment and (E) wk4 post-treatment mice livers. Scale bar = 100µm.

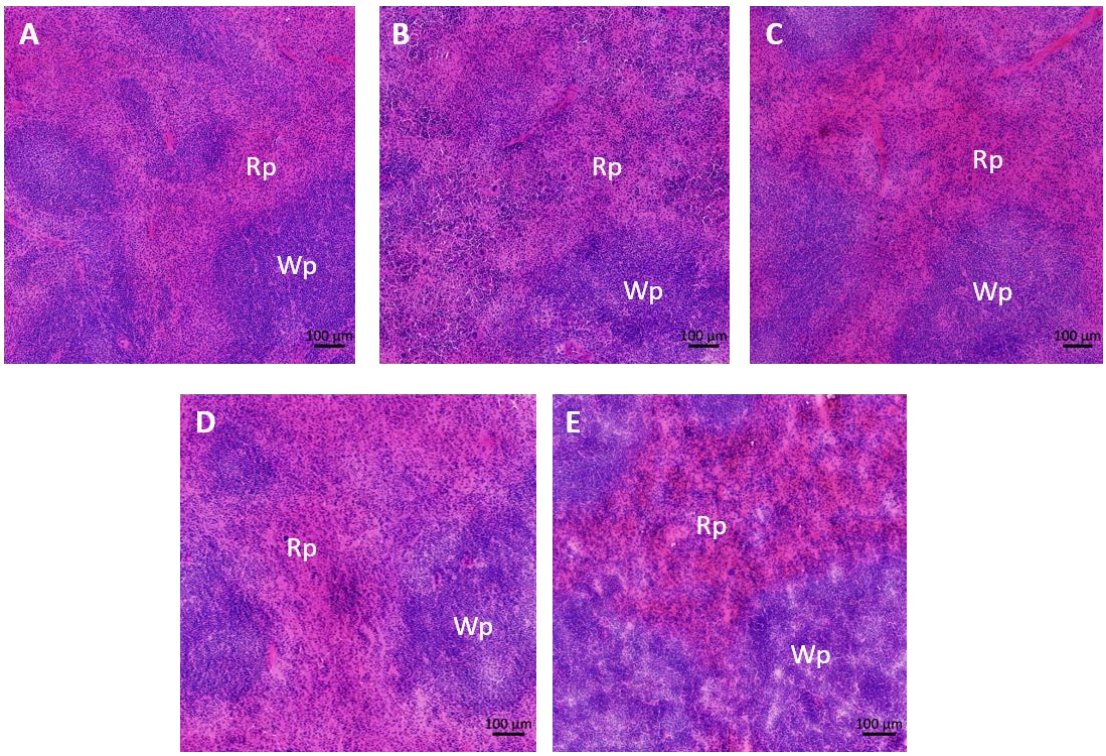

Figure 5.11 Representative Haematoxylin and Eosin stained spleen images of treated mice. Post-mortem spleens were harvested and 8-10µm frozen sections were stained with Haematoxylin and Eosin (H & E) as described in **Chapter 2** (Methods and Materials). Images are representative of (A) uninfected, (B) wk1 post-treatment, (C) wk2 post-treatment, (D) wk3 post-treatment and (E) wk4 post-treatment mice spleens. Scale bar = 100µm, Rp= Red pulp and Wp= White Pulp.

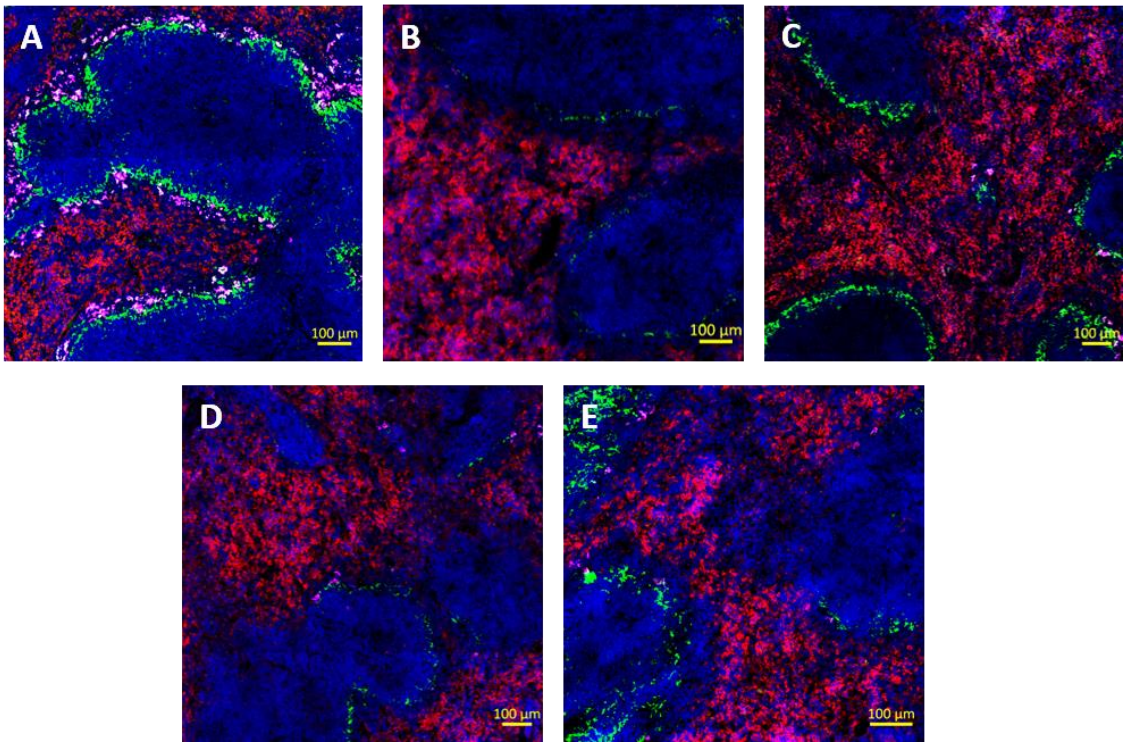

Figure 5.12 Representative IF stained spleen images of treated mice. Frozen spleen sections of 8-10µm thickness were stained with IF markers for different populations of splenic macrophages. (A) Uninfected, (B) wk1 post-treatment, (C) wk2 post-treatment, (D) wk3 post-treatment and (E) wk4 post-treatment, spleen sections were stained for red pulp macrophages (F4/80) and marginal zone macrophages, MMM (CD169) and MZM (SIGNR1). Images were counterstained with DAPI for nuclei and collected on Axio Scan slide scanner. Scale bar = 100µm, F4/80 = Red, CD169 = Green, SIGNR1 = Magenta, DAPI= Blue.

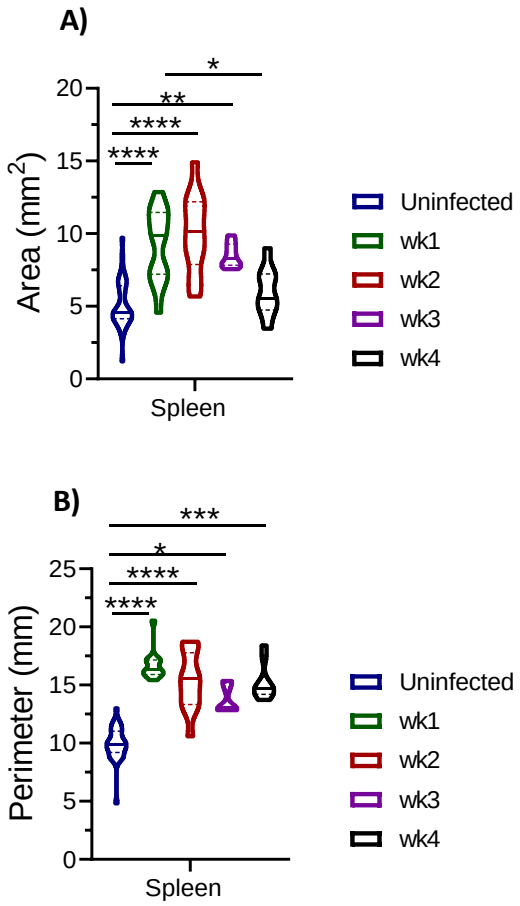

Figure 5.13 Area and perimeter of spleen after treatment. Segmentation analysis was done on the IF stained spleens using StrataQuest TissueGnostics software to calculate (A) area and (B) perimeter of spleen sections with 2-3 ROI per sample. Data are representative of n= 11 uninfected (includes 2-3 mice per time-point) and treated mice at n= 3 wk1, n=3 wk2, n=3 wk3 and n=3 wk4 post-treatment. Data shown as median with quartiles and were analysed using non-parametric Kruskal-Wallis test with Dunn's post-hoc test, *, $p < 0.05$; **, $p < 0.01$; ***, $p < 0.001$; ****, $p < 0.0001$.

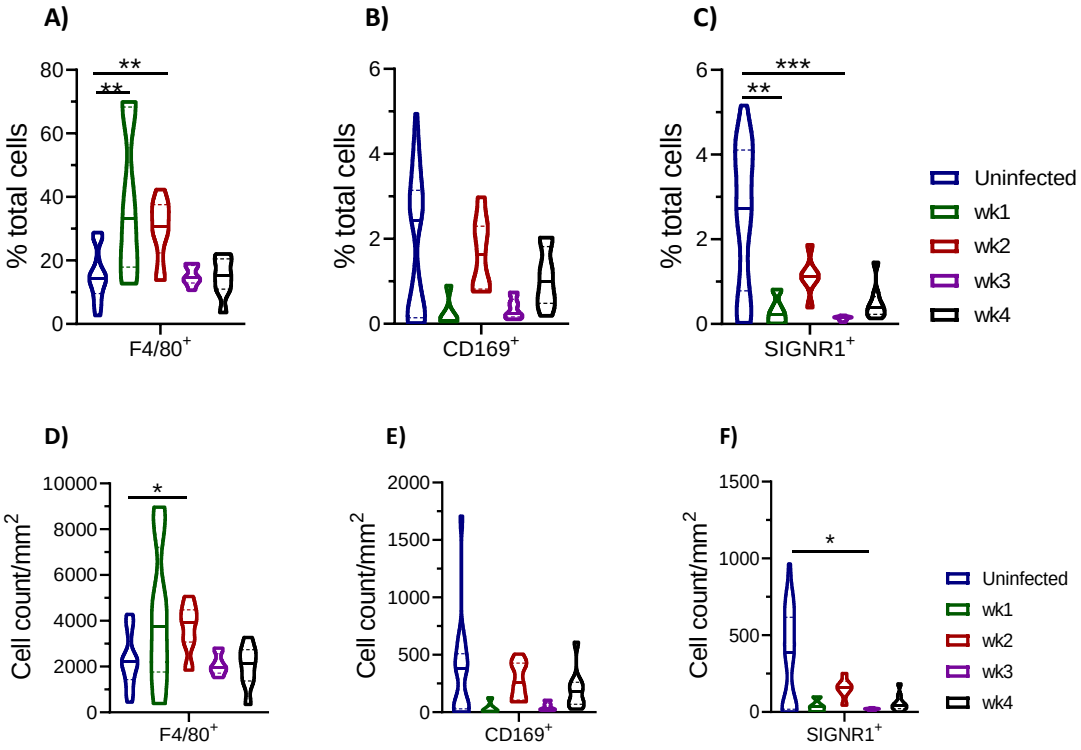

Figure 5.14 Response of splenic macrophages to treatment. Segmentation analysis was done on the IF stained spleen sections using StrataQuest TissueGnostics software. Graphs show the percentage/total cells of (A) F4/80$^+$, (B) CD169$^+$ and (C) SIGNR1$^+$ cells. Cell count of (D) F4/80$^+$, (E) CD169$^+$ and (F) SIGNR1$^+$ cells per unit area (mm^2) was also calculated. Data are representative of n= 11 uninfected (includes 2-3 mice per time-point) and treated mice at n= 3 wk1, n=3 wk2, n=3 wk3 and n=3 wk4 post-treatment. Data shown as median with quartiles and were analysed using non-parametric Kruskal-Wallis test with Dunn's post-hoc test, *, $p < 0.05$; **, $p < 0.01$; ***, $p < 0.001$.

5.3.3 Production of iNOS by macrophages during infection and after treatment

As activated tissue macrophages such as splenic RP macrophages have been associated with enhanced phagocytosis, we were interested to investigate the role of activated macrophages in VL induced cytopenias during infection and post-treatment (213). Frozen sections of liver and spleen of d28 infected and weekly post-treatment experimental mice were stained with immunofluorescent markers for tissue macrophages (F4/80) and iNOS. Segmentation analysis was done on IF stained tissues using StrataQuest TissueGnostics software as described earlier.

Segmentation analysis on IF stained liver sections **(Figure 5.15 A-F)** showed Kupffer cells are increased during infection which decreases after the clearance of parasites post-treatment **(Figure 5.16 A-C)**. Our analysis also shows that the cells inside the granulomas were producing more iNOS than the cells outside the granulomas, with a significant reduction post-treatment **(Figure 5.16 D-E)**. Our data on double-positive cells i.e. iNOS producing Kupffer cells, inside and outside the granulomas ($F4/80^+$ $iNOS^+$), illustrates an increased number of $F4/80^+$ $iNOS^+$ cells at d28 of infection inside the granulomas with a significant reduction after successful treatment **(Figure 5.16 F-G)**. Together these data suggest that Kupffer cells have increased activation of iNOS during infection in an attempt to clear the parasites which decreases after the resolution of granulomas and parasite clearance.

Segmentation analysis was also done on the IF stained spleen sections **(Figure 5.17 A-F)** using StrataQuest TissueGnostics image analysis software. Our analysis shows the expansion of spleen mainly red pulp (RP) at d28 post-infection followed by a reduction after treatment **(Figure 5.18A-C)**. It is mainly due to the enlargement of spleen in response to parasite presence inside RP macrophages.

Our analysis shows an increase in $F4/80^+$ RP macrophages during infection followed by a gradual reduction after treatment **(Figure 5.19 A-C)**. However, it is important to mention that despite a significant reduction in the weight of spleens after treatment, they were bigger in size than the normal spleens even after four weeks post-treatment (data shown in **Figure 5. 8B**).

Interestingly, our analysis on $iNOS^+$ cells shows an increase in the number iNOS producing cells during infection with a further increase after treatment mainly in the RP

than the WP region **(Figure 5.19 D-F)**. Similarly, an increase in double-positive cells ($F4/80^+$ $iNOS^+$) i.e. iNOS producing RP macrophages, was observed at d28 of infection as compared to uninfected/untreated control mice spleens **(Figure 5.19 G-I)**. A further increase in the number of double-positive cells was seen within one week after treatment with a significant reduction at week-4 post-treatment **(Figure 5.19 G-I)**. This data suggest that splenic RP macrophages produce more iNOS in response to treatment perhaps to aid the clearance of parasites.

Increased production of iNOS by macrophages in infected mice livers and spleens could explain excessive blood cell phagocytosis however, an increase in splenic iNOS post-treatment despite the progressive recovery of blood counts need further studies.

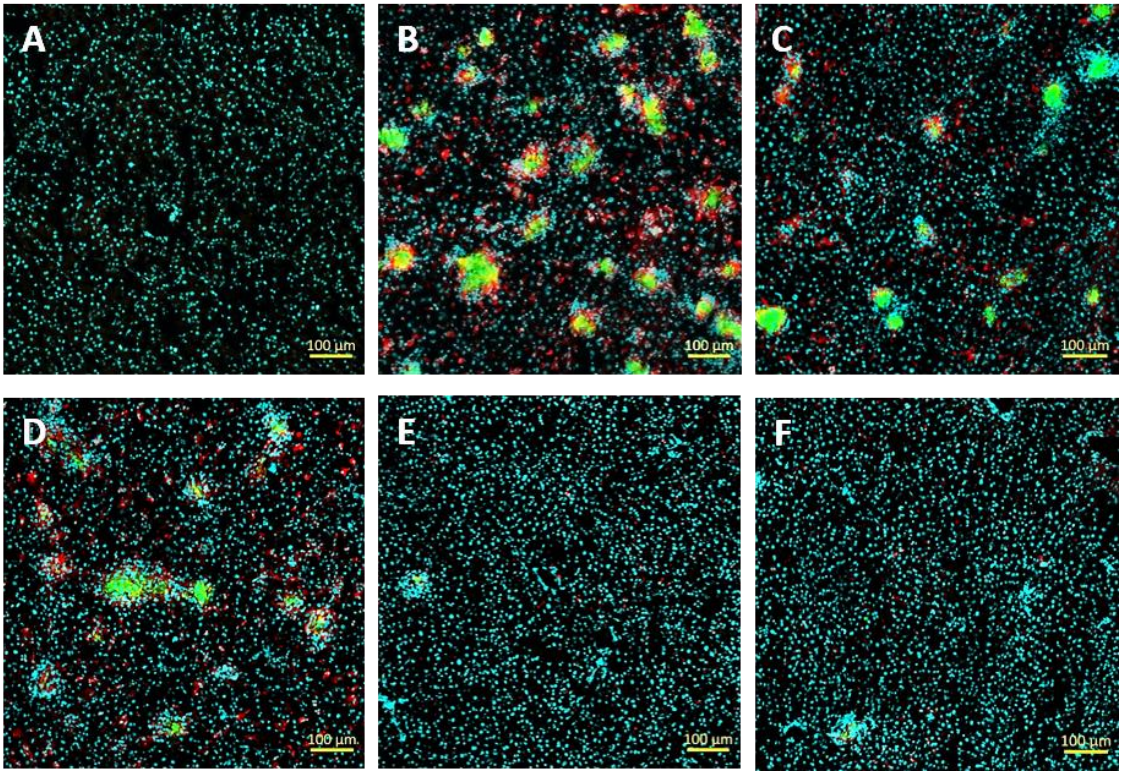

Figure 5.15 Reduction in hepatic iNOS expression in response to treatment. Frozen liver sections of 8-10µm thickness were stained with F4/80 for Kupffer cells along with iNOS antibody and counterstained with DAPI for nuclei. Segmentation analysis was done on the IF stained liver sections using StrataQuest TissueGnostics software. Images are representative of (A) uninfected, (B) d28, (C) wk1, (D) wk2, (E) wk3 and (F) wk4 post-treatment. Scale bar, 100µm, F4/80 = Red, iNOS = Green and DAPI = Turquoise.

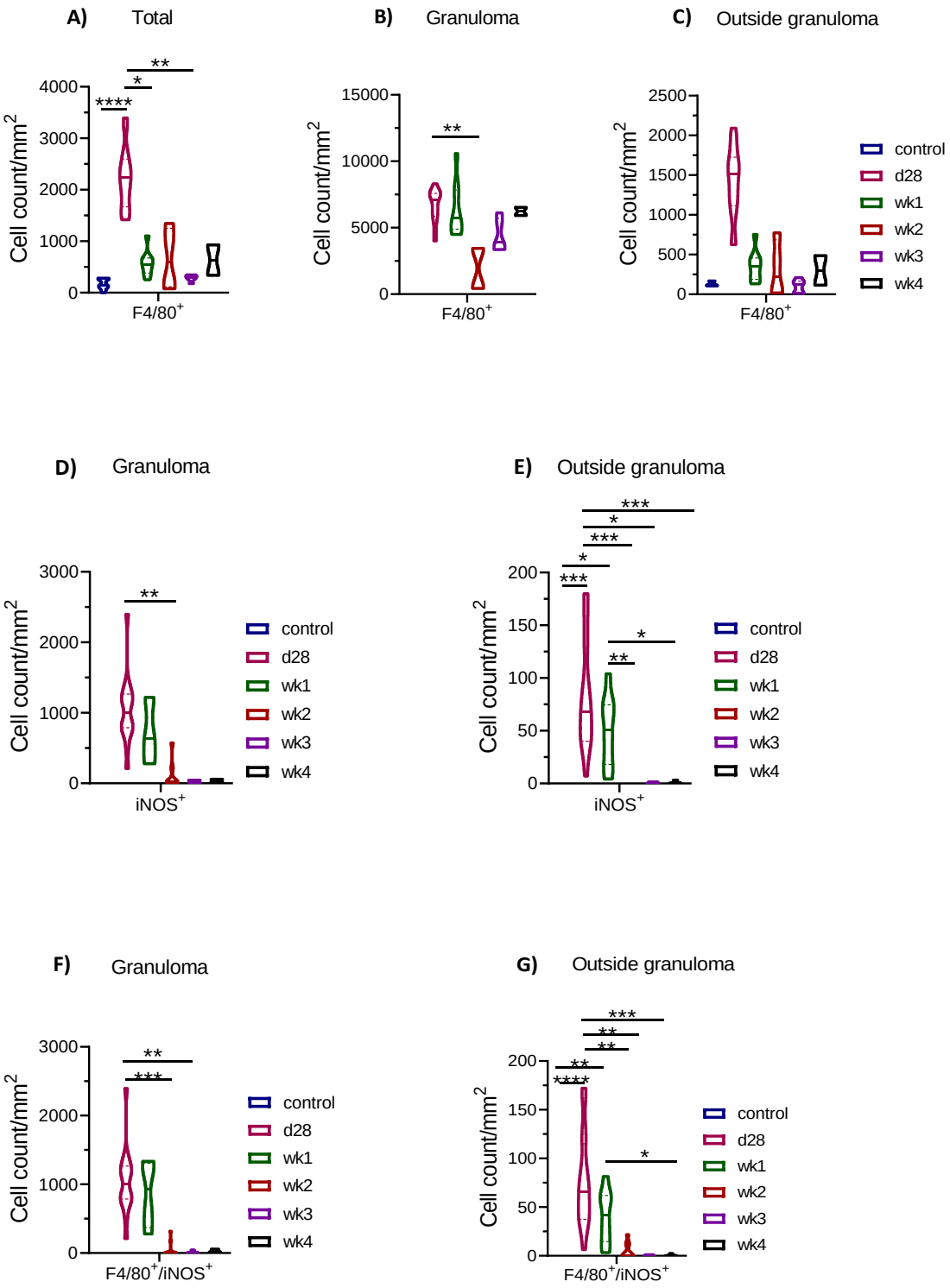

Figure 5.16 iNOS expression in Kupffer cells. Segmentation analysis was done on the IF stained liver sections using StrataQuest TissueGnostics software. Graphs show the cell count/unit area (mm^2) for (A) total $F4/80^+$ Kupffer cells, (B) $F4/80^+$ cells in granulomas and (C) outside granulomas. Cell count/unit area (mm^2) of (D) $iNOS^+$ cells inside

granulomas and (E) outside granulomas, double-positive cells ($F4/80^+$ $iNOS^+$) (F) inside granulomas and (G) outside granulomas. Data are representative of n= 3 controls (uninfected/untreated), n=5 d28 infected and treated mice at wk1, wk2, wk3 and wk4 (n=3 each) post-treatment. Data shown as median with quartiles and were analysed using non-parametric Kruskal-Wallis test with Dunn's post-hoc test, *, $p < 0.05$; **, $p < 0.01$; ***, $p < 0.001$; ****, $p < 0.0001$.

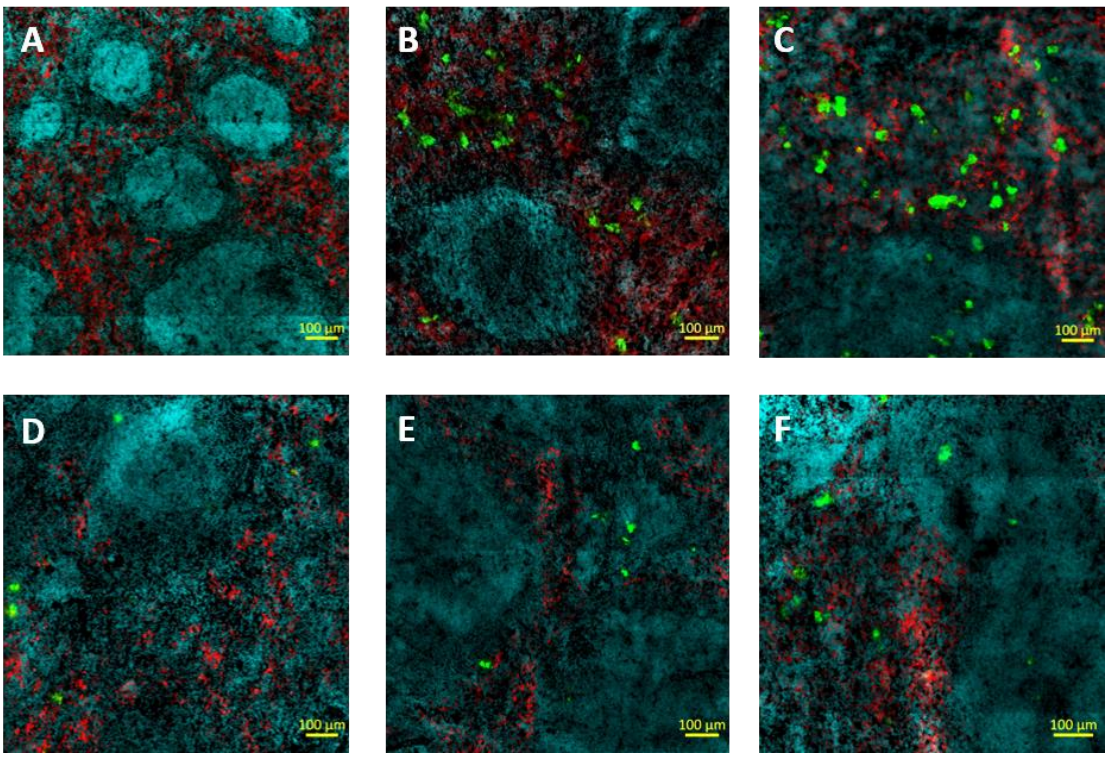

Figure 5.17 Splenic iNOS expression in response to treatment. Frozen spleen sections of 8-10µm thickness were stained with F4/80 for RP macrophages along with iNOS antibody and counterstained with DAPI for nuclei. Segmentation analysis was done on the IF stained spleen sections using StrataQuest TissueGnostics software. Images are representative of (A) uninfected, (B) d28, (C) wk1, (D) wk2, (E) wk3 and (F) wk4 post-treatment. Scale bar, 100µm, F4/80 = Red, iNOS = Green and DAPI = Turquoise.

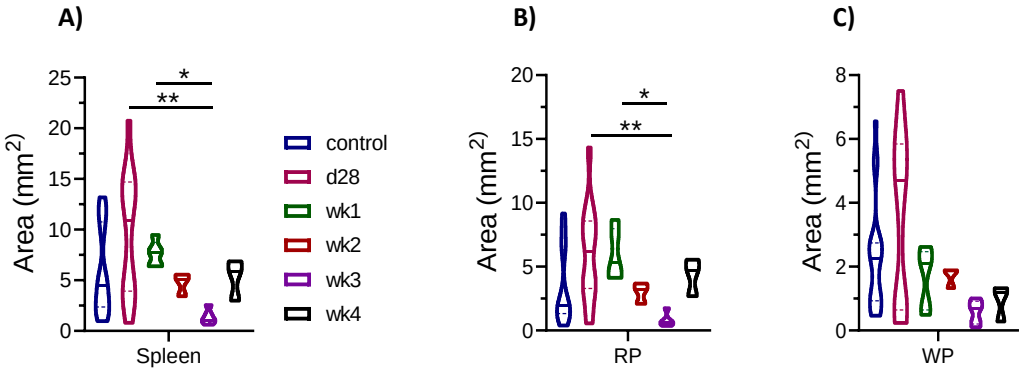

Figure 5.18 Splenic area in response to treatment. Segmentation analysis was done on the IF stained spleen sections using StrataQuest TissueGnostics software. Graphs show the (A) total area of spleen, (B) red pulp (RP) area and (C) white pulp (WP) area of n= 3 controls (uninfected/untreated), n=5 d28 infected and treated mice at wk1, wk2, wk3 and wk4 (n=3 each) post-treatment. Data shown as median with quartiles and were analysed using non-parametric Kruskal-Wallis test with Dunn's post-hoc test, *, $p < 0.05$; **, $p < 0.01$.

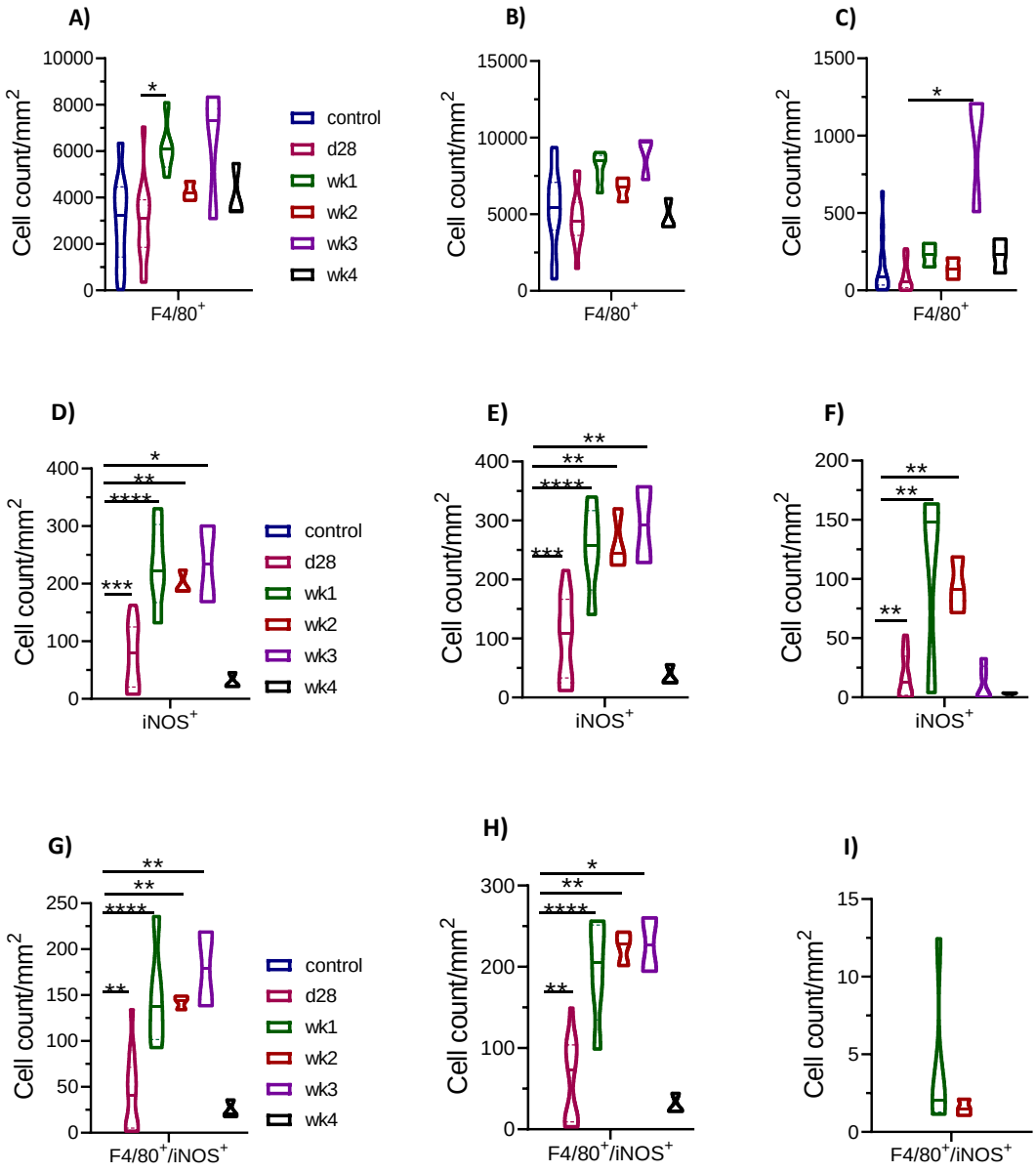

Figure 5.19 iNOS expression in splenic RP macrophages. Segmentation analysis was done on the IF stained spleen sections using StrataQuest TissueGnostics software. Graphs show the cell count/unit area (mm^2) for (A) total $F4/80^+$ RP macrophages, (B) $F4/80^+$ cells in RP and (C) WP during infection and after treatment. Cell count/ unit area (mm^2) of (D) total $iNOS^+$ cells, (E) $iNOS^+$ in RP and (F) WP, and double-positive cells ($F4/80^+$ $iNOS^+$) (G) in total, in (H) RP and (I) WP. Data are representative of n=3 controls (uninfected/untreated), n=5 d28 infected and treated mice at wk1, wk2, wk3 and wk4 (n=3 each) post-treatment. Data shown as median with quartiles and were analysed using non-parametric Kruskal-Wallis test with Dunn's post-hoc test, *, $p < 0.05$; **, $p < 0.01$; ***, $p < 0.001$; ****, $p < 0.0001$.

5.4 Discussion

VL is a systemic disease involving three major organs; liver, spleen and BM, with the dysfunctional immune system and defective haematological profile. As already mentioned, haematological complications have been studied less during disease and after clinical cure. Although studies have suggested that haematological complications are reversible after treatment as reviewed by Varma and Naseem, no data are available in experimental models of the infection (96). Our results on the mechanisms of thrombocytopenia are suggestive of multifactorial pathogenesis, with decreased production of platelets from defective MKs (**Chapter 3**) and enhanced clearance by peripheral mechanisms (**Chapter 4**). Our data on external stimulation of BM MKs have also shown that the damage to MKs is not permanent as these cells retain their potential to produce platelets on stimulation. Similarly, platelet recovery after treatment is suggestive of a transient effect of infection on platelet production however, further studies are required to study the ultrastructure of MKs in treated mice. Recovery of erythrocyte and leucocyte counts in peripheral blood are also suggestive of temporary defects in their production or consumption in the body which are reversible after clinical cure. Intriguingly, the rate of recovery of blood counts are suggestive of the restoration of these underlying mechanisms after treatment and could be used as non-invasive cost-effective markers to assess treatment response.

The immune system is hijacked by the parasite to allow long-term persistence of parasites in tissue macrophages. Clinical and experimental studies have shown that the clearance of parasites from tissues results in the recovery of immune system (114,214). Restoration of normal tissue architecture after treatment is hard to study in humans as most of the diagnostic techniques are invasive and expensive. Although post-treatment resolution of hepatic granulomas in infected mice have been observed in experimental studies, post-treatment changes in other tissues are not studied in detail (114). Further studies are needed to study the long-term effects of treatment on immune system for better understanding of the immune response and the risk of relapse. Normal liver architecture is important for the production of TPO, and the granuloma formation in the liver results in defective TPO production which could be responsible for defective cell cycle, differentiation/proliferation of HSCs and reduced platelet production (**Chapter 3**) (101). As spleen is important to filter harmful blood-borne microorganisms and removal of

old/effete blood cells, architectural changes in the spleens of infected mice might risk the filtration of invading microbes making these immunocompromised patients more prone to infections. Increase in the number of RP splenic macrophages could be responsible for the cell clearance leading to reduction in the number of circulating cells as suggested in other infections (149). Our analysis on the post-mortem livers shows a gradual reduction in their size after treatment along with the restoration of their normal tissue microarchitecture however, splenomegaly remained persistent until four weeks post-treatment and poor recovery of marginal zone macrophages, especially SIGNR1^{+} MZM macrophages. However, the recovery of blood counts could be related to parasite clearance, and/or restoration of normal size and architecture of liver and spleen after treatment. As already discussed, studies on EVL are suggestive of the role of spleen but our data suggest that the correlation between platelet count and spleen weight is lost after treatment. Further studies are required to study the effects of treatment on BM resident cells and tissue microenvironment, and parasite clearance which will be helpful in understanding these mechanisms more clearly and also to predict the relapse or long-term consequences of VL.

Parasite mainly resides inside tissue macrophages avoiding the antimicrobial mechanisms in chronic infection. The role of reactive oxygen and nitrogen species have been described in VL and other infections which are produced as a consequence of immune activation and have been associated with damage to the tissue architecture (87). Interestingly, our results show a reduction in the number of iNOS^{+} Kupffer cells after treatment mainly due to the resolution of infection however, an increase in the number of iNOS^{+} splenic RP macrophages is observed. Increased iNOS activation by inflammatory cells mainly splenic RP macrophages is suggestive of the role of immune system in the clearance of remaining parasites. However, the restoration of blood counts despite increased iNOS production is suggestive of decreased cell destruction while spleen is clearing parasites and other immune cells or the production is doubled to compensate for the destruction. Although we could not measure inflammatory cytokines in post-treatment groups but studies on AmBisome® treated VL mice are suggestive of normalisation of cytokines within one week after treatment (114).

In summary, the results in this chapter demonstrate for the first time in an experimental model of VL that thrombocytopenia is rapidly reversed, in concert with the partial restoration of homeostasis that accompanies successful drug treatment.

Chapter 6. Sequential secondary infection in drug-treated *L. donovani*-infected mice

6.1 Introduction

VL is mainly endemic in countries with poor socioeconomic conditions and health care services. Patients are generally diagnosed at an advance stage with complications, as treatment affordability is a hindrance to timely and proper care. Other infections such as malaria, HIV, helminthic infections are also common in VL-endemic regions and represent a huge burden on health care facilities, in addition to carrying a high risk of morbidity and mortality (115,116). Polyparasitism is a common diagnosis in VL-endemic regions and VL patients are diagnosed with co-infections like HIV, malaria and others, which are not only difficult to treat but also lead to a debilitating illness (116,117). Drugs like miltefosine and AmBisome® work well for a single infection, but the response is poor in co-infected cases (as discussed in **Chapter 5**). Clinical and experimental studies to understand the pathogenesis of co-infections have increased in recent years, but the extent to which prior treated-VL impacts the subsequent infections has not been studied. Apart from co-infections, post-treatment infections in VL patients are expected due to immunocompromised status and high exposure to other endemic infections such as HIV and malaria. In a clinical setting, this is likely due to lack of long-term follow-up, and poor or absent patient registries in these countries.

Both VL and malaria are among the most important infectious diseases on the WHO list of tropical diseases with an overlapping geographical distribution, and high morbidity and mortality (https://www.who.int/topics/tropical_diseases/en/). Malaria and VL, both present with similar clinical features including the tissues involved and cytopenias (158). Similar to VL, studies conducted on malaria have proposed multiple mechanisms responsible for anaemia and thrombocytopenia (153,171). However, due to commonality of symptoms, the risk of misdiagnosis or delayed diagnosis is very common in endemic countries. VL/malaria co-infection has been reported from endemic African and Asian regions with a prevalence of 3-4% in Ethiopia, 5.9% in India and 19% in Uganda (117,173,215,216).

Previously, few experimental studies have been conducted to understand the immunobiology of VL with co-infections. A delayed but fully functional anti-leishmanial granulomatous response was seen in *L. donovani*-infected mice with pre-existing *S. mansoni* infection although granulomas failed to develop around the parasites in pre-existing *S. mansoni* granulomas (217). Experimental studies on malaria/CL co-infection have shown a delayed cutaneous lesion formation whereas, malaria severity was mainly dependent on the strain of *leishmania* (156). Interestingly, increased resistance to the development of *Streptococcus pneumoniae* sepsis was observed in *L. donovani*-infected mice (198). These studies are suggestive of the immune response in delay, control or exacerbation of both or either infection which is likely to exist in human co-infections. Despite the risk of post-treatment infections, no clinical studies or data are available to date. Therefore, we were interested to study the responses of VL to other infections after the clinical cure is achieved using an experimental murine model.

Here, we used rodent malaria as a model of secondary infection in VL treated mice due to geographical representation and a significant overlap of clinical presentation especially haematological complications (117). Our data on post-treatment VL model show a complete recovery of blood counts along with the parasite clearance and restoration of tissue architecture. There are several strains of *Plasmodium* known which cause rodent malaria with findings similar to malaria in humans. Rodent plasmodia are broadly divided into fatal and non-fatal types, with an acute or chronic pattern of infection (218). *Plasmodium berghei ANKA* causes severe fatal malaria with cerebral symptoms and severe anaemia similar to *P. falciparum* in humans (219). *P. chabaudi AS* is generally used to study non-fatal chronic malaria in animal models while *P. yoelii* is another non-virulent strain of chronic rodent malaria. Both of these strains are commonly used as experimental models to study immunopathology of chronic infection (218). Different strains of rodent plasmodia are used in experimental studies as a model of co-infection and superimposed infections, depending on the questions being addressed. Experimental studies involving malaria co-infection with cutaneous leishmaniasis and schistosomiasis have shown growth inhibition of one or the other parasites (156,163). Although VL and malaria are endemic in Indian and African regions, the effects of post-treatment infections have not been studied in experimental models. In order to study the haematological complications of malaria in VL treated mice, we infected mice with previously drug-treated VL, with a non-fatal strain of *P. chabaudi* (220).

6.2 Aims

The aims of this study were;

1. To determine the haematological response to *P. chabaudi* infection in drug-treated *L. donovani*-infected mice
2. To determine the parasitological response to *P. chabaudi* infection in mice with previously treated VL

6.3 Results: Rodent malaria- a pilot experiment

A pilot experiment was performed in C57BL/6 mice to evaluate the kinetics of malaria infection, adverse events with the severity of infection and associated haematological features (**Figure 6.1).** A non-virulent strain of chronic rodent malaria, *P. chabaudi* was used to avoid the risk of high fatality in a model of secondary infection.

C57BL/6 mice were infected with 1 x 10^5 infected erythrocytes via tail vein injection and kept under a strict 12-hour light-dark cycle to maintain the natural life-cycle of *Plasmodium*. Mice were bled within 2 hours of the beginning of dark cycle at each specified time-point to monitor the level of parasitaemia as well as peripheral blood counts. Mice were weighed every day and checked two to three times a day for any signs of disease severity, as per project license recommendations (**Figure 6.1**).

Parasitaemia was measured on Giemsa stained blood smears by counting the number of infected erythrocytes with trophozoites/1000 total erythrocytes x 100. Infected RBCs (iRBCs) were observed within 5 days of infection and numbers increased exponentially from day-7 of infection **(Figure 6.2A)**. Mice started to lose weight with increasing parasitaemia **(Figure 6.2B)**. Weight loss and clinical signs of stress were suggestive of severe infection. The experiment was terminated after eight days of infection to avoid any further complications. Post-mortem liver and spleen weights were measured for the extent of organomegaly, which shows a significant increase in the size of livers and spleens of malaria infected mice as compared to uninfected mice **(Figure 6.3A & B)**.

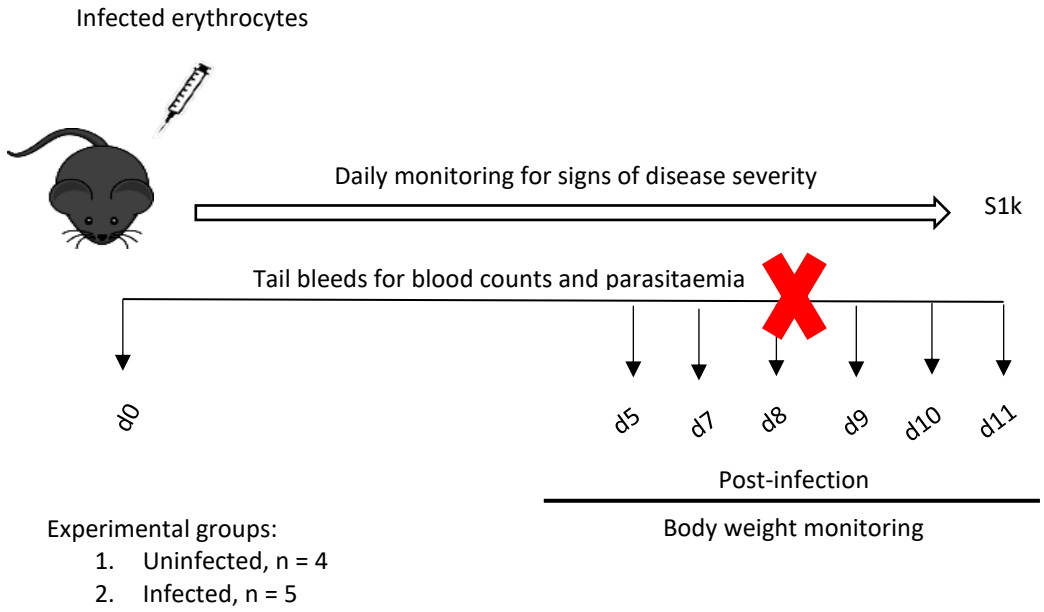

Figure 6.1 Schematic of malaria infection in C57BL/6 mice. Mice were infected with 1 x 10^5 infected erythrocytes via tail vein injection, and bled before and after infection at specified time-points for blood counts and parasitaemia. Daily monitoring of body weight and signs of severity of the disease was done at least two to three times a day during the course of infection. The experiment was terminated at d8 of infection after the parasitaemia and blood count assessment, due to the emergence of signs of stress in some mice. Parasitaemia (%) was calculated by manual count of trophozoite infected erythrocytes/1000 erythrocytes x 100, on the thin blood smears.

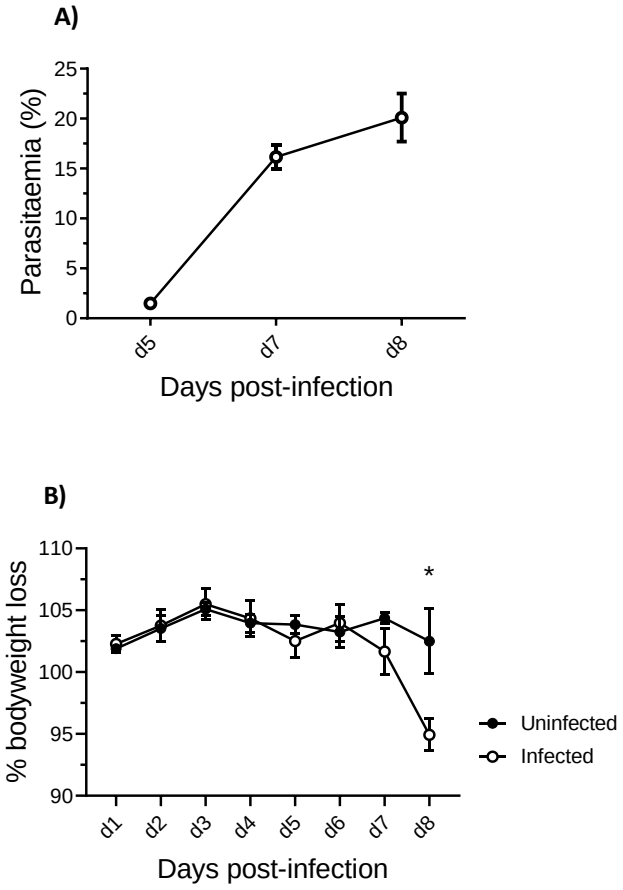

Figure 6.2 Parasitaemia and weight loss in infected mice. Infected mice were checked for (A) parasitaemia at d5, d7 and d8 of infection and monitored every day for any changes in the (B) body weight throughout infection and represented as % of body weight loss. Data show the results of n=4 uninfected and n=5 infected mice at each time-point. Data shown as mean ± SD and were analysed using an unpaired t test comparing uninfected vs infected mice, *, $p < 0.05$.

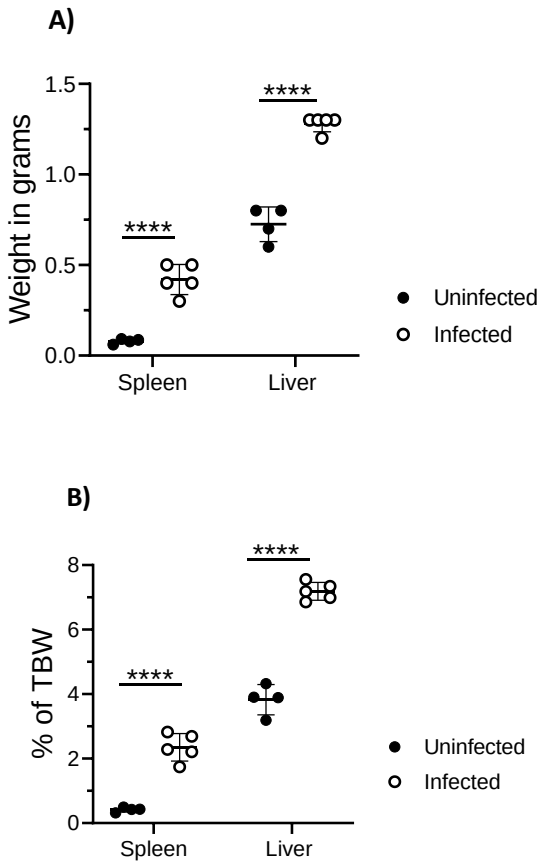

Figure 6.3 Changes in the organ weights in response to malaria. Post-mortem weight of spleens and livers was measured in uninfected and infected mice, represented as (A) weight in grams and (B) % of total body weight. Data show the mean ± SD of n=4 uninfected and n=5 infected mice and analysed using unpaired t test comparing the weight of spleens and livers of uninfected vs infected mice, ****, $p < 0.0001$.

6.3.1 Haematological profile of malaria infected mice

Haematological complications are one of the predominant features of malaria similar to VL and other infections (221). Malaria infected C57BL/6 mice were bled before and after the infection at the time-points specified in the experimental protocol. Malaria infected mice showed progressive thrombocytopenia with increasing parasitaemia **(Figure 6.4A)**. MPV was raised in infected as compared to uninfected mice at the peak of parasitaemia **(Figure 6.4B)**. Malaria infected mice also showed a drop in RBC counts, Hb and Hct with increasing parasitaemia suggestive of infection-induced anaemia **(Figure 6.5A, B & C)**. Other red cell indices i.e. MCV, MCH and MCHC were also consistent with the findings shown in clinical and experimental models **(Figure 6.5D, E & F)**. RDW was also increased in infected mice as compared to uninfected mice which suggests the presence of erythrocytes of variable sizes **(Figure 6.5G)**. Total WBC count and individual leucocyte counts were also checked and showed a slight increase in the number of circulating leucocytes, most probably due to immune response to the infection **(Figure 6.6A-E)**.

6.3.2 Tissue microarchitectural changes in malaria

Disruption of tissue architecture is usually associated with human and murine malaria (222,223). To determine whether this was also evident in our model, frozen sections of spleens and livers with a maximum thickness of 8-10µm were stained with haematoxylin and eosin (H & E) and immunofluorescent (IF) markers for tissue macrophages **(Figure 6.7 and 6.8)**. Segmentation analysis on stained sections showed an increase in the area and perimeter of both spleen and liver sections **(Figure 6.9A-D)**.

IF demonstrated that tissue macrophages in both the spleen (RP macrophages) and liver (Kupffer cells) of malaria infected mice were increased compared to uninfected mice **(Figure 6.10A-H)**. In the spleen, there was a significant reduction in the number of marginal zone macrophages (MZM) and marginal metallophilic macrophages (MMM) indicative of the disruption of marginal zone **(Figure 6.10A-H)**.

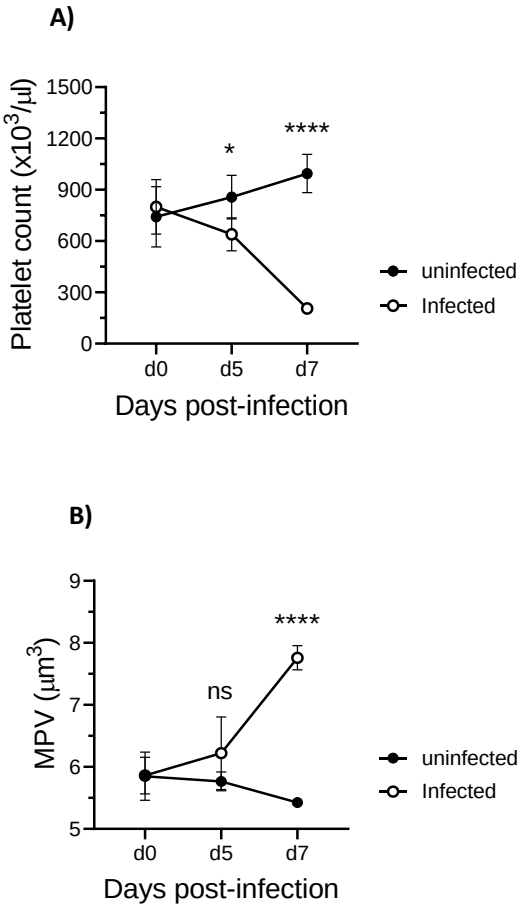

Figure 6.4 Thrombocytopenia in rodent malaria. C57BL/6 malaria infected and uninfected mice were bled at d0 (pre-infection) and then at d5 and d7 post-infection for blood counts. (A) Platelet counts and (B) MPV were measured at each time-point. Data are representative of n=4 uninfected and n=5 infected mice. Data shown as mean ± SD and were analysed using unpaired t test comparing uninfected vs infected groups at each time-point, p value, ns, non-significant; *, $p < 0.05$; ****, $p < 0.0001$.

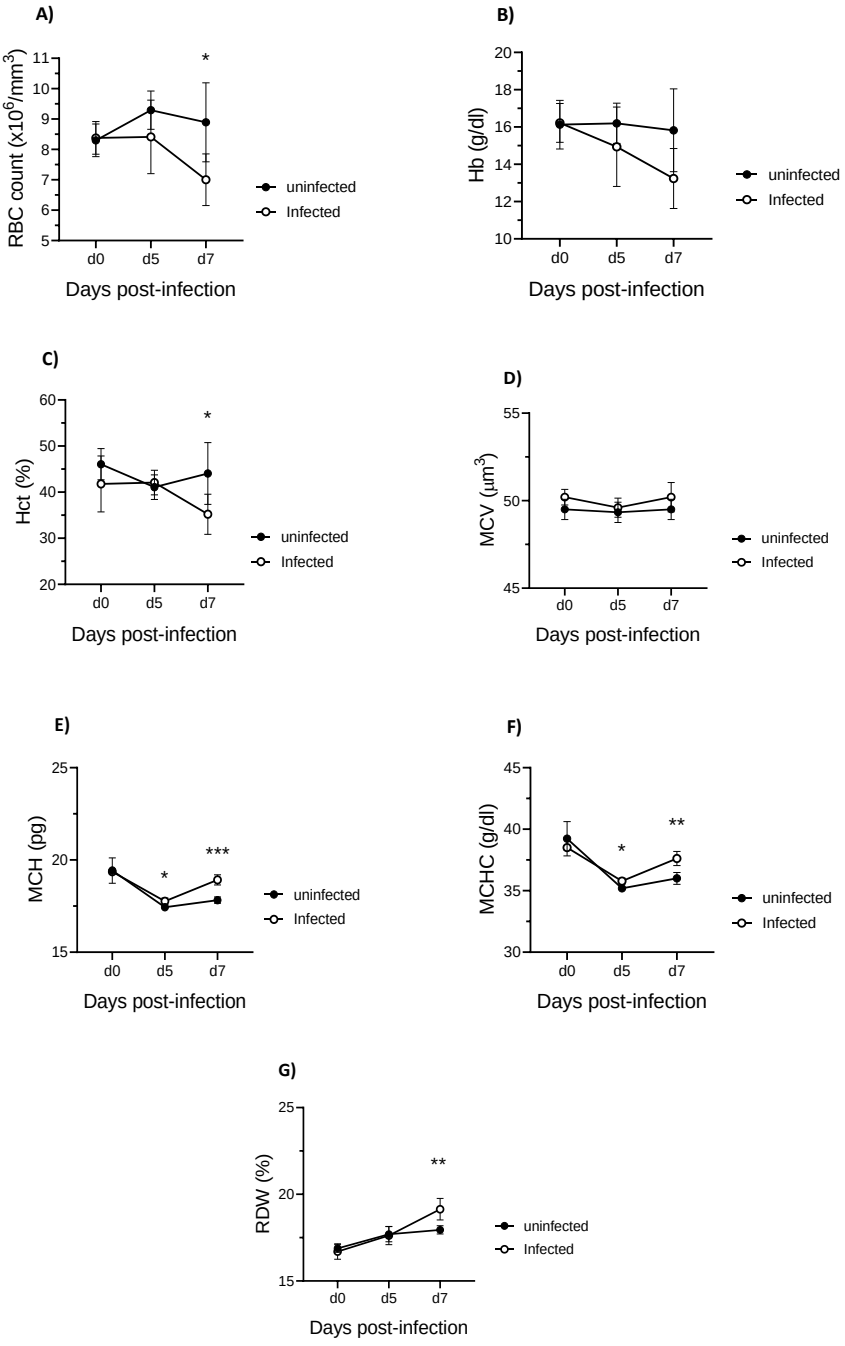

Figure 6.5 Changes in erythrocyte counts and indices in malaria infected mice. C57BL/6 malaria infected and uninfected mice were bled at d0 (pre-infection) and then at d5 and d7 post-infection for blood counts. Graphs are representative of (A) RBC count, (B) Hb, (C) Hct, (D) MCV, (E) MCH, (F) MCHC and (G) RDW at each time-point. Data show the results of n=4 uninfected and n=5 infected mice. Data shown as mean ± SD and were analysed using unpaired t test comparing uninfected vs infected groups at each time-point, *, $p < 0.05$; **, $p < 0.01$; ***, $p < 0.001$.

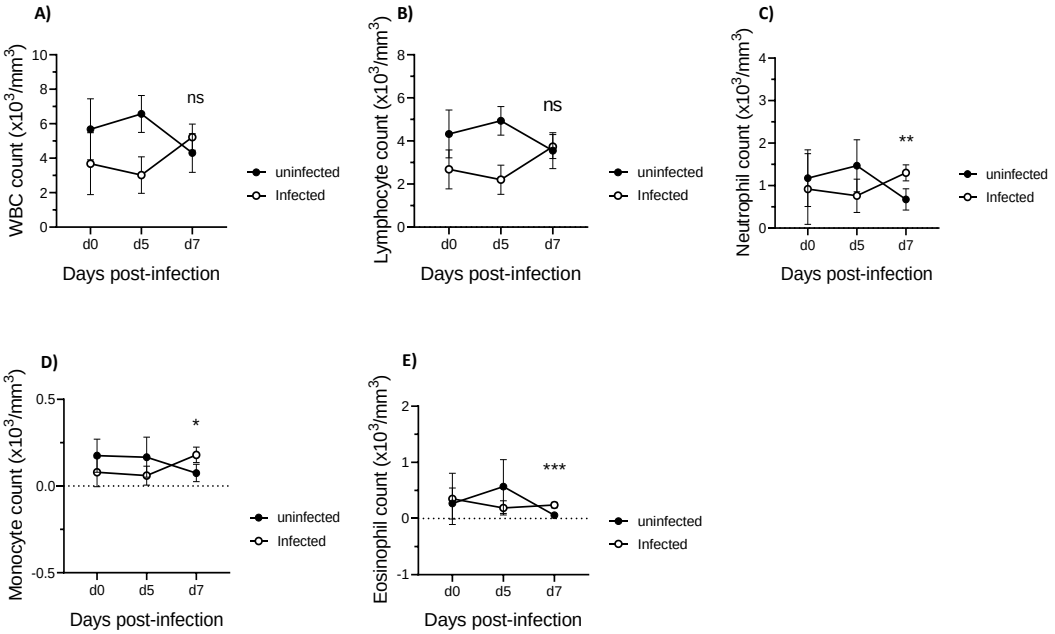

Figure 6.6 Changes in leucocyte counts in malaria infected mice. C57BL/6 malaria infected and uninfected mice were bled at d0 (pre-infection) and then at d5 and d7 post-infection for blood counts. Graphs are representative of (A) WBC count, (B) Lymphocyte count, (C) Neutrophil count, (D) Monocyte count and (E) Eosinophil count at each time-point for n=4 uninfected and n=5 infected mice. Data shown as mean ± SD and were analysed using unpaired t test comparing uninfected vs infected groups at d7 time-point, p value, ns, non-significant; *, $p < 0.05$; **, $p < 0.01$; ***, $p < 0.001$.

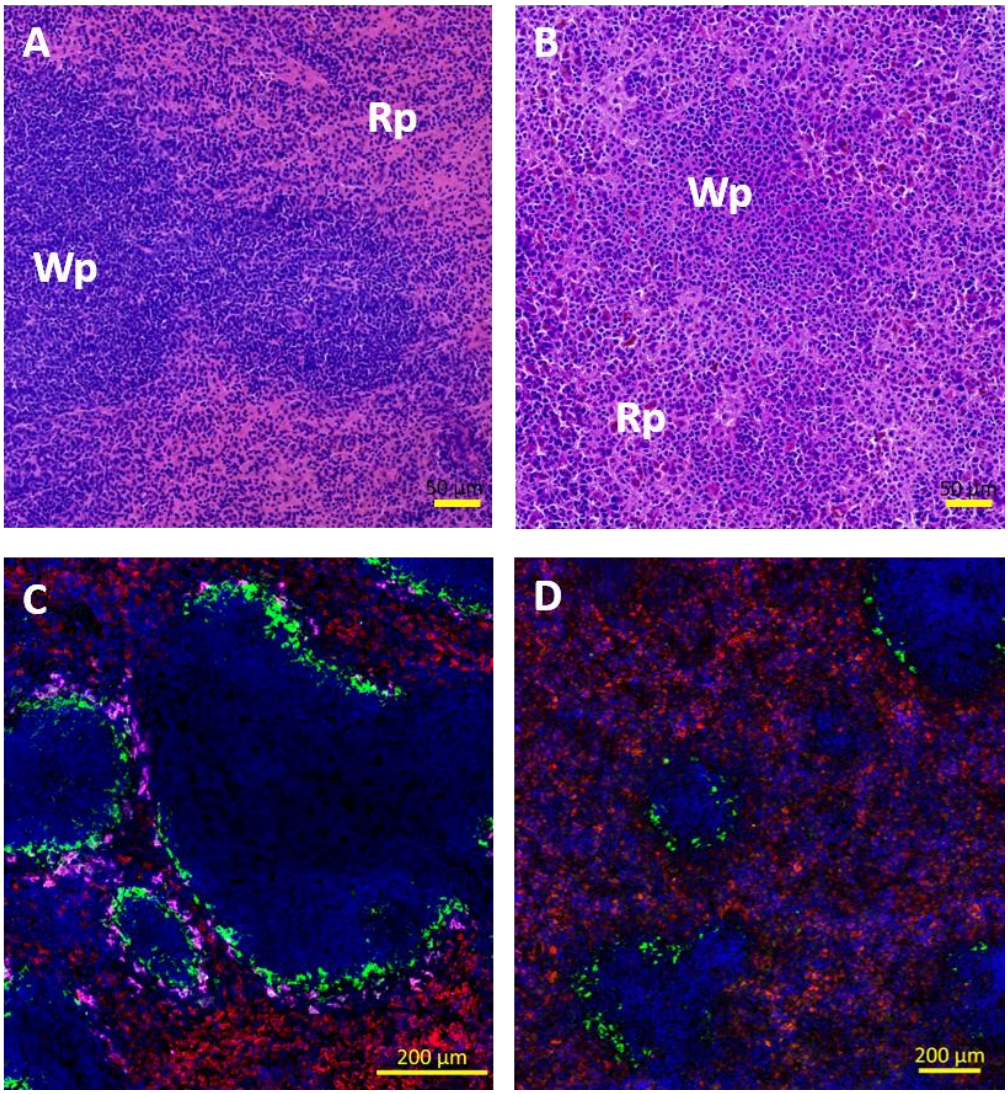

Figure 6.7 Representative H & E and IF stained spleen images of malaria infected mice. Frozen spleen sections of 8-10µm thickness were stained with H & E and IF markers as described in Materials and Methods (**Chapter 2**). Images show H & E stained (A) uninfected and (B) d8 infected spleens and IF stained (C) uninfected and (D) d8 infected spleens with macrophage markers. Spleens were stained with F4/80 for RP macrophages (red), CD169 for MMM (green) and SIGNR1 for MZM (magenta) for splenic macrophages and counterstained with DAPI for nuclei (blue). Images were collected using AxioScan slide scanner at 20x resolution. Scale bar, 50µm (H & E), 200µm (IF) images. Wp = White pulp, Rp = Red pulp.

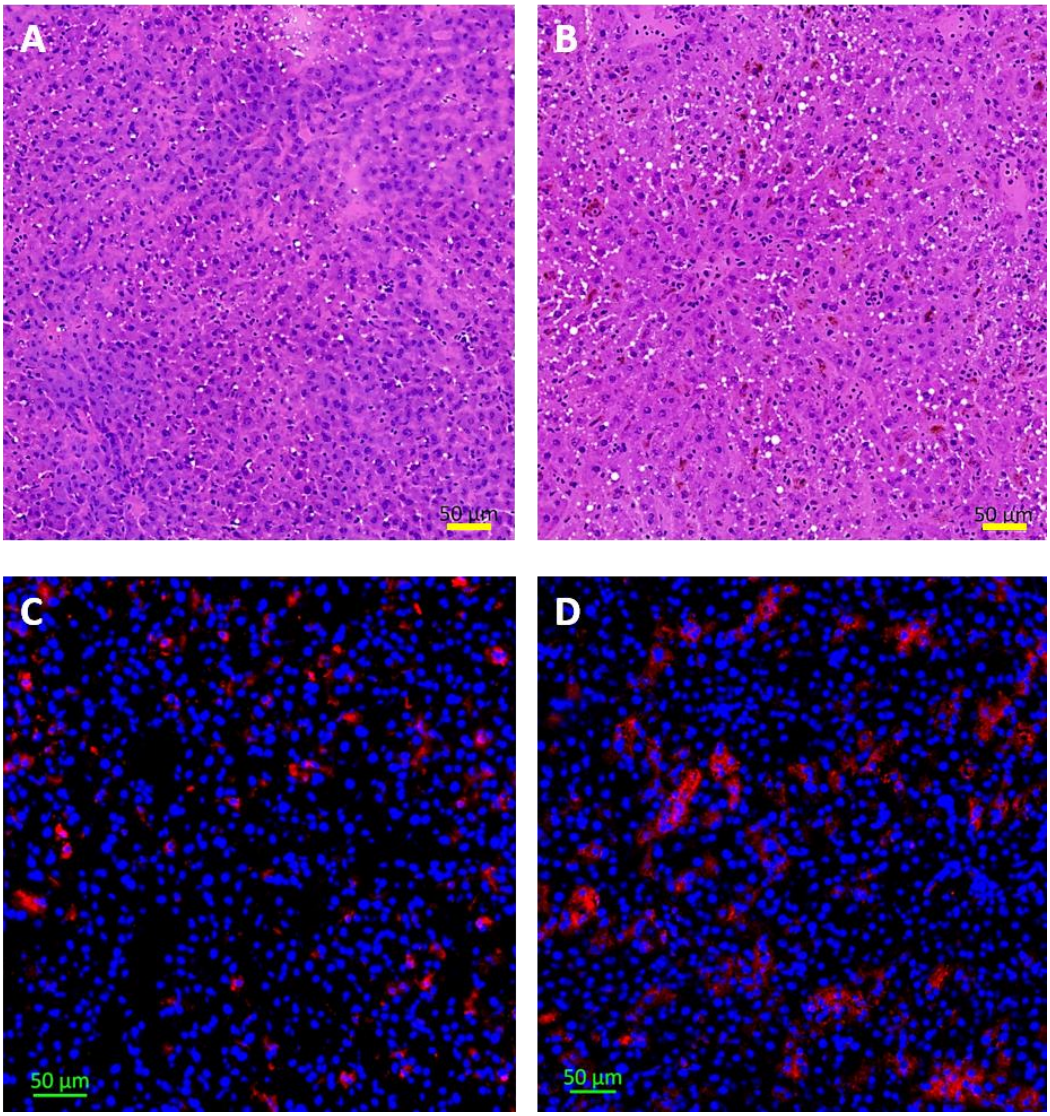

Figure 6.8 Representative H & E and IF stained liver images of malaria infected mice. Frozen liver sections of 8-10µm thickness were stained with H & E and IF markers as described in Materials and Methods (**Chapter 2**). Images show H & E stained (A) uninfected and (B) d8 infected livers and IF stained (C) uninfected and (D) d8 infected livers. Liver sections were stained with F4/80 for Kupffer cells (red) and counterstained with DAPI for nuclei (blue). Images were collected using AxioScan slide scanner at 20x resolution. Scale bar, 50µm.

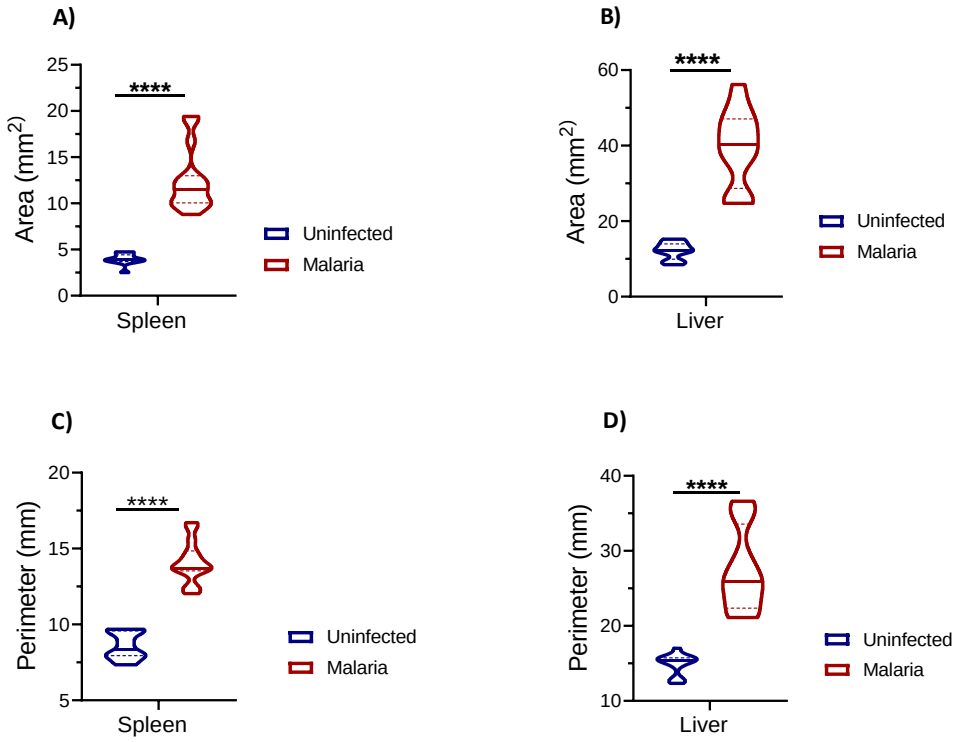

Figure 6.9 Area and perimeter analysis on IF stained images of malaria infected mice. Segmentation analysis was done on IF stained images using StrataQuest TissueGnostics software. Area of (A) spleen and (B) liver sections was calculated along with the perimeter of (C) spleen and (D) liver sections. Data are representative of n=4 uninfected and n=5 infected mice with 2-3 ROI per samples. 1 ROI= 1 tissue section. Data were analysed using Mann Whitney non-parametric test comparing median (with quartiles) of uninfected vs infected data for each parameter, ****, $p < 0.0001$.

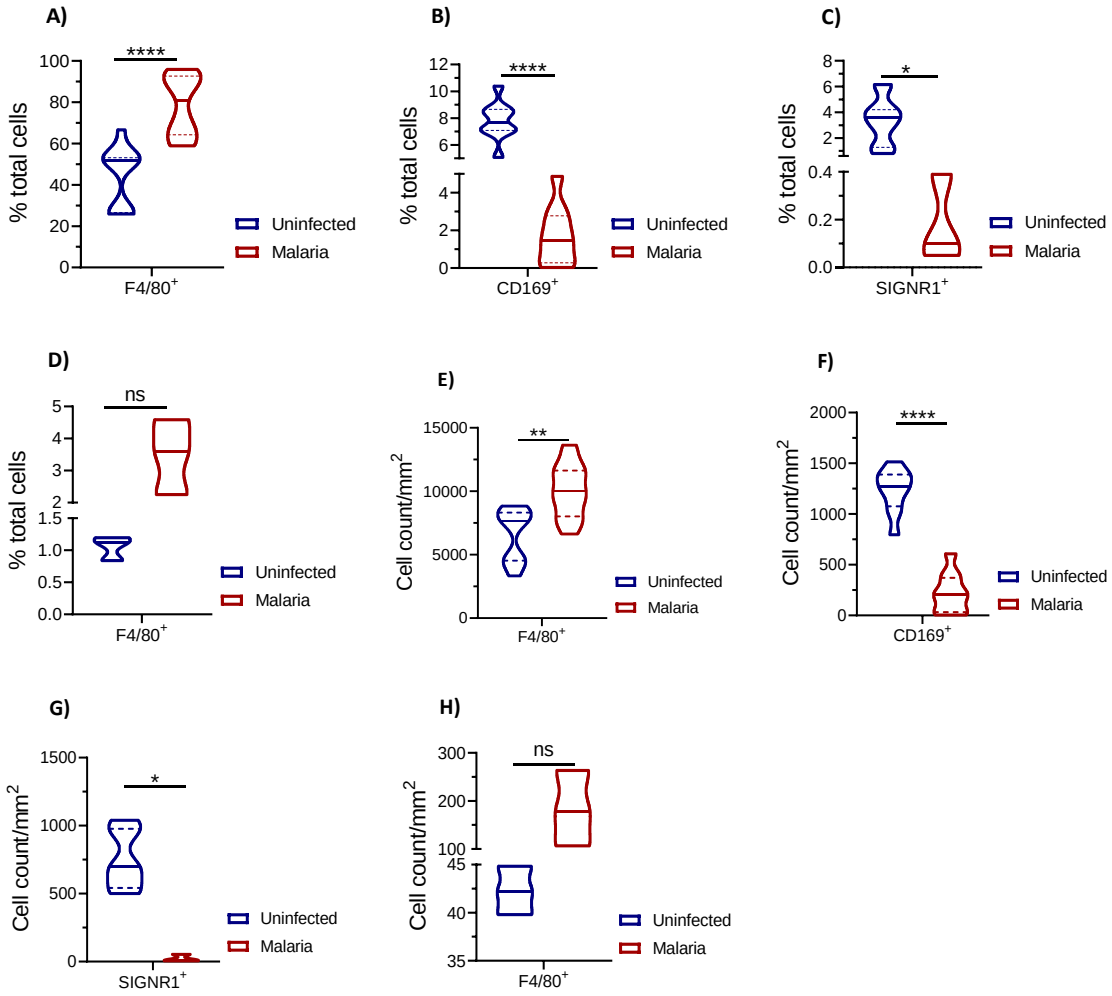

Figure 6.10 Spleen and liver macrophages in response to malaria. Segmentation analysis was done on IF stained spleen and liver images using StrataQuest TissueGnostics software. Data show the % of cells per total number of cells for splenic RP macrophages, (A) F4/80$^+$ and marginal zone macrophages: (B) CD169$^+$ and (C) SIGNR1$^+$, and (D) F4/80$^+$ hepatic Kupffer cells. Cell count/unit area (mm^2) of total spleen for F4/80$^+$ RP macrophages, CD169$^+$ MMM and SIGNR1$^+$ MZM macrophages, and F4/80$^+$ Kupffer cells is shown in (E), (F), (G) and (H) respectively. Data are representative of n=4 uninfected and n=5 infected mice with 2-3 ROI per samples. 1 ROI= 1 tissue section. Data were analysed using Mann Whitney non-parametric test comparing median (with quartiles) of uninfected vs infected data for each parameter with p value, ns, non-significant; *, $p < 0.05$; ****, $p < 0.0001$.

6.4 Malaria as a secondary infection in drug-treated *L. donovani*-infected mice

L. donovani-infected mice were treated with a single dose of AmBisome® and left for four weeks to allow the clearance of parasites to below detectable levels and recovery of blood and bone marrow parameters (see **Chapter 5**). Five cohorts of mice were used: 1. Uninfected mice (C); 2. Mice receiving 1 x 10^5 *P. chabaudi* iRBCs (M); 3. *L. donovani*-infected mice (VU); 4. Drug-treated *L. donovani*-infected mice receiving 1 x 10^5 *P. chabaudi* iRBCs (VM); 5. Drug-treated *L. donovani*-infected mice (VT) **(Figure 6.11)**. Parasitaemia, blood parameters and body weight changes were monitored during the course of infection in all groups.

6.4.1 Response to malaria in VL treated mice

In malaria infected mice, iRBCs started appearing in the blood circulation at d5 post-infection, peaking around d9 followed by a progressive decline **(Figure 6.12A)**. In drug-treated *L. donovani*-infected mice, the trend and peak parasitaemia were similar but the kinetics was delayed **(Figure 6.12A)**. A delay in the rise and drop of parasitaemia in drug-treated *L. donovani*-infected mice could be due to the immune protection provided by previous *L. donovani* infection.

To determine whether malaria as a secondary infection induced any signs of relapse or appearance of amastigotes in the tissues of drug-treated *L. donovani*-infected mice, post-mortem liver and spleen impression smears were stained with Giemsa solution and LDU's were calculated as described earlier. No parasites were seen on the impression smears of drug-treated *L. donovani*-infected mice irrespective of whether they received secondary malaria challenge. Hence, there was no evidence of parasitological relapse after exposure to *P. chabaudi* **(Figure 6.12B)**. The relatively low parasite burden of VU mice by d56 of primary infection is expected given the normal course of *L. donovani* infection in C57BL/6 mice **(Figure 6.12B)**.

Our data show that the signs of delayed response to malaria by VM group as compared to group M mice. Although weight loss was a prominent feature of malaria in both groups,

the VM group mice showed a delayed overall response to malaria including weight loss as shown by the % of body weight loss and total body weight (grams) **(Figure 6.13A & C)**. No change in the body weights of other groups was noticed **(Figure 6.13B & D)**.

Post-mortem organ weights were also measured to estimate the extent of organomegaly in infected mice. Our results show an increase in the spleen and liver weights of VT, VM and group M mice as compared to other control groups **(Figure 6.14A-E)**. No significant difference in the weight of kidneys was noticed in malaria infected groups.

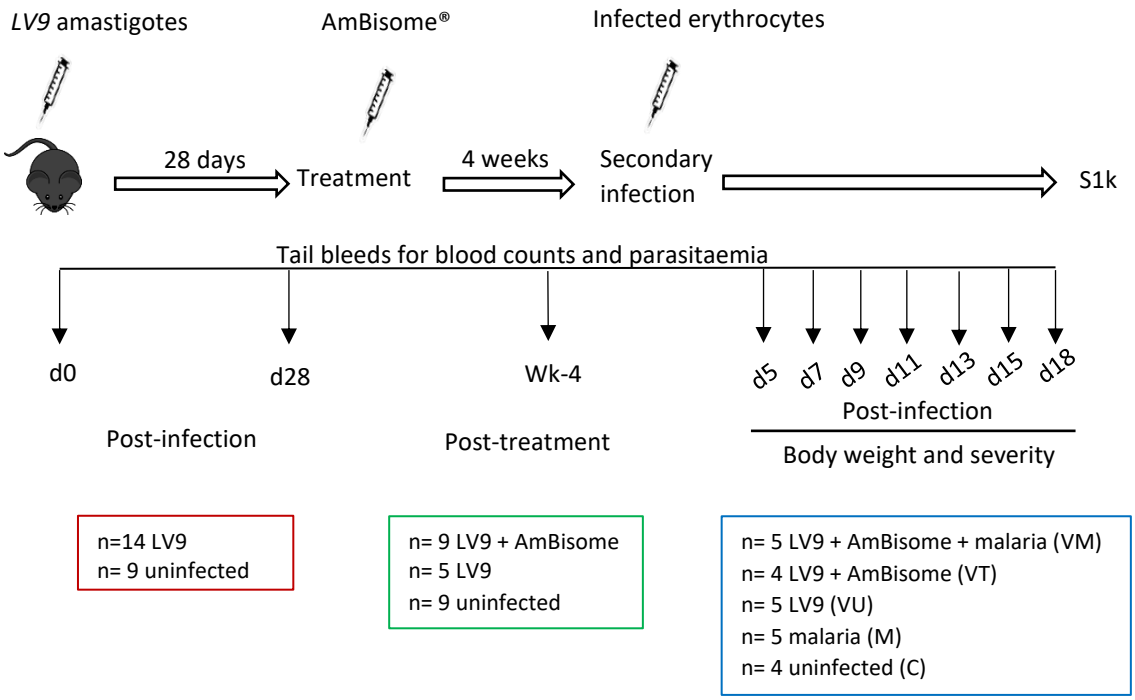

Figure 6.11 Schematic of malaria as a secondary infection in drug treated *L. donovani*-infected mice. C57BL/6 mice were infected with *LV9* amastigotes (n=14) via tail vein injection followed by treatment with a single dose of 8mg/kg of AmBisome® intravenously at d28 post-infection (n=9). A group of uninfected (M; n=5) and four weeks VL treated mice (VM; n=5) were infected with 1 x 10^5 *P. c. chabaudi (AS)* infected erythrocytes via tail vein injections. A group of VL untreated (VU; n=5), VL treated (VT; n=4) and uninfected/untreated (C; n=4) were included as controls. All mice were bled at d0 (pre-infection), at d28 of VL infection, four weeks post-AmBisome® treatment (Wk-4) and then at d5, d7, d9, d11, d13, d15 and d18 of malaria for blood counts and parasitaemia. Parasitaemia was measured on Giemsa stained blood smears by counting the number of infected erythrocytes with plasmodium trophozoites/1000 total erythrocytes x 100. Mice were monitored for any changes in the total body weight and clinical signs of disease severity. Mice were sacrificed at d18 post-bleed and tissues were harvested for further analysis.

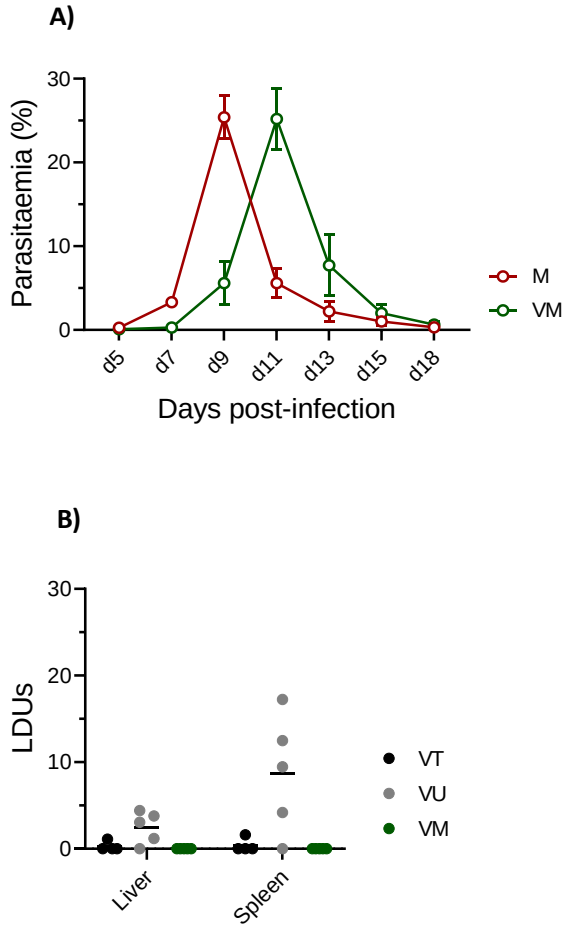

Figure 6.12 *P. chabaudi* parasitaemia and LDUs in infected mice. Both groups of malaria infected mice were bled at specified time-points and (A) parasitaemia was calculated on the blood smears by counting infected erythrocytes with trophozoites as described earlier. Data show the mean ± SD of n=5 M and n=5 VM mice. (B) LDUs on liver and spleen impression smears were also counted for n=4 VT, n=5 VU and n=5 VM mice.

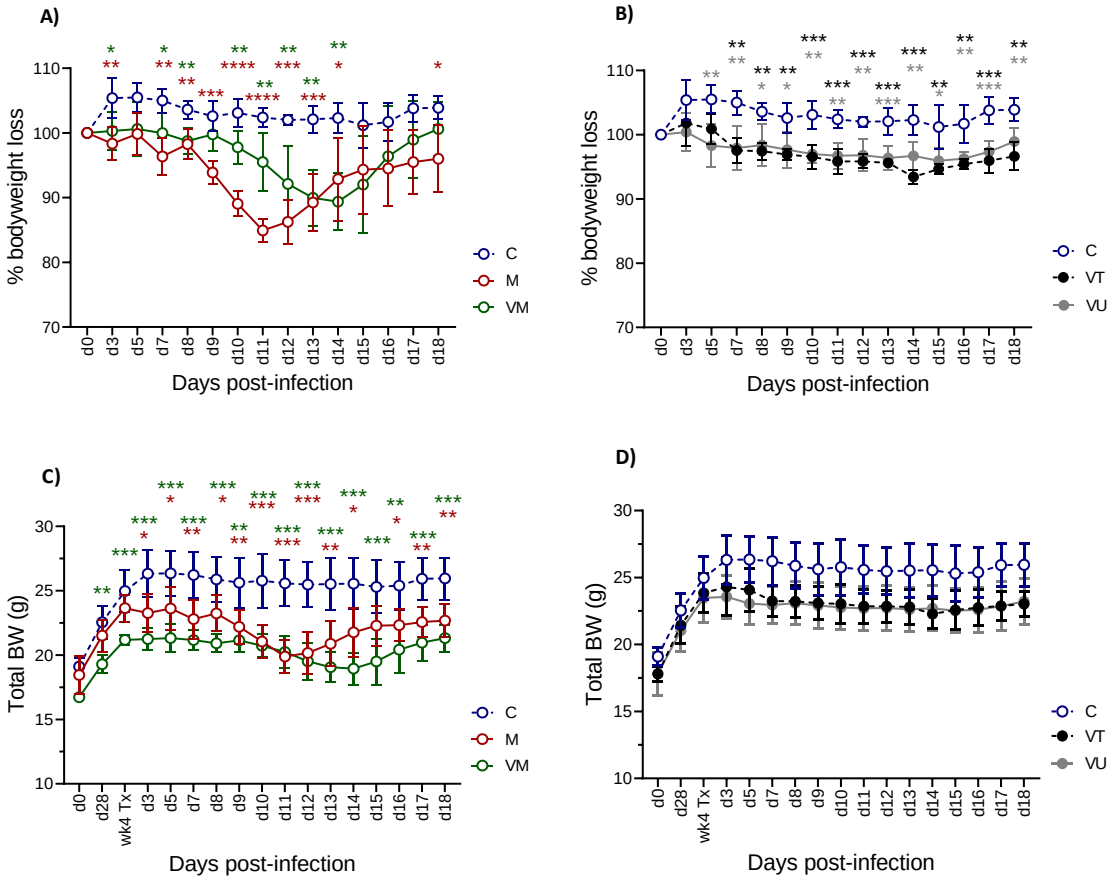

Figure 6.13 Weight loss in malaria infected mice. Total body weight was measured in all malaria infected and control groups, before and after malaria infection. Data (A & B) show the % of body weight loss of group C, M, VM, VT and VU mice. Graphs (C & D) show the mean ± SD of weight in grams of all mice at each time-point along with pre-infection (d0), d28 of VL (d28), four weeks post-AmBisome® treatment (wk-4) and post-malaria at specified days. Data show the results of n=4 C, n=4 VT, n=5 VU, n=5 M and n=5 VM mice. Data were analysed using ANOVA with Dennett's post-hoc test comparing mean (± SD) of M and VM groups with C group (A & C), and VT and VU groups with C group (B & D), *, $p < 0.05$; **, $p < 0.01$; ***, $p < 0.001$ and ****, $p < 0.0001$.

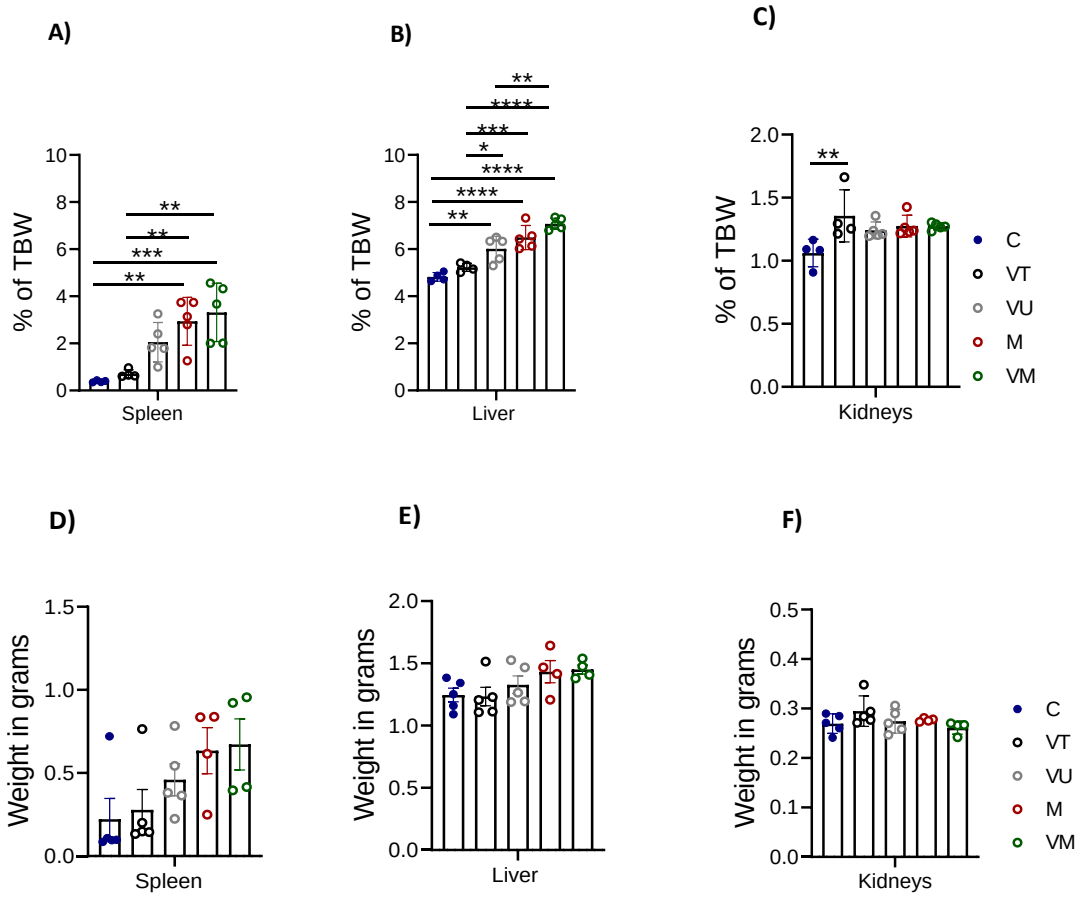

Figure 6.14 Organomegaly in response to malaria. Post-mortem organ weights were measured in all experimental groups. Data show the weight of (A) spleen, (B) liver and (C) kidneys as a % of total body weight. Weight of (D) spleen, (E) liver and (F) kidneys is also shown in grams. Data are representative of n=4 C, n=4 VT, n=5 VU, n=5 M and n=5 VM mice. Data shown as mean ± SEM and were analysed using ANOVA with Tukey's as post-hoc test, *, $p < 0.05$; **, $p < 0.01$; ***, $p < 0.001$ and ****, $p < 0.0001$.

6.4.2 Haematological response to malaria in VL treated mice

Platelet count and MPV (**Figure 6.15**), erythrocyte count and indices (**Figure 6.16**) and leucocyte counts (**Figure 6.17**) for uninfected/untreated control mice (C), drug-treated *L. donovani*-infected mice (VT), *L. donovani*-infected mice untreated (VU), malaria infected (M) and drug-treated *L. donovani*-infected mice given malaria (VM) mice were derived from routine blood draws.

Our findings show a delayed haematological response to malaria in VM mice as compared to M mice, consistent with the kinetics of infection. A delayed onset of thrombocytopenia and early recovery of platelet count was noticed in VM mice as compared to M mice **(Figure 6.15A)**. However, the rate of thrombocytopenia progression and severity was similar in malaria infected groups. No difference in the platelet count was noticed in C and VT mice but a partial restoration of platelet count was seen in VU mice **(Figure 6.15B)**. Similarly, the increase in platelet volume (MPV) was also delayed in VM mice as compared to M but no difference was noticed in control groups **(Figure 6.15C and D)**.

Similar to thrombocytopenia, malaria-induced anaemia was delayed in the VM group in comparison to M group, assessed by RBC count, Hb and Hct **(Figure 6.16A, C and E)**. Control groups showed no alteration in any of these parameters **(Figure 6.16B, D and F)**. Other red cell indices MCV, MCH, MCHC and RDW showed a similar pattern in all groups **(Figure 6.16G-N)**.

Total WBC count started rising with increasing parasitaemia in M group however, leucocytosis was delayed to a later stage in VM mice **(Figure 6.17A)**. Our data show an increase in total WBC count after d13 of malaria when parasitaemia started dropping in the peripheral blood as shown in **Figure 6.12A**. A delayed increase in the lymphocyte, monocyte, granulocyte and eosinophil count was noticed in VM group as compared to M group **(Figure 6.17C, E and G)**. Interestingly, total and individual leucocyte counts remained higher even after a complete decline in parasitaemia in malaria infected groups. No difference was noticed in control groups **(Figure 6.17B, D, F and H)**.

Together these data suggest that haematological changes in the peripheral blood are sensitive to the presence of parasites in the circulation and change according to the stage of infection.

We previously identified a correlation between platelet counts and organ weights in VL mice (**Chapter 3**). This was also the case for platelet counts and spleen weights in both M and VM, and also the VU mice **(Figure 6.18A-F)**. However, that correlation is lost in VT mice similar to uninfected/untreated controls (C) suggesting that normal size is important for the maintenance of platelet counts within the normal range **(Figure 6.18B and F)**. Correlation between platelet counts and liver weights was not significant in any group **(Figure 6.18A-F)**.

6.4.3 Thrombopoietin production in single and sequentially infected mice

As previously discussed (**Chapter 3**), TPO plays a significant role in platelet production. Therefore, we measured serum TPO levels by Quantikine TPO ELISA as per manufacturer's guidelines in blood samples from all groups of mice **(Figure 6.19)**. VT mice had similar levels of TPO compared to C mice, indicative of their treatment response and significant restoration of blood homeostasis. VU, VM and M mice all displayed reduced serum TPO levels, approximating 50% of that seen in C mice. Hence, both infections reduce TPO levels to a similar extent with no indication of synergistic activity.

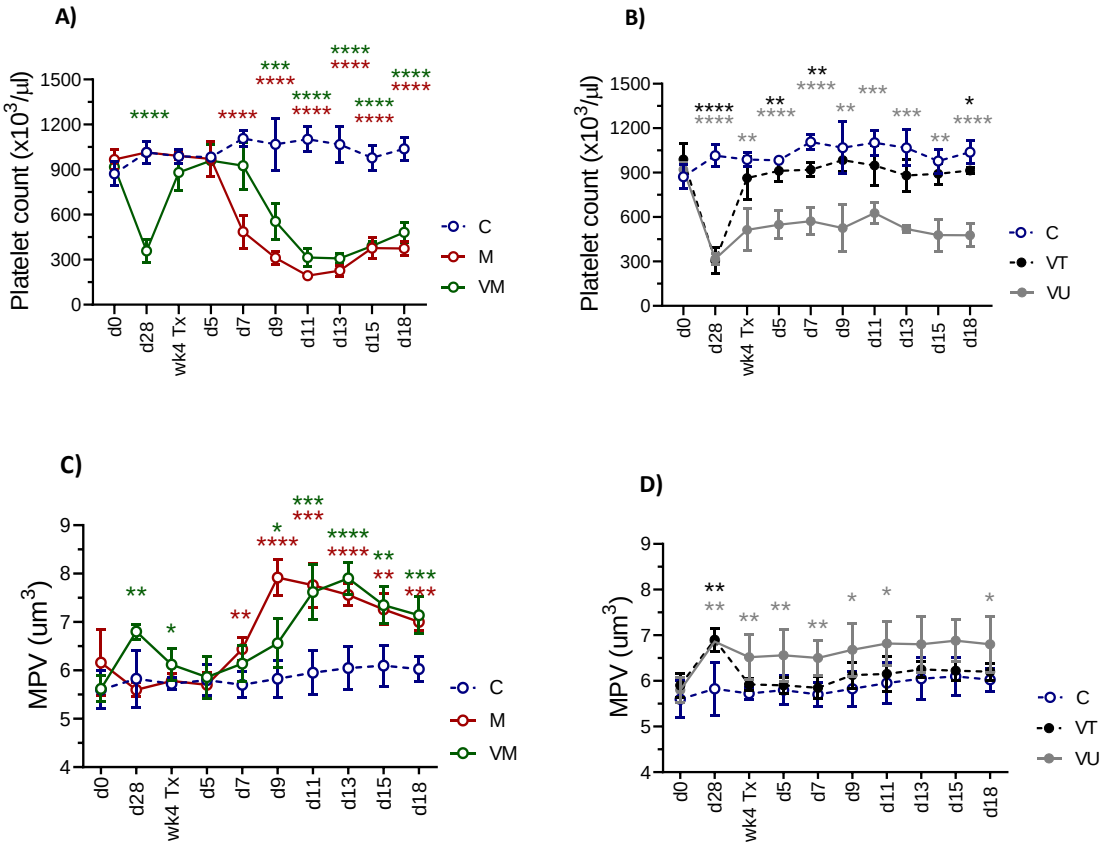

Figure 6.15 Platelet count changes in VL treated and malaria infected mice. Mice were bled at specified time-points for blood counts as shown in **Figure 6.11**. Data are representative of platelet counts (A & B) and MPV (C & D) of n=4 C, n=4 VT, n=5 VU, n=5 M and n=5 VM mice from a single experiment. Data were analysed using ANOVA with Dennett's post-hoc test comparing mean (± SD) of M and VM groups with C group (A & C), and VT and VU groups with C group (B & D), *, $p < 0.05$; **, $p < 0.01$; ***, $p < 0.001$ and ****, $p < 0.0001$.

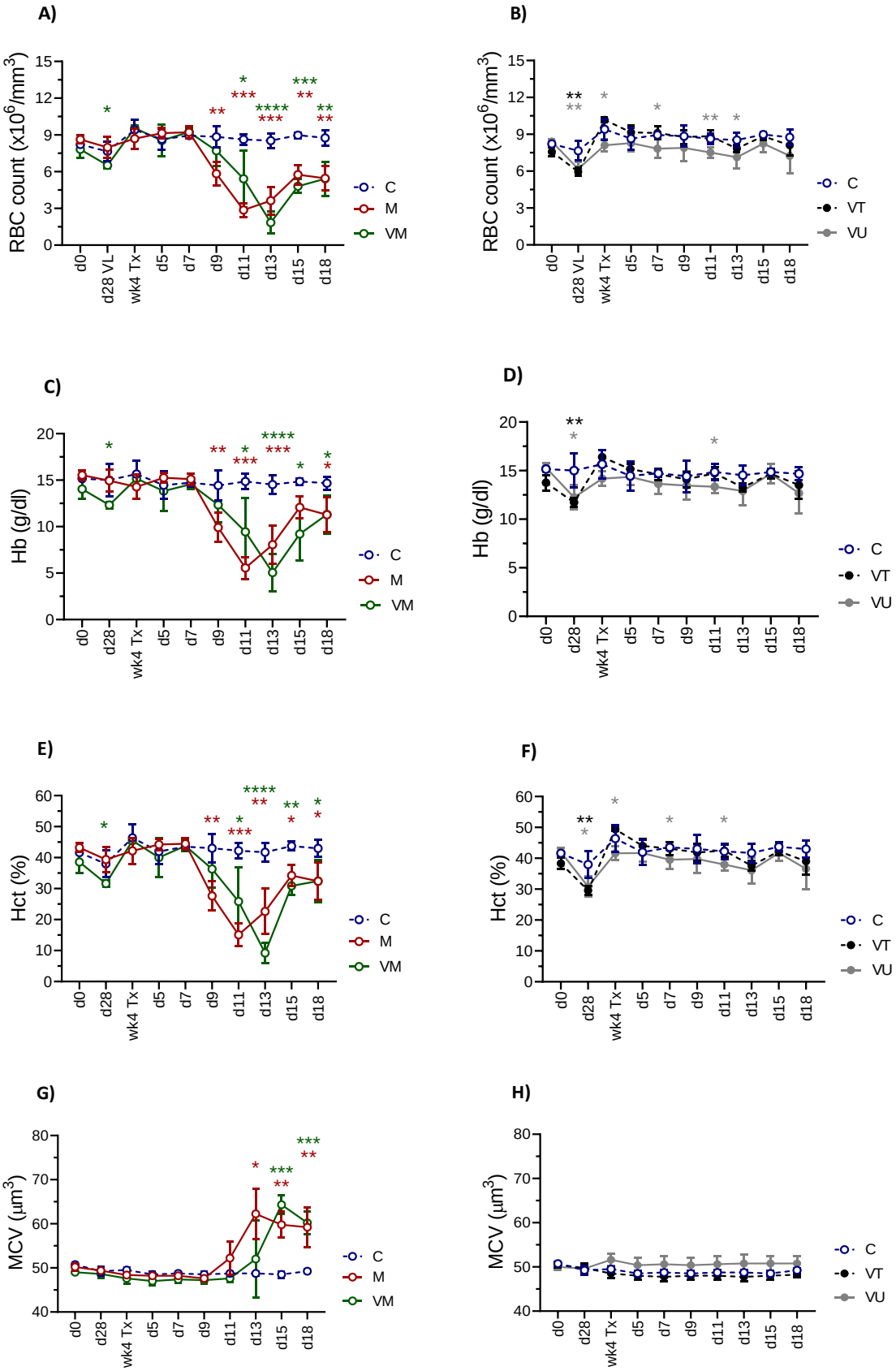
A)
RBC count (x10^6/mm^3)
C
M
VM
B)
RBC count (x10^6/mm^3)
C
VT
VU
C)
Hb (g/dl)
C
M
VM
D)
Hb (g/dl)
C
VT
VU
E)
Hct (%)
C
M
VM
F)
Hct (%)
C
VT
VU
G)
MCV (µm^3)
C
M
VM
H)
MCV (µm^3)
C
VT
VU
d0
d28 VL
wk4 Tx
d5
d7
d9
d11
d13
d15
d18

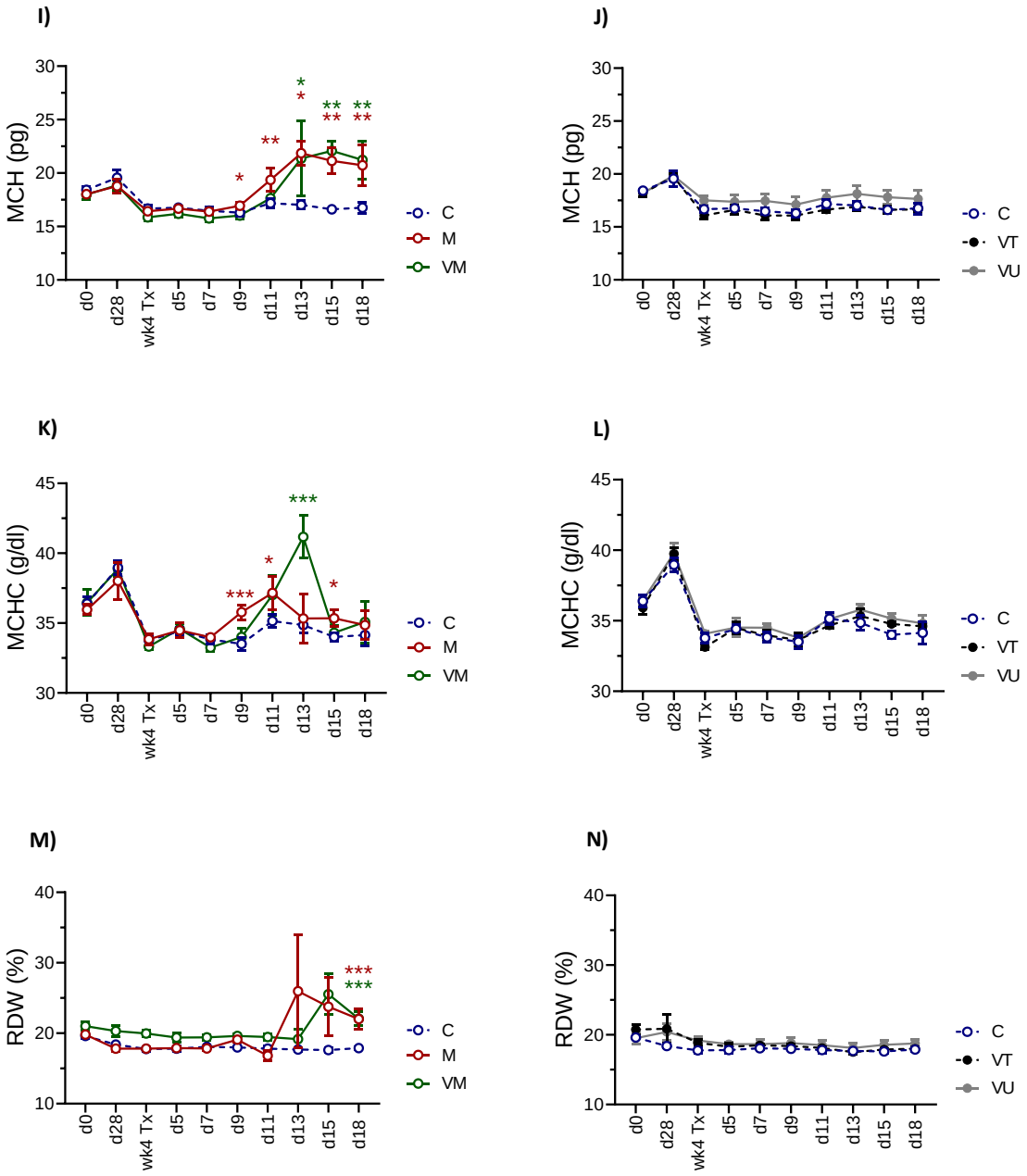

Figure 6.16 Erythrocyte count and red cell indices in VL treated and malaria infected mice. Mice were bled at specified time-points for blood counts as shown in **Figure 6.11**. Data are representative of (A & B) RBC count, (C & D) Hb, (E & F) Hct, (G & H) MCV, (I & J) MCH, (K & L) MCHC and (M & N) RDW of n=4 C, n=4 VT, n=5 VU, n=5 M and n=5 VM mice. Data were analysed using ANOVA with Dennett's post-hoc test comparing mean (± SD) of M and VM groups with C group (A, C, E, G, I, K and M), and VT and VU groups with C group (B, D, F, H, J, L and N), *, $p < 0.05$; **, $p < 0.01$; ***, $p < 0.001$ and ****, $p < 0.0001$.

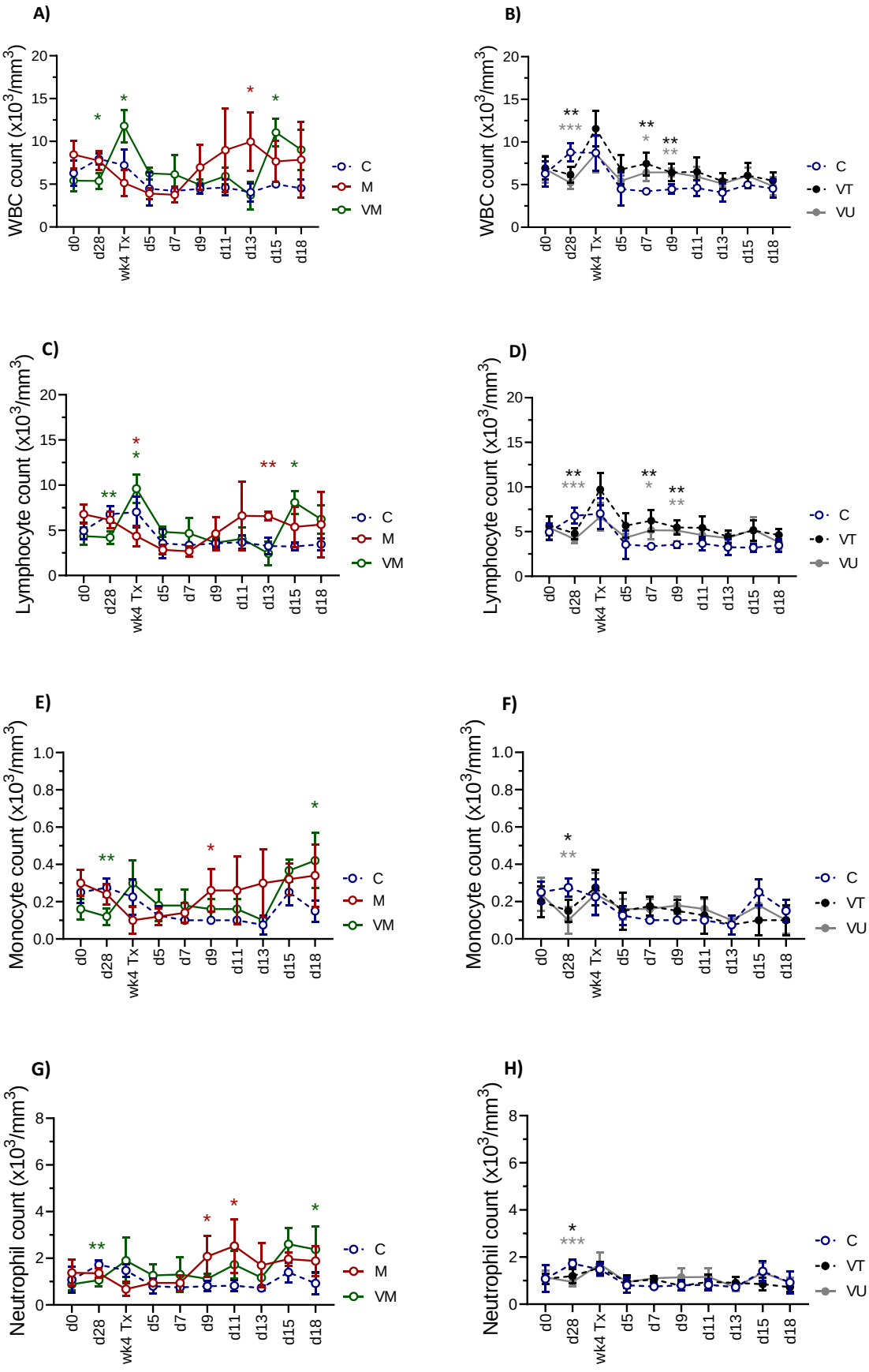
A)
WBC count (x10^3/mm^3)
C
M
VM
B)
WBC count (x10^3/mm^3)
C
VT
VU
C)
Lymphocyte count (x10^3/mm^3)
C
M
VM
D)
Lymphocyte count (x10^3/mm^3)
C
VT
VU
E)
Monocyte count (x10^3/mm^3)
C
M
VM
F)
Monocyte count (x10^3/mm^3)
C
VT
VU
G)
Neutrophil count (x10^3/mm^3)
C
M
VM
H)
Neutrophil count (x10^3/mm^3)
C
VT
VU
d0
d28
wk4 Tx
d5
d7
d9
d11
d13
d15
d18

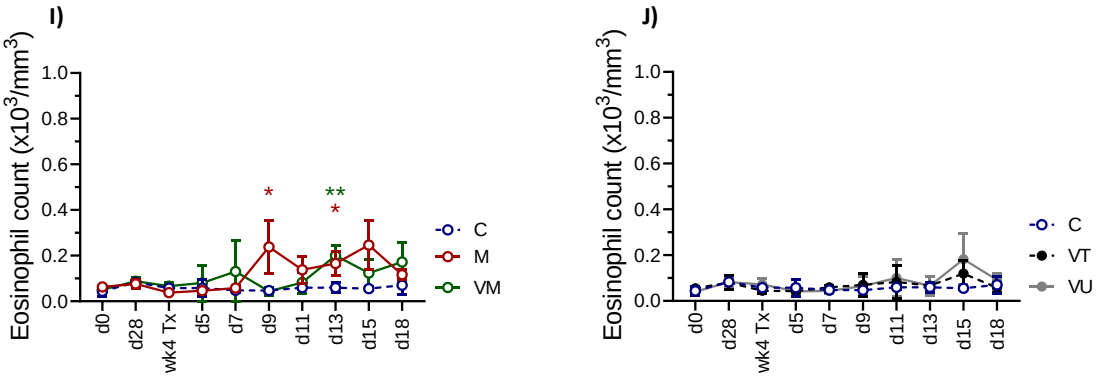

Figure 6.17 Leucocyte count changes in VL treated and malaria infected mice. Mice were bled at specified time-points for blood counts as shown in **Figure 6.11**. Data are representative of (A & B) WBC count, (C & D) lymphocyte count, (E & F) Monocyte count, (G & H) Neutrophil count and (I & J) Eosinophil count of n=4 C, n=4 VT, n=5 VU, n=5 M and n=5 VM mice. Data were analysed using ANOVA with Dennett's post-hoc test comparing mean (± SD) of M and VM groups with C group (A, C, E, G and I), and VT and VU groups with C group (B, D, F, H and J), *, $p < 0.05$; **, $p < 0.01$ and ***, $p < 0.001$.

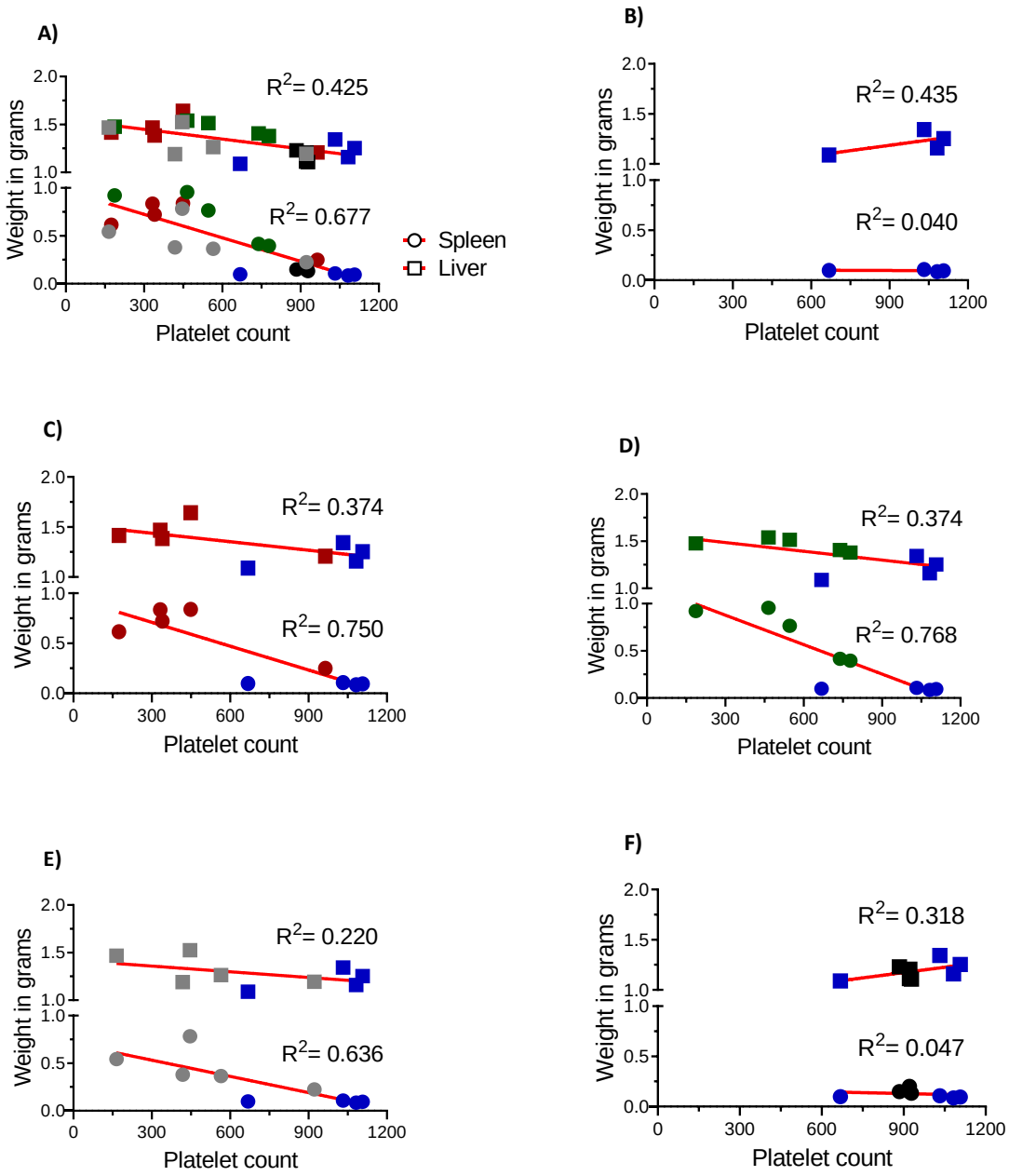

Figure 6.18 Correlation between platelet count and organ weights. Pre-mortem platelet counts and post-mortem organ weights (Livers; □ and spleens; ○) were measured and analysed using linear regression. Data are representative of (A) all data sets together, (B) group C alone and with (C) M, (D) VM, (E) VU and (F) VT mice. Data show the results of a single experiment with n=4 C (in blue), n=4 VT (in black), n=5 VU (in grey), n=5 M (in red) and n=5 VM (in green) mice.

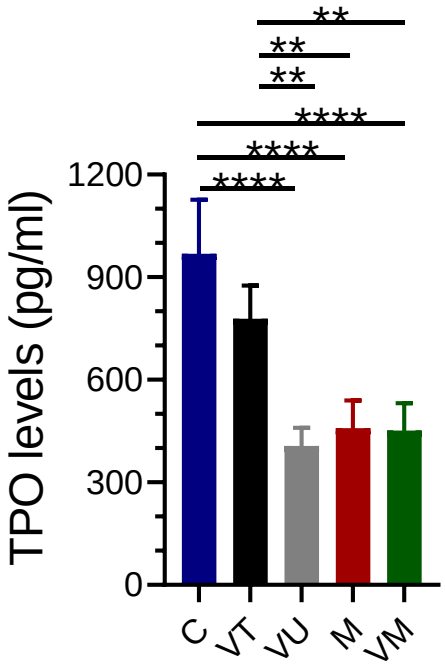

Figure 6.19 Serum thrombopoietin levels. Thrombopoietin levels (TPO) were measured in the serum samples by ELISA using anti-mouse TPO Quantikine serum ELISA kits (R & D, Biotechnic). Data show the results of a single experiment with n=4 C, n=4 VT, n=5 VU, n=5 M and n=5 VM mice. Data shown as mean ± SD and were analysed using ANOVA with Tukey's as post-hoc test, **, $p < 0.01$; ****, $p < 0.0001$.

6.4.4 Tissue remodelling after sequential secondary infection

We used the developed immunochemistry approaches to examine whether there were any synergistic/antagonistic effects on splenic architecture between single and sequentially infected mice. No significant difference was noticed in the area and perimeter between M and VM groups, and VU group **(Figure 6.20A-D)**.

IF staining on frozen sections of livers indicated an increase in the number of F4/80$^+$ Kupffer cells in M group as compared to VM **(Figure 6.21A & B)**. However, F4/80$^+$ RP macrophages were decreased in the spleens of malaria infected groups compared to C group **(Figure 6.22A & D)**. There was no significant difference in the number (or percentage) of F4/80$^+$ cells in between VM and M mice. Interestingly, the destruction of splenic marginal zone in malaria was similar to VL **(Figure 6.22B-C, E-F)**. Our findings also suggest the recovery of RP macrophages and MMM (CD169$^+$) macrophages in VT mice as compared to VU mice, however, secondary exposure to malaria in treated groups results in the loss of these macrophages. Complete restoration of MZM (SIGNR1$^+$) macrophages was not even seen in VT spleens, a further reduction was noticed in malaria infected spleens **(Figure 6.22C & F)**. Representative images of IF stained livers and spleens for each group are shown in **Figure 6**.**23** and **Figure 6**.**24**.

H & E stained liver sections showed the architectural changes consistent with malaria as described in the literature including the presence of red coloured malaria pigment, hemozoin (**Figure 6.25**). Hemozoin has a well-described role in innate immune responses correlating with disease severity in humans and experimental murine models (224). Architectural damage such as the expansion of RP and disruption of WP in malaria infected spleens was confirmed on H & E stained splenic images **(Figure 6.26)**.

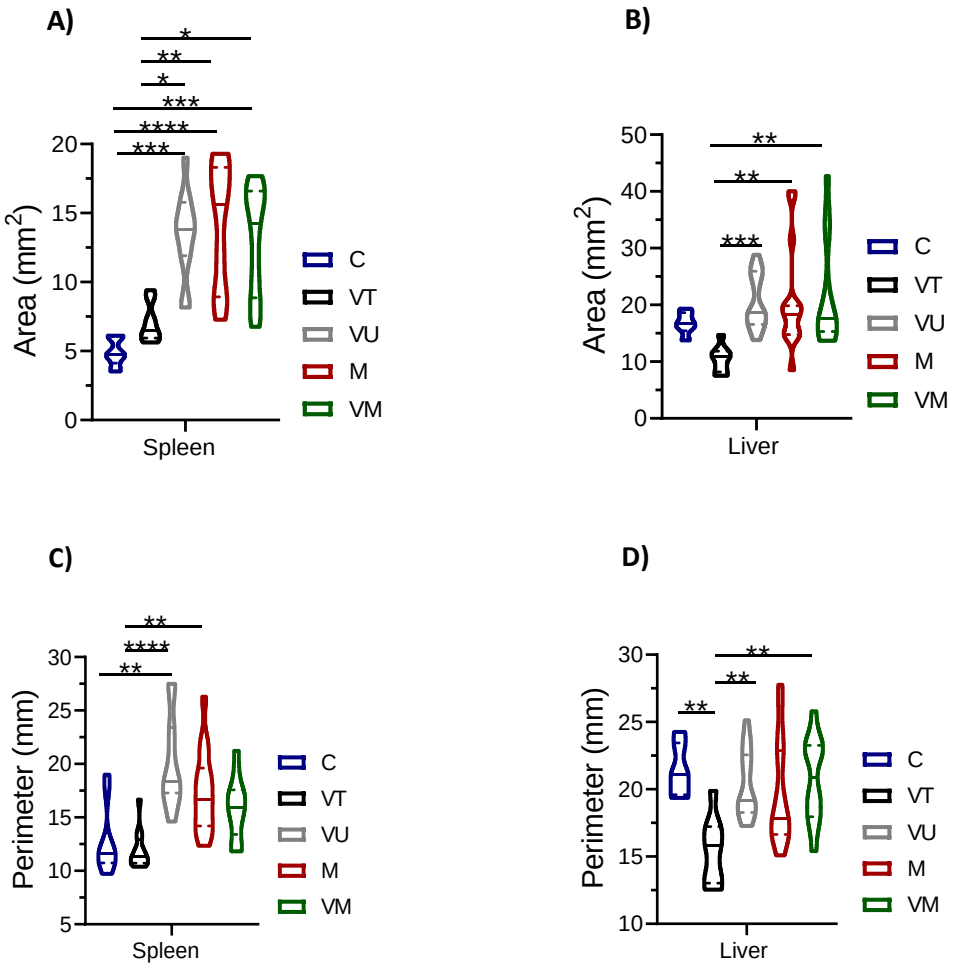

Figure 6.20 Area and perimeter analysis on IF stained images. Segmentation analysis was done on IF stained images using StrataQuest TissueGnostics software. Area of (A) spleen and (B) liver sections was calculated along with the perimeter of (C) spleen and (D) liver sections. Data are representative of n=4 C, n=4 VT, n=5 VU, n=5 M and n=5 VM mice with 2-3 ROI per sample (1 ROI = 1 tissue section). Data shown as median with quartiles and were analysed using Kruskal Wallis with post-hoc Dunn's test comparing the median of each group, *, $p < 0.05$; **, $p < 0.01$; ***, $p < 0.001$ and ****, $p < 0.0001$.

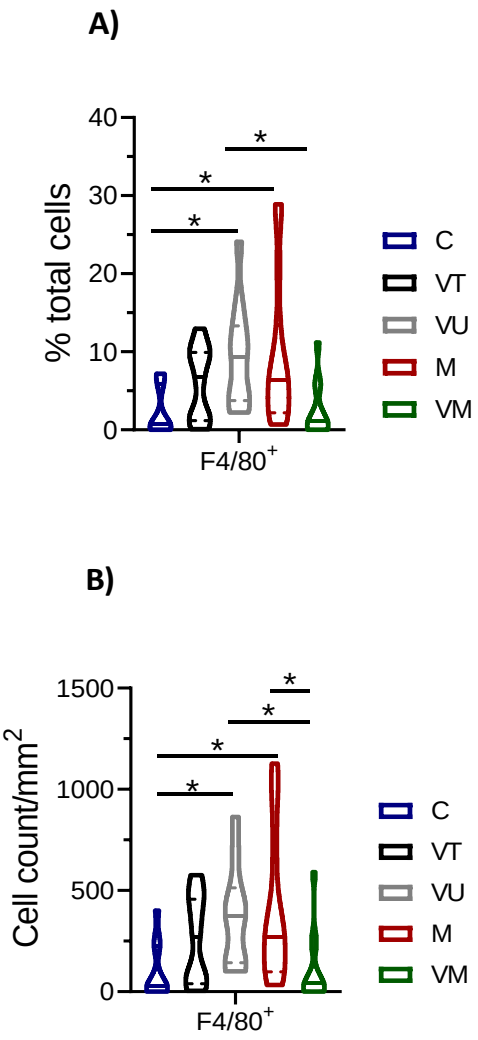

Figure 6.21 F4/80$^+$ Kupffer cells in response to malaria. Segmentation analysis was done on IF stained liver images using StrataQuest TissueGnostics software. Graphs show the (A) % of F4/80$^+$ cells per total number of cells and (B) cell count/unit area (mm^2) of n=4 C, n=4 VT, n=5 VU, n=5 M and n=5 VM mice with 2-3 ROI per sample (1 ROI = 1 tissue section). Data shown as median with quartiles and were analysed using Kruskal Wallis with post-hoc Dunn's test comparing the median of each group, *, $p < 0.05$.

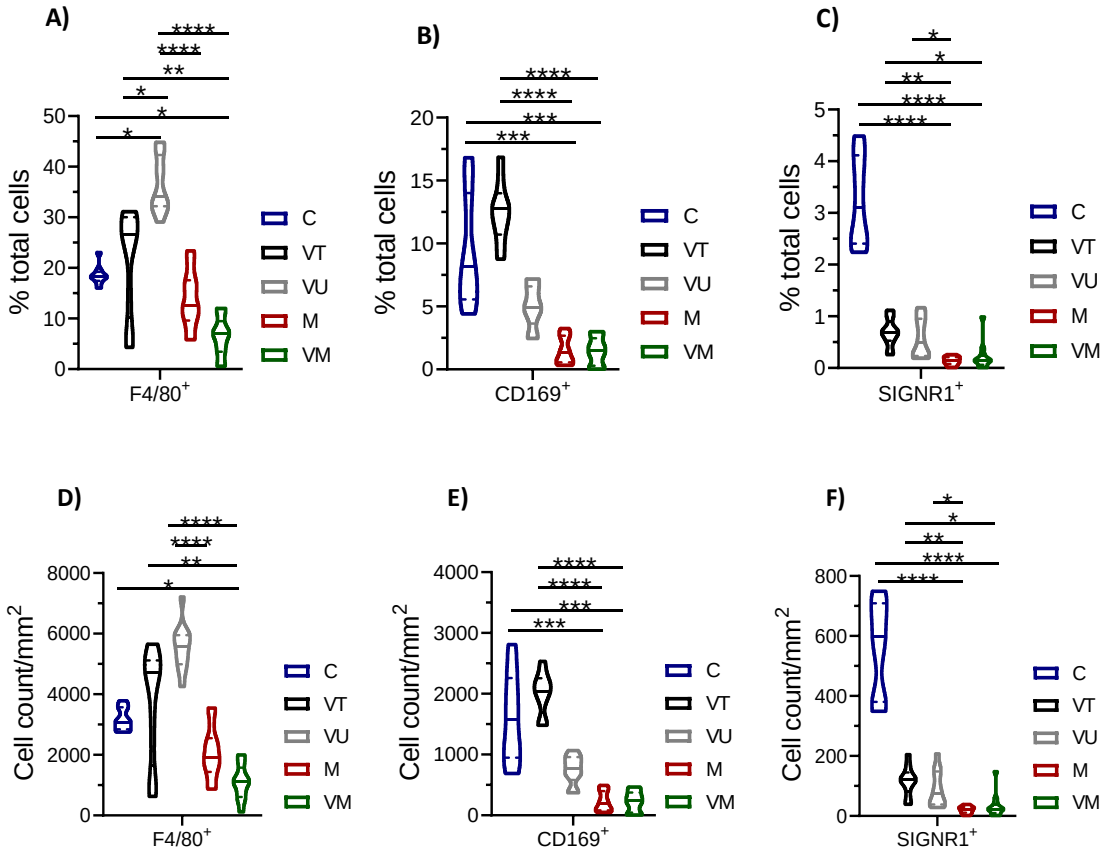

Figure 6.22 Splenic macrophages in response to malaria. Segmentation analysis was done on IF stained spleen images using StrataQuest TissueGnostics software. Graphs show the % of cells per total number of cells for (A) F4/80$^+$ RP macrophages, (B) CD169$^+$ MMM and (C) SIGNR1$^+$ MZM of n=4 C, n=4 VT, n=5 VU, n=5 M and n=5 VM mice with 2-3 ROI per sample (1 ROI = 1 tissue section). Cell count/unit area (mm^2) for F4/80$^+$ cells, CD169$^+$ and SIGNR1$^+$ macrophages are shown in (D), (E) and (F), respectively. Data shown as median with quartiles and were analysed using Kruskal Wallis with post-hoc Dunn's test comparing the median of each group, *, $p < 0.05$; **, $p < 0.01$; ***, $p < 0.001$ and ****, $p < 0.0001$.

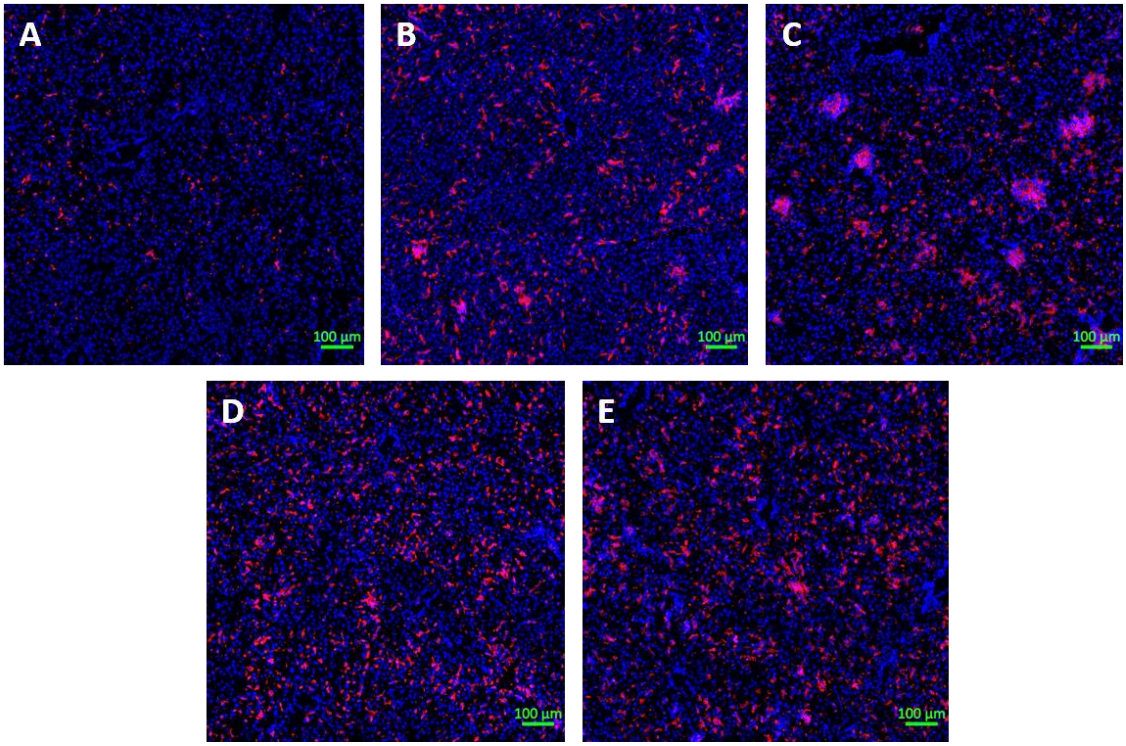

Figure 6.23 Representative IF stained liver images. Images are representative of groups (A) C, (B) VT, (C) VU, (D) M and (E) VM mice. Liver sections of 8-10µm thickness were stained with F4/80 for Kupffer cells (red) followed by counterstaining with DAPI for the nuclei (blue). Images were collected at AxioScan slide scanner at 20x resolution. Scale bars, 100µm.

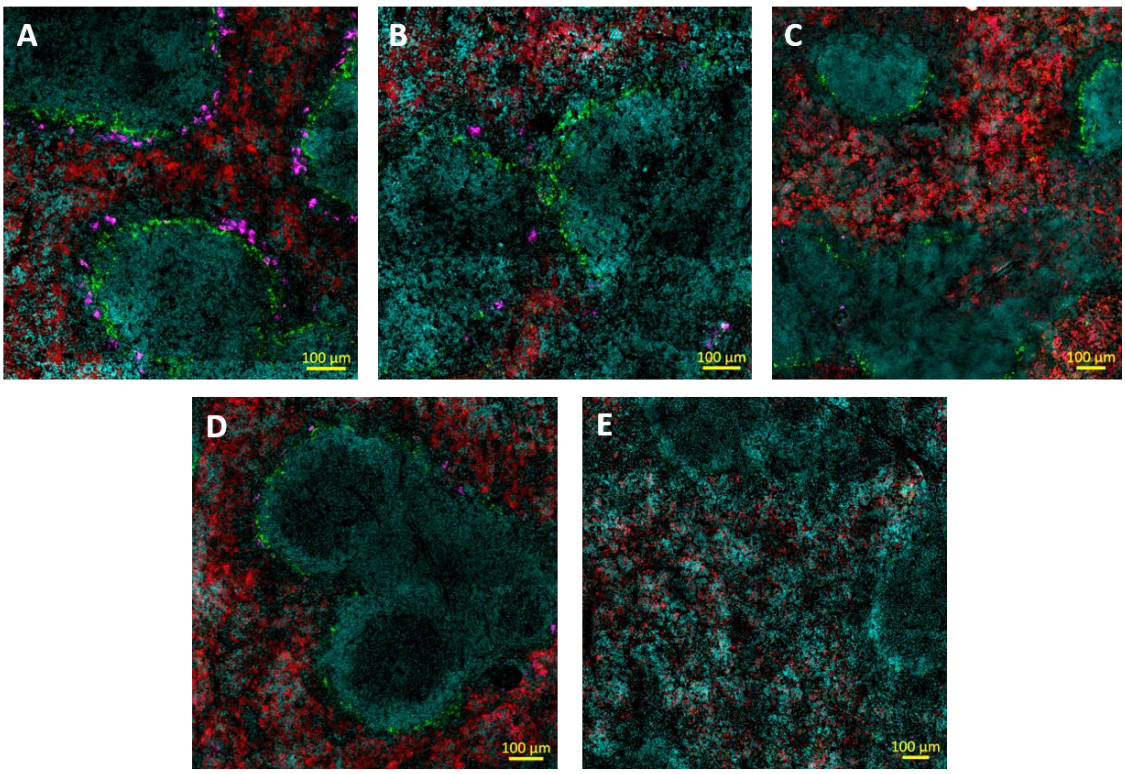

Figure 6.24 Representative IF stained spleen images. Frozen spleen sections of 8-10µm thickness were stained with IF markers for different populations of splenic macrophages. Tissue sections were stained with F4/80 (red) for RP macrophages, CD169 (green) for MMM and SIGNR1 (magenta) for MZM splenic macrophages. Tissues sections were counterstained with DAPI (turquoise) for nuclei. Images are representative of groups (A) C, (B) VT, (C) VU (C), (D) M and (E) VM mice. Images were collected at AxioScan slide scanner at 20x resolution. Scale bar, 100µm.

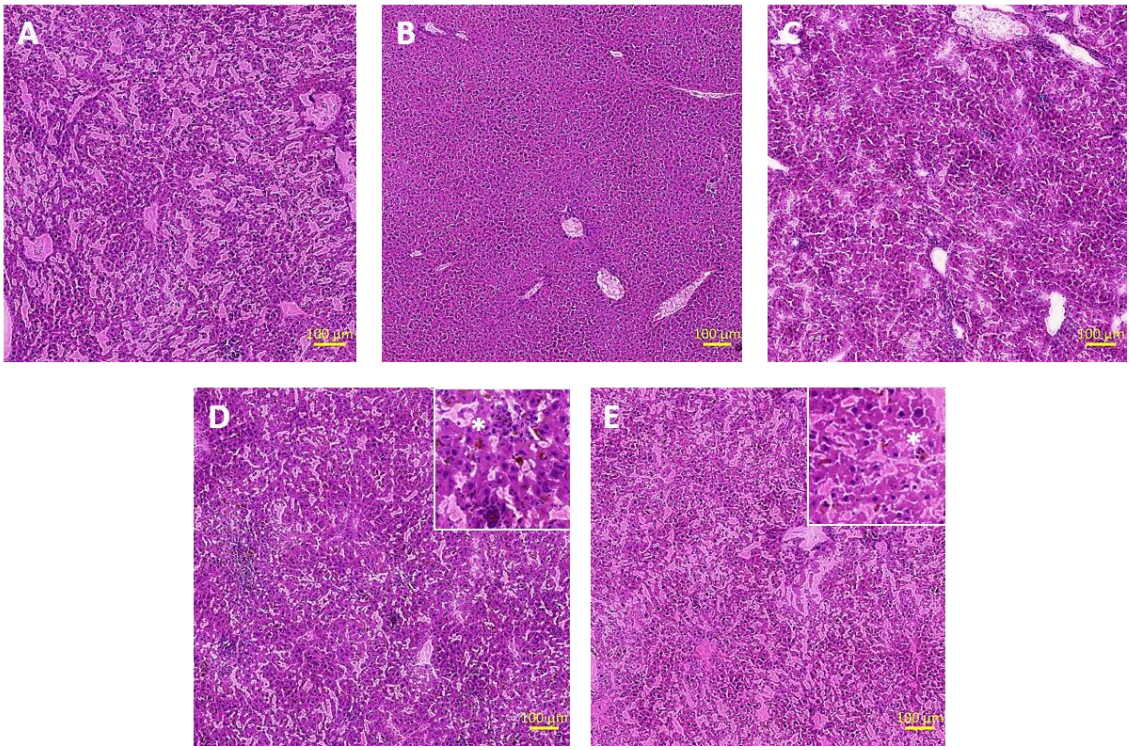

Figure 6.25 Representative H & E stained liver images. Frozen liver sections of 8-10µm thickness were stained with H & E as described in Materials and Methods (**Chapter 2**). Images show the H & E stained livers of group (A) C, (B) VT, (C) VU, (D) M and (E) VM mice. Architectural changes with the presence of orange-red coloured malaria pigment, hemozoin (*) was noticed in malaria infected mice. Images were collected at AxioScan slide scanner at 20x resolution. Scale bar, 100µm.

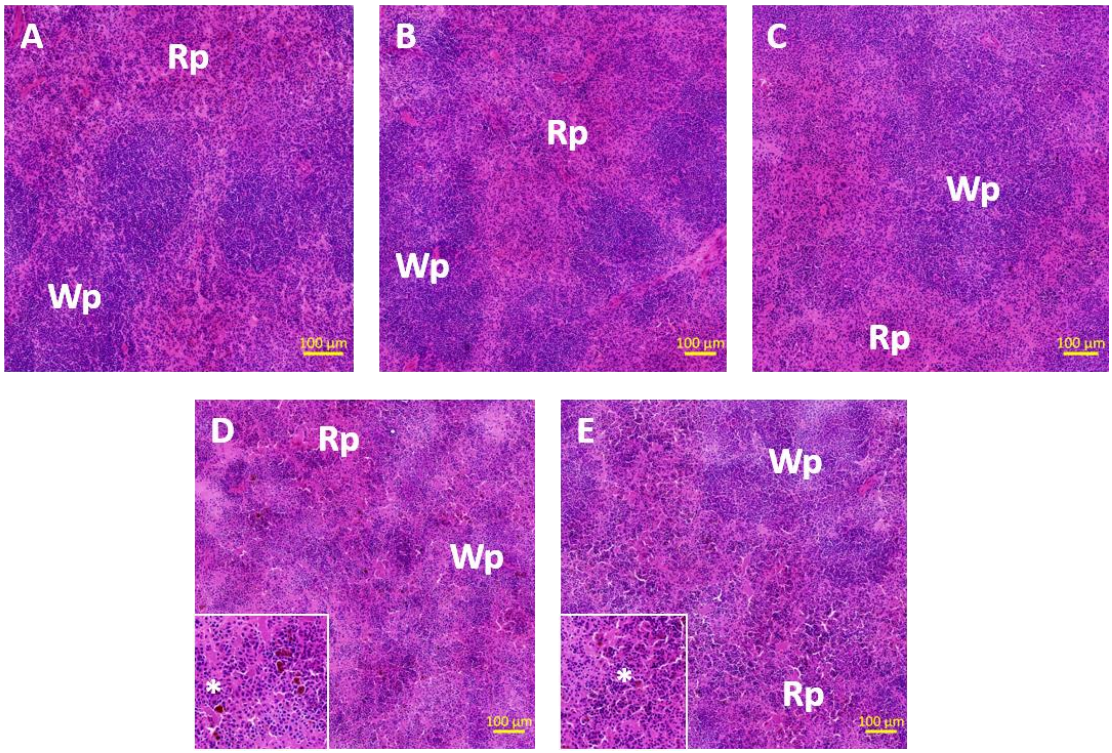

Figure 6.26 Representative H & E stained spleen images. Frozen spleen sections of 8-10µm thickness were stained with H & E as described in Materials and Methods (**Chapter 2**). Representative spleen images of group (A) C, (B) VT, (C) VU, (D) M, and (E) VM mice. Architectural changes with the presence of orange-red coloured malaria pigment, hemozoin (*) was noticed in malaria infected mice. Images were collected at AxioScan slide scanner at 20x resolution. Scale bar, 100µm. Wp = white pulp, Rp = red pulp.

6.5 Discussion

Malaria is a parasitic disease caused by an endoparasite, *Plasmodium* in both humans and animals, is a leading parasitic cause of morbidity and mortality among infections around the globe followed by leishmaniasis (167,225). Both leishmaniasis and malaria are classified as tropical diseases with extensive overlap of geographical and clinical presentation therefore, most likely to co-exist and difficult to diagnose and treat (117). There is a rapid increase in the number of cases being diagnosed with co-infections however, in most of the cases either the diagnosis or treatment is delayed due to unavailability or unaffordability of health care facilities. VL patients are more prone to infections due to weakened immune system, delayed diagnosis and lack of proper treatment. Multiple infections have been seen to co-exist with VL, with HIV being the most common diagnosis and fatal among others. Although clinical studies and few experimental studies have been done to understand the role of immune system in co-infections or VL untreated cases, however, no studies are conducted on the effects of exposure to another infection after clinical cure. Polyparasitism could alter the course and outcome of one or other infection due to immune modulation, delayed or missed diagnosed and the effect of chemotherapeutics (156).

In the present study, we established a model of sequential secondary infection with a non-lethal strain of rodent plasmodium in a drug-treated VL mouse model. Our data suggest that the disease kinetics of *P. chabaudi* are delayed in AmBisome® treated *L. donovani*-infected mice. However, the severity of infection was similar in both groups. Interestingly, no *Leishmania* relapse was noticed in mice with secondary malaria infection (VM) and VL mice left untreated (VU) started to resolve the infection as well. Our data are suggestive of delayed malaria pathogenesis in VL treated mice (VM) model most probably due to the immune protection provided by previous exposure to VL.

A pilot experiment was done to estimate the severity of malaria and changes in the total body weight and blood counts. Results of our pilot malaria experiment were helpful in establishing a model of secondary infection. Our data show a delayed onset of parasitaemia in the blood which could be due to VL induced architectural changes in the tissues especially liver, which is critical for the development of parasite. Similar to parasitaemia, delayed weight loss and cytopenias were seen in VL treated (VM) mice as compared to malaria infected (M) group. Experimental study involving superimposed

infection with *P. yoelii* in mice infected with *L. braziliensis* showed reduced parasitaemia as compared to mice infected with *P. yoelii* only (156). Interestingly, a higher parasitaemia was noticed in mice previously exposed to *L. amazonensis* in the same study (156). These findings suggest that the disease response and outcome is mainly dependent on the strain of parasite involved however, these findings are not confirmed on the *L. donovani*-infected or treated models. A normal granulomatous response to superimposed *L. donovani* infection in general, while a failed response to *L. donovani* parasites inside the developed *Schistosoma* granulomas is suggestive of the role of Th2 biased microenvironment (217).

Although it is difficult to say whether the VL response to co-infections is dependent on innate or acquired immune responses, there are few possibilities based on the findings of above mentioned studies. A Th2 skewed environment does not prevent the development of Th1 mediated granulomatous response however, similar to *L. donovani* infection, malaria involves a complicated Th1/Th2 response (217). As discussed in **Chapter 1**, self-limiting hepatic stage of VL is dependent on effective Th1 response while Th2 cytokines are decisive of disease progression, similarly, the acute malaria is mainly dependent on Th1 responses however, exacerbation of Th1 cytokines is associated with disease severity (217). Together, these studies suggest a role of pro-inflammatory cytokines in delaying the kinetics of malaria in a mouse model. However, our mice were recovered from VL before malaria infection with the restoration of haematological profiles and tissue architecture (see **Chapter 5**), might have resolved the immune responses, although cytokine levels were not determined in this experiment. These findings are critical as parasitic co-infections are very common and may alter the disease response which might be critical especially for treatment response.

Another possible explanation could be the residual architectural changes in VL treated mice tissue parenchyma. Our data are suggestive of complete restoration of liver architecture post-treatment but a poor recovery of splenic marginal zone mainly MZM ($SIGNR1^+$ cells) and also an increased iNOS expression in splenic macrophages post-treatment were seen (see **Chapter 5**). Together, this data suggest that the anatomical disruption, active phagocytic cells and increased NO production might disturb the normal progression of malaria. There is a possibility that NO producing tissue macrophages kill the iRBC inoculum immediately after injection and it takes longer time to replicate and infect erythrocytes to produce symptomatic infection. Inflammatory environment with

excess of cytokines is another possibility which could delay the onset of infection or haematological response in VL treated mice.

The haematological effects of polyparasitism or post-treatment infections are not well-studied however, cytopenias mainly anaemia and thrombocytopenia are commonly seen during infections. Although the blood counts and tissue architecture are restored to normal after VL treatment (see **Chapter 5**), exposure to malaria resulted in a decrease in the blood cell counts along with reduced TPO production and damage to liver and spleen architecture. Architectural damage to liver and spleen with macrophage hyperplasia is well-studied in malaria however, no data are available on the tissue damage in co-infections. Our data suggest a complete resolution of infection in the liver with the restoration of tissue architecture post-treatment however, the splenic marginal zone of treated mice was not fully recovered. Slow recovery of MMM macrophages and a poor recovery of MZM macrophages was seen, which was further damaged in treated mice exposed to malaria. MZM macrophages play a critical role in clearing blood-borne pathogens although a less severe superimposed *S. pneumoniae* infection was seen in *L. donovani*-infected mice suggestive of protective role of RP macrophages in the absence of MZM macrophages (198). We could not investigate the direct role of immune system in delaying malaria after VL treatment however, our data are suggestive of immune modulation which needs further studies for better understanding. Studying the underlying immune mechanisms and haematological consequences is challenging in clinical studies however, experimental models can be used to study the post-treatment changes in VL mice and disease kinetics of co- and secondary infections.

Chapter 7. Concluding Discussion

7.1 Thrombocytopenia in experimental VL is multifactorial

Murine models are widely used to study VL and show many features consistent with human disease. Thrombocytopenia is one of the predominant features in naturally infected humans and dogs, and also experimental models. However, the mechanisms remain poorly understood. We used a well-characterised C57BL/6 mouse model to understand the pathogenesis of thrombocytopenia in experimental VL. Our data are suggestive of progressive thrombocytopenia post-infection due to defective platelet production and enhanced clearance of the platelets.

Our study is the first to describe the ultrastructural changes such as reduced DMS and platelet territories but a normal polyploid nucleus in mature BM MKs in infected mice. Previously, it is shown that the number of BM MKs remain unaltered at d28 post-infection (O. Preham thesis; http://etheses.whiterose.ac.uk/13654/). BM MK ultrastructural changes were reversible on additional stimulation via induced ITP as was a recovery in platelet count. Nevertheless, recovery after induced ITP did not normalise platelet count in infected mice, suggestive of other mechanisms that promote thrombocytopenia in addition to defective production. Therefore, we investigated the role of other tissues involved in the production or clearance of platelets.

The BM, liver and spleen are the major organs involved in the platelet production or clearance, and also a reservoir of *L. donovani* parasites in VL. Therefore, we attempted to also investigate the role of liver and spleen. Our data show a significant reduction in the levels of circulating TPO and hepatic *Thpo* mRNA at d28 of infection but increased TPO protein in infected liver hepatocytes. We report for the first time that TPO production is spatially regulated in the infected livers most likely due to the activation of the JAK-STAT signalling pathway by inflammatory cytokines in hepatocytes closer to granulomas. There is a possibility that the reduced circulating level is due to defective TPO release by hepatocytes into the circulation as blood sinuses are lined by inflammatory granulomas which are either altering the TPO release mechanisms or newly released TPO is cleared by Kupffer cells before being released into the circulation or sequestered by splenic macrophages. The binding of desialylated platelets to hepatic

AMR is known to play a key role in the TPO production and a mechanism of platelet clearance under normal physiological conditions. There was an increase in the percentage of desialylated platelets at d28 post-infection in our experimental mice which might be responsible for enhanced platelet clearance due to excessive desialylation, and also increased TPO transcription. The decreased *Thpo* mRNA could be explained by our assay limitation as we were using *hprt* as our housekeeping gene, which is expressed by myeloid cells and expansion in myeloid compartment is seen in infected livers, therefore, resulting in dilution of signals derived from hepatocyte mRNA. The use of hepatocyte-specific housekeeping gene such as albumin would be a better choice and probably true representative of *Thpo* accumulation in infected livers.

We also attempted to investigate the role of spleen in platelet clearance as previous studies have shown that excessive splenic clearance might be responsible for thrombocytopenia (O. Preham thesis; http://etheses.whiterose.ac.uk/13654/). We were not successful in fully depleting macrophages from infected mice spleens after clodronate treatment. Complete depletion of tissue macrophages in uninfected mice did not show any change in the platelet counts. These findings suggest that most probably tissue macrophages are not the major source of removing the old platelets from circulation under normal physiological conditions, which is consistent with the recent data on platelet clearance, which suggests that liver is the major tissue responsible for the clearance of old platelets (38). We also show that there was an increase in the level of IgG bound platelets, generally cleared by tissue macrophages in infections and ITP as shown by other studies (208,225). There is a possibility that splenic macrophages play an important role in clearing these IgG bound platelets resulting in thrombocytopenia as evident from splenectomised infected mice data (O. Preham thesis; http://etheses.whiterose.ac.uk/13654/). However, further studies are needed to understand the role of splenic macrophages in platelet clearance using genetic mice models of macrophage depletion as discussed in **Chapter 4**.

In summary, our findings are suggestive of multifactorial pathogenesis of thrombocytopenia in EVL, with both defective platelet production and enhanced clearance play an important role. **Figure 7.1** shows a summary of our addition to pre-existing mechanisms proposed as a cause of VL induced thrombocytopenia.

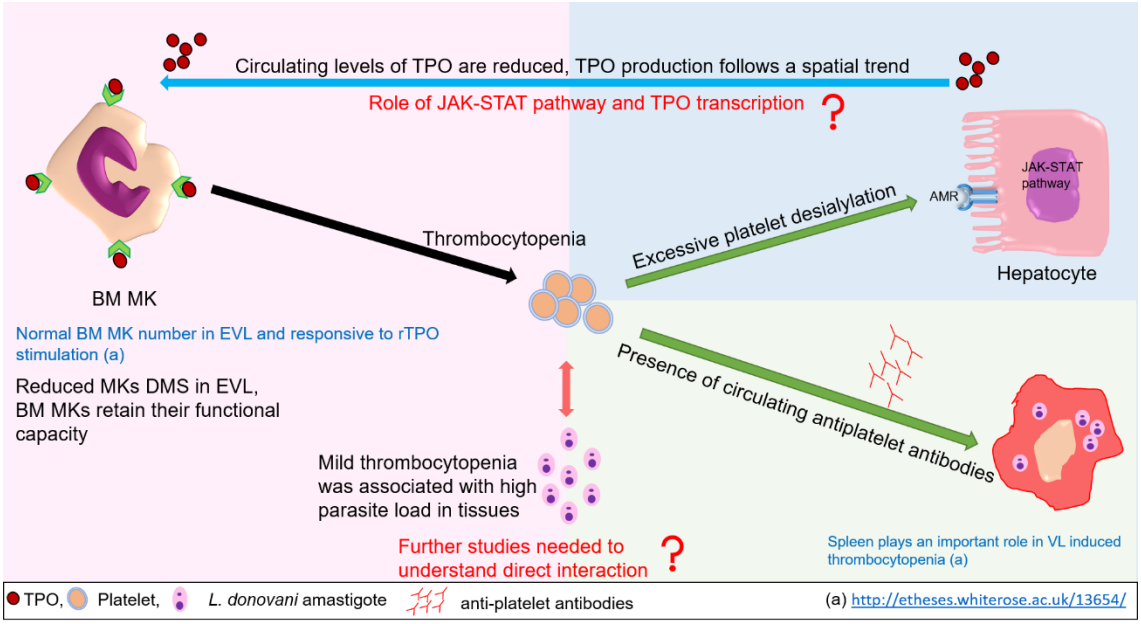

Figure 7.1 Summary of thrombocytopenia mechanisms in VL including our findings. Multiple mechanisms have been proposed based on the findings of clinical and experimental studies as described in **Chapter 1**. Our new data on understanding the underlying mechanisms of VL-induced thrombocytopenia include: ultrastructural changes in BM MKs in infected mice, spatial regulation of TPO and excessive clearance indicted by the presence of anti-platelet antibodies and increase in desialylated platelets. Our preliminary data are suggestive of the protective role of platelets in limiting VL as shown by high tissue parasite burden in less thrombocytopenic infected mice i.e. mice treated with rTPO. Further studies are needed to determine the platelet-parasite interaction in the circulation and tissue macrophages in VL.

7.2 Haematological profile and tissue architecture is reversible after treatment

Our findings using post-treatment murine VL model show a restoration of blood counts and tissue microarchitecture after the parasites are cleared from the resident tissues. As discussed above, thrombocytopenia has multifactorial pathogenesis in EVL, therefore, the progressive recovery of platelet counts is suggestive of restoration of normal platelet production and elimination of excessive platelet clearance mechanisms post-treatment. Post-treatment recovery of platelet counts is consistent with our data on the functional capacity of BM MKs, increased platelet production after exogenous stimulation. Together these data suggest that the damage to the BM MKs is not permanent which could be true for the whole BM as seen by the restoration of other blood cell counts post-treatment. There is no sufficient clinical or experimental evidence available on the recovery of blood counts post-treatment however, normal blood counts are noticed in VL patients after the clinical cure is achieved (96). Hence, platelets and other blood cell counts recovery post-treatment could be used as a surrogate marker for the successful treatment and tissue restoration.

Previously, studies on post-treatment VL models have shown a trend towards the recovery of tissue microarchitecture and a reduction in the inflammatory cytokines (114). Here we show that the liver microarchitecture is reversible with the resolution of hepatic granulomas after four weeks post-treatment. Recovery of hepatic morphology also resulted in normal circulating levels of TPO. Our data on splenic microarchitecture show the restoration of red and white pulp along with marginal zone macrophages. $CD169^{+}$ MMM macrophages were quicker to recovery as compared to $SIGNR1^{+}$ MZM macrophages which is consistent with the published literature (226).

Our data are first to investigate the post-treatment changes in the blood counts and tissue microarchitecture for four consecutive weeks after a single dose of AmBisome®. Although tissue morphology is difficult to study in human VL patients, experimental models are a good choice to understand the role of tissue recovery in controlling infection, understanding the risk factors for poor treatment response and relapse as well as response to co- and secondary infections.

7.3 Delayed disease kinetics of *P. chabaudi* malaria in treated EVL mice

Polyparasitism is a common finding and now considered an integral part of the studies conducted on infection models to understand the course and outcome of infections due to immune modulation, delayed diagnosed and effectiveness of available treatment options (156). Malaria and VL are the most deadly tropical infections with a huge overlap of geographical and clinical presentations (117,167,225). Therefore, VL patients are at a high risk for malaria as a co-infection or post-treatment infection, which could be a limitation for the timely and accurate diagnosis, leading to fatal outcomes by altering the pathogenesis of each other. Although VL/co-infections are now studied in clinical and experimental models, data on sequential infection post-treatment has been overlooked despite high risk of relapse and risk of multiple infections due to immunocompromised status. Therefore, there is a need to understand the pathogenesis of secondary infections in treated humans and experimental models.

Our data on sequential secondary infection with *P. chabaudi* rodent malaria in *L. donovani*-infected mice treated for four weeks show an overall delayed malaria kinetics however, the severity of disease was comparable in malaria infected groups. Previous leishmaniasis/malaria co-infection studies have shown a decreased *P. yoelii* parasitaemia in mice infected with *L. braziliensis* while increased parasitaemia in mice exposed to *L. amazonensis* (156). However, superimposed VL in mice infected with *S. mansoni* showed defective Th1 response to *L. donovani* amastigotes in *S. mansoni* egg granulomas while a less severe *S. pneumoniae* co-infection was seen in VL infected mice (198,217).

A delay in the onset of thrombocytopenia, anaemia and weight loss was seen in treated *L. donovani*-infected mice as compared to malaria infected control mice. Thrombocytopenia and anaemia have been associated with the severity of malaria with multifactorial pathogenesis (227–229). Here we show a delay in cytopenias in treated mice which could be due to the VL induced tissue microarchitectural changes, cytokines or immune modulation. However, we treated VL mice before challenging them with malaria to minimise the risk of complications and also to see the tissue response to a second infection after recovery. There was no relapse or cytopenias noted in our VL treated control mice throughout the experiment therefore, the tissue architectural changes were likely due to

malaria rather than VL and their effects on blood counts were more representative of malaria than VL.

The delayed response to malaria in VL treated mice could be dependent on various factors including the role of Th1/Th2 immune response, increased cytokine levels, increased NO production to clear the parasites as shown by increased expression of iNOS post-treatment or tissue microarchitecture of VL treated mice. Although our *L. donovani*-infected mice were treated before malaria, there is a possibility that the remnant Th1/Th2 environment in treated mice played a protective role in the acute phase of malaria however, was not efficient to control disease progression. It has been shown previously that the T cell responses and cytokines production such as IFNγ, TNF, IL-6 and IL-10 plays an important role in the malaria progression in leishmaniasis/co-infection models (156). Another possibility is the destruction of *Plasmodium* iRBCs by tissue macrophages. Although iNOS expression does not show a direct effect on *plasmodia* (230–232), it is likely that *P. chabaudi* iRBCs were destroyed by iNOS expressing activated macrophages, immediately after administration, and the surviving iRBCs took longer to expand the number of parasites to reach the infective stage. Our data show a higher expression of iNOS in macrophages after treatment. However, further studies are needed to understand these mechanisms in detail post-treatment or after exposure to secondary infections.

Appendix

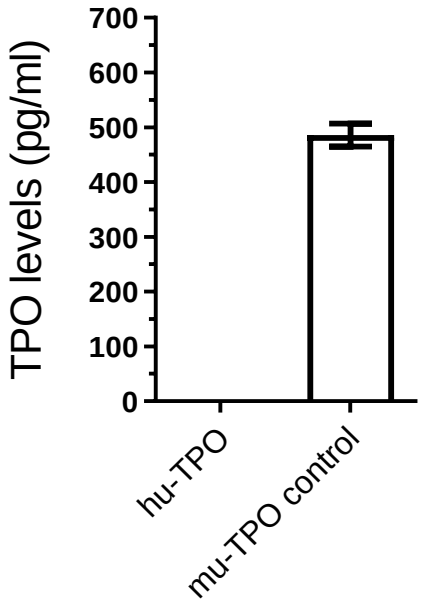

Supplementary Figure 1. No detectable human-TPO in hu-rTPO treated mice serum. Mouse thrombopoietin Quantikine ELISA was performed by adding an equal volume of human recombinant-TPO (hu-rTPO; used for rTPO treatment of infected and uninfected mice) to control wells as mouse TPO control (provided with the assay) followed by the addition of mouse-TPO conjugate, similar to other controls and experimental samples. All samples were processed as per manufacturer's protocol and optical density was measured as described in **Chapter 2**. No TPO was detectable in the hu-TPO control wells, suggestive of ELISA specificity to mu-TPO only. Data expressed as mean ± SD.

Abbreviations

ACD	Acid Citrate Dextrose
ADP	Adenosine diphosphate
AF	Alexa Fluor
AMR	Ashwell-Morrell receptor
ANOVA	Analysis of Variance
APC	Antigen presenting cells
ARRIVE	Animal Research: Reporting of *In Vivo* Experiments
ASGPR	Asialoglycoprotein receptor
BALB/c	Albino, laboratory-bred strain of mice
BM	Bone marrow
BSA	Bovine serum albumin
BSF	Biological services facility
BSS	Bernard-Soulier syndrome
c-Mpl	Myeloproliferative leukaemia protein, also known as thrombopoietin receptor (TPO-R)
C57BL/6	Common laboratory-bred strain of mice, often referred to as C57 black 6, C57, black 6 or B6.
CAMT	Congenital amegakaryocytic thrombocytopenia
CBC	Complete blood count
CCD	Charge-coupled device
CD	Cluster of differentiation
cDNA	Complementary DNA
CL	Cutaneous leishmaniasis
CL3	Containment level 3 (Category 3 laboratory)
CLD	Chronic liver disease
CLEC4F	C-type lectin domain family 4 member F is a protein that in humans is encoded by the CLEC4F gene
CO_2	Carbon dioxide
GM-CSF	Granulocyte macrophage colony-stimulating factor
DAPI	4′,6-diamidino-2-phenylindole

DAT	Direct antiglobulin test
DC	Dendritic cell
DMS	Demarcation membranous system
DNA	Deoxyribonucleic acid
DNase	Deoxyribonuclease
dNTP	deoxynucleotides tri-phosphate
DTR	Diphtheria toxin receptor
EBV	Epstein-Barr virus
ECM	Extracellular matrix
EDTA	Ethylenediaminetetraacetic acid
ELISA	Enzyme-linked immunosorbent assay
EM	Electron microscopy
EPO	Erythropoietin
ET	Essential thrombocythaemia
EVL	Experimental visceral leishmaniasis
FGF	Fibroblast-growth factor
FITC	Fluorescein Isothiocyanate
FLT	FMS-like tyrosine kinase
Glc-NAc	N-Acetylglucosamine
GPs	Glycoproteins
GPS	Gray platelet syndrome
GT	Glanzmann thrombasthenia
HCV	Hepatitis-C virus
HEPES	4-(2-hydroxyethyl)-1-piperazineethanesulfonic acid
HIV	Human immunodeficiency virus
HSC	Haematopoietic stem cell
hu-TPO	Human thrombopoietin
IF	Immunofluorescence
IFN	Interferon
IL	Interleukin
iNOS or NOS2	Inducible or type-2 nitric oxide synthase

iRBCs	Infected red blood cells
IRF	Interferon regulatory factor
ITP	Immune thrombocytopenia
IU	International units
IVIS	*In vivo* imaging system
IVS	Invagination membranous system
JAK	Janus Kinase
LDU	Leishman Donovan unit
LN2	Liquid nitrogen
LSM	Confocal laser scanning microscopes
LT HSCs	Long-term Haematopoietic stem cells
LV9	Ethiopian strain of *Leishmania donovani*
MAL-II	Maackia Amurensis lectin-II
MARCO	Macrophage Receptor with Collagenous structure
MCH	Mean cell haemoglobin
MCHC	Mean corpuscular haemoglobin concentration
MCL	Mucocutaneous leishmaniasis
MCV	Mean cell volume
MEP	Megakaryocyte-erythroid progenitor
MFI	Median fluorescence intensity
MK	Megakaryocyte
MMM	Marginal metallophilic macrophages
MPS	Mononuclear phagocyte system
MPV	Mean platelet volume
mu-TPO	Mouse thrombopoietin
MYH9-related disorders	Inherited disorders due to mutations in the MYH9 gene
MZ	Marginal zone
MZM	Marginal zone macrophages
NO	Nitric oxide
OCT	Cryo embedding matrix

PBS	Phosphate-buffered saline
PCR	Polymerase chain rection
PE	Phycoerythrin
PF 4	Platelet factor 4
PFA	Paraformaldehyde
PKDL	Post kala-azar dermal leishmaniasis
PRP	Platelet rich plasma
RBC	Red blood cell
RCA	Ricinus Communis Agglutinin
RDW	Red blood cell distribution width
RNA	Ribonucleic acid
RNase	Ribonuclease
RNI	Reactive nitrogen intermediates
RNS	Reactive nitrogen species
ROI	Reactive oxygen intermediates/Region of interest
ROS	Reactive oxygen species
RP	Red pulp
RPMI	Roswell park memorial institute
RT	Room temperature
rTPO	Recombinant thrombopoietin
S1k	Schedule 1 killing
SCF	Stem cell factor
SD	Standard deviation
SEM	Standard error of the mean/median
SIGNR1	C-type lectin SIGNR1 (the murine homolog of human dendritic cell-specific intracellular adhesion molecule-grabbing nonintegrin [SIGN])
SNA	Sambucus Nigra
SPF	Specific-pathogen free
STAT	Signal transducer and activator of transcription
TBW	Total body weight
TEM	Transmission electron microscopy
TF	Technology facility

TGF-β	Transforming growth factor-beta
Th1	T-helper type 1 lymphocytes
Th2	T-helper type 2 lymphocytes
TLR	Toll-like receptor
TNF	Tissue necrosis factor
TPO	Thrombopoietin
VL	Visceral Leishmaniasis
vWF	von Willebrand factor
WBC	White blood cell
WHO	World Health Organisation
WP	White pulp

References

1. Tomaiuolo M, Brass LF, Stalker TJ. Regulation of Platelet Activation and Coagulation and Its Role in Vascular Injury and Arterial Thrombosis. Interv Cardiol Clin. 2017 Jan;6(1):1–12. Available from: https://www.ncbi.nlm.nih.gov/pubmed/27886814

2. Swinkels M, Rijkers M, Voorberg J, Vidarsson G, Leebeek FWGG, Jansen AJGG. Emerging Concepts in Immune Thrombocytopenia. Vol. 9, Frontiers in Immunology. Frontiers Media S.A.; 2018. p. 880. Available from: https://www.frontiersin.org/article/10.3389/fimmu.2018.00880

3. Holinstat M. Normal platelet function. Cancer Metastasis Rev. 2017 Jun;36(2):195–8. Available from: https://www.ncbi.nlm.nih.gov/pubmed/28667366

4. Youssefian T, Drouin A, Massé J-M, Guichard J, Cramer EM. Host defense role of platelets: engulfment of HIV andStaphylococcus aureus occurs in a specific subcellular compartment and is enhanced by platelet activation. Blood. 2002 Jun 1;99(11):4021–9. Available from: https://doi.org/10.1182/blood-2001-12-0191

5. Assinger A. Platelets and Infection – An Emerging Role of Platelets in Viral Infection. Vol. 5, Frontiers in Immunology. 2014. p. 649. Available from: https://www.frontiersin.org/article/10.3389/fimmu.2014.00649

6. Kerrigan SW, Cox D. Platelet–bacterial interactions. Cell Mol Life Sci. 2010;67(4):513–23. Available from: https://doi.org/10.1007/s00018-009-0207-z

7. McMorran BJ, Marshall VM, de Graaf C, Drysdale KE, Shabbar M, Smyth GK, et al. Platelets Kill Intraerythrocytic Malarial Parasites and Mediate Survival to Infection. Science. 2009 Feb 6;323(5915):797 LP – 800. Available from: http://science.sciencemag.org/content/323/5915/797

8. Italiano JE. Unraveling mechanisms that control platelet production. Semin Thromb Hemost. 2013;39(1):15–24.

9. Leslie M. Beyond Clotting: The Powers of Platelets. Science. 2010 Apr30;328(5978):562,LP-564.
   Available from: http://science.sciencemag.org/content/328/5978/562

10. van der Heyde HC, Gramaglia I, Sun G, Woods C. Platelet depletion by anti-CD41 (αIIb) mAb injection early but not late in the course of disease protects against Plasmodium berghei pathogenesis by altering the levels of pathogenic cytokines. Blood. 2005 Mar 1;105(5):1956–63. Available from: https://doi.org/10.1182/blood-2004-06-2206

11. Wachtman LM, Skolasky RL, Tarwater PM, Esposito D, Schifitto G, Marder K, et al. Platelet Decline: An Avenue for Investigation Into the Pathogenesis of Human Immunodeficiency Virus–Associated Dementia. Arch Neurol. 2007 Sep 1;64(9):1264–72. Available from: https://doi.org/10.1001/archneur.64.9.1264

12. Semple JW, Italiano JE, Freedman J. Platelets and the immune continuum. Nat Rev Immunol. 2011;11(4):264–74. Available from: https://doi.org/10.1038/nri2956

13. SMYTH SS, MCEVER RP, WEYRICH AS, MORRELL CN, HOFFMAN MR, AREPALLY GM, et al. Platelet functions beyond hemostasis. J Thromb Haemost. 2009 Nov 1;7(11):1759–66. Available from: https://doi.org/10.1111/j.1538-7836.2009.03586.x

14. Elaine M. Keohane SJL and JMW. Rodak's Hematology (Fifth Edition). 2016.

15. Kapur R, Semple JW. Immune Functions of Platelets. In: Antibody Therapy. Springer International Publishing; 2018. p. 241–59.

16. Sørensen AL, Rumjantseva V, Nayeb-Hashemi S, Clausen H, Hartwig JH, Wandall HH, et al. Role of sialic acid for platelet life span: exposure of β-galactose results in the rapid clearance of platelets from the circulation by asialoglycoprotein receptor–expressing liver macrophages and hepatocytes. Blood. 2009 Aug 20;114(8):1645–54. Available from: https://doi.org/10.1182/blood-2009-01-199414

17. Patel SR, Hartwig JH, Italiano Jr. JE. The biogenesis of platelets from megakaryocyte proplatelets. J Clin Invest. 2005 Dec 1;115(12):3348–54. Available from: https://doi.org/10.1172/JCI26891

18. Mazzi S, Lordier L, Debili N, Raslova H, Vainchenker W. Megakaryocyte and polyploidization. Exp Hematol. 2018;57:1–13. Available from: https://doi.org/10.1016/j.exphem.2017.10.001

19. Lee HO, Davidson JM, Duronio RJ. Institute of Human Virology 2009 Journal

Club Series Suzanne Gartner , PhD “ An Introduction to Endoreplication ” 725 West Lombard Street 3rd Floor Light Well Refreshments Endoreplication : polyploidy with purpose. Genes Dev. 2010;23:2461–77.

20. Eckly A, Heijnen H, Pertuy F, Geerts W, Proamer F, Rinckel J-Y, et al. Biogenesis of the demarcation membrane system (DMS) in megakaryocytes. Blood. 2014 Feb 6;123(6):921–30. Available from: https://doi.org/10.1182/blood-2013-03-492330

21. Cuenca-Zamora JE, Ferrer-Marín F, Rivera J, Teruel-Montoya R. Tubulin in Platelets: When the Shape Matters. Vol. 20, International Journal of Molecular Sciences . 2019.

22. Thon JN, Montalvo A, Patel-Hett S, Devine MT, Richardson JL, Ehrlicher A, et al. Cytoskeletal mechanics of proplatelet maturation and platelet release. J Cell Biol. 2010 Nov 15;191(4):861–74. Available from: https://www.ncbi.nlm.nih.gov/pubmed/21079248

23. Deutsch VR, Tomer A. Megakaryocyte development and platelet production. Br J Haematol. 2006;134(5):453–66.

24. Lefrançais E, Ortiz-Muñoz G, Caudrillier A, Mallavia B, Liu F, Sayah DM, et al. The lung is a site of platelet biogenesis and a reservoir for haematopoietic progenitors. Nature. 2017;544(7648):105–9. Available from: http://dx.doi.org/10.1038/nature21706

25. Kaushansky K. Thrombopoietin: a tool for understanding thrombopoiesis. J Thromb Haemost. 2003 Jul 1;1(7):1587–92. Available from: https://doi.org/10.1046/j.1538-7836.2003.00273.x

26. Kaushansky K. Thrombopoietin. N Engl J Med. 1998 Sep 10;339(11):746–54. Available from: https://doi.org/10.1056/NEJM199809103391107

27. Bruno S, Gunetti M, Gammaitoni L, Dane A, Cavalloni G, Sanavio F, et al. In vitro and in vivo megakaryocyte differentiation of fresh and ex-vivo expanded cord blood cells: rapid and transient megakaryocyte reconstitution. Haematologica. 2003 Jan 1;88(4):379 LP-387. Available from: http://www.haematologica.org/content/88/4/379

28. Afdhal N, McHutchison J, Brown R, Jacobson I, Manns M, Poordad F, et al.

Thrombocytopenia associated with chronic liver disease. J Hepatol. 2008 Jun 1;48(6):1000–7.
Available from: https://www.sciencedirect.com/science/article/pii/S0168827808002213

29. Arriazu E, Ruiz de Galarreta M, Cubero FJ, Varela-Rey M, Pérez de Obanos MP, Leung TM, et al. Extracellular matrix and liver disease. Antioxid Redox Signal. 2014 Sep 1;21(7):1078–97. Available from: https://www.ncbi.nlm.nih.gov/pubmed/24219114

30. Kurokawa T, Ohkohchi N. Platelets in liver disease, cancer and regeneration. World J Gastroenterol. 2017;23(18):3228–39.

31. Kaushansky K. Thrombopoietin: the primary regulator of platelet production. Blood. 1995 Jul 15;86(2):419–31. Available from: https://doi.org/10.1182/blood.V86.2.419.bloodjournal862419

32. Machlus KR, Italiano Jr. JE. The incredible journey: From megakaryocyte development to platelet formation. J Cell Biol. 2013 Jun 10;201(6):785–96. Available from: https://doi.org/10.1083/jcb.201304054

33. Ishikawa T, Ichida T, Matsuda Y, Sugitani S, Sugiyama M, Kato T, et al. Reduced expression of thrombopoietin is involved in thrombocytopenia in human and rat liver cirrhosis. J Gastroenterol Hepatol. 1998;13(9):907–13.

34. Bleeker JS, Hogan WJ. Thrombocytosis: diagnostic evaluation, thrombotic risk stratification, and risk-based management strategies. Thrombosis. 2011;2011:536062. Available from: https://www.ncbi.nlm.nih.gov/pubmed/22084665

35. Li R, Hoffmeister KM, Falet H. Glycans and the platelet life cycle. Platelets. 2016 Sep 17;27(6):505–11. Available from: https://pubmed.ncbi.nlm.nih.gov/27135356

36. Cho J, Kim H, Song J, Cheong JW, Shin JW, Yang WI, et al. Platelet storage induces accelerated desialylation of platelets and increases hepatic thrombopoietin production. J Transl Med. 2018;16(1):1–9. Available from: https://doi.org/10.1186/s12967-018-1576-6

37. Li Y, Fu J, Ling Y, Yago T, McDaniel JM, Song J, et al. Sialylation on O-glycans protects platelets from clearance by liver Kupffer cells. Proc Natl Acad Sci. 2017 Aug 1;114(31):8360 LP –8365. Available from: http://www.pnas.org/content/114/31/8360

38. Deppermann C, Kratofil RM, Peiseler M, David BA, Zindel J, Castanheira FVES, et al. Macrophage galactose lectin is critical for Kupffer cells to clear aged platelets. J Exp Med. 2020;217(4).

39. Knutson M, Wessling-Resnick M. Iron Metabolism in the Reticuloendothelial System. Crit Rev Biochem Mol Biol. 2003 Jan 1;38(1):61–88. Available from: https://doi.org/10.1080/713609210

40. Coelho HCC, Lopes SCP, Pimentel JPD, Nogueira PA, Costa FTM, Siqueira AM, et al. Thrombocytopenia in Plasmodium vivax Malaria Is Related to Platelets Phagocytosis. PLoS One. 2013 May 28;8(5):e63410. Available from: https://doi.org/10.1371/journal.pone.0063410

41. Grozovsky R, Giannini S, Falet H, Hoffmeister KM, Herv´ H, Falet H, et al. Regulating billions of blood platelets: Glycans and beyond. Blood. 2015 Oct 17;126(16):1877–84.

42. Nomura S. Advances in Diagnosis and Treatments for Immune Thrombocytopenia. Clin Med Insights Blood Disord. 2016 Jul 1;9:15.

43. Stasi R. How to approach thrombocytopenia. Hematol Am Soc Hematol Educ Progr. 2012;2012:191–7. Available from: https://pubmed.ncbi.nlm.nih.gov/23233580

44. Ballmaier M, Germeshausen M, Schulze H, Cherkaoui K, Lang S, Gaudig A, et al. c-mpl mutations are the cause of congenital amegakaryocytic thrombocytopenia. Blood. 2001 Jan 1;97(1):139–46. Available from: https://doi.org/10.1182/blood.V97.1.139

45. Pecci A, Ragab I, Bozzi V, De Rocco D, Barozzi S, Giangregorio T, et al. Thrombopoietin mutation in congenital amegakaryocytic thrombocytopenia treatable with romiplostim. EMBO Mol Med. 2018 Jan;10(1):63–75. Available from: https://pubmed.ncbi.nlm.nih.gov/29191945

46. D'Andrea G, Chetta M, Margaglione M. Inherited platelet disorders: thrombocytopenias and thrombocytopathies. Blood Transfus. 2009 Oct;7(4):278–92. Available from: https://www.ncbi.nlm.nih.gov/pubmed/20011639

47. NURDEN AT. Qualitative disorders of platelets and megakaryocytes. J Thromb Haemost. 2005 Aug 1;3(8):1773–82. Available from: https://doi.org/10.1111/j.1538-7836.2005.01428.x

48. Lanza F. Bernard-Soulier syndrome (hemorrhagiparous thrombocytic dystrophy). Orphanet J Rare Dis. 2006 Nov 16;1:46. Available from: https://www.ncbi.nlm.nih.gov/pubmed/17109744

49. Aster RH. Pooling of platelets in the spleen: role in the pathogenesis of "hypersplenic" thrombocytopenia. J Clin Invest. 1966 May 1;45(5):645–57. Available from: https://doi.org/10.1172/JCI105380

50. Young NS, Scheinberg P, Calado RT. Aplastic anemia. Curr Opin Hematol. 2008 May;15(3):162–8. Available from: https://www.ncbi.nlm.nih.gov/pubmed/18391779

51. Giannini E, Borro P, Botta F, Fumagalli A, Malfatti F, Podestà E, et al. Serum thrombopoietin levels are linked to liver function in untreated patients with hepatitis C virus-related chronic hepatitis. J Hepatol. 2002 Nov 1;37(5):572–7. Available from: https://www.sciencedirect.com/science/article/pii/S016882780200274X

52. Wang C-S, Yao W-J, Wang S-T, Chang T-T, Chou P. Strong Association of Hepatitis C Virus (HCV) Infection and Thrombocytopenia: Implications from a Survey of a Community with Hyperendemic HCV Infection. Clin Infect Dis [Internet]. 2004 Sep 15;39(6):790–6. Available from: https://doi.org/10.1086/423384

53. Zhang W, Nardi MA, Borkowsky W, Li Z, Karpatkin S. Role of molecular mimicry of hepatitis C virus protein with platelet GPIIIa in hepatitis C–related immunologic thrombocytopenia. Blood. 2009 Apr 23;113(17):4086–93. Available from: https://doi.org/10.1182/blood-2008-09-181073

54. Kolb-Mäurer A, Goebel W. Susceptibility of hematopoietic stem cells to pathogens: role in virus/bacteria tropism and pathogenesis. FEMS Microbiol Lett. 2003 Sep 1;226(2):203–7. Available from: https://doi.org/10.1016/S0378-1097(03)00643-8

55. Gibellini D, Clò A, Morini S, Miserocchi A, Ponti C, Re MC. Effects of human immunodeficiency virus on the erythrocyte and megakaryocyte lineages. World J Virol.2013;2(2):91–101. Available from: https://www.ncbi.nlm.nih.gov/pubmed/24175233

56. SANJO A, SATOI J, OHNISHI A, MARUNO J, FUKATA M, SUZUKI N. Role of elevated platelet-associated immunoglobulin G and hypersplenism in thrombocytopenia of chronic liver diseases. J Gastroenterol Hepatol. 2003 Jun

1;18(6):638–44. Available from: https://doi.org/10.1046/j.1440-1746.2003.03026.x

57. Adinolfi LE, Giordano MG, Andreana A, Tripodi M-F, Utili R, Cesaro G, et al. Hepatic fibrosis plays a central role in the pathogenesis of thrombocytopenia in patients with chronic viral hepatitis. Br J Haematol. 2001 Jun 1;113(3):590–5. Available from: https://doi.org/10.1046/j.1365-2141.2001.02824.x

58. Peck-Radosavljevic M, Wichlas M, Zacherl J, Stiegler G, Stohlawetz P, Fuchsjäger M, et al. Thrombopoietin induces rapid resolution of thrombocytopenia after orthotopic liver transplantation through increased platelet production. Blood. 2000 Feb 1;95(3):795–801. Available from: https://doi.org/10.1182/blood.V95.3.795.003k25_795_801

59. Kurokawa T, Zheng Y-W, Ohkohchi N. Novel functions of platelets in the liver. J Gastroenterol Hepatol. 2016 Apr 1;31(4):745–51. Available from: https://doi.org/10.1111/jgh.13244

60. Tribulatti MV, Mucci J, Van Rooijen N, Leguizamón MS, Campetella O. The Sialidase from Trypanosoma cruzi Induces Thrombocytopenia during Acute Chagas Disease by Reducing the Platelet Sialic Acid Contents. Infect Immun. 2005 Jan 1;73(1):201 LP – 207. Available from: http://iai.asm.org/content/73/1/201

61. Grewal PK, Uchiyama S, Ditto D, Varki N, Le DT, Nizet V, et al. The Ashwell receptor mitigates the lethal coagulopathy of sepsis. Nat Med. 2008;14(6):648–55. Available from: https://doi.org/10.1038/nm1760

62. Tao L, Zeng Q, Li J, Xu M, Wang J, Pan Y, et al. Platelet desialylation correlates with efficacy of first-line therapies for immune thrombocytopenia. J Hematol Oncol. 2017;10(1):10–3.

63. Riswari SF, Tunjungputri RN, Kullaya V, Garishah FM, Utari GSRR, Farhanah N, et al. Desialylation of platelets induced by Von Willebrand Factor is a novel mechanism of platelet clearance in dengue. PLOS Pathog. 2019 Mar 8;15(3):e1007500. Available from: https://doi.org/10.1371/journal.ppat.1007500

64. Kullaya V, de Jonge MI, Langereis JD, van der Gaast-de Jongh CE, Bull C, Adema GJ, et al. Desialylation of Platelets by Pneumococcal Neuraminidase A Induces ADP-Dependent Platelet Hyperreactivity. Infect Immun. 2018 Oct;86(10).

65. Li MF, Li XL, Fan KL, Yu YY, Gong J, Geng SY, et al. Platelet desialylation is a novel mechanism and a therapeutic target in thrombocytopenia during sepsis: An open-label, multicenter, randomized controlled trial. J Hematol Oncol. 2017;10(1):1–10.

66. Qadri SM, Donkor DA, Nazy I, Branch DR, Sheffield WP. Bacterial neuraminidase-mediated erythrocyte desialylation provokes cell surface aminophospholipid exposure. Eur J Haematol. 2018 May;100(5):502–10.

67. Sosman JA, Verma A, Moss S, Sorokin P, Blend M, Bradlow B, et al. Interleukin 10-induced thrombocytopenia in normal healthy adult volunteers: evidence for decreased platelet production. Br J Haematol. 2000 Oct 1;111(1):104–11. Available from: https://doi.org/10.1111/j.1365-2141.2000.02314.x

68. Iga D, Tomimatsu M, Endo H, Ohkawa S-I, Yamada O. Improvement of thrombocytopenia with disappearance of HCV RNA in patients treated by interferon-α therapy: possible etiology of HCV-associated immune thrombocytopenia. Eur J Haematol. 2005 Nov 1;75(5):417–23. Available from: https://doi.org/10.1111/j.1600-0609.2005.00524.x

69. Ready PD. Epidemiology of visceral leishmaniasis. Clin Epidemiol. 2014 May 3;6:147–54. Available from: https://www.ncbi.nlm.nih.gov/pubmed/24833919

70. Torres-Guerrero E, Quintanilla-Cedillo MR, Ruiz-Esmenjaud J, Arenas R. Leishmaniasis: a review. F1000Research. 2017 May 26;6:750. Available from: https://www.ncbi.nlm.nih.gov/pubmed/28649370

71. Rodrigues V, Cordeiro-Da-Silva A, Laforge M, Silvestre R, Estaquier J. Regulation of immunity during visceral Leishmania infection. Parasites and Vectors. 2016;9(1):1–13. Available from: http://dx.doi.org/10.1186/s13071-016-1412-x

72. WHO. WHO | Leishmaniasis [Online]. WHO. World Health Organization; 2018 [cited 2020 Jan 28]. Available from: https://www.who.int/gho/neglected_diseases/leishmaniasis/en/

73. WHO. WHO [Online]. Epidemiological situation. 2017 [cited 2020 Jan 27]. Available from: https://www.who.int/leishmaniasis/epidemic/special_conditions_hiv_coinfection/en/

74. Kaye P, Scott P. Leishmaniasis: complexity at the host–pathogen interface. Nat Rev Microbiol. 2011;9(8):604–15. Available from: https://doi.org/10.1038/nrmicro2608

75. Sundar S, Rai M. Laboratory diagnosis of visceral leishmaniasis. Clin Diagn Lab Immunol. 2002 Sep;9(5):951–8. Available from: https://pubmed.ncbi.nlm.nih.gov/12204943

76. Sundar S, Singh RK, Maurya R, Kumar B, Chhabra A, Singh V, et al. Serological diagnosis of Indian visceral leishmaniasis: direct agglutination test versus rK39 strip test. Trans R Soc Trop Med Hyg. 2006 Jun 1;100(6):533–7. Available from: https://doi.org/10.1016/j.trstmh.2005.08.018

77. Balasegaram M, Ritmeijer K, Lima MA, Burza S, Ortiz Genovese G, Milani B, et al. Liposomal amphotericin B as a treatment for human leishmaniasis. Expert Opin Emerg Drugs. 2012;17(4):493–510.

78. Rosenthal E, Marty P. Recent understanding in the treatment of visceral leishmaniasis. J Postgrad Med. 2003 Jan 1;49(1):61–8. Available from: http://www.jpgmonline.com/article.asp?issn=0022-3859

79. Moafi M, Rezvan H, Sherkat R, Taleban R. Leishmania Vaccines Entered in Clinical Trials: A Review of Literature. Int J Prev Med. 2019 Jun 7;10:95. Available from: https://www.ncbi.nlm.nih.gov/pubmed/31360342

80. Murray HW, Berman JD, Davies CR, Saravia NG. Advances in leishmaniasis. Lancet. 2005 Oct 29;366(9496):1561–77. Available from: https://www.sciencedirect.com/science/article/pii/S0140673605676295?via%3Dihub

81. Dayakar A, Chandrasekaran S, Kuchipudi S V., Kalangi SK. Cytokines: Key Determinants of Resistance or Disease Progression in Visceral Leishmaniasis: Opportunities for Novel Diagnostics and Immunotherapy. Front Immunol. 2019;10(APR):670.
Available from: https://www.frontiersin.org/article/10.3389/fimmu.2019.00670

82. Nylén S, Sacks D. Interleukin-10 and the pathogenesis of human visceral leishmaniasis. Trends Immunol. 2007 Sep 1;28(9):378–84. Available from: https://www.sciencedirect.com/science/article/pii/S1471490607001834

83. Medina-Colorado AA, Osorio EY, Saldarriaga OA, Travi BL, Kong F, Spratt H, et al. Splenic CD4+ T Cells in Progressive Visceral Leishmaniasis Show a Mixed Effector-Regulatory Phenotype and Impair Macrophage Effector Function through

Inhibitory Receptor Expression. PLoS One. 2017 Jan 19;12(1):e0169496. Available from: https://doi.org/10.1371/journal.pone.0169496

84. Bogdan C, Röllinghoff M, Diefenbach A. Reactive oxygen and reactive nitrogen intermediates in innate and specific immunity. Curr Opin Immunol. 2000;12(1):64–76.

85. Bogdan C, Röllinghoff M, Diefenbach A. The role of nitric oxide in innate immunity. Immunol Rev. 2000;173(1):17–26.

86. Liew FY, Li Y, Millott S, Millott S. Tumor necrosis factor-alpha synergizes with IFN-gamma in mediating killing of Leishmania major through the induction of nitric oxide. *J Immunol*. 1990;145(12):4306-4310.

87. Carneiro PP, Conceição J, Macedo M, Magalhães V, Carvalho EM, Bacellar O. The Role of Nitric Oxide and Reactive Oxygen Species in the Killing of Leishmania braziliensis by Monocytes from Patients with Cutaneous Leishmaniasis. PLoS One. 2016 Feb 3;11(2):e0148084. Available from: https://doi.org/10.1371/journal.pone.0148084

88. Zafra R, Jaber JR, Pérez-Ecija RA, Barragán A, Martínez-Moreno A, Pérez J. High iNOS expression in macrophages in canine leishmaniasis is associated with low intracellular parasite burden. Vet Immunol Immunopathol. 2008 Jun;123(3–4):353–9.

89. Stäger S, Rafati S. CD8(+) T cells in leishmania infections: friends or foes? Front Immunol. 2012 Jan 24;3:5. Available from: https://www.ncbi.nlm.nih.gov/pubmed/22566891

90. Schietinger A, Greenberg PD. Tolerance and exhaustion: defining mechanisms of T cell dysfunction. Trends Immunol. 2014 Feb;35(2):51–60. Available from: https://pubmed.ncbi.nlm.nih.gov/24210163

91. Wherry EJ. T cell exhaustion. Nat Immunol. 2011;12(6):492–9. Available from: https://doi.org/10.1038/ni.2035

92. Phillips R, Svensson M, Aziz N, Maroof A, Brown N, Beattie L, et al. Innate killing of Leishmania donovani by macrophages of the splenic marginal zone requires IRF-7. PLoS Pathog. 2010 Mar 12;6(3):e1000813–e1000813. Available from: https://pubmed.ncbi.nlm.nih.gov/20300600

93. Ghalib HW, Piuvezam MR, Skeiky YA, Siddig M, Hashim FA, El-Hassan AM, et al. Interleukin 10 production correlates with pathology in human Leishmania donovani infections. J Clin Invest. 1993;92(1):324–9.

94. Mege J-L, Meghari S, Honstettre A, Capo C, Raoult D. The two faces of interleukin 10 in human infectious diseases. Lancet Infect Dis. 2006 Sep 1;6(9):557–69. Available from: https://www.sciencedirect.com/science/article/pii/S1473309906705771

95. Means RT. The anaemia of infection. Best Pract Res Clin Haematol. 2000;13(2):151–62.
Available from: http://www.sciencedirect.com/science/article/pii/S1521692699900658

96. Varma N, Naseem S. Hematologic Changes in Visceral Leishmaniasis/Kala Azar. Indian J Hematol Blood Transfus. 2010;26(3):78–82. Available from: https://doi.org/10.1007/s12288-010-0027-1

97. Nicolato R de C, de Abreu RT, Roatt BM, Aguiar-Soares RD de O, Reis LES, Carvalho M das G, et al. Clinical forms of canine visceral Leishmaniasis in naturally Leishmania infantum-infected dogs and related myelogram and hemogram changes. PLoS One. 2013 Dec 23;8(12):e82947–e82947. Available from: https://pubmed.ncbi.nlm.nih.gov/24376612

98. Dos Santos PL, de Oliveira FA, Santos MLB, Cunha LCS, Lino MTB, de Oliveira MFS, et al. The Severity of Visceral Leishmaniasis Correlates with Elevated Levels of Serum IL-6, IL-27 and sCD14. PLoS Negl Trop Dis. 2016 Jan 27;10(1):e0004375–e0004375.
Available from: https://www.ncbi.nlm.nih.gov/pubmed/26814478

99. Pinto AI, Brown N, Preham O, Doehl JSP, Ashwin H, Kaye PM. TNF signalling drives expansion of bone marrow CD4+T cells responsible for HSC exhaustion in experimental visceral leishmaniasis. PLoS Pathog. 2017 Jul 1;13(7).

100. Abidin BM, Hammami A, Stäger S, Heinonen KM. Infection-adapted emergency hematopoiesis promotes visceral leishmaniasis. PLOS Pathog. 2017 Aug 7;13(8):e1006422. Available from: https://doi.org/10.1371/journal.ppat.1006422

101. Preham O, Pinho FA, Pinto AI, Rani GF, Brown N, Hitchcock IS, et al. CD4+ T Cells Alter the Stromal Microenvironment and Repress Medullary Erythropoiesis

in Murine Visceral Leishmaniasis. Front Immunol. 2018;9:2958.

102. Lafuse WP, Story R, Mahylis J, Gupta G, Varikuti S, Steinkamp H, et al. Leishmania donovani infection induces anemia in hamsters by differentially altering erythropoiesis in bone marrow and spleen. PLoS One. 2013;8(3):e59509–e59509. Available from: https://www.ncbi.nlm.nih.gov/pubmed/23533629

103. Vilela RB, Bordin JO, Chiba AK, Castelo A, Barbosa MC. RBC-associated IgG in patients with visceral leishmaniasis (kala-azar): a prospective analysis. Transfusion. 2002;42(11):1442–7.

104. Wickramasinghe SN, Abdalla SH, Kasil EG. Ultrastructure of bone marrow in patients with visceral leishmaniasis. J Clin Pathol. 1987;40(3):267–75.

105. Engwerda CR, Kaye PM. Organ-specific immune responses associated with infectious disease. Immunol Today. 2000;21(2):73–8. Available from: http://www.sciencedirect.com/science/article/pii/S0167569999015492

106. Costa ASA, Costa GC, Aquino DMC de, Mendonça VRR de, Barral A, Barral-Netto M, et al. Cytokines and visceral leishmaniasis: a comparison of plasma cytokine profiles between the clinical forms of visceral leishmaniasis . Vol. 107, Memórias do Instituto Oswaldo Cruz . scielo ; 2012. p. 735–9.

107. Terrazzano G, Cortese L, Piantedosi D, Zappacosta S, Di Loria A, Santoro D, et al. Presence of anti-platelet IgM and IgG antibodies in dogs naturally infected by. Vet Immunol Immunopathol. 2006 May 1;110(3–4):331–7. Available from: https://www.sciencedirect.com/science/article/pii/S016524270500320X

108. Ciaramella P, Pelagalli A, Cortese L, Pero ME, Corona M, Lombardi P, et al. Altered platelet aggregation and coagulation disorders related to clinical findings in 30 dogs naturally infected by Leishmania infantum. Vet J. 2005;169(3):465–7. Available from: https://www.sciencedirect.com/science/article/pii/S109002330400070X?via%3Dihub

109. Gebreyohannes EA, Bhagvathula AS, Abegaz TM, Seid MA. Treatment outcomes of visceral leishmaniasis in Ethiopia from 2001 to 2017: A systematic review and meta-analysis. Infect Dis Poverty. 2018 Oct 19;7(1).

110. Braga SS. Multi-target drugs active against leishmaniasis: A paradigm of drug repurposing. Eur J Med Chem. 2019 Dec 1;183:111660. Available from:

https://www.sciencedirect.com/science/article/pii/S0223523419308049?via%3Dihub

111. Wasunna M, Njenga S, Balasegaram M, Alexander N, Omollo R, Edwards T, et al. Efficacy and Safety of AmBisome in Combination with Sodium Stibogluconate or Miltefosine and Miltefosine Monotherapy for African Visceral Leishmaniasis: Phase II Randomized Trial. PLoS Negl Trop Dis. 2016 Sep 14;10(9):e0004880. Available from: https://doi.org/10.1371/journal.pntd.0004880

112. Tollemar J, Klingspor L, Ringdén O. Liposomal amphotericin B (AmBisome) for fungal infections in immunocompromised adults and children. Clin Microbiol Infect. 2001 Jan 1;7:68–79. Available from: https://www.sciencedirect.com/science/article/pii/S1198743X15301026?via%3Dihub

113. Burza S, Sinha PK, Mahajan R, Lima MA, Mitra G, Verma N, et al. Risk factors for visceral leishmaniasis relapse in immunocompetent patients following treatment with 20 mg/kg liposomal amphotericin B (Ambisome) in Bihar, India. PLoS Negl Trop Dis. 2014;8(1):e2536.

114. Forrester S, Siefert K, Ashwin H, Brown N, Zelmar A, James S, et al. Tissue-specific transcriptomic changes associated with AmBisome® treatment of BALB/c mice with experimental visceral leishmaniasis. Wellcome open Res . 2019 Dec 10;4:198. Available from: https://www.ncbi.nlm.nih.gov/pmc/articles/PMC6961418/

115. Hotez PJ, Molyneux DH, Fenwick A, Ottesen E, Ehrlich Sachs S, Sachs JD. Incorporating a rapid-impact package for neglected tropical diseases with programs for HIV/AIDS, tuberculosis, and malaria. PLoS Med. 2006 Jan;3(5):e102–e102. Available from: https://www.ncbi.nlm.nih.gov/pubmed/16435908

116. Supali T, Verweij JJ, Wiria AE, Djuardi Y, Hamid F, Kaisar MMM, et al. Polyparasitism and its impact on the immune system. Int J Parasitol. 2010;40(10):1171–6.
Available from: http://www.sciencedirect.com/science/article/pii/S0020751910001827

117. van den Bogaart E, Berkhout MMZZ, Adams ER, Mens PF, Sentongo E, Mbulamberi DB, et al. Prevalence, features and risk factors for malaria co-infections amongst visceral leishmaniasis patients from Amudat Hospital, Uganda. PLoS Negl Trop Dis. 2012/04/10. 2012 Apr;6(4):e1617–e1617. Available from: https://www.ncbi.nlm.nih.gov/pubmed/22506087

118. Akuffo H, Costa C, van Griensven J, Burza S, Moreno J, Herrero M. New insights into leishmaniasis in the immunosuppressed. PLoS Negl Trop Dis. 2018 May 10;12(5):e0006375. Available from: https://doi.org/10.1371/journal.pntd.0006375

119. van Griensven J, Balasegaram M, Meheus F, Alvar J, Lynen L, Boelaert M. Combination therapy for visceral leishmaniasis. The Lancet Infectious Diseases. 2010.

120. Van Griensven J, van Henten S, Mengesha B, Kassa M, Adem E, Seid ME, et al. Longitudinal evaluation of asymptomatic Leishmania infection in HIV-infected individuals in North-West Ethiopia: A pilot study. PLoS Negl Trop Dis. 2019;13(10):30–45.

121. Mathur P, Samantaray JC, Vajpayee M, Samanta P. Visceral leishmaniasis/human immunodeficiency virus co-infection in India: the focus of two epidemics. J Med Microbiol. 2006 Jul 1;55(7):919–22. Available from: https://www.microbiologyresearch.org/content/journal/jmm/10.1099/jmm.0.46574-0

122. Redhu NS, Dey A, Balooni V, Singh S. Leishmania–HIV co-infection: An emerging problem in India. AIDS. 2006;20(8). Available from: https://journals.lww.com/aidsonline/Fulltext/2006/05120/Leishmania_HIV_co_infection__An_emerging_problem.24.aspx

123. Yona S, Gordon S. From the Reticuloendothelial to Mononuclear Phagocyte System – The Unaccounted Years. Vol. 6, Frontiers in Immunology. 2015. p. 328. Available from: https://www.frontiersin.org/article/10.3389/fimmu.2015.00328

124. Hume DA. Differentiation and heterogeneity in the mononuclear phagocyte system. Mucosal Immunol. 2008;1(6):432–41.

125. Chen S, Yang J, Wei Y, Wei X. Epigenetic regulation of macrophages: from homeostasis maintenance to host defense. Cell Mol Immunol. 2019;(17). Available from: http://www.ncbi.nlm.nih.gov/pubmed/31664225

126. Mebius RE, Kraal G. Structure and function of the spleen. Nat Rev Immunol. 2005;5(8):606–16. Available from: https://doi.org/10.1038/nri1669

127. Borges Da Silva H, Fonseca R, Pereira RM, Cassado ADA, Álvarez JM, D'Império Lima MR. Splenic Macrophage Subsets and Their Function during

Blood-Borne Infections. Front Immunol. 2015 Sep 22;6(SEP):480. Available from: https://www.ncbi.nlm.nih.gov/pubmed/26441984

128. Jones C, Virji M, Crocker PR. Recognition of sialylated meningococcal lipopolysaccharide by siglecs expressed on myeloid cells leads to enhanced bacterial uptake. Mol Microbiol. 2003 Sep 1;49(5):1213–25. Available from: https://doi.org/10.1046/j.1365-2958.2003.03634.x

129. Heikema AP, Koning RI, Duarte dos Santos Rico S, Rempel H, Jacobs BC, Endtz HP, et al. Enhanced, Sialoadhesin-Dependent Uptake of Guillain-Barré Syndrome-Associated Campylobacter jejuni Strains by Human Macrophages. Flynn JL, editor. Infect Immun. 2013 Jun 1;81(6):2095 LP – 2103. Available from: http://iai.asm.org/content/81/6/2095

130. Chang Y-C, Olson J, Louie A, Crocker PR, Varki A, Nizet V. Role of macrophage sialoadhesin in host defense against the sialylated pathogen group B Streptococcus. J Mol Med. 2014;92(9):951–9. Available from: https://doi.org/10.1007/s00109-014-1157-y

131. Ercoli G, Fernandes VE, Chung WY, Wanford JJ, Thomson S, Bayliss CD, et al. Intracellular replication of Streptococcus pneumoniae inside splenic macrophages serves as a reservoir for septicaemia. Nat Microbiol. 2018;3(5):600–10. Available from: https://doi.org/10.1038/s41564-018-0147-1

132. de Porto APNA, Lammers AJJ, Bennink RJ, ten Berge IJM, Speelman P, Hoekstra JBL. Assessment of splenic function. Eur J Clin Microbiol Infect Dis. 2010 Dec;29(12):1465–73. Available from: https://www.ncbi.nlm.nih.gov/pubmed/20853172

133. Cadili A, de Gara C. Complications of Splenectomy. Am J Med. 2008 May1;121(5):371–5.
Available from: https://www.sciencedirect.com/science/article/pii/S000293430800185X

134. Davies LC, Jenkins SJ, Allen JE, Taylor PR. Tissue-resident macrophages. Nat Immunol. 2013;14(10):986–95. Available from: https://doi.org/10.1038/ni.2705

135. Mebius RE, Kraal G. Structure and function of the spleen. Nat Rev Immunol. 2005;5(8):606–16. Available from: https://doi.org/10.1038/nri1669

136. Ishibashi H, Nakamura M, Komori A, Migita K, Shimoda S. Liver architecture, cell function, and disease. 2009 p. 399–409.

137. Krishna M. Microscopic anatomy of the liver. Vol. 2, Clinical Liver Disease. John Wiley and Sons Inc.; 2013.

138. Zhou Z, Xu M-J, Gao B. Hepatocytes: a key cell type for innate immunity. Cell Mol Immunol. 2016;13(3):301–315. Available from: https://doi.org/10.1038/cmi.2015.97

139. Bilzer M, Roggel F, Gerbes AL. Role of Kupffer cells in host defense and liver disease. Vol. 26, Liver International. 2006. p. 1175–86.

140. Krizhanovsky V, Yon M, Dickins RA, Hearn S, Simon J, Miething C, et al. Senescence of Activated Stellate Cells Limits Liver Fibrosis. Cell. 2008 Aug 22;134(4):657–67.

141. Tsutsui H, Nishiguchi S. Importance of kupffer cells in the development of acute liver injuries in mice. Int J Mol Sci. 2014;15(5):7711–30.

142. McFarlane E, Perez C, Charmoy M, Allenbach C, Carter KC, Alexander J, et al. Neutrophils Contribute to Development of a Protective Immune Response during Onset of Infection with Leishmania donovani. Infect Immun. 2008 Feb 1;76(2):532 LP – 541. Available from: http://iai.asm.org/content/76/2/532

143. Sheel M, Engwerda CR. The diverse roles of monocytes in inflammation caused by protozoan parasitic diseases. Trends Parasitol. 2012 Oct 1;28(10):408–16. Available from: https://www.sciencedirect.com/science/article/pii/S1471492212001262

144. Murray HW, Nathan CF. Macrophage microbicidal mechanisms in vivo: reactive nitrogen versus oxygen intermediates in the killing of intracellular visceral Leishmania donovani. J Exp Med. 1999 Feb 15;189(4):741–6. Available from: https://www.ncbi.nlm.nih.gov/pubmed/9989990

145. Engwerda CR, Ato M, Cotterell SEJ, Mynott TL, Tschannerl A, Gorak-Stolinska PMA, et al. A Role for Tumor Necrosis Factor-α in Remodeling the Splenic Marginal Zone during Leishmania donovani Infection. Am J Pathol. 2002 Aug 1;161(2):429–37.
Available from: https://www.sciencedirect.com/science/article/pii/S0002944010641995

146. Hermida M d'El-R, de Melo CVB, Lima IDS, Oliveira GG de S, Dos-Santos WLC. Histological Disorganization of Spleen Compartments and Severe Visceral Leishmaniasis. Front Cell Infect Microbiol. 2018 Nov 13;8:394. Available from:

https://www.ncbi.nlm.nih.gov/pubmed/30483481

147. Cotterell SEJ, Engwerda CR, Kaye PM. Enhanced Hematopoietic Activity Accompanies Parasite Expansion in the Spleen and Bone Marrow of Mice Infected with Leishmania donovani. Infect Immun. 2000 Apr 1;68(4):1840 LP – 1848. Available from: http://iai.asm.org/content/68/4/1840

148. Cotterell SEJ, Engwerda CR, Kaye PM. Leishmania donovani infection of bone marrow stromal macrophages selectively enhances myelopoiesis, by a mechanism involving GM-CSF and TNF-α. Blood. 2000 Mar 1;95(5):1642–51. Available from: https://doi.org/10.1182/blood.V95.5.1642.005k10_1642_1651

149. Elmakki E. Hypersplenism. Journal of Biology, Agriculture and Healthcare. 2012;2(10):89-99.

150. Jandl JH, Aster RH. Increased splenic pooling and the pathogenesis of hypersplenism. Am J Med Sci. 1967 Apr;253(4):383–98.

151. CASSERD F, FINCH CA, GIBLETT ER, HOUGHTON B, MOTULSKY AG. Studies on the pathogenesis of splenic anemia. Blood. 1956 Dec;11(12):1118–31.

152. Martins RN, Cleva R de, Gouveia ÉM, Ghosn NB, Herman P. Correlação entre esplenomegalia e plaquetopenia na forma hepatoesplênica da esquistossomose mansônica. Vol. 23, ABCD. Arquivos Brasileiros de Cirurgia Digestiva (São Paulo). scielo ; 2010. p. 254–8.

153. Lacerda MVG, Mourão MPG, Coelho HC, Santos JB. Thrombocytopenia in malaria: Who cares? Mem Inst Oswaldo Cruz. 2011;106(SUPPL. 1):52–63.

154. WHO. WHO | World malaria report 2019 [Online]. Available from: https://www.who.int/malaria/publications/world-malaria-report-2019/en/

155. Ademola IO, Odeniran PO. Co-infection with Plasmodium berghei and Trypanosoma brucei increases severity of malaria and trypanosomiasis in mice. Acta Trop. 2016 Jul 1;159:29–35. Available from: https://www.sciencedirect.com/science/article/pii/S0001706X16301255

156. Pinna RA, Silva-dos-Santos D, Perce-da-Silva DS, Oliveira-Ferreira J, Villa-Verde DMSS, De Luca PM, et al. Malaria-Cutaneous Leishmaniasis Co-infection: Influence on Disease Outcomes and Immune Response. Frontiers in Microbiology

Frontiers Research Foundation; 2016 p. 982. Available from: https://www.frontiersin.org/article/10.3389/fmicb.2016.00982

157. Mendonça VRR, Andrade BB, Souza LCL, Magalhães BML, Mourão MPG, Lacerda MVG, et al. Unravelling the patterns of host immune responses in Plasmodium vivax malaria and dengue co-infection. Malar J. 2015;14(1):315. Available from: https://doi.org/10.1186/s12936-015-0835-8

158. van den Bogaart E, Berkhout MMZ, Nour ABYM, Mens PF, Talha A-BA, Adams ER, et al. Concomitant malaria among visceral leishmaniasis in-patients from Gedarif and Sennar States, Sudan: a retrospective case-control study. BMC Public Health. 2013 Apr 11;13:332. Available from: https://www.ncbi.nlm.nih.gov/pubmed/23577673

159. Magalhães BML, Alexandre MAA, Siqueira AM, Melo GC, Gimaque JBL, Bastos MS, et al. Case report: Clinical profile of concurrent dengue fever and Plasmodium vivax malaria in the Brazilian Amazon: Case series of 11 hospitalized patients. Am J Trop Med Hyg. 2012 Dec;87(6):1119–24.

160. Hotez PJ, Molyneux DH, Fenwick A, Ottesen E, Sachs SE, Sachs JD. Incorporating a rapid-impact package for neglected tropical diseases with programs for HIV/AIDS, tuberculosis, and malaria: A comprehensive pro-poor health policy and strategy for the developing world. Vol. 3, PLoS Medicine. 2006. p. 576–84.

161. HARTGERS FC, YAZDANBAKHSH M. Co-infection of helminths and malaria: modulation of the immune responses to malaria. Parasite Immunol. 2006 Oct 1;28(10):497–506. Available from: https://doi.org/10.1111/j.1365-3024.2006.00901.x

162. Sanches-Vaz M, Temporão A, Luis R, Nunes-Cabaço H, Mendes AM, Goellner S, et al. Trypanosoma brucei infection protects mice against malaria. PLoS Pathog. 2019;15(11):e1008145. Available from: http://www.ncbi.nlm.nih.gov/pubmed/31703103

163. Moriyasu T, Nakamura R, Deloer S, Senba M, Kubo M, Inoue M, et al. Schistosoma mansoni infection suppresses the growth of Plasmodium yoelii parasites in the liver and reduces gametocyte infectivity to mosquitoes. PLoS Negl Trop Dis. 2018 Jan 1;12(1).

164. Yoshida A, Maruyama H, Kumagai T, Amano T, Kobayashi F, Zhang M, et al. Schistosoma mansoni infection cancels the susceptibility to Plasmodium chabaudi through induction of type 1 immune responses in A/J mice. Int Immunol. 2000 Aug 1;12(8):1117–25. Available from: https://doi.org/10.1093/intimm/12.8.1117

165. Egima CM, Macedo SF, Sasso GRS, Covarrubias C, Cortez M, Maeda FY, et al. Co-infection with Trypanosoma cruzi protects mice against early death by neurological or pulmonary disorders induced by Plasmodium berghei ANKA. Malar J. 2007;6(1):90. Available from: https://doi.org/10.1186/1475-2875-6-90

166. Legesse M, Erko B, Balcha F. Increased parasitaemia and delayed parasite clearance in Schistosoma mansoni and Plasmodium berghei co-infected mice. Acta Trop. 2004 Jul 1;91(2):161–6. Available from: https://www.sciencedirect.com/science/article/pii/S0001706X04000725

167. WHO. WHO | This year's World malaria report at a glance. WHO [Online]. 2019;(December):1–10. Available from: https://www.who.int/malaria/media/world-malaria-report-2018/en/#Global%20and%20regional%20malaria%20burden,%20in%20numbers

168. WHO. WHO | Epidemiological situation. World Health Organization; 2019.

169. Petney TN, Andrews RH. Multiparasite communities in animals and humans: frequency, structure and pathogenic significance. Int J Parasitol. 1998 Mar 1;28(3):377–93.
Available from: https://www.sciencedirect.com/science/article/pii/S0020751997001896

170. Griffiths EC, Pedersen AB, Fenton A, Petchey OL. The nature and consequences of coinfection in humans. J Infect. 2011/06/16. 2011 Sep 1;63(3):200–6. Available from: https://www.sciencedirect.com/science/article/pii/S0163445311003914?via%3Dihub

171. White NJ. Anaemia and malaria. Malar J. 2018;17(1):371. Available from: https://doi.org/10.1186/s12936-018-2509-9

172. Ghimire PG, Ghimire P, Adhikari J, Chapagain A. A case report of visceral leishmaniasis and malaria co-infection with pancytopenia and splenomegaly - a diagnostic challenge. BMC Infect Dis. 2019;19(1):849. Available from: https://doi.org/10.1186/s12879-019-4478-1

173. Aschale Y, Ayehu A, Worku L, Tesfa H, Birhanie M, Lemma W. Malaria-visceral

leishmaniasis co-infection and associated factors among migrant laborers in West Armachiho district, North West Ethiopia: community based cross-sectional study. BMC Infect Dis. 2019;19(1):239. Available from: https://doi.org/10.1186/s12879-019-3865-y

174. Semple JW. Animal models of immune thrombocytopenia (ITP). Ann Hematol. 2010;89(1):37–44. Available from: https://doi.org/10.1007/s00277-009-0882-8

175. Duncan SM, Myburgh E, Philipon C, Brown E, Meissner M, Brewer J, et al. Conditional gene deletion with DiCre demonstrates an essential role for CRK3 in Leishmania mexicana cell cycle regulation. Mol Microbiol. 2016 Jun 1;100(6):931–44. Available from: https://doi.org/10.1111/mmi.13375

176. Prévost N, Kato H, Bodin L, Shattil SJBT-M in E. Platelet Integrin Adhesive Functions and Signaling. In: Integrins. Academic Press; 2007. p. 103–15. Available from: http://www.sciencedirect.com/science/article/pii/S0076687907260069

177. Bhasin TS, Sharma S, Manjari M, Mannan R, Kansal V, Chandey M, et al. Changes in megakaryocytes in cases of thrombocytopenia: Bone marrow aspiration and biopsy analysis. J Clin Diagnostic Res. 2013;7(3):473–9.

178. Pokharel S, Upadhyaya P, Karki S, Paudyal P, Pradhan B, Poudel P. Megakaryocytic alterations in thrombocytopenia: A bone marrow aspiration study. J Pathol Nepal. 2016;6(11):914–21.

179. Eckly A, Strassel C, Freund M, Cazenave JP, Lanza F, Gachet C, et al. Abnormal megakaryocyte morphology and proplatelet formation in mice with megakaryocyte-restricted MYH9 inactivation. Blood. 2009;113(14):3182–9.

180. Yurdakul P, Dalton J, Beattie L, Brown N, Erguven S, Maroof A, et al. Compartment-specific remodeling of splenic micro-architecture during experimental visceral leishmaniasis. Am J Pathol. 2011 Jul;179(1):23–9.

181. de Freitas EO, Leoratti FM de S, Freire-de-Lima CG, Morrot A, Feijó DF. The Contribution of Immune Evasive Mechanisms to Parasite Persistence in Visceral Leishmaniasis. Vol. 7, Frontiers in Immunology . 2016. p. 153. Available from: https://www.frontiersin.org/article/10.3389/fimmu.2016.00153

182. Schulze H, Korpal M, Hurov J, Kim S-W, Zhang J, Cantley LC, et al.

Characterization of the megakaryocyte demarcation membrane system and its role in thrombopoiesis. Blood. 2006 May 15;107(10):3868–75. Available from: https://doi.org/10.1182/blood-2005-07-2755

183. White JG, Key NS, King RA, Vercellotti GM. A 'touch' of the White platelet syndrome. Platelets. 2005 Sep 1;16(6):346–61. Available from: https://doi.org/10.1080/09537100500124376

184. White JG, Key NS, King RA, Vercellotti GM. The White platelet syndrome: a new autosomal dominant platelet disorder. Platelets. 2004 May;15(3):173–84.

185. Sampaio MJA de Q, Cavalcanti NV, Alves JGB, Fernandes Filho MJC, Correia JB. Risk Factors for Death in Children with Visceral Leishmaniasis. PLoS Negl Trop Dis. 2010 Nov 2;4(11):e877. Available from: https://doi.org/10.1371/journal.pntd.0000877

186. Makar RS, Zhukov OS, Sahud MA, Kuter DJ. Thrombopoietin levels in patients with disorders of platelet production: Diagnostic potential and utility in predicting response to TPO receptor agonists. Am J Hematol. 2013;88(12):1041–4.

187. Petroianu A, De Oliveira AE, Alberti LR. Hypersplenism in Schistosomatic Portal Hypertension. Arch Med Res. 2005 Sep 1;36(5):496–501. Available from: https://www.sciencedirect.com/science/article/pii/S0188440905001396

188. McCormick PA, Murphy KM. Splenomegaly, hypersplenism and coagulation abnormalities in liver disease. Best Pract Res Clin Gastroenterol. 2000;14(6):1009–31.

189. Bankoti R, Stäger S. Differential Regulation of the Immune Response in the Spleen and Liver of Mice Infected with Leishmania donovani. J Trop Med. 2012;2012:639304. Available from: https://pubmed.ncbi.nlm.nih.gov/21811511

190. Provan D, Stasi R, Newland AC, Blanchette VS, Bolton-Maggs P, Bussel JB, et al. International consensus report on the investigation and management of primary immune thrombocytopenia. Blood. 2010 Jan 14;115(2):168–86. Available from: https://doi.org/10.1182/blood-2009-06-225565

191. Kashiwagi H, Tomiyama Y. Pathophysiology and management of primary immune thrombocytopenia. Int J Hematol. 2013;98(1):24–33. Available from:

https://doi.org/10.1007/s12185-013-1370-4

192. Qiu J, Liu X, Li X, Zhang X, Han P, Zhou H, et al. CD8+ T cells induce platelet clearance in the liver via platelet desialylation in immune thrombocytopenia. Sci Rep. 2016;6(1):27445. Available from: https://doi.org/10.1038/srep27445

193. Aslam R, Kapur R, Segel GB, Guo L, Zufferey A, Ni H, et al. The spleen dictates platelet destruction, anti-platelet antibody production, and lymphocyte distribution patterns in a murine model of immune thrombocytopenia. Exp Hematol. 2016;44(10):924-930.e1. Available from: http://dx.doi.org/10.1016/j.exphem.2016.07.004

194. Rumjantseva V, Grewal PK, Wandall HH, Josefsson EC, Sørensen AL, Larson G, et al. Dual roles for hepatic lectin receptors in the clearance of chilled platelets. Nat Med. 2009;15(11):1273–80. Available from: https://doi.org/10.1038/nm.2030

195. Bader JE, Enos RT, Velázquez KT, Carson MS, Nagarkatti M, Nagarkatti PS, et al. Macrophage depletion using clodronate liposomes decreases tumorigenesis and alters gut microbiota in the AOM/DSS mouse model of colon cancer. Am J Physiol Gastrointest Liver Physiol. 2018 Jan 1;314(1):G22–31. Available from: https://pubmed.ncbi.nlm.nih.gov/29025731

196. van Rooijen N, Hendrikx E. Liposomes for Specific Depletion of Macrophages from Organs and Tissues BT- Liposomes: Methods and Protocols, Volume 1: Pharmaceutical Nanocarriers. In: Weissig V, editor. Totowa, NJ: Humana Press; 2010. p. 189–203. Available from: https://doi.org/10.1007/978-1-60327-360-2_13

197. Cines DB, Bussel JB, Liebman HA, Luning Prak ET. The ITP syndrome: pathogenic and clinical diversity. Blood. 2009 Jun 25;113(26):6511–21. Available from: https://doi.org/10.1182/blood-2009-01-129155

198. Kirby AC, Beattie L, Maroof A, Van Rooijen N, Kaye PM. SIGNR1-negative red pulp macrophages protect against acute streptococcal sepsis after Leishmania donovani-induced loss of marginal zone macrophages. Am J Pathol. 2009 Sep;175(3):1107–15. Available from: https://pubmed.ncbi.nlm.nih.gov/19644016

199. Mai LT, Smans M, Silva-Barrios S, Fabié A, Stäger S. IRF-5 Expression in Myeloid Cells Is Required for Splenomegaly in L. donovani Infected Mice. Vol. 10, Frontiers in Immunology. 2020. p. 3071. Available from:

https://www.frontiersin.org/article/10.3389/fimmu.2019.03071

200. Goren I, Allmann N, Yogev N, Schürmann C, Linke A, Holdener M, et al. A Transgenic Mouse Model of Inducible Macrophage Depletion: Effects of Diphtheria Toxin-Driven Lysozyme M-Specific Cell Lineage Ablation on Wound Inflammatory, Angiogenic, and Contractive Processes. Am J Pathol. 2009;175(1):132–47.
Available from: http://www.sciencedirect.com/science/article/pii/S0002944010605305

201. Hua L, Shi J, Shultz LD, Ren G. Genetic Models of Macrophage Depletion. Methods Mol Biol. 2018;1784:243–58. Available from: https://pubmed.ncbi.nlm.nih.gov/29761404

202. Aref S, Sleem T, El Menshawy N, Ebrahiem L, Abdella D, Fouda M, et al. Antiplatelet antibodies contribute to thrombocytopenia associated with chronic hepatitis C virus infection. Hematology. 2009 Oct;14(5):277–81. Available from: https://pubmed.ncbi.nlm.nih.gov/19843383

203. WHO. Leishmaniasis Key facts [Online]. 2017. p. 2013–4. Available from: http://www.who.int/en/news-room/fact-sheets/detail/leishmaniasis

204. Moore EM, Lockwood DN. Treatment of visceral leishmaniasis. J Glob Infect Dis. 2010 May;2(2):151–8. Available from: https://pubmed.ncbi.nlm.nih.gov/20606971

205. Herwaldt BL, Berman JD. Recommendations for treating leishmaniasis with sodium stibogluconate (pentostam) and review of pertinent clinical studies. Am J Trop Med Hyg. 1992;46(3):296–306.

206. Sane SA, Shakya N, Gupta S. Immunomodulatory effect of picroliv on the efficacy of paromomycin and miltefosine in combination in experimental visceral leishmaniasis. Exp Parasitol. 2011;127(2):376–81. Available from: http://dx.doi.org/10.1016/j.exppara.2010.09.003

207. Jain K, Jain NK. Novel therapeutic strategies for treatment of visceral leishmaniasis. Drug Discov Today. 2013 Dec 1;18(23–24):1272–81. Available from: https://www.sciencedirect.com/science/article/pii/S1359644613002687

208. Sundar S, Singh A, Rai M, Prajapati VK, Singh AK, Ostyn B, et al. Efficacy of Miltefosine in the Treatment of Visceral Leishmaniasis in India After a Decade of

Use. Clin Infect Dis. 2012 May 9;55(4):543–50. Available from: https://doi.org/10.1093/cid/cis474

209. Rahman M, Ahmed BN, Faiz MA, Chowdhury MZU, Islam QT, Sayeedur R, et al. Phase IV trial of miltefosine in adults and children for treatment of visceral leishmaniasis (kala-azar) in Bangladesh. Am J Trop Med Hyg. 2011;85(1):66–9.

210. Sundar S, Singh A. Recent developments and future prospects in the treatment of visceral leishmaniasis. Ther Adv Infect Dis. 2016;3(3–4):98–109.

211. Ritmeijer K, ter Horst R, Chane S, Aderie EM, Piening T, Collin SM, et al. Limited Effectiveness of High-Dose Liposomal Amphotericin B (AmBisome) for Treatment of Visceral Leishmaniasis in an Ethiopian Population With High HIV Prevalence. Clin Infect Dis. 2011 Oct 19;53(12):e152–8. Available from: https://doi.org/10.1093/cid/cir674

212. Diro E, Blesson S, Edwards T, Ritmeijer K, Fikre H, Admassu H, et al. A randomized trial of AmBisome monotherapy and AmBisome and miltefosine combination to treat visceral leishmaniasis in HIV co-infected patients in Ethiopia. PLoS Negl Trop Dis. 2019 Jan 17;13(1):e0006988–e0006988. Available from: https://pubmed.ncbi.nlm.nih.gov/30653490

213. A-Gonzalez N, Castrillo A. Origin and specialization of splenic macrophages. Cell Immunol.2018;330:151–8.
Available from: http://www.sciencedirect.com/science/article/pii/S0008874918302259

214. Banerjee A, De M, Ali N. Complete Cure of Experimental Visceral Leishmaniasis with Amphotericin B in Stearylamine-Bearing Cationic Liposomes Involves Down-Regulation of IL-10 and Favorable T Cell Responses. J Immunol. 2008 Jul 15;181(2):1386 LP – 1398. Available from: http://www.jimmunol.org/content/181/2/1386

215. Ferede G, Diro E, Getie S, Getnet G, Takele Y, Amsalu A, et al. Visceral Leishmaniasis-Malaria Coinfection and Their Associated Factors in Patients Attending Metema Hospital, Northwest Ethiopia: Suggestion for Integrated Vector Management. Chattopadhyay R, editor. Malar Res Treat. 2017;2017:6816913. Available from: https://doi.org/10.1155/2017/6816913

216. Nandy A, Addy M, Guha SK, Maji AK, Chauahuri D, Chatterjee P. Co-existent

kala-azar and malaria in India. Trans R Soc Trop Med Hyg. 1995;89(5):516.

217. Hassan MF, Zhang Y, Engwerda CR, Kaye PM, Sharp H, Bickle QD. The Schistosoma mansoni hepatic egg granuloma provides a favorable microenvironment for sustained growth of Leishmania donovani. Am J Pathol. 2006;169(3):943–53. Available from: http://dx.doi.org/10.2353/ajpath.2006.051319

218. Otto TD, Böhme U, Jackson AP, Hunt M, Franke-Fayard B, Hoeijmakers WAM, et al. A comprehensive evaluation of rodent malaria parasite genomes and gene expression. BMC Biol. 2014;12(1):86. Available from: https://doi.org/10.1186/s12915-014-0086-0

219. De Oca MM, Engwerda C, Haque A. Plasmodium berghei ANKA (PbA) Infection of C57BL/6J Mice: A Model of Severe Malaria BT - Mouse Models of Innate Immunity: Methods and Protocols. In: Allen IC, editor. Methods in Molecular Biology. Totowa, NJ: Humana Press; 2013. p. 203–13. Available from: https://doi.org/10.1007/978-1-62703-481-4_23

220. Brugat T, Cunningham D, Sodenkamp J, Coomes S, Wilson M, Spence PJ, et al. Sequestration and histopathology in Plasmodium chabaudi malaria are influenced by the immune response in an organ-specific manner. Cell Microbiol [Internet]. 2014 May;16(5):687–700. Available from: https://pubmed.ncbi.nlm.nih.gov/24003897

221. Akinosoglou KS, Solomou EE, Gogos CA. Malaria: A haematological disease. Hematology. 2012;17(2):106–14.

222. Cadman ET, Abdallah AY, Voisine C, Sponaas AM, Corran P, Lamb T, et al. Alterations of splenic architecture in malaria are induced independently of toll-like receptors 2, 4, and 9 or MyD88 and may affect antibody affinity. Infect Immun. 2008 Sep;76(9):3924–31.

223. Autino B, Corbett Y, Castelli F, Taramelli D. Pathogenesis of malaria in tissues and blood. Mediterr J Hematol Infect Dis. 2012;4(1):e2012061–e2012061. Available from: https://pubmed.ncbi.nlm.nih.gov/23170190

224. Olivier M, Van Den Ham K, Shio MT, Kassa FA, Fougeray S. Malarial pigment hemozoin and the innate inflammatory response. Front Immunol. 2014 Feb 5;5:25. Available from: https://pubmed.ncbi.nlm.nih.gov/24550911

225. WHO. Leishmaniasis [Online]. WHO. 2019 [cited 2020 Jan 30]. Available from: https://www.who.int/news-room/fact-sheets/detail/leishmaniasis

226. Chen Y, Pikkarainen T, Elomaa O, Soininen R, Kodama T, Kraal G, et al. Defective Microarchitecture of the Spleen Marginal Zone and Impaired Response to a Thymus-Independent Type 2 Antigen in Mice Lacking Scavenger Receptors MARCO and SR-A. J Immunol. 2005 Dec 15;175(12):8173 LP – 8180. Available from: http://www.jimmunol.org/content/175/12/8173

227. Lampah DA, Yeo TW, Malloy M, Kenangalem E, Douglas NM, Ronaldo D, et al. Severe malarial thrombocytopenia: a risk factor for mortality in Papua, Indonesia. J Infect Dis. 2015 Feb 15;211(4):623–34. Available from: https://pubmed.ncbi.nlm.nih.gov/25170106

228. Hanson J, Phu NH, Hasan MU, Charunwatthana P, Plewes K, Maude RJ, et al. The clinical implications of thrombocytopenia in adults with severe falciparum malaria: a retrospective analysis. BMC Med. 2015;13(1):97. Available from: https://doi.org/10.1186/s12916-015-0324-5

229. Castro-Gomes T, Mourão LC, Melo GC, Monteiro WM, Lacerda MVG, Braga ÉM. Potential Immune Mechanisms Associated with Anemia in Plasmodium vivax Malaria: a Puzzling Question. Maurelli AT, editor. Infect Immun. 2014 Oct 1;82(10):3990 LP – 4000. Available from: http://iai.asm.org/content/82/10/3990

230. Gillman BM, Batchelder J, Flaherty P, Weidanz WP. Suppression of Plasmodium chabaudi Parasitemia Is Independent of the Action of Reactive Oxygen Intermediates and/or Nitric Oxide. Infect Immun. 2004 Nov 1;72(11):6359 LP-6366. Available from: http://iai.asm.org/content/72/11/6359

231. van der Heyde HC, Gu Y, Zhang Q, Sun G, Grisham MB. Nitric Oxide Is Neither Necessary Nor Sufficient for Resolution of Plasmodium chabaudi Malaria in Mice. J Immunol. 2000 Sep 15;165(6):3317 LP – 3323. Available from: http://www.jimmunol.org/content/165/6/3317

232. Hawkes M, Opoka RO, Namasopo S, Miller C, Conroy AL, Serghides L, et al. Nitric oxide for the adjunctive treatment of severe malaria: hypothesis and rationale. Med Hypotheses. 2011 Sep;77(3):437–44. Available from: https://pubmed.ncbi.nlm.nih.gov/21745716

Publications/other contributions

1. Olivier Preham, Flaviane A. Pinho, Ana Isabel Pinto, Gulab Fatima Rani, Najmeeyah Brown, Ian S. Hitchcock, Hiro Goto and Paul M. Kaye. **$CD4^+$ T Cells Alter the Stromal Microenvironment and Repress Medullary Erythropoiesis in Murine Visceral**. Frontiers in Immunology (2018).

2. James P. Hewitson, Katie A. West, Kylie R. James, Gulab Fatima Rani, Nidhi Dey, Audrey Romano, Najmeeyah Brown, Sarah A. Teichmann, Paul M. Kaye and Dimitris Lagos. **Malat1 Suppresses Immunity to Infection through Promoting Expression of Maf and IL-10 in Th Cells.** The Journal of Immunology (2020).

3. Tess A Stanly, Rakesh Suman, Gulab Fatima Rani, Peter O' Toole, Paul M. Kaye and Ian S. Hitchcock. **Quantitative Optical Diffraction Tomography Imaging of Platelets: in Health and Disease.** Frontiers in Physiology (2020).

4. Gulab Fatima Rani, Olivier Preham, Najmeeyah Brown, Helen Ashwin, Ian S. Hitchcock, Paul M. Kaye. **Understanding the Mechanisms Underlying Thrombocytopenia in Visceral Leishmaniasis.** Poster presentation at 61st ASH Annual Meeting & Exposition, Orlando, Florida (2019).

5. Vector Laboratories image contest (2018) winning image. **Macrophage populations in normal adult WT mouse spleen** (https://vectorlabs.com/galleries/gulab-fatima-rani-university-of-york).

6. Gulab Fatima Rani, Olivier Preham, Helen Ashwin, Najmeeyah Brown, Ian S. Hitchcock, Paul M. Kaye. **Mechanisms of Thrombocytopenia in Murine Visceral Leishmaniasis are Multifactorial** (working title)-in preparation (2020).

7. Gulab Fatima Rani, Helen Ashwin, Najmeeyah Brown, Ian S. Hitchcock, Paul M. Kaye. **Hematological Consequences of Malaria Infection in Mice Previously Treated for Visceral Leishmaniasis** (working title) – in preparation (2020).

8. Oliver J Herd, Gulab Fatima Rani, James P Hewitson, Karen Hogg, Andrew P Stone, Nichola Cooper, David G Kent, Paul G Genever, Ian S Hitchcock. **An Adapting Bone Marrow Creates a Nurturing Environment for Hematopoiesis During Immune Thrombocytopenia Progression in Mice** (working title) – in preparation (2020).